Demixing Alkyl piperidines for CO2 capture : A thermodynamic approach

Alexander Rowland Lowe

N° d'Ordre : 2772

UNIVERSITE BLAISE PASCAL
U.F.R. Sciences et Technologies
ECOLE DOCTORALE DES SCIENCES FONDAMENTALES
N° 897

THÈSE

Présentée pour obtenir le grade de
DOCTEUR D'UNIVERSITE

Spécialité : Chimie-Physique
Par : **Alexander Rowland Lowe**
Master of Science (University of Guelph, Canada)

Alkyl pipéridine démixantes pour le captage du CO_2: Approche thermodynamique
Demixing Alkyl Piperidines for CO_2 Capture: A Thermodynamic Approach

Soutenue publiquement le 12 décembre 2016, devant la commission d'examen

Examinateurs :
Christophe Coquelet, Professeur, Ecole Nationale Supérieure des Mines, ParisTech, Fontainebleau, (Président de Jury)
Aline Auroux, Directrice de Recherche Emérite, IRCELYON, Lyon, (Rapporteure)
Ilham Mokbel, Maître de Conférences, Université Jean Monnet St Etienne- Université de Lyon, (Rapporteure)
Denis Lourdin, Directeur de Recherche, INRA, Anger-Nantes (Examinateur)

Directeurs de Thèse :
Karine Ballerat-Busserolles, Ingénieure de Recherche, CNRS, Clermont-Ferrand
Jean-Yves Coxam, Maître de Conférences, Université Blaise Pascal, Clermont-Ferrand

Co-Encadrant :
Yohann Coulier, Ingénieur de Recherche, CNRS, Clermont-Ferrand

New Prestige Class:

Doctor of Physical Chemistry / Docteur de Chimie-Physique

Quotes from past scientists who inspired me keep learning.

“Il n'est pas certain que tout soit incertain.” Blaise Pascal

“Thermodynamics is a funny subject. The first time you go through it, you don't understand it at all. The second time you go through it, you think you understand it, except for one or two small points. The third time you go through it, you know you don't understand it, but by that time you are so used to it, so it doesn't bother you anymore.” Arnold Sommerfeild

Résumé : L'augmentation de la concentration de dioxyde de carbone (CO_2) dans l'atmosphère depuis la révolution industrielle a conduit à l'augmentation de la température moyenne du globe. Pour limiter l'accroissement des températures atmosphériques moyennes, la quantité de dioxyde de carbone émise dans l'atmosphère doit être réduite. Une des solutions envisagée sur les sources fixes est le captage et le stockage du CO_2. Ce procédé d'absorption/désorption, bien connu dans le traitement du gaz naturel, est onéreux et peu efficace pour le traitement du gaz des sources fixes et doit être optimisé.

La solution proposée s'appuie sur l'utilisation de solvants démixants, présentant une séparation de phase équilibre liquide-liquide (LLE) en solution aqueuse en fonction de la température. Ce manuscrit présente une étude réalisée pour la famille des alkyl-pipéridines connues pour ses séparations de phase. Cette étude permettra d'évaluer l'influence de la taille, de la position et du nombre de substituants sur les propriétés thermodynamiques d'intérêt pour le procédé.

Pour étudier les LLE des solutions aqueuses démixantes, en particulier dans le cas des solutions chargées en gaz, deux instruments ont été mis au point. Il a été possible de démontrer que les changements opérés sur les diagrammes de phase des amines sont liés aux réactions chimiques mises en jeu lors de la dissolution du CO_2. Pour les alkyl-pipéridines tertiaire on observe la température de démixtion diminue avec l'addition de CO_2, allant avec la formation de carbonates. Avec les alkyl-pipéridines secondaires la température de démixtion augmente, ce qui est lié à la présence en solution de carbamates qui stabilisent la solution aqueuse. Le comportement des amines secondaires très encombrées, qui ne peuvent donc pas formées de carbamates, est similaire à celui des amines tertiaires, ce qui est cohérent avec les conclusions précédentes.

Une étude approfondies des propriétés thermodynamiques d'excès (V^E, C_p^E et H^E) des alkyl-pipéridines en solution aqueuse a également permis de démontrer des relations structure - propriétés. La position du substituant sur le cycle pipéridine a une influence considérable et prévisible sur l'intensité des propriétés d'excès, alors que la nature de l'amine (secondaire ou tertiaire) va influencer la position de l'extremum de cette propriété.

Enfin, une modélisation thermodynamique rigoureuses des solubilités et des enthalpies de dissolution du CO_2 dans les solutions aqueuses de pipéridines a permis de déterminer les constantes de formation des carbamates dans les solutions aqueuses de 3- et 4-méthylpipéridines.

Abstract: The increase of carbon dioxide (CO_2) concentration in the atmosphere, since the industrial revolution has led to the rise in the average global climate temperature. To prevent the escalation of global climate temperatures the amount of CO_2 emitted into the atmosphere must be reduced. One solution is carbon capture and sequestration which removes CO_2 from fixed sources. The absorption/desorption cycle is well known for the treatment of acid gas, but is expensive and not as efficient for the treatment of gas from fixed/industrial sources.

A solution to this problem is the use of aqueous demixing amine solvents which present a liquid-liquid phase equilibrium (LLE) as a function of temperature. This manuscript presents a study done to measure the LLE and thermodynamic properties of the alkyl piperidine family, which can be used for carbon capture processes. This work evaluates the effect of the size, position and number of alkyl substituents on the thermodynamic properties of interest in the carbon capture process.

To study the LLE of aqueous demixing solutions, particularly gas loaded solutions, two novel apparatuses were developed. The results demonstrate that the changes in the amine phase diagrams are related to the chemical reactions involved with dissolution of CO_2. The tertiary alkyl piperidines displayed reduced demixing temperature with the addition of CO_2 due to the formation of carbonate species. The secondary alkyl piperidines display an increasing demixing temperature which is related to the formation of carbamate species which stabilizes the solution. Secondary alkyl piperidines that are severely sterically hindered, which cannot produce carbamates, behave similarly to the tertiary amine which is coherent with the preceding conclusion.

The structure property relationship concerning the excess thermodynamic properties (V^E,C_P^E and H^E) of aqueous solutions were studied in depth. This revealed that the position of the substituents on the cyclic ring has a considerable and obvious influence on the intensity of the excess properties, along with the class of the amine, whether secondary or tertiary, will influence the positions of the extrema of the excess property.

To conclude, a rigorous thermodynamic model based on the CO_2 solubility and the enthalpy of solution for CO_2 in aqueous solutions of alkyl piperidine, allowed for the determination of the carbamate formation constants of 3- and 4-methylpiperidine.

Mots clés / Key words : Captage du CO_2 / CO_2 capture, Amines démixantes / Demixing amines, Équilibre de phase / Phase equilibria, Enthalpies de solution / Enthalpy of Solution, Solubilités de CO_2 / CO_2 Solubility, Volumes Molair / Molar volumes, Densité / Density, Capacité calorifique molair / Molar heat capacity, Enthalpies molair d'excès / Excess molar enthalpy, alkyl-pipéridine / alkyl piperidine.

Acknowledgements / Remercîments

Back in 2011 I read a journal article from my main thesis supervisor during my master's degree. I then had the opportunity to meet her when she visited and little did I know then that I would have the opportunity to be her Ph.D student. Since that time I have now completed my Ph.D at the Université de Blaise Pascal, now Université Clermont Auvergne, as her student. From her I have learned that there are many different points of view in science particularly the way of looking at data and evaluating them. Her energy and intensity are limitless and served as motivation during my studies. My thesis co-supervisor I met in 2013 during my masters during a visit at the laboratory in Guelph. His insight in chemical thermodynamics and theory and data helped me further understand chemical thermodynamics and the relationships between what we observe in the nature of materials. The discussions I have had with him have helped me interpret my data and expand my understanding of molecular interactions. To Dr. Karine Ballerat-Busserolles and Dr. Jean-Yves Coxam, I would like to sincerely thank you both for the three year spent working with you and learning from you, it has been a privilege.

The reporters and examiners in my Ph.D defence: Prof. Christophe Coquelet (Centre thermodynamique de Procedee, Dr. Aline Auroux (Ircelyon), Dr. Ilham Mokbel (Univ. Claude Bernard) and Dr. Denis Lourdin (INRA Nates). It was a pleasure to have you examine me and hold me accountable to my work. Your comments and suggestions have giving me insight into the areas which I need to improve my knowledge.

None of my time here would have been possible without Dr. Yohann Coulier. I met him back in 2012 as a post-doc and I am happy for his recommendation to the group. He helped me to the best of his ability and I am happy for his efforts and to know him. His ability to focus on complex task is an admirable trait, exemplified by his marathon running. To my fellow student, Barbara Liborio (soon to be Dr. Liborio), sharing this experience with you has been a pleasure. The back and forth help we gave each other help me better understand the problems engineers face and gave me motivation to finish degree. I would also like to give a special thank you to Nicole Nénot, for her cheerful demeanour and encouragement.

The boys of CALNESIS, Dr. Mickael Simond and Dr. Jean-Claude Neyt, I would like to thank you both for the early years getting started. In both learning french and learning where to go for a drink and beer, i.e. Nota Bene, the campus bar with the best atmosphere I have been to, run by the best barkeep, Fred Gaume. The few games of pool we had during the first year were great.

The TIM group is a fantastic group of scientists and technicians who have helped me in one way or another throughout the program. Some of which have offered advice or a small distraction from work at the after lunch coffee or celebration of a grand achievement. Working with you has been a pleasure: Dr. Jean-Micheal Andanson, Dr. Margarida Costa Gomes, Dr. Alain Dequidt, Julien Devemy, Dr. Florent Gujon, Dr. Passcale Husson, Prof. Patrice Malfreyt, Prof. Agilio Padua, Laure Pison, Dr. Sabine Sarraute. While not part of the TIM group but part of the building I would like to thanks Professor Jean-Pierre Grolier, for sharing the history of chemical thermodynamics between Canada and France.

The organic chemists of chemistry 4 with who I would like to thank are Dr. Arnaude Gautier, Dr. Frederico Cisnetti, Dr. Gettano Angelici, Dr. Clémentine Gibrad, Dr. Jacob Hansen, Dr. Egon Heuson, Dr. Geoffrey Dumonteil and most importantly Radhe Shyam. It was a pleasure to meet you and get to know you. You are a great group of organic chemists and beer drinkers. Learning french was both a challenge with you guys and a pleasure.

To the bureaux d'Auvergne Société Chimique de France Club Jeunes, Audrey Diouf-Lewis, Dr. Amira Farhaoui and Dr. Yannick Esvan. The club we managed to run produced a few good events for everyone. The Christmas party, le journée scientifique, and student oral competition. It was nice working with you and you are great group of people.

To my fellow pre docs and post docs and no doc, who was part of the journey. Many thanks to Emilie Bordes, Thibaud Dreher, Joao Franca, Ludovic Garnier, Kevin Kempfer, Dr. Leila Moura, Dr. Makha Ndao, Dr. Inès Otero Fernandez, Dr. Yarick Grosu, Sven Plappert, Pablo Sanchez, Laura Sivet, Dr. José Solano, Gunjita Singh, Dr. Dusan

Stosic, Dr. Joana Szala-Bilnik, Dr. Julian Tay and Darius Yeadon. Many of you are still on your journey I hope you find the end of it soon thank you for the time I got to spend with you. Meeting you was great way to learn of new cultures and new and different sciences.

Outside of the ICCF and school I would like to thank Jessica Addley, Chantel Nguyen, David Alberti Morales, David Roberti, AntoineTavin, Meghana Upadhyaya, Nathanael Lampe (soon to be Dr), Martyna Zidonis, Dr. Ben Pesch. Meeting and getting to knowing each of you has been a big enjoyment in my life and the helpful distractions have helped me recover from hard weeks of work to get back into the next week.

I would also like to thank the international collaborators Dr. John Carroll, Dr Jenny Cox, Dr. Peter Tremaine, Dr. Olivia Fandiño Torres, and Christine McGregor.

Finally my parents, Geoffrey and Linda Lowe, and brothers Andrew and Christopher, thank you for your support over the past few years. I would also family in grandparents Joan and Stanley Lowe, my aunt Barbra Roberts and Mike Roberts for letting me spend the holidays with them in Manchester. As well as my aunts, uncles and cousins in Scotland who I had the opportunity to visit.

There are many things in life which add complexity to daily tasks. Balancing work and personal relationships is difficult thing to do. Learning how is even harder, I would like to thank you all very much. Merci beaucoup.

I apologise for not writing any acknowledgements in French, for I know I would not be able to full express my gratitude to all of you adequately. Mais encore, merci beaucoup à tout le monde pour trois grandes années.

Table of Contents

Table of Figures

Table of Tables

LIST of Abbreviations and Symbols

Abbreviation

CO_2	Carbon dioxide / Dioxyde de carbon
DPD	Dimethylpiperidine / Diméthylpipéridine
EPD	Ethylpiperidine / Éthylpipéridine
e-NRTL	Electrolyte Non-Random Two Liquid Model
Eth	Ethanol / Éthanol
LCST	Lower Critical Solution Temperature / Température de Solution Critique Inférieur
LLE	Liquid-liquid equilibrium / Équilibre liquide-liquide
MPD	Methylpiperidine / Méthylpipéridine
N	Nitrogen / Azote
NRTL	Non-Random Two Liquid Models
UCST	Upper Critical Solution Temperature / Température de Solution Critique Supérieur
UNIQUAC	UNIversal QUAsi Chemical

Symbols

A B C Fitting parameter

A_φ	Debye-Hückel coefficients for an extensive property / Parametre de Debye-Hückel pour un propriété étendu
b	Coefficient in the Pitzer equation / Coefficient dans l'équation de Pitzer
β	Virial parameter for the Pitzer equation / paramètre viriel pour l'équation de Pitzer
C_p	Isobaric molar heat capacity / Capacité calorifique molaire isobare
c_p	Specific heat capacity / Capacité calorifique spécifique

D	Dielectric Constant /Constante diélectrique
G	Molar Gibbs Energy / Énergie libre de molaire Gibbs
$\overline{G}_i$	Partial Molar Gibbs Energy / Énergie libre de molaire Gibbs partiel
H	Molar Enthalpy / Enthalpie molarie
I	Ionic strength / Force ionique
IP	Interaction parameters / Paramètres d'interaction
K	Equilibrium constant / Constant d'equilibre
k	Calibration constant / Constant de calibration
k_H	Henry's constant / Constante de Henry
M	Molecular weight / Masse moleculaire
m	Molality in moles per kilogram of solvent / Molalité en mole par kilograms de solvant
S	Molar Entropy / Entropie Molaire
R	Ideal Gas Constant / Constante des gaz parfaits
r	Radius of the molecule or ion / Radius de la molecule ou de l'ion
T	Temperature in Kelvin / Temperature en Kelvin
V	Molar Volume / Volume molaire
kg	kiliogram / kilogramme
mL	milliliters / millilitres
MPa	Megapascal / Megapascal
n	Number of moles / Nombre de moles
P	Power / Puissance
p	Pressure / Pression
f	Fugacity / Fugacité

w Water / Eau

w_a Weight percent amine in water amine solution / Pourcentage en masse d'aminé dans une solution d'eau amine

x_a Mole fraction of amine in water amine solution / Fraction molaire de l'aminé dans une solution d'eau amine

z Charge on an ion /Charge de l'ion

Greek Symbols

α Loading charge /Taux de charge

Δ Difference / Difference

ν Stoichiometric coefficient / Coefficient Stoichiométrique

γ Activity coefficient, anisotropy / Coefficient d'activité

ρ Density of a liquid / Masse volumique d'une liquide

σ Standard uncertainty / deviations standard

μ Chemical potential / Potential chimique

ϕ Fugacity coefficient / Coefficient de fugacité

τ Period of vibration / Période de résonnacne

Subscripts

a Amine, activity / activité

i Species / Espèce

r At the reference temperature, Reduced property / A la temperature de reference, Propriété réduite

t Total amount of species / Quantité totale d'espèces

s Solution

sc Critical Solution Temperature / Température critique de la solution

w Water / Eau

Superscripts

α Phase one / Phase une

β Phase two / Phase deux

E Excess property / Propriété excès

^{o} Hypothetical one molal standard state or ideal gas standard state / Un état standard molaire standard ou un état de gaz idéal

* Pure substance / Substance pure

sat Saturation

v Vapour / Vapeur

0 Résumé en Française

Un changement climatique est un phénomène naturel apparaissant régulièrement sur notre planète. L'échelle de temps pour ce changement est normalement de l'ordre de centaines de milliers d'années. Cependant le changement climatique qui se produit actuellement a lieu depuis le début de la révolution industrielle, donc sur une échelle de temps très réduite d'une centaine d'années. A cette époque, les émissions anthropiques de gaz à effet de serre se sont intensifiées, le dioxyde de carbone (CO_2) étant le plus important. Il est responsable d'environ 60% du réchauffement climatique. Le taux de CO_2 dans l'atmosphère a augmenté rapidement, passant de 260 ppm dans les années 80 (Wigley, 1983) à la valeur actuelle de plus de 400 ppm mesurée à l'observatoire de Mauna Loa, Hawaï. Le groupe d'experts internationaux sur le changement climatique (GIEC) prédit un taux de 570 ppm de dioxyde de carbone dans l'atmosphère d'ici 2100. La température sur terre serait alors augmentée de 2°C et le niveau moyen de la mer de 38 cm (Stewart and Hessami, 2005).

L'augmentation de la population et l'utilisation des énergies fossiles pour la demande croissante en énergie sont les causes principales de l'augmentation des émissions de CO_2 (Pachauri et al., 2014). En attendant un développement des énergies alternatives, les technologies de captage et de séquestration du CO_2 (CSC) peuvent être envisagées pour prévenir l'augmentation du taux de celui-ci dans l'air (Ellina Levina et al., 2013). Ces technologies doivent être utilisées sur les centrales électriques et les sites industriels consommateurs d'énergies fossiles afin de répondre à cette demande. Le rapport du GIEC suppose que le captage et stockage du CO_2 (CSC) peut réduire de 14% les émissions de CO_2 par rapport à celles de 2005 (Ellina Levina et al., 2013).

Le procédé de captage le plus communément envisagé, est le procédé dit de « lavage aux amines ». Ce procédé postcombustion utilise des solutions aqueuses d'alkanolamines pour absorber sélectivement

le dioxyde de carbone dans les effluents industriels. Ce procédé de lavage aux amines est déjà mis en place pour séparer le CO_2 dans le traitement du gaz naturel (Maddox et al., 1987). Il a également récemment été appliqué pour capter le CO_2 provenant de centrales à charbon, par exemple au Boundary Dam Power Station au Canada, (Mumford et al., 2015). L'amine actuellement considérée comme référence en Europe est la monoéthanolamine. Parmi les autres solvants classiques on trouve la méthyldiéthanolamine, la diéthanolamine, la 2-amino-2-méthyl-1-propanol ou des mélanges d'amines, de pipérazine et d'ammoniac.

Le procédé repose sur des cycles d'absorption-désorption du CO_2, et son schéma de principe est représenté en Figure 0-1. Le dioxyde de carbone contenu dans les effluents gazeux est absorbé sélectivement par une solution liquide dans un absorbeur. Le mécanisme d'absorption est principalement chimique, basé sur les réactions acido-basiques et sur la formation de carbonates, bicarbonates ou de carbamates. La solution chargée est régénérée par désorption dans une colonne de régénération. Le solvant régénéré retourne dans l'absorbeur, et le dioxyde de carbone est compressé et transporté pour être stocké ou réutilisé. Le problème clé de cette technologie est son coût énergétique. En effet, la désorption du dioxyde de carbone est fortement endothermique. Elle a lieu dans une colonne de régénération où la solution chargée est chauffée autour de 120°C.

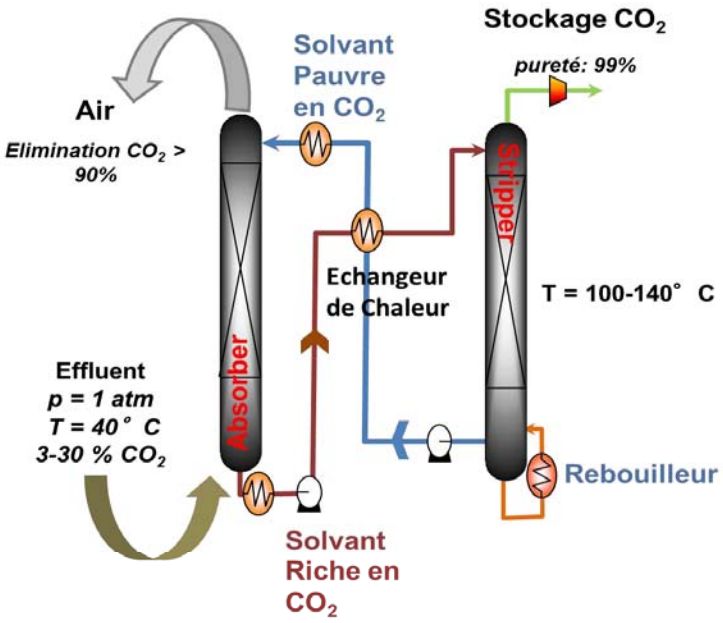

Figure 0-1 Schéma de principe d'une unité de captage post-combustion de dioxyde de carbone.

Il est nécessaire d'imaginer des procédés innovants permettant une réduction notable du coût énergétique du traitement. Parmi les nombreuses solutions envisagées, une des options est l'utilisation de solvants démixants (Zhang et al., 2011; Gomez et al., 2014). Ces nouveaux solvants présentent une séparation de phases liquide-liquide qui facilite le relargage du CO_2 capté et la régénération du solvant pour une utilisation industrielle.

Ces solvants démixants sont homogènes à température ambiante et présentent une séparation de phase liquide-liquide en augmentant la température. Le procédé DMX^{TM}, qui est basé sur le principe du solvant démixant, a été proposé et breveté par IFP Energies nouvelles (IFPEn). Le schéma de fonctionnement est présenté en Figure 0-2. Dans la première étape du procédé, le dioxyde de carbone est chimiquement absorbé par une solution aqueuse d'amine, selon le même schéma que dans le cas du « lavage aux amines » classique (figure 0-1). La solution chargée en CO_2 est alors envoyée vers un décanteur où la température de la solution est augmentée jusqu'à séparation de phases. La phase la plus

lourde est composée principalement d'eau, de sels carbonés et de sels d'amine, alors que la phase supérieure contient principalement les amines qui n'ont pas réagi. Dans le procédé de séparation, seule la phase aqueuse chargée est envoyée vers l'unité de régénération, la phase amine étant renvoyée directement vers l'absorbeur. L'intérêt de travailler avec des amines dites démixantes, est que seule une partie de la solution est envoyée vers l'unité de régénération. Le coût de la régénération est ainsi réduit du fait d''une quantité plus faible de solution à régénérer.

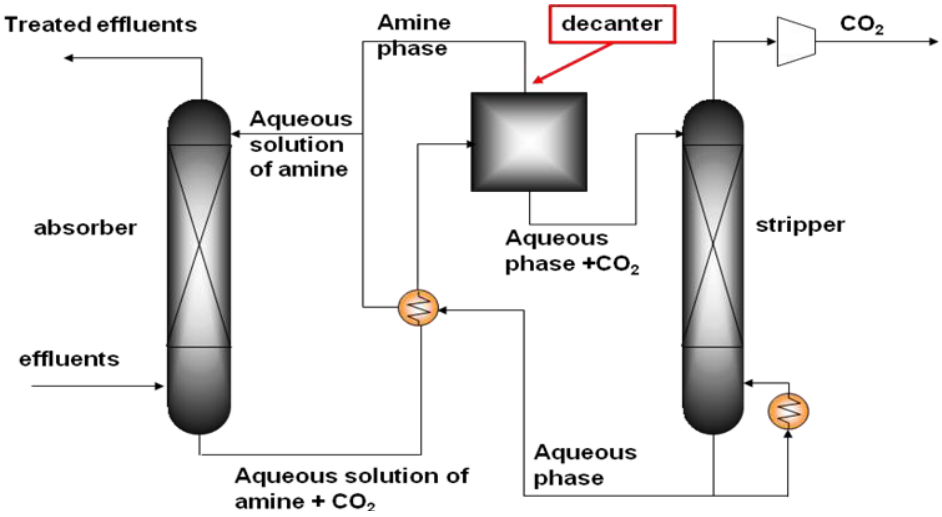

Figure 0-2: Schéma du procédé utilisant les solutions d'amines démixantes (Gomez et al., 2014)

L'étude proposée ici va contribuer à la compréhension des équilibres thermodynamiques des systèmes {eau-amine} et {eau-amine-CO_2}, où l'amine est une pipéridine substituée. Le choix des substitutions est établis afin de mettre en évidence des relations structure-propriétés (démixion-absorption). Les pipéridines sont déjà bien connues pour présenter une séparation de phases liquide-liquide de type LCST (lower critical solution temperature). Le but est d'élaborer des règles systématiques et transférables, à partir d'une étude thermodynamique, afin de pouvoir aider au design de molécules spécifiquement efficaces pour des procédés de captage de CO_2, économiques et adaptables à

la nature des effluents industriels à traiter. D'après la représentation du procédé montré en Figure 0-3, un schéma physico-chimique et un schéma de procédé peuvent être établis:

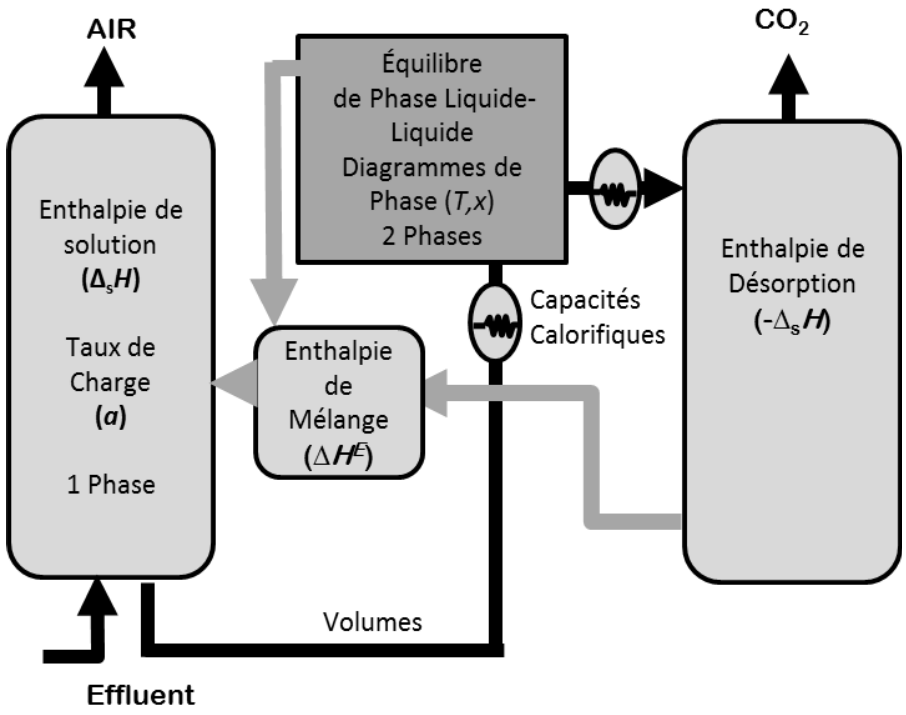

Figure 0-3: Schéma physico-chimique du procédé de captage de CO_2

Le côté gauche de la figure 0-3 correspond à la dissolution du CO_2, où l'enthalpie de solution et la solubilité du CO_2 à la température de l'absorbeur (environ 40°C), sont les grandeurs caractéristiques choisies pour représenter le processus. Le côté droit correspond à la colonne de régénération, l'enthalpie de régénération dans cette partie est l'opposé de l'enthalpie de dissolution, à la température de la colonne (autour de 120°C). Dans cette colonne, seule la phase aqueuse riche en dioxyde de carbone est considérée. La partie centrale haute représente l'étape de séparation liquide-liquide qui a lieu dans le décanteur. La transition d'une à deux phases, ou l'équilibre liquide-liquide, est la caractéristique principale de cette opération. Finalement, le carré central bas correspond au mélange de la phase

régénérée riche en eau, provenant du régénérateur, et de la phase riche en amine, provenant du décanteur. Elle est caractérisée par l'enthalpie de mélange ou d'excès {eau-amine}. Les données de capacités calorifiques et de densités sont nécessaires au dimensionnement des échangeurs thermiques du procédé.

La pipéridine a une structure hétérocyclique saturée avec un groupe azoté. Elle a, avec l'addition de groupements alkyles, des valeurs de pK_a allant de 10 pour la N-méthylpipéridine à 11,1 pour la pipéridine. Le pK_a dépend de la position, du nombre et de la taille des groupements alkyles. La pipéridine est complètement soluble quelle que soit la composition dans le domaine de températures et de pressions étudiés dans ce travail. L'addition d'un groupe méthyle va engendrer une séparation de phases liquide-liquide avec l'augmentation de la température, en solution aqueuse (Stephenson, 1993; Góral et al., 2012a; Góral et al., 2012b). L'augmentation de la longueur de chaine du groupe alkyle ou l'augmentation du nombre de groupes alkyles vont également modifier les températures critiques de solution, T_{sc}, ainsi que la composition critique de solution, x_{sc},. L'équilibre de phases est lié à la structure de la molécule, cependant le mécanisme de cette relation est aujourd'hui inconnu. La Figure 0-4 illustre les différentes structures des pipéridines étudiées dans ce projet. Le nom des produits chimiques et leurs acronymes est listés dans le Tableau 0-1.

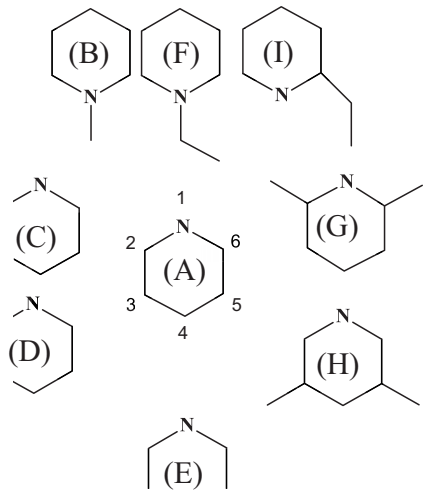

Figure 0-4: Structure des alkyl-pipéridines étudiées dans ce le projet: (A) Pipéridine, (B) N-méthylpipéridine, N-MPD (C) 2-méthylpipéridine, 2-MPD (D) 3-méthylpipéridine, 3-MPD (E) 4- méthylpipéridine (F) N-éthylpipéridine, N-EPD (G) 2,6-diméthylpipéridine, 2,6-DPD (H) 3,5-diméthylpipéridine, 3,5-DP, (I) 2-éthylpipéridine, 2-EPD.

Tableau 0-1: Liste des amines étudiées et leurs acronymes

Produits chimique	Acronymes
N-méthylpipéridine	N-MPD
2-méthylpipéridine	2-MPD
3-méthylpipéridine	3-MPD
4- méthylpipéridine	4-MPD
2,6-dimethylpipéridine	2,6-DPD
3,5-diméthylpipéridine	3,5-DPD
N-éthylpipéridine	N-EPD

Cette thèse a été réalisée dans le cadre d'un projet nommé DACOOTA, (**D**emixing **A**mines for **CO_2** capture : **T**hermodynamic and Spectroscopic **A**pproach). Il s'agit d'une collaboration internationale entre une équipe de recherche de l'institut de Chimie de Clermont-Ferrand (équipe Thermodynamique et Interactions Moléculaires, thématique « Captage du CO_2 ») et le « Hydrothermal Chemistry Group» de l'Université de Guelph, au Canada. Les financements de ce projet ont été fournis

par l'Agence Nationale de la Recherche (ANR) pour l'équipe française et le Conseil de Recherches en Sciences Naturelles et en Génie du Canada (CRSNG). Cette collaboration permet de mettre en commun les compétences de chaque groupe. Le groupe "captage du CO_2 " est spécialisé dans les mesures expérimentales de solubilité du CO_2, des équilibres liquide-liquide, des enthalpies de mélange, des capacités calorifique d'excès et des masses volumiques de fluides. Le « Hydrothermal Chemistry Group » de l'Université de Guelph est spécialisé dans l'étude des propriétés thermodynamiques et de transport des solutions aqueuses aux hautes températures et hautes pressions. Dans le cadre de ce projet, la spectroscopie RAMAN a été utilisée pour déterminer la spéciation en solution après absorption du dioxyde de carbone dans les solutions d'amine, avant et après démixtion.

Le but de ma thèse est de caractériser expérimentalement les systèmes {eau-amine} et {eau-amine-CO2}, en particulier les équilibres liquide-liquide pour une famille de pipéridines substituées. L'étude thermodynamique permettra de répondre à plusieurs questions importantes :

- Comment la structure de la molécule affecte-t-elle les propriétés physico chimiques et les équilibres de phases?
- y a-t-il des relations entre la structure des pipéridines et les propriétés thermodynamiques ou les équilibres de phases, qui peuvent être utilisées pour concevoir de nouvelles molécules?

Les outils utilisés dans ma thèse sont principalement expérimentaux. Les températures d'équilibre liquide-liquide des solutions aqueuses d'amine ont été mesurées avec et sans dioxyde de carbone. Pour les systèmes binaires {eau-amine}, les densités, les capacités calorifiques spécifiques et les enthalpies d'excès ont été étudiées en fonction de la température. Pour les systèmes ternaires {eau-amine-CO_2}, mon travail a porté sur la mesure et la représentation des enthalpies de solution et des solubilités.

Les données expérimentales d'enthalpies de solution ont été utilisées pour ajuster les modèles représentatifs de la dissolution du gaz dans la solution aqueuse. Pour cela un modèle thermodynamique

γ-υ a été ajusté sur les données enthalpiques obtenues aux faibles taux de charge et sur les données de solubilités obtenues en fonction de la température et de la pression. Ce modèle thermodynamique permet une estimation des constantes d'équilibre de formation du carbamate et de la spéciation en solution.

La suite de ce chapitre va présenter les principaux résultats obtenus au cours de mon travail de thèse. Une des grandes avancées de ce travail réside dans la mise au point d'une méthode pour la mesure des températures de séparation de phases dans des solutions chargées en gaz. Cette méthode, ainsi que les principaux résultats expérimentaux sont présentés par la suite. Après une présentation des principales propriétés thermodynamiques des solutions binaires (volumes, capacités calorifiques et enthalpies d'excès) obtenues, suivra la présentation des enthalpies de solution du CO_2 dans les solutions aqueuses d'amine, et leur modélisation thermodynamique.

0.1 Équilibre de phase liquide-liquide

La température de séparation de phases liquide-liquide, LLE, a été déterminée pour des solutions aqueuses de pipéridine, notamment à différents taux de charges en CO_2, en utilisant la méthode du point de trouble. Elle est basée sur la détermination optique de la température à laquelle la solution n'est plus homogène, quand il existe un équilibre entre deux phases liquides. Cette propriété a pour origine la différence dans l'indice de réfraction entre une solution homogène et une émulsion, où des gouttes d'un liquide sont dispersées dans un second. Les mélanges hétérogènes diphasiques sont opaques, alors que les solutions homogènes monophasiques sont transparentes. La Figure 0-5 illustre ces différences observables visuellement.

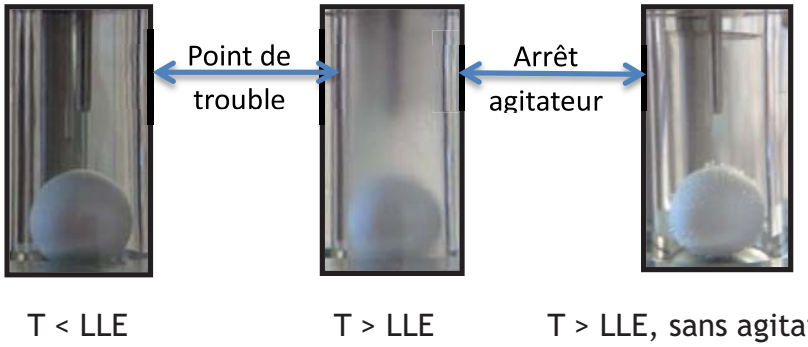

Figure 0-5: Illustration de la visualisation de la séparation de phase lors de l'augmentation de température.

Deux équipements différents ont été utilisés pour réaliser ces mesures : la cellule d'équilibre de phases SPM 20 de la société Thar Instruments et une cellule en saphir développée en collaboration avec le « Centre Thermodynamique des Procédés » de Mines ParisTech. Ces deux équipements sont représentés sur la Figure 0-6.

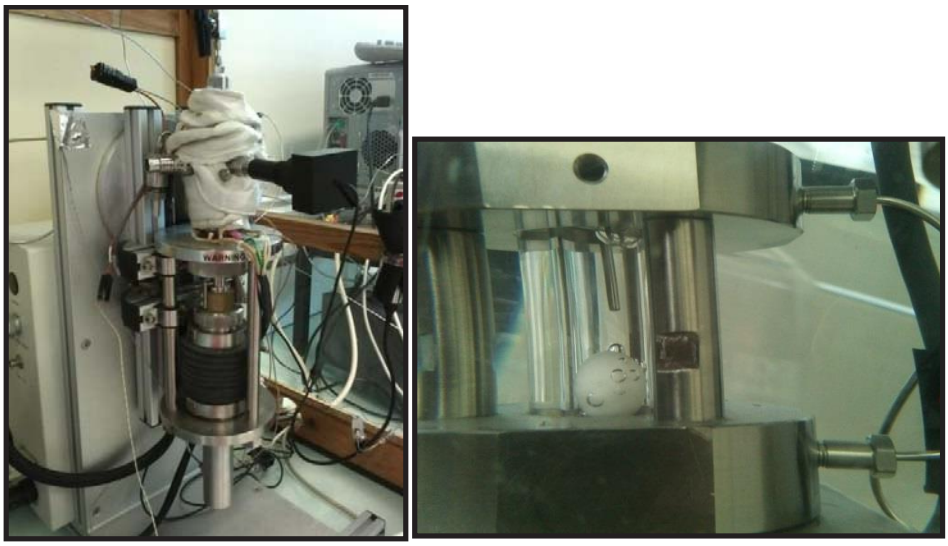

Figure 0-6: Photo de gauche: L'instrument de Thar Instruments ; à droite: cellule en saphir (CTP).

Les principales caractéristiques de ces deux appareils sont données dans le Tableau 0-2 suivant.

Tableau 0-2: Caractéristiques des cellules d'équilibre de phase.

	Cellule Thar Instrument	Cellule en saphir
T (K)	T ambiante – 393	270 – 393
Control of T	Ruban chauffant	Bain thermostatique
p (MPa)	1 – 40	1 – 8
Control de la pression	Volume tampon	Volume tampon
Volume interne (mL)	10 - 20 ajustable	4.4
Visualisation de l'échantillon	Fenêtre de saphir	Echantillon entier

La procédure pour déterminer le point de trouble est la même quelle que soit la cellule utilisée. Une fois la cellule entièrement remplie avec la solution homogène sans phase vapeur, la température est augmentée dans la cellule à une vitesse contrôlée (0,2 à 1 K/min) pour trouver l'intervalle de température où la solution devient trouble. L'augmentation et la diminution lente de la température dans cet intervalle permet alors d'affiner la lecture de la température du point de trouble. Le changement de la turbidité est observé visuellement. L'incertitude sur la température de point de trouble a été estimée pour la reproductibilité à $\sigma T = 2$ K, alors que l'incertitude sur la mesure est $\sigma T = 0.5$ K.

0.2 Les systèmes aqueux binaires

Pour les systèmes aqueux binaires, les données d'équilibre de phases de la littérature sont rares et ne sont pas toujours cohérentes. Elles sont au nombre de quatre pour la N-MPD, de deux pour 3-MPD et 4-MPD, et une seule référence existe pour 2,6-DPD, 3,5-DPD et N-EPD. Ces équilibres de phases ont donc été déterminés au cours de cette thèse et comparés aux mesures obtenues par Stephenson (Stephenson, 1993). Un exemple de diagramme *T-x* est montré sur la **Figure 0-7**.

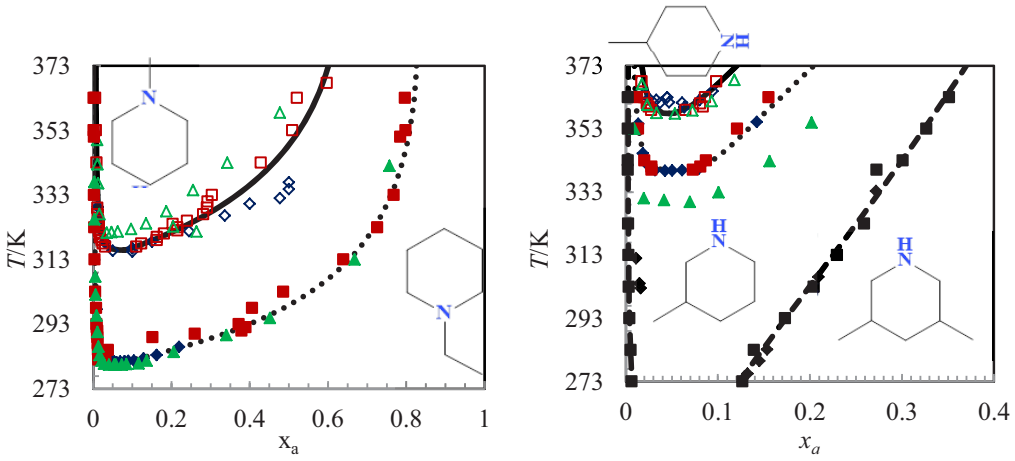

Figure 0-7: diagrammes de phases des systèmes binaires étudiés :A gauche : amines tertiaires : N-MPD (◇,□,△) et N-EPD (◆, ■, ▲) (◆ Ce travaille, ◇ Coulier Y et al. 2010, △ Flaschner and MacEwen, 1908; ▲ Flaschner, 1909; □, ■ Stephenson, 1993) ; à droite : amines secondaires : 4-MPD, (◇ □ △). 3-MPD, (◆ ■ ▲) 3,5-DPD (◆, ■). (◇, ◆ Ce travaille, △ Flaschner and MacEwen, 1908; ▲ Flaschner, 1909; □, ■, ■ Stephenson, 1993)

Les diagrammes permettent d'identifier deux caractéristiques majeures : la température de solution critique (LCST) et le domaine de concentration sur lequel la solution démixe. Il apparait clairement que les amines tertiaires démixent sur un large domaine de fractions molaires (jusqu'à x_a=0.85 pour la N-EPD) alors que les amines secondaires (figure de droite) ne démixent que sur un domaine restreint de fractions molaires (jusqu'à x_a=0.4 pour la 3,5-DPD). De plus d'une manière générale, les LCST des amines secondaires sont plus hautes que celles de leurs équivalents tertiaires (comparaison de N-MPD avec 3- et 4- MPD). L'addition d'un deuxième groupe méthyl ou l'augmentation de la longueur de la chaine d'un groupe alkyle diminue drastiquement la LCST ainsi que la largeur du domaine de séparation de phases.

Les données d'équilibre de phases ont été corrélées grâce à des équations mathématiques. Celles-ci décrivent l'enveloppe de phase et les températures critiques inférieures de solution.

0.3 Les systèmes aqueux ternaires

Pour les systèmes ternaires, il a été nécessaire de mettre au point un protocole afin de préparer les solutions aqueuses chargées, avec une quantité connue de gaz. La méthodologie s'appuie sur une

méthode couramment utilisée au laboratoire pour des mesures d'enthalpie de dissolution de gaz dans les solutions aqueuses d'amines (Arcis et al., 2011). Une unité de mélange a donc été ajoutée en amont de la cellule de mesure d'équilibre de phases (voir section 4.3.3 du manuscrit).

Cette technique a été utilisée pour préparer les solutions aqueuses de 2-MPD chargée en CO_2. Quelques résultats sont reportés en Figure 0-8 (figure de gauche) Nous avons pu démontrer que la température de séparation de phases augmente avec le taux de charge en CO_2, pour une concentration en amine constante. De plus, plus la concentration en amine est élevée, plus la température de séparation de phase augmente rapidement avec le taux de charge.

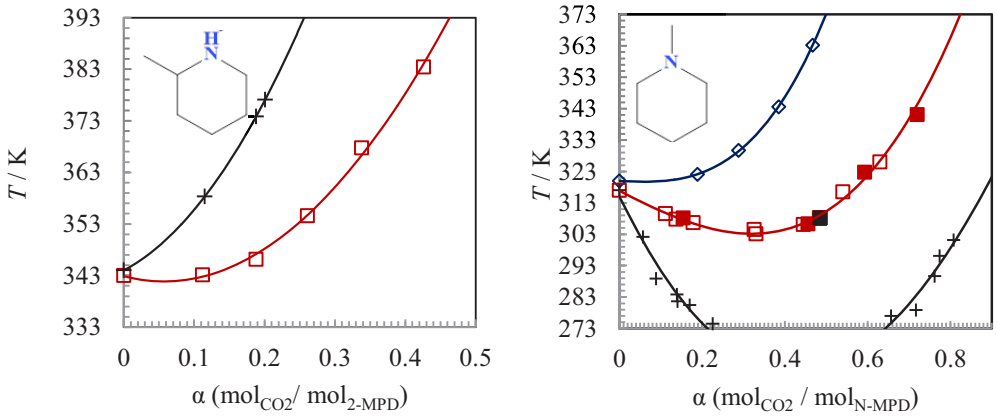

Figure 0-8: LLE en fonction du taux de charge en CO_2, pour les solutions aqueuses de 2-MPD (gauche) et N-MPD (droite). Les symboles sont : ◇ 10 w_a%, (□ , ■) 20 w_a % et + 40 w_a%,

L'étude de la séparation de phases dans les solutions aqueuses de N-MPD a montré un comportement très différent (Figure 0-8, graphe de droite). Les températures d'équilibre de phase diminuent avec l'absorption de faibles quantités de CO_2. Cette décroissance est d'autant plus importante que la fraction molaire d'amine en solution aqueuse augmente. Cependant, pour les plus forts taux de charge, la LLE augmente à nouveau. Pour une solution à 40% en masse d'amine (x_a = 0.1), avec un taux

de charge de CO_2 compris entre 0.2 et 0.6, la solution était diphasique quel que soit le domaine de température étudié.

Lors de la dissolution du CO_2 dans la solution aqueuse de N-MPD, les réactions chimiques conduisent à la formation de carbonates et de bicarbonates. La présence de ces sels abaisse la solubilité de l'amine dans la solution. Cet effet est connu sous l'appellation « salting-out ». La différence principale entre N-MPD et 2-MPD est la possibilité pour la 2-MPD de former des carbamates en solution aqueuse. Si on considère que cette espèce est responsable des différences de comportement entre les deux amines, alors il faut supposer que ce carbamate stabilise la solution. Cette hypothèse est corroborée par les résultats obtenus avec les 3- et 4- MPD. En effet en présence de CO_2, 3-MPD et 4-MPD ne présentent plus de séparation de phases liquide-liquide quelle que soit la quantité de CO_2 absorbée sur le domaine de température étudié. La plus grande différence entre ces trois amines est l'encombrement de l'azote de la pipéridine. Dans le cas de la 2-MPD, celui-ci est plutôt encombré, les carbamates ne sont donc pas stables, ce qui conduit à des LLE inférieures à celles obtenues avec la 3-MPD et la 4-MPD.

Cette hypothèse est renforcée par l'étude de la 2,6-DPD. Dans le cas où l'azote de la pipéridine est encore plus encombré (un groupement CH_3 sur chaque carbone entourant l'azote), les carbamates ne peuvent plus se former, et le diagramme de phases obtenu est similaire au diagramme de phases de la N-MPD (amine tertiaire). Dans les 2 systèmes (2,6-DPD et N-MPD), le carbone est principalement absorbé sous forme de carbonates et de bicarbonates.

L'influence de la longueur de la chaine alkyle est analysée en comparant les équilibres de phases obtenus en fonction du taux de charge, pour la N-EPD et la N-MPD. Les températures de séparation de phases étant plus basses avec la N-EPD, Il a été nécessaire de concevoir un nouveau système de préparation du mélange du CO_2 avec la solution aqueuse. La solution est préparée à l'aide d'une

méthode *pVT* statique : une quantité contrôlée de CO_2 était insérée dans un cylindre à température, pression et volume connus. Ensuite une quantité également connue de solution aqueuse est insérée dans le cylindre. L'ensemble est maintenu sous agitation, dans un bain froid (autour de zéro degré), jusqu'à homogénéisation du mélange. Les résultats obtenus pour la N-EPD montrent que la forme du diagramme de phase est similaire à celle de N-MPD. Les températures de séparation de phases quant-à-elles sont plus basses avec N-EPD que celles obtenues avec la N-MPD.

0.4 Les propriétés thermodynamiques des solutions aqueuses

Nous nous sommes intéressés aux propriétés thermodynamiques des solutions aqueuses binaires en fonction de la température. Ici encore, peu de données sont disponibles dans la littérature. Dans le passé, le laboratoire a étudié les propriétés d'excès de la N-MPD et de la 2-MPD (Coulier et al., 2010; Coulier et al., 2015). Le travail présenté dans cette section concerne les données thermodynamiques des systèmes binaires {eau + alkyl-pipéridine}. L'objectif est de comparer les données thermodynamiques à la structure moléculaire afin de trouver des relations structure-propriétés.

Trois différentes propriétés thermodynamiques ont été mesurées :

- Les densités (volumes d'excès),
- Les capacités calorifiques (capacités calorifiques d'excès),
- Les enthalpies d'excès.

Les densités ont été obtenues sur une gamme de températures allant de 288.15 K à 328.15 K, à pression atmosphérique en utilisant un densimètre SODEV 02D. Un microcalorimètre microSC de SETARAM a permis d'obtenir les capacités calorifiques des N-, 2-, 3-, 4- méthylpipéridines pures et en solution aqueuse. Enfin les enthalpies d'excès des solutions ont été mesurées avec un calorimètre fluxmétrique SETARAM B 2.15, équipé d'une cellule de mélange à écoulement développé au laboratoire. La

description des méthodes expérimentales peut être trouvée dans la section 5.2 du manuscrit. Un exemple des résultats obtenus est donné sur la Figure 0-9 où sont représentées les trois propriétés thermodynamiques à une température donnée, pour les quatre amines étudiées.

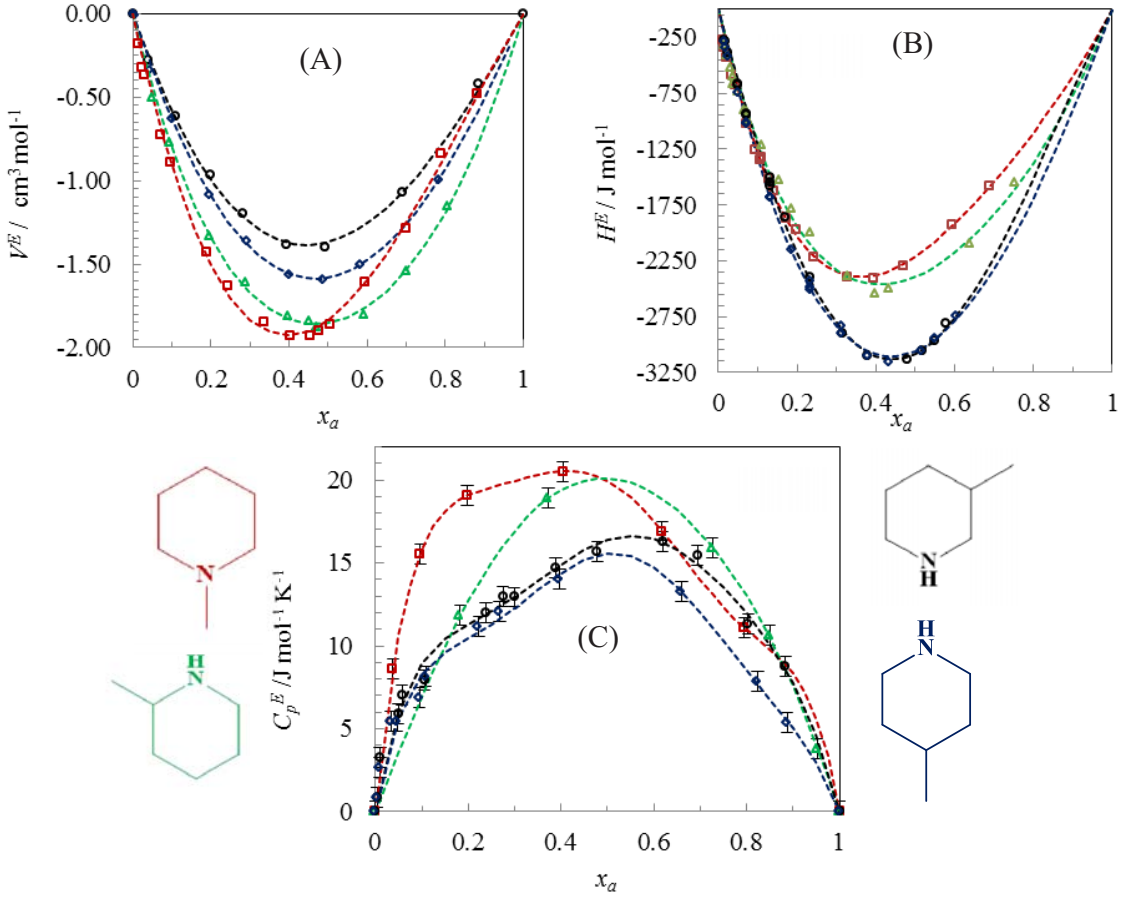

Figure 0-9: Propriétés thermodynamiques des methyl-pipéridines en solution aqueuse; (A) Volume molaire d'excès à 25°C; (B) Enthalpie molaire d'excès à 40°C (C) Capacité Calorifique molaire d'excès à 35°C.

Les données montrent une relation entre les propriétés thermodynamiques et la structure moléculaire des pipéridines. Pour les amines secondaires (2-, 3-, 4- MPD), l'extremum obtenu pour des grandeurs d'excès est centré autour d'une fraction molaire comprise entre 0.45 et 0.5. Cette valeur se décale vers les plus basses fractions molaires pour la N-MPD qui est une amine tertiaire. De plus, il apparait aussi clairement que les valeurs maximales obtenues pour N-MPD et 2-MPD d'une part, et pour

3-MPD et 4-MPD d'autre part sont similaires quelle que soit la propriété. Par exemple, les enthalpies d'excès des N- et 2- methylpipéridines ont une valeur proche de -2300 $J.mol^{-1}$ alors que cette valeur est de -3200 $J.mol^{-1}$ pour les 3- et 4-MPD. La valeur maximale de la propriété est donc sans doute liée plutôt à la proximité du méthyl envers l'azote du cycle, alors que la position du maximum est liée à la notion de degrés de substitution de l'azote.

0.5 Enthalpies de solution du dioxyde de carbone dans les solutions aqueuses de 4-MPD et 3-MPD

Cette section présente les mesures des enthalpies de solution ($\Delta_{sol}H_{CO_2}$) du CO_2 dans les solutions aqueuses de 3-méthylpipéridine (3-MPD) et 4-méthylpipéridine (4-MPD). Ces deux amines ont une LCST supérieure à 338 K (Stephenson, 1993). Les enthalpies de solution pour la 3-MPD et la 4-MPD sont mesurées à 318 K et 338 K, et à des pressions de 0.5, 1.0 et 1.5 MPa. Les solutions aqueuses ont été préparées à des compositions allant de $15w_a\%$ à $40w_a\%$. L'appareil de mesure est le calorimètre SETARAM BT 2.15, utilisant une cellule de mélange développée au laboratoire, et similaire à celle utilisée pour la mesure des enthalpies d'excès présentées précédemment. Un exemple de résultats est reporté sur la Figure 0-10

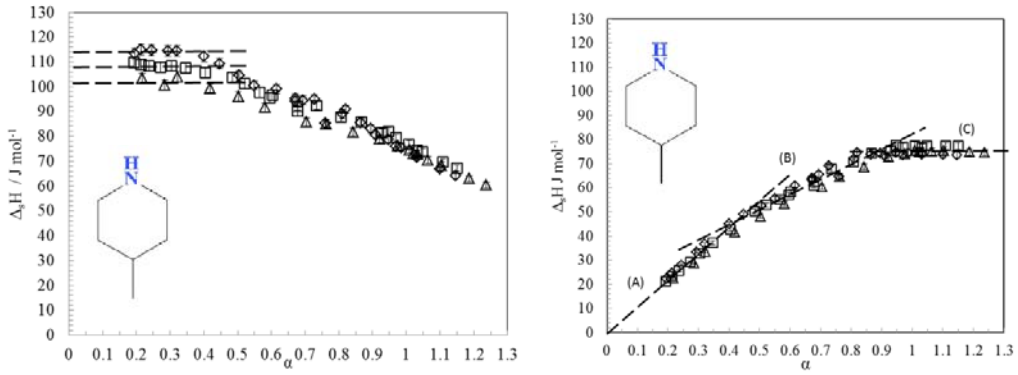

Figure 0-10: Enthalpies de solution par mole de CO_2 (courbe de gauche) et par mole d'amine (courbe de droite) en fonction du taux de charge en CO_2, dans une solution aqueuse de 4-MPD à 40% en masse, et pour trois pressions : ◇ (0.43 MPa), □ (0.95 MPa), et △ (1.45 MPa)

Les résultats obtenus pour l'enthalpie de solution par mole d'amine (figure de droite) mettent en évidence trois domaines principaux qui correspondent respectivement à une dissolution totale (solution insaturée), et à une dissolution partielle (solution saturée) du CO_2 :

- Pour des taux de charge inférieurs à 0.5, le CO_2 est totalement dissous (A). Ce domaine correspond à une augmentation linéaire quand les enthalpies sont exprimées par mole d'amine. Dans ce domaine la valeur d'enthalpie de solution aux faibles taux de charge exprimée par mole de CO_2 (courbes de gauche) est constante dans la limite de l'incertitude expérimentale. Elle est couramment utilisée pour discuter des énergies de régénération; elle représente (au signe près) l'énergie nécessaire pour l'inversion de la réaction d'absorption. Ce plateau existe tant que le mécanisme d'absorption ne change pas.

- pour des taux de charge supérieurs à 0.9 (solution saturée, C), il y a coexistence de deux phases en équilibre: une phase liquide saturée en CO_2, et une phase gaz constituée de CO_2, d'eau et d'amine. Dans ce domaines on observe une diminution de l'enthalpie calculée par mole de CO_2 et ~~à~~ un plateau, quand l'enthalpie est calculée par mole d'amine. La limite de solubilité du CO_2 est déterminée graphiquement à

partir de la représentation de l'enthalpie par mole d'amine. Elle correspond au premier point sur le plateau.

- pour les taux de charge compris entre 0.5 et 0.9, (domaine B), l'enthalpie par mole d'amine augmente avec une pente différente de celle observée aux faibles taux de charge et diminue sur la courbe tracée par mole de CO_2. Ce changement de pente correspond à un changement dans le mécanisme d'absorption chimique du gaz.

Un modèle thermodynamique rigoureux a été développé pour représenter l'absorption du CO_2 dans les solutions aqueuses de 3-MPD et 4-MPD. Ce modèle d'équilibre de phases permet d'analyser les mécanismes de dissolution à partir de la prédiction des spéciations en solution et des enthalpies de solution en fonction du taux de charge. Le modèle repose sur la résolution d'un système d'équations représentant les équilibres chimiques et physiques en solution. Ce modèle est basé sur une approche γ–ϕ pour décrire les équilibres liquide-vapeur. Les coefficients de fugacité ϕ sont estimés par une équation du viriel tronquée. Les coefficients d'activité γ de la phase liquide sont calculés à partir d'un modèle de Pitzer (Pitzer, 1973; Edwards et al., 1978). Il est décrit en détail dans l'article de (Arcis et al., 2008).

L'utilisation de ce modèle nécessite la connaissance des constantes d'équilibre des réactions mises en jeu au cours de l'absorption du gaz: dissociation de l'eau, protonation de l'amine, formation d'hydrogénocarbonates, de carbonates et de carbamates. Le modèle requiert également la connaissance des constantes de Henry et pressions de vapeur saturante pour la représentation des équilibres physiques du CO_2, de l'eau et de l'amine.

Dans l'approche γ–ϕ, en convention asymétrique, l'équilibre entre les deux phases liquide et gaz est défini par la loi de Henry pour le CO_2 et les amines, alors que l'équilibre vapeur-liquide est défini par la loi de Raoult pour l'eau. Pour décrire la phase liquide, le modèle repose sur la connaissance des

constantes d'équilibre des réactions en fonction de la température. Connaissant les constantes de protonation des amines, les constantes de formation des carbonates et des hydrogénocarbonates, et en ajustant le modèle sur les données d'équilibre liquide-vapeur et des enthalpies de solution, il a été possible de déterminer une valeur pour la constante de formation des carbamates dans les solutions de 3-MPD et de 4-MPD. La résolution du système d'équations conduit à la détermination de la spéciation en fonction des conditions de composition initiale en amine, pression, température et taux de charge en CO_2.

Les valeurs obtenues grâce au modèle décrit précédemment, en particulier les constantes de formation des carbamates, et la spéciation en solution seront confrontées ultérieurement aux données obtenues dans le cadre de ce projet par le laboratoire canadien partenaire de ce projet. La détermination de spéciation en solution doit être réalisée à l'aide de méthodes spectroscopiques RMN ou RAMAN.

0.6 Conclusion

En conclusion, deux nouvelles méthodes dynamiques et une méthode de mélange statique ont été développés pour déterminer les équilibres liquide-liquide des solutions aqueuses de méthyl et éthyl pipéridines en présence de dioxyde de carbone, de 273 K à 393 K. Les données collectées ont prouvé la grande précision et reproductibilité des techniques développées.

Les alkyls pipéridines ont pu être divisées en différentes catégories basées sur leur structure et les équilibres chimiques en solution.

- Les pipéridines tertiaires telles que la N-MPD et la N-EPD ne produisent pas de carbamates avec le CO_2. La présence de CO_2 permet la formation de carbonates et de bicarbonates dans la solution aqueuse. Ces sels déstabilisent la solution par un effet « salting-out » et les LLE sont abaissées.

- Les amines secondaires, telles que la 3-MPD et la 4-MPD, peuvent former des carbamates en solution, ce qui stabilise les solutions, et augmente les LLE. Ces amines ne démixent plus lorsqu'on ajoute du CO_2 en solution sur le domaine de température étudié.
- Les amines secondaires légèrement encombrées, comme la 2-MPD, forment peu de carbamates ou forment des carbamates instables, ce qui conduit à une augmentation plus modérée de la LLE avec l'addition de CO_2.
- Enfin, les amines secondaires très encombrées comme la 2,6-DPD ne permettent pas la formation de carbamate, et le diagramme LLE de cette amine est similaire à celui de la N-MPD.

L'étude des propriétés thermodynamiques d'excès des solutions aqueuses de méthylpipéridines a également mis en évidence des relations entre la structure de la molécule et leur évolution. En effet, les grandeurs d'excès présentent les caractéristiques suivantes :

- Les pipéridines tertiaires ont un extrémum centré sur des valeurs de fraction molaire autour de x_a=0.4 alors que les amines secondaires ont un extrémum centré sur une fraction molaire entre 0.45 et 0.5.

- la valeur de l'extremum des propriétés d'excès dépend de la position du groupement méthyl sur le cycle de la pipéridine : lorsque le CH_3 est situé en position 1 ou 2 sur le cycle la valeur absolue des propriétés énergétiques est plus importante que lorsqu'il est en position 3 ou 4. La propriété volumique a un comportement inverse.

Enfin, la détermination des enthalpies de solution aux faibles taux de charge et la solubilité du CO_2 dans les solutions aqueuses d'amine a donné des informations importantes sur les mécanismes de dissolution du CO_2 dans les solutions aqueuses de 3- et 4-méthylpipéridine. L'utilisation de ces données

pour ajuster un modèle thermodynamique robuste a permis l'estimation des constantes de formation des carbamates. Celles-ci ont été ajustées à partir d'un modèle thermodynamique γ–ϕ en corrélant des données de solubilité et des données d'enthalpie de solution. Ces constantes de carbamate complètent l'étude des équilibres chimiques en solution.

Les résultats obtenus, combinés aux données de spéciation déterminées par le laboratoire de l'Université de Guelph vont permettre de fournir un panorama complet des processus de dissolution du CO_2 dans les solutions aqueuses d'amines démixantes.

A partir de ces résultats, les premières relations structure-propriétés ont pu être établies. L'étape suivante résidera dans l'amélioration des propriétés physicochimiques de ces nouveaux solvants en ajustant leur formulation, et en ajoutant éventuellement un solvant physique qui pourrait optimiser les diagrammes de phase, en réduisant les capacités calorifiques ou les enthalpies de régénération des solutions chargées.

1 Introduction

1.1 Environmental Context

1.1.1 Increasing Temperature of the Earth

A change in climate is normally a natural phenomenon which occurs regularly on our planet with the change in atmospheric gasses (Lüthi et al., 2008). The natural history of life on this planet life has regularly evolved and moved to find suitable habitat which is more agreeable for a specific organism. The time scale for climate change usually happens over hundreds of thousands of years. Natural selection has been able to play a major role over this time scale, allowing for species to develop an adaptation to the change of the natural environment. The current situation is with climate change is occurring on a rapid time scale of about 100 years, starting at the beginning of the industrial revolution. Over time anthropogenic emissions of pollutants into the environment started become more massive. One of the many pollutants emitted is carbon dioxide which is known to be responsible for approximately 60% of the global warming. The amount of carbon dioxide has risen rapidly from 260 ppm in the 1880's (Wigley, 1983) to the currently above 400 ppm measured at the Mauna Loa Observatory in Hawaii. The International Panel on Climate Change predicts that by 2100 the atmosphere may contain up to 570 ppm of CO_2. This would increase the climate temperature by 2°C and mean seal level by 38 cm (Stewart and Hessami, 2005). The reason for the continued increase carbon dioxide is increase in energy demand by increasing world population and production from fossil fuels (Pachauri et al., 2014). The simplest solution to stop the rise of CO_2 in the atmosphere is to switch to renewable energy technologies. These technologies are not mature enough to meet modern and future energy demands. Until they are ready, transition technology, carbon capture and sequestration can be used to help mitigate the increasing CO_2 levels (Ellina Levina et al., 2013).

1.1.2 Technological Solutions

While renewable energies are the ideal way to reduce carbon dioxide emissions the current technological standards are not capable of meeting the modern energy demands with respect to the human population. At present carbon capture and storage technologies, CCS, are used in conjunction with fossil fuel consuming power plants to meet current energy demands. The report from the Intergovernmental Panel on Climate Change suggests that CCS can reduce 14 % of the CO_2 emissions (Ellina Levina et al., 2013).

There are however, many different technologies present for capturing carbon dioxide in post combustion systems. The most conceptually simple system uses aqueous sodium hydroxide solutions to capture carbon dioxide, otherwise known as the soda lime processes (Goeppert et al., 2012). This technology however uses high temperatures, up to 900 °C, to regenerate the sodium hydroxide. Calcium looping is another high temperature strategy which relies on the equilibrium of calcium oxide solids and carbon dioxide gas to equilibrate to form calcium carbonate (Fan et al., 2012). While forming the calcium carbonate is relatively easy the process to reform calcium oxide is much slower. The temperature necessary are also quite high. In both systems some heat can be recovered for power generation. Lower temperature but undeveloped options include ionic liquids, which can be tuned for physical or chemical absorption of carbon dioxide (Hanming et al., 2012). However, these systems currently suffer from production costs. Zeolites are one technology which could be used to trap carbon dioxide within their pores (Chue et al., 1995). The downsides are diffusion of gases through the zeolites and water reducing their absorption ability. Metal organic frameworks have shown promise in high pressure systems with high thermal resistance (Millward and Yaghi, 2005). They can also be tuned much like ionic liquids depending on the metal involved. However, impurities such as water can interfere with absorption. The last technology and the most well know and currently in use is amine

scrubbing technologies. These technologies have reviewed the most attention from the scientific community and has been part of many review articles.(Olajire, 2010; Wang et al., 2011; Boot-Handford et al., 2013; Mumford et al., 2015)

The process uses homogenous solutions of aqueous alkanoamines to collect carbon dioxide from power plant effluents, otherwise known as amine scrubbing solutions. It is this technology where current and past research is seeking improvement to reduce carbon emissions from fixed sources. On the continents of North America, Europe, Australia and Asia the amine scrubbing processes are already in place to remove carbon dioxide from coal fire power plants (Mumford et al., 2015). The amine of choice is currently monoethanolamine, MEA. This is not the only solvent currently in use for carbon capture. Other solvent systems include methyldiethanolamine, blended amine solvent systems, piperazine and ammonia.

Currently the industrial technologies feasible in the near future are based on a CO_2 separation from post-combustion effluent by gas dissolution in chemical absorbent solutions. The technology is mature enough to be integrated into industrial sites without strong modification of the plant. The process is schematically represented in Figure 1-1.

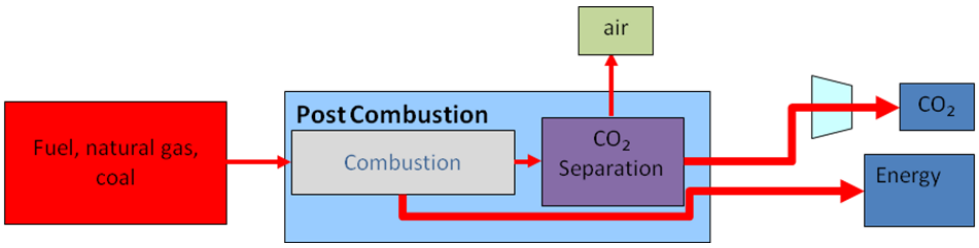

Figure 1-1: Schematic representation of post-combustion process.

The principle is based on CO_2 absorption-desorption cycles. Carbon dioxide contained in gaseous effluents is absorbed by liquid solvents in which the gas is selectively soluble. Currently the

most selective absorbents are the aqueous solutions of alkanolamine (Maddox et al., 1987) used already beneficially in the decarbonation of natural gases. The mechanism of absorption is mainly due to acid-base and carbamate formation reactions, making it a "chemical absorbent" process. The solvent solution charged with carbon dioxide is regenerated by desorption in a regenerator column and the regenerated solvent is returned to the absorber, while carbon dioxide is compressed and transported to be stored or reused as seen in Figure 1-2.

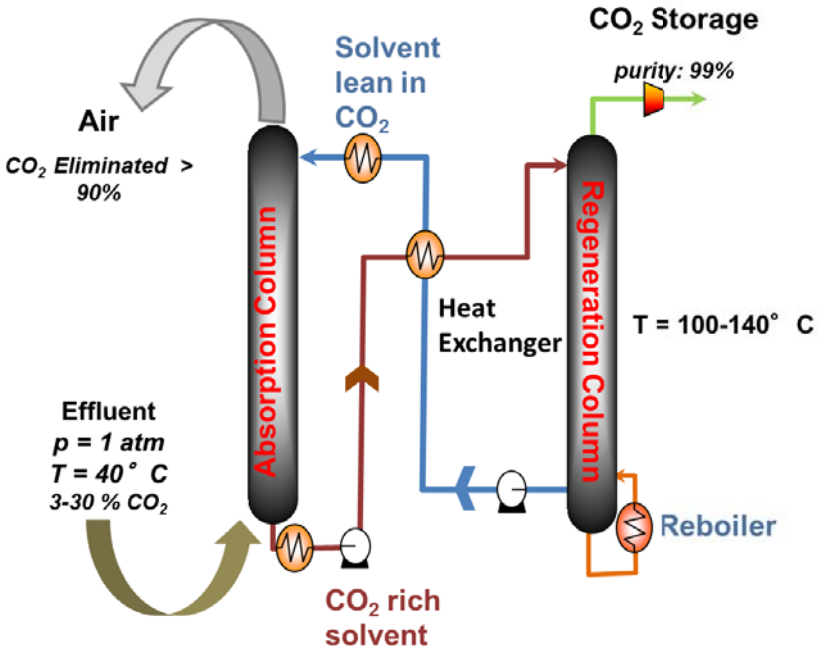

Figure 1-2 : Simplified representation of post-combustion carbon dioxide capture unit.

The central problem of this technology concerns the cost of carbon dioxide treatment. In the cycling process, desorption of carbon dioxide from alkanolamine solution is highly energy consuming. The separation takes place in a regeneration column where the solution is typically heated up to about 120°C, and this operation represents the most expensive step of the whole process. It is thus necessary to imagine new breakthrough processes allowing substantial energetic cost reduction. One option is the use of demixing solvents (J. Zhang et al., 2011; Gomez et al., 2014).

1.2 DACOOTA Project

The aim of this research project is to contribute to a better physico-chemical understanding and a quantitative description of the mechanisms of carbon dioxide dissolution in aqueous solutions of a new class of amine absorbents known as demixing amines. These new solvents for CCS present a liquid-liquid phase separation that facilitates the release of the captured carbon dioxide and then the regeneration of the solvent through an industrial process.

These are aqueous solutions containing amines which present a liquid-liquid phase separation with a temperature increase depending on the composition of the solution (Figure 1-3). The DMX^{TM} process, which is based on this demixing solvent concept, has been recently proposed and patented by IFP Energies nouvelles (IFPEn), European Patent EP2168659 (Bouillon et al., 2012).

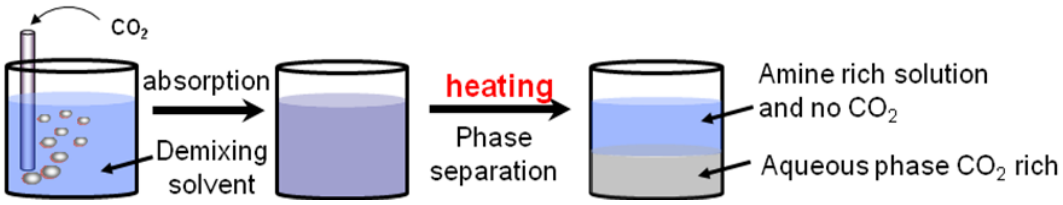

Figure 1-3: Liquid-liquid phase separation for ternary solution {water + amine + carbon dioxide}.

In the first step of the process, carbon dioxide is chemically absorbed by an aqueous solution of amine. In the next step, the temperature of the solution is increased until to have a phase splitting into two phases of the ternary solution of carbon dioxide, amine and water. The heavier (lower) phase is composed mainly of water, carbonated salts and amine salts, while the upper phase contains principally the unreacted amine. In the separation process, the only phase that should be sent to the stripper is the charged water solution, while the amine phase is directly returned to the absorber.

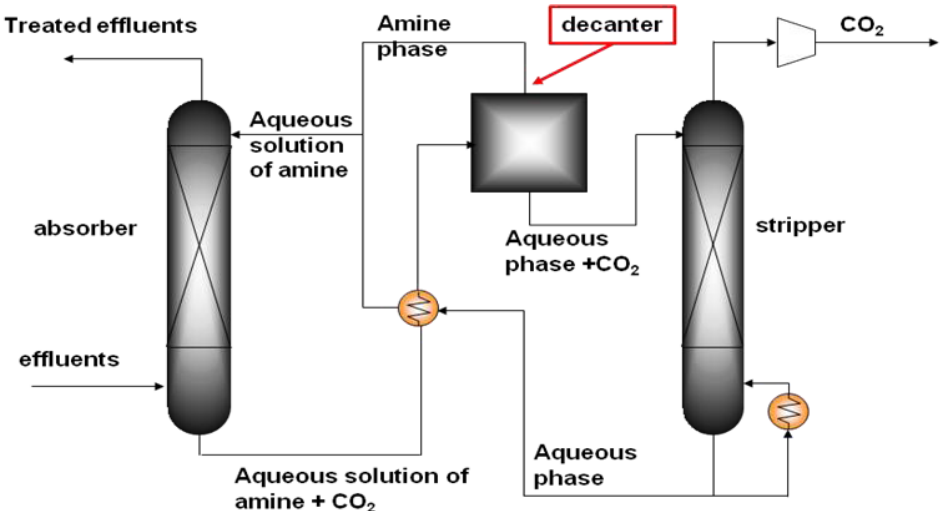

Figure 1-4: Simplified schematic representation of the industrial process using a demixing amine. (Gomez et al., 2014)

The interest of working with such a regime is that only a fraction of the absorbent solution is sent to the stripper. The cost of the regeneration is therefore reduced due to a smaller quantity of solvent to be treated.

1.2.1 The Data to Collect

The proposed study will contribute to the understanding of thermodynamic equilibria in aqueous alkyl piperidine solutions and alkyl piperidine solution charged with carbon dioxide to elucidate the structure-property relationships for the studied alkyl piperidines. The purpose of this study is to elaborate systematic rules from the study of model molecules that can be useful for designing specific molecules suitable for the carbon capture process. From the representation of the process shown in Figure 1-4, a physico-chemical and engineering scheme can be represented as follows:

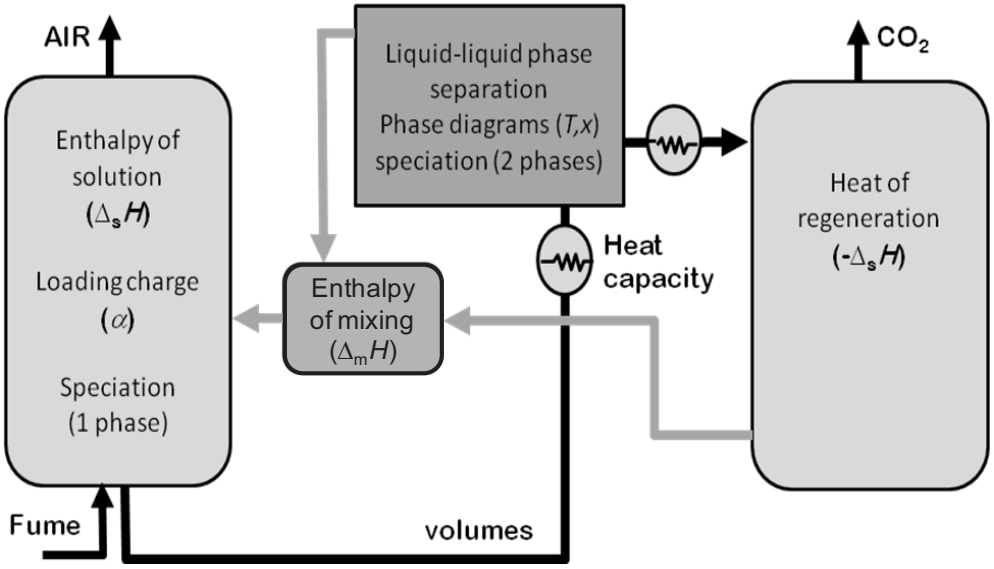

Figure 1-5: Thermodynamic and physico-chemical representation of the process.

The left side depicts the CO_2 dissolution process, where the enthalpy of solution and the solubility of CO_2 at the temperature of the absorption column (around 40°C) are the main characteristics. The right side corresponds to the regeneration column; the enthalpy of regeneration in this section corresponds to the opposite of the enthalpy of solution at the temperature of the stripper (up to 120°C). In this section only the CO_2 rich phase is considered. The upper central section concerns the liquid-liquid separation step of the process corresponding to the decanter in Figure 1-4, the transition between the one and two phase systems and characterization of the latter one. Finally, the lower central square corresponds to the mixing of the regenerated water-rich phase and amine-rich phase coming directly from the decanter. The volumetric and heat capacity data are important from the engineering point of view to calculate the size of the columns and the energy that should be supplied to the decanter to phase separate, and they are also used in thermodynamic models. However, in order to get a more profound understanding of such systems, and to be able to elaborate the structure-property rules, this simplified

engineering scheme is not detailed enough since the mechanism of CO_2 capture by absorption in aqueous solutions of amine is a combination of physical dissolution and different chemical reactions.

1.2.2 Recent Bibliography on Phase-Change Solvent

Several studies on phase-change solvents such as the DMX™ process development (Raynal et al., 2011; Raynal et al., 2011), thermomorphic biphasic solvent (TBS) systems (Zhang et al., 2011) and mixed phase-changed solvents (Liebenthal et al., 2013) have been reported in the literature. TBS have been widely studied by Zhang et al. and Tan (Tan, Y. H., 2010; Zhang et al., 2011; J. Zhang et al., 2011; Zhang et al., 2012a; Zhang et al., 2012b; Zhang et al., 2013).The solvent is an aqueous mixture of lipophilic amines exhibiting a liquid-liquid phase transition upon heating leading to a high carbon dioxide desorption at temperatures well below the boiling point of aqueous solutions. This technology uses heterogeneous absorbent solutions which becomes homogeneous upon carbon dioxide absorption and returns to two phases through heating. The organic phase acts as an extractive agent, removing the amines from the aqueous phase and thus favourably displacing the regeneration equilibrium. Zhang et al. (Zhang et al., 2012b) have intensively worked on replacing steam stripping used for carbon dioxide release with nucleation or agitation techniques. They point out that there is an advantage of adding a hydrophobic organic solvent to reduce the operating temperature for carbon dioxide desorption (Zhang et al., 2011). Mixed phase-changed solvents have been investigated by Svendsen and coworkers (Arshad et al., 2013; Ciftja et al., 2013; Monteiro et al., 2013; Pinto et al., 2014; Pinto et al., 2014; Arshad et al., 2014; Monteiro et al., 2015) as a part of the European Union project iCap (2010-2013). This biphasic solvent is based on an aqueous mixture of amines which can form two phases upon CO_2 absorption. The process is very similar to the one developed by Raynal et al. (Raynal et al., 2011). The heats of absorption of CO_2 (Arshad et al., 2013), speciation at equilibrium (Ciftja et al., 2013) and vapour-liquid

equilibrium data (Xu et al., 2014; Arshad et al., 2014; Monteiro et al., 2015), for aqueous blends of amine have been reported by Svendsen and coworkers. Screening investigations (Xu et al., 2012; Ye et al., 2015) to evaluate the CO_2 absorption and desorption facilities of phase-change solvents have been completed.

Previous researches on demixing amines were the subject of a task included in the project ACACIA (Gomez et al., 2014), co-financed by the Unique Interministerial Fund (FUI) and certified by Axelera (French Chemistry and Environment competitive cluster). This project, coordinated by IFPEn and RHODIA, aims to reduce the costs of CO_2 capture processes. In this project ICCF-TIM obtained first data on aqueous solutions of demixing amines. Different molecules were synthesized by our partners in the project and tested. It was found that the relation between amine structure and demixing properties must be carefully analysed in order to avoid future costly screening investigations. The development of efficient tools for the design of specific amines will require numerous and systematic studies because of the complexity of the problems. In this work the structure-properties relationships of the alkyl piperidine family were investigated in order to design suitable demixing amines for CO_2 absorption.

1.3 The Alkyl Piperidine Family

Piperidine is a saturated heterocyclic ring structure with one nitrogen group. Piperidine and alkyl derivative are basic compounds with pK_a values ranging from 10 (N-methylpiperidine) to 11.1 (piperidine) depending on the position, number and size of the alkyl group. Piperidine is completely soluble in all water-piperidine compositions within the experimental parameters investigate. The addition of a simple methyl group to any position of the ring structure will cause the aqueous solution of alkyl piperidine to display a liquid-liquid phase equilibrium with increasing temperature (Stephenson,

1993; Góral et al., 2012a; Góral et al., 2012b). Increasing the alkyl chain length or number of alkyl groups are already known to have different effects on the temperature and composition of the critical solution temperature, T_{sc}, and the critical solution composition, x_{sc}, of the solution. The phase equilibria are directly related with the structure of the molecule; however the mechanism of this relationship is currently unknown. Figure 1-6, illustrates the different structures of alkyl piperidine structures under investigation.

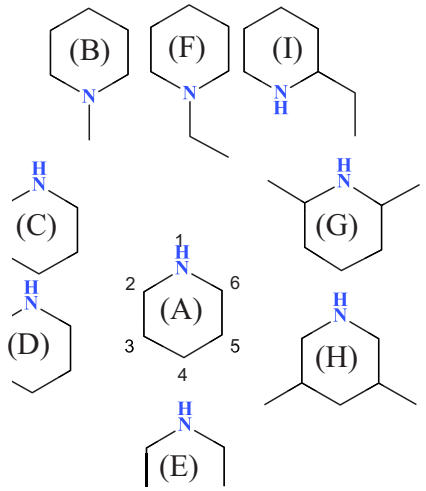

Figure 1-6: Structures of the alkyl piperidines investigated (A) Pipereridine, (B) N-Methylpiperidine, N-MPD (C) 2-Methylpiperidine, 2-MPD (D) 3-Methylpiperidine, 3-MPD (E) 4-Methylpiperidine(F) N-Ethylpiperidine, N-EPD (G) 2,6-Dimethylpiperidine, 2,6-DPD(H) 3,5-Dimethylpiperidine, 3,5-DPD (I) 2-Ethylpiperidine, 2-EPD.

1.3.1 Molecular Structure

The molecular structure of some of the alkyl piperidines have been investigated in the literature. The methods of the investigation used a variety of different spectroscopic and computational techniques (Eliel et al., 1980; Gulluoglu et al., 2007). Moving the methyl group will allow us to study the influence of inductive effects and steric hindrance on protonation and carbamate formation equilibrium. It is

accepted that the methyl groups for the alkyl piperidines are placed in the equatorial position rather than axial position.

Outside of liquid state studies, crystallographic experiments have been done with piperidine and 4-methylpiperidine (Freytag and Jones, 1999; Jiang et al., 2007; Jiang et al., 2008). The studies had shown a preference for carbamates to exist in the equatorial position of the ring structure. For 4-methylpiperidine, the structure of both methyl and carbamates were found in the equatorial position.

1.3.2 Thermodynamic Properties

Studies on thermodynamic properties of these alkyl piperidines are sparse in the literature. Piperidine has the largest and most comprehensive volume of information to date with thermodynamic values on the pK_a (Bates and Bower, 1956), pure and solution densities (Afzal et al., 2008; Marczak et al., 2015), pure heat capacities (Conti, G et al., 1976; Messerly et al., 1988), mixing enthalpies at 298.15 K (Kul and Lieu, 2010). However, the gap in the literature appears to be closing. The temperature dependant pK_a values for N-methylpiperidine, 2-methylpiperidine, 3-methylpiperidine, 4-methylpiperidine and 2,6-dimethylpiperidine were examined by (Ballerat-Busserolles et al., 2014) and (Blais et al., 1974). Carbamate formation constants currently do not exist in the current literature data base. The densities have been measured for the N-methylpiperidine and 2-methylpiperidine in the work of (Coulier et al., 2010; Marczak et al., 2013). The excess heat capacities of the N-methylpiperidine and 2-methylpiperidine have recently been added to the literature together with their excess enthalpies (Coulier et al., 2015) and the heat capacities of the pure values of 2-methylpiperidine in past literature (Messerly et al., 1988).

1.4 Thesis Goals

It is the goal of this thesis is to measure the thermodynamic and liquid-liquid phase equilibrium of the alkyl piperidine family. It is with this thermodynamic data it should be possible to answer an import question. How does the structure of the molecules affect the thermodynamic properties and phase equilibria? Are there and trends in the behaviour of the thermodynamic properties or liquid-liquid phase equilibria which can be useful to design new molecules? It is these questions this thesis will explore. The tools which are used are experimental. Liquid-liquid equilibrium temperatures of aqueous alkyl piperidine with and without carbon dioxide have been measured. Using standard thermodynamic techniques the densities, specific heat capacities and excess enthalpies are measured for the aqueous solutions of alky-piperidine, and solution enthalpy of carbon dioxide in aqueous alkyl piperidines. Carbamate constants have been estimated using a thermodynamic model combined with the experimental solution enthalpy.

2 Review of Thermodynamic Theory

2.1 Chemical Equilibrium

Chemical equilibrium is the state in which both reactants and products are present within concentrations which have no further tendency to change with time (Atkins and de Paula, 2010). Equation 2-1 is a generalized equilibrium reaction:

$$\nu_A \mathrm{A} + \nu_B \mathrm{B} \rightleftharpoons \nu_C C + \nu_D \mathrm{D} \qquad \textbf{Eq 2-1}$$

where A and B are the reactants, and C and D are the final products of the reaction. The Greek characters ν with the superscripts *a, b, c* and *d* are defined as the stoichiometric coefficients of reactions. The

product of the activities of the reactants and products raised to the power of their stoichiometry defines the equilibrium constant, *K*.

$$K = \prod_i a_i^{\upsilon_i} = \prod_i (m_i \gamma_i)^{\upsilon_i} \qquad \textbf{Eq 2-2}$$

To define the equilibrium constants the stoichiometry is negative for the reactants while products of the reaction are positive. The molality based activity coefficient convention being adopted, then the activities a_i, are defined as the products of the molality (mol kg^{-1}) of the solutes m_i and the activity coefficient of ionic solutes in solution γ_i divided by a fugacity reference.

The first model for calculating the activity coefficients of a solute in dilute solution is the Debye-Hückel equation:

$$\ln\gamma = \frac{A|z_+ z_-|\sqrt{I}}{1 + B\,\mathring{a}\sqrt{I}}\ , \qquad \textbf{Eq 2-3}$$

Here terms of *A* and *B* are the Debye-Hückel constants that are dependent on the solvent and temperature, *z* is the charge of the ion, and $\mathring{a}$ is a theoretical term which is the distance of closest approach between anions and cations. The *A* term is osmotic coefficient parameter while the *B* term is fixed between the values of 0.5 to 2.0. The ionic strength of the solution is needed to calculate activity coefficients for weak electrolyte solutions. The ionic strength is calculated using equation 2-4

$$I = \frac{1}{2}\sum_i m_i z_i^2 \qquad \textbf{Eq 2-4}$$

This model works to estimate activity coefficients for dilute solutions with ionic strengths below 0.1 mol kg^{-1}.

2.1.1 Vapour-Liquid Equilibrium

Vapour-liquid equilibrium is a two-state relationships between which volatile molecules move from either the gas phase to the liquid phase or vice versa. The conditions of the phase equilibrium are dependent on both temperature and pressure and composition of the system. Calculations of the equilibrium compositions are typically done using the isofugacity condition.

$$f_i^v(T,p,y) = f_i^l(T,p,x) \qquad \textbf{Eq 2-5}$$

Where f_i^v and f_i^l are the fugacity of the components in the vapour and the liquid phase. The y and x components represent the mole fractions of all the species in the gas phase and in the liquid phase. The fugacity is typically related to state variables which can be experimentally measured. Which case the fugacities of the vapour phase is related to the fugacity coefficient, ϕ_i. For the liquid phase the fugacity is calculated with activity coefficients, γ_i.

The vapour phase fugacity of each species is related to the composition of the species at the system pressure and temperature.

$$f_i^v(T,p,y) = \phi_i(T,p,y)\, y_i\, p \qquad \textbf{Eq 2-6}$$

At constant temperature and vapour phase composition the fugacity coefficient of an individual component species in a mixture can be calculated using the following relation.

$$\mathrm{R}T \ln \phi_i = \int_0^P \left(\overline{V}_i - V_i \right) dp \qquad \textbf{Eq 2-7}$$

The value of $\overline{V}_i$ is the partial molar volumes of the species in the gas mixture and V_i is the molar volume of the pure gas in the ideal gas state. The partial molar volumes are typically calculated using equations of state which has the ability of representing the pressure dependence of the species. In the past truncated virial coefficients have successfully been used to represent partial molar volumes.

The liquid phase fugacity is related to the activity coefficient for an individual species, γ_i, which are composition, pressure and temperature dependent,

$$f_i^l \left(T, p, x_i \right) = \gamma_i \left(T, p, x \right) x_i f^{ref} \qquad \textbf{Eq 2-8}$$

where f^{ref} is an arbitrary reference fugacity to describe the equilibrium to a pure state or infinite dilution state and x_i is the molar fraction. The pure state or solvent is usually described by Raoult's law which best describes the behaviour of a solvent with the addition of solute particles at saturation.

In this case equation 2-8 becomes

$$f_i^l \left(T, p, x_i \right) = \gamma_i \left(T, p, x \right) x_i \phi_i^{sat} \left(T \right) p_i^{sat} \left(T \right). \qquad \textbf{Eq 2-9}$$

Where υ_i^{sat} and p_i^{sat} are the fugacity of the pure saturated vapour and the saturation vapour pressure of the solvent, *solv*, at equilibrium. In order to account for the pressure dependence of the activity coefficients, the Poynting term must be applied.

$$f_i^l\left(T,p,x_i\right)=\gamma_i\left(T,p,x\right)x_i\varphi_i^{sat}\left(T\right)p_{solv}^{sat}\left(T\right)\exp\left[V^{*,sat}\left(p-p_{solv}^{sat}\right)/RT\right] \qquad \textbf{Eq 2-10}$$

The equation uses the pure molar volume $V^{*,sat}$ of the solvent at saturation. Since it is representation of the liquid phase these values can be assumed to be independent of pressure.

For the description of the solute species Henry's Law constant, k_H, is used to describe the physical dissolution of a species in the solvent and the saturation pressure of the solvent p_{solv}^{sat}.

$$f_i^l\left(T,p,x\right)=\gamma_i\left(T,p,x\right)x_i k_{H,i}\left(T,p_{solv}^{sat}\right)\exp\left[\overline{V}_i^{\infty}\left(p-p_{solv}^{sat}\right)/RT\right] \qquad \textbf{Eq 2-11}$$

The rest of equation 2-11 is similar to equation 2-10 however uses the infinite dilution value, $\overline{V}_i^{\infty}$, of the solution species to account for the pressure effects.

2.1.2 Liquid-Liquid Equilibrium

The liquid-liquid phase equilibrium like, vapour-liquid equilibrium is a physical process where molecules prefer to be in a specific state or environment with the respect to pressure, temperature and composition. At the critical solution temperature a homogenous solution will become two phases or vice versa. In figure 2-1, is an example diagram of closed loop liquid-liquid phase equilibrium.

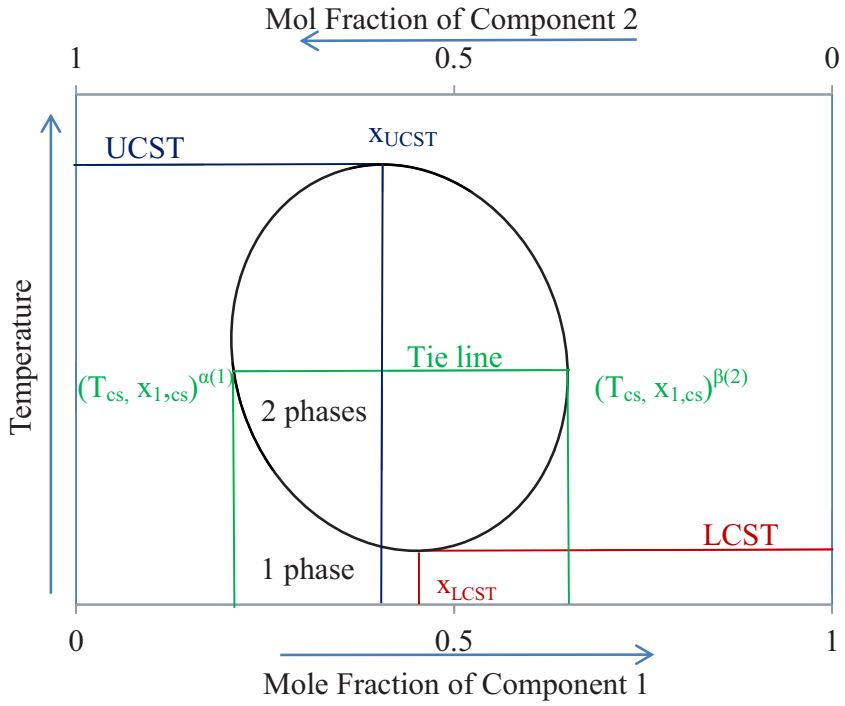

Figure 2-1: Example diagram of liquid-liquid phase equilibrium.

The interior of the loop is a 2 phase system, heterogenous, with the exterior representing a single homogenous phase. If a solution is changing from a 2 phase system to 1 phase system the maximum of the curve is called the upper critical solution temperature, UCST. At the lowest temperature where there is a phase change the minimum of the curve is called the lower critical solution temperature, LCST. At temperatures below the UCST or above LCST are critical temperatures and critical compositions where the homogenous phase becomes heterogeneous and vice versa. A tie line relates the two phases together, α phase 1 and β phase 2, at isothermal condition. The least dense phase resting on top of the bottom dense phase. The chemical potential of the two phases are equal to each other.

$$\mu^{\alpha}\left(T,p,x^{\alpha}\right)=\mu^{\beta}\left(T,p,x^{\beta}\right) \qquad \textbf{Eq 2-12}$$

To calculate the composition of both phases the concept of isoactivity is used to describe the behaviour of both states.

$$f_i^{\alpha}\left(T,p,x^{\alpha}\right)=f_i^{\beta}\left(T,p,x^{\beta}\right) \qquad \textbf{Eq 2-13}$$

The equal activities are expanded in their component concepts of chemical composition, x_i, and activity coefficients, γ_i.

$$x_i^{\alpha}\gamma_i^{\alpha}\left(T,p,x^{\alpha}\right)=x_i^{\beta}\gamma_i^{\beta}\left(T,p,x^{\beta}\right) \qquad \textbf{Eq 2-14}$$

The fugacities are related to the excess Gibbs energies, as will be defined later in section 2.2.1, which are calculated using an activity coefficient model. These models are regressed to the available liquid-liquid equilibrium data.

2.2 Maxwell's Relations of Thermodynamic Properties

The equilibrium constant is related to the standard partial Gibbs free energy of the system, as seen in equation 2-15,

$$\Delta G^{o} = -\mathrm{R}T\ln K \qquad \textbf{Eq 2-15}$$

The partial derivatives of the standard Gibbs free energy of reaction with respect to pressure yield the standard partial molar volume of reaction, $\Delta V°$. The partial derivatives of the standard Gibbs free energy

with respect to temperature yields the standard partial molar enthalpy of reaction, $\Delta H°$, and entropy of reaction, $\Delta S°$. Equation 2-16 is the partial derivative with respect to pressure at constant temperature.

$$\Delta V° = \left(\frac{\partial \Delta G°}{\partial p} \right)_T \qquad \textbf{Eq 2-16}$$

Expression for the $\Delta H°$ and $\Delta S°$ are derived from the temperature-dependent partial derivatives of the Gibbs free energy.

$$\Delta H° = -T^2 \left[\frac{\partial \left(\frac{\Delta G°}{T} \right)}{\partial T} \right]_p \qquad \textbf{Eq 2-17}$$

$$\Delta S° = -\left(\frac{\partial \Delta G°}{\partial T} \right)_p \qquad \textbf{Eq 2-18}$$

The partial derivative of the enthalpy of reaction yield the standard partial molar heat capacity of reaction, $\Delta C_p°$,

$$\Delta C_p° = \left(\frac{\partial \Delta H°}{\partial T} \right)_p \qquad \textbf{Eq 2-19}$$

2.2.1 Partial Molar Properties and Excess Molar Properties

The derivative of the Gibbs energy, *G,* with respect to the molar composition of a sample is equal to partial molar Gibbs energy, $\overline{G}_i$, the chemical potential of an individual species in solution,

$$\mu_i = \overline{G}_i = \left(\frac{\partial G}{\partial n_i} \right)_{T,p,n_{j \neq i}} \qquad \textbf{Eq 2-20}$$

The chemical potential is related to the standard state properties via the following equations.

$$\mu_i - \mu_i^{\circ} = \mathrm{R}T \ln\left(f_i \,/\, f_i^{\circ} \right) \qquad \textbf{Eq 2-21}$$

Where the $\mu_i°$ is the chemical potential of the standard state, f_i, is fugacity of species and f_i° is the standard state fugacity. The fugacity ratios can be written as an activity which can be further defined by an activity coefficient and composition variable.

A general relationship to the partial molar property of a solute can be expressed as $\overline{Y_2}$ which is an extensive property, *Y,* of a binary solution:

$$\overline{Y_2} = \left(\frac{\partial Y}{\partial n_2} \right)_{p,T,n_1} \qquad \textbf{Eq 2-22}$$

By extension of this idea, the sum of all individual partial molar properties with the know amount will equal the molar property of the solution.

$$Y = n_1 \overline{Y_1} + n_2 \overline{Y_2} \qquad \textbf{Eq 2-23}$$

With respect to the molar fraction of the components will give rise to the molar property of solution Y_m

$$Y_m = x_1\overline{Y}_1 + (1-x_1)\overline{Y}_2 \qquad \textbf{Eq 2-24}$$

The equations can also be written in fashion where the molar properties are written as derivatives of the composition.

$$\partial Y_m = \overline{Y}_1 \partial x_1 + \overline{Y}_2 \partial(1 - x_1) \qquad \textbf{Eq 2-25}$$

The partial molar properties can then be expressed as

$$\overline{Y}_1 = Y_m + (1-x_1)\left(\frac{\partial Y_m}{\partial x_1}\right) \qquad \textbf{Eq 2-26}$$

$$\overline{Y}_2 = Y_m - x_1\left(\frac{\partial Y_m}{\partial x_1}\right) \qquad \textbf{Eq 2-27}$$

At infinite dilution the partial molar property, $\overline{Y}_1^{\infty}$ is represented by in equation 2-28,

$$\overline{Y}_1^{\infty} = \lim_{x_1 \to 0}\left[Y_m + (1-x_1)\left(\frac{\partial Y_m}{\partial x_1}\right)\right] \qquad \textbf{Eq 2-28}$$

The change in the Gibbs energy can also be used to express the mixing of two individual liquids to make a solution. This can be defined as the Gibbs energy of mixing, ΔG_{mix}, which is related to the chemical potential of the species in solution. The mixing functions, ΔY_{mix}, are described as.

$$\Delta Y_{mix} = Y_m - Y^{ideal}$$ **Eq 2-29**

The molar properties and *ideal* properties can be expanded into their partial molar properties and pure molar properties

$$\Delta Y_{mix} = \left(x_1 \overline{Y_1} + x_2 \overline{Y_2} \right) - \left(x_1 Y_1^* + x_2 Y_2^* \right)$$ **Eq 2-30**

followed by taking the first derivative with respect to x_1.

$$\left(\frac{\partial \Delta Y_{mix}}{\partial x_1} \right)_{T,p} = \left(\overline{Y}_1 - Y_1^* \right) + x_1 \left(\frac{\partial \overline{Y}_1}{\partial x_1} \right) - \left(\overline{Y}_2 - Y_2^* \right) + x_2 \left(\frac{\partial \overline{Y}_2}{\partial x_1} \right)$$ **Eq 2-31**

Applying the Gibbs Duhem equation,

$$x_1 \left(\frac{\partial \overline{Y_1}}{\partial x_1} \right)_{T,p} + x_2 \left(\frac{\partial \overline{Y}_2}{\partial x_1} \right)_{T,p} = 0$$ **Eq 2-32**

results in equation 2-33.

$$\left(\frac{\partial \Delta Y_{mix}}{\partial x_1} \right)_{T,p} = \left(\overline{Y_1} - Y_1^* \right) - \left(\overline{Y_2} - Y_2^* \right)$$ **Eq 2-33**

Followed by multiplying both sides of the equation by x_1 and adding the ΔY_{mix} then rearranging the equation gives the partial molar properties

$$\overline{Y_2} = \Delta Y_{mix} + Y_2^* - x_1 \left(\frac{\partial \Delta Y_{mix}}{\partial x_1} \right)_{T,p} \qquad \textbf{Eq 2-34}$$

$$\overline{Y_2} = \Delta Y_{mix} + Y_1^* + (1 - x_1) \left(\frac{\partial \Delta Y_{mix}}{\partial x_1} \right)_{T,p} \qquad \textbf{Eq 2-35}$$

The partial molar properties at infinite dilution are equal to

$$\overline{Y}_1^{\infty} = Y_1^* + \lim_{x_1 \longrightarrow 0} \left[\Delta Y_{mix} + (1 - x_1) \left(\frac{\partial \Delta Y_{mix}}{\partial x_1} \right)_{T,p} \right] \qquad \textbf{Eq 2-36}$$

Excess functions are thermodynamic properties of solution that in excess of those of an ideal solution at the same conditions of temperature, pressure and compositions. For an ideal solution all excess functions are zero. For example G^E, the excess Gibbs energy, is defined by,

$$G^E = G^{Real}_{(T,p,x)} - G^{Ideal}_{(T,p,x)} \qquad \textbf{Eq 2-37}$$

The value of G^{real} is Gibbs energy of the real solution, and G^{ideal} solution where an ideal solution for all excess functions is zero.

The partial molar excess function g_i^E is defined in a manner analogous to that used for partial molar thermodynamic properties (eq 2-20),

$$\frac{\bar{g}_i^{\mathrm{E}}}{\mathrm{R}T} = \left(\frac{\partial n_T g^{\mathrm{E}} / \mathrm{R}T}{\partial n_i} \right)_{T,p,n_{j \neq i}} \qquad \textbf{Eq 2-38}$$

This can be written to express the non-ideality in term of ideal and real fugacities. In this case fugacities are used as the place holder for these values as seen in equation 2-39.

$$g_i^{\mathrm{E}} = \mathrm{R}T \ln\left(f_i / f_{ideal} \right) \qquad \textbf{Eq 2-39}$$

Using equation 2-8 in equation 2-38 and activity coefficient of an ideal solution being equal to unity, the definition of the partial excess Gibb energy becomes,

$$g_i^{\mathrm{E}} = \mathrm{R}T \ln\left(\gamma_i x_i f_i^{\circ} / x_i f_i^{\circ} \right) = \mathrm{R}T \ln\left(\gamma_i \right) \qquad \textbf{Eq 2-40}$$

The excess functions above can be differentiated by the same relations described in equations 2-19 to 2-22 to give the excess properties V^E, H^E, S^E and $C_p{}^E$.

2.3 Thermodynamic Models for Phase Equilibrium.

The chemical and physical behaviour is calculated at equilibrium using the isofugacity criteria. In this work, the γ-φ approach is considered to model phase equilibria. The non-ideal component for the liquid phase is calculated using activity coefficient, γ and the non-ideal component for the vapour phase is calculated using fugacity coefficients, υ. Over time, many different models have been developed in an attempt to accurately estimate activity coefficients as a function of temperature, pressure and

composition with a variety of different systems. This section is designed to be a terse description of the models currently in use for CO_2 solubility and phase equilibrium.

2.3.1 The Kent and Eisenberg Model

The Kent-Eisenberg model (Kent, R. L. and Eisenberg, B., 1976) has been used extensively among primary amine, secondary amine as well as tertiary amine because of its simplicity and favourable predictions. It was first used to represent the CO_2 and H_2S partial pressures over aqueous solutions of monoethanolamine (MEA) and diethanol-amine (DEA) (Lee et al., 1976). It assumes that all activity and vapour-phase fugacity coefficients equal to one and regressed two of the chemical equilibrium constants representing the amine equilibria to experimental data. (Jou et al., 1982), modified this model to include tertiary alkanolamines. Based on this assumption that, the researched system is in an ideal state, the Kent-Eisenberg model is the only suitable at certain temperature and pressure range. For a different system, this model was applied with good prediction when conditions were not rigid. When the system is not taken as ideal state, activity coefficients which take non-idealities into account are needed. As the data became available the accuracy of the model for some systems has claimed to rival (Luo et al., 2016) more thermodynamically consistent models such as the e-NRTL model and UNIQUAC models. However, because it treats the system ideally the results are less accurate at higher temperatures and pressures.

2.3.2 Ion interaction model from Pitzer modified by Edwards

The ion interaction model from Pitzer is probably the most well-known model to chemists and chemical engineers. It was created in 1970's and has been applied to many different aqueous solutions (Pitzer, 1973; Pitzer and Kim, 1974). The equations have been successful for modelling activity

coefficients for geochemical systems (Bea et al., 2010) as well as the volatility of weak electrolytes in solution (Edwards et al., 1978). The activity coefficients are calculated using the extended Debye Hückel equation which describes the electrolytes in solution,

$$\ln\gamma = -Az^2\left[\frac{\sqrt{I}}{1+1.2\sqrt{I}} + \frac{2}{1.2}\ln\left(1+1.2\sqrt{I}\right)\right] + IP \qquad \textbf{Eq 2-41}$$

The ion interaction parameters, IP, are estimated using available thermodynamic data to generate the parameters for the equation below:

$$IP = 2\sum m_j\left\{\beta_{ij}^0 + \frac{\beta_{ij}^1}{2I}\left[1-\left(1+2\sqrt{I}\right)\exp\left(-2\sqrt{I}\right)\right]\right\} - \frac{z_i^2}{4I^2}\sum_{j\neq w}\sum_{k\neq w} m_j m_k \beta_{ij}^1\left\{\left(1+2\sqrt{I}+2I\right)\exp\left(-2\sqrt{I}\right)\right\} \qquad \textbf{Eq 2-42}$$

These parameters are additions made by (Edwards et al., 1978), where β^0 and β^1 are interaction parameters chose to be equal zero for ions of the same charge. The activity of water is conveniently calculated using the Gibbs-Duhem equation.

$$\ln a_{H_2O} = M_w\left\{\frac{2A_\varphi I^{3/2}}{1+b\sqrt{I}} - \sum_{i'w}\sum_{j'w} m_i m_j\left[\beta_{i,j}^0 + \beta_{i,j}^1 exp\left(-2\sqrt{I}\right)\right] - \sum_{i'w} m_i\right\} \qquad \textbf{Eq 2-43}$$

The Pitzer equation modified by Edwards has been used successfully in the past to model the solubility of vapour-liquid equilibrium of CO_2 solubility aqueous amine solutions (Rumpf and Maurer, 1993; Arcis et al., 2009; Arcis et al., 2011).

2.3.3 Deshmukh-Mather

This model was developed in the early 1980's with (Deshmukh and Mather, 1981) and developed from the idea that the Kent Eisenberg model required more thermodynamic rigour, but with less parameters than ion interaction model from Pitzer. The activity coefficients of the model are calculated using the Debye Hückel equation, equation 2-7, with the ion interaction parameter defined using the following equation

$$IP = \sum_{\substack{j=1 \\ j \neq w}} m_j \beta_{ij} \qquad \textbf{Eq 2-44}$$

This simple expression for the interaction parameter is required for all other species in solution (Carroll and Mather, 1996; Benamor and Aroua, 2005). The activity of water is assumed to behave ideally and unlike the Pitzer interaction model which uses the Gibbs-Duhem equation to calculate the activity of water.

2.3.4 Electrolyte-Non Random two Liquid Model / E-NRTL

Probably one of the most well used models for modelling phase equilibria both is **n**on-**r**andom **t**wo **l**iquid model or NRTL (Renon and Prausnitz, 1968). The e-NRTL model has proved to be the most popular activity coefficient model. The popularity of the model is large enough that a company has been

dedicated to the refinement and licencing of the model *i.e.* AspenTech. The excess Gibbs energy term for the e-NRLT model is a two component equation developed to represent the long range and short range interactions of molecules. The long range interactions are calculated using the reformulation of the Debye Huckel equation from (Pitzer, 1980) to represent the long range ion-ion interactions and the Born expression. The expression accounts for the excess Gibbs energy of transfer from infinite dilution in the mixed solvent to infinite dilution in the aqueous phase.

$$g_{PDH}^{\mathrm{E}} = -\mathrm{R}T\left(\sum_k x_k\right)\left(1000/M_s\right)^{1/2}\left(4A_\phi I_x/\rho\right)\ln\left(1+\rho I_x^{1/2}\right) \qquad \textbf{Eq 2-45}$$

Values of M_s are the molar mass of solvent, A_v, is a function of the mixed solvent dielectric constant and mixed solvent density. ρ is the distance of closest approach and I_x is the ionic strength of the solution.

$$g_{BORN}^{\mathrm{E}} = \mathrm{R}T\left(e^2/2k\mathrm{T}\right)\left(1/D_s - 1/D_w\right)\left(\sum_i x_i z_i^2/r_i\right)10^{-2} \qquad \textbf{Eq 2-46}$$

The value of e is the charge of the electron, k is the boltzmann constant, D_s and D_w are the dielectric constants of the solution and water. The value of x is the molar fraction, z charge of the solution and r is the radius of the molecule or ion. The short range parameters for the local composition are written as

$$\frac{g^{E}_{NRTL}}{RT} = \sum_{m} X_m \frac{\sum_{j} \tau_{jm} G_{jm} X_j}{\sum_{k} G_{km} X_k} + \sum_{c} X_c \sum_{a'} \frac{X_a \sum_{j} G_{jc,a'c} \tau_{jc,a'c}}{\left(\sum_{a''} X_{a''}\right)\left(\sum_{k} X_k G_{kc,a'c}\right)} + \sum_{a} X_a \sum_{c'} \frac{X_{c'} \sum_{j} G_{ja,c'a} \tau_{ja,ca}}{\left(\sum_{c''} X_{c''}\right)\left(\sum_{k} X_k G_{ka,c'a}\right)} \quad \textbf{Eq 2-47}$$

Where $X_i = x_i C_i$ where C_j is equal to 1 for molecules and Z_i for the ions. The parameters of G_{xx} are related to adjustable parameter τ_{xx}, and the value of α_{xx} is a non-randomness factor. The sub scripts of c, a and m denote the cation, anion and molecule species. The equations of all the general parameters for the short range parameters listed below

$$G_{cm} = \sum_{a} X_a G_{ca,m} \Big/ \sum_{a'} X_{a'} \quad \textbf{Eq 2-48}$$

$$G_{am} = \sum_{c} X_c G_{ca,m} \Big/ \sum_{c'} X_{c'} \quad \textbf{Eq 2-49}$$

$$\alpha_{cm} = \sum_{a} X_a \alpha_{ca,m} \Big/ \sum_{a'} X_{a'} \quad \textbf{Eq 2-50}$$

$$\alpha_{am} = \sum_{c} X_c \alpha_{ca,m} \Big/ \sum_{c'} X_{c'} \quad \textbf{Eq 2-51}$$

$$G_{jc,a'c} = \exp\left(-\alpha_{jc,a'c} \tau_{jc,a'c}\right) \quad \textbf{Eq 2-52}$$

$$G_{ja,c'a} = \exp\left(-\alpha_{ja,c'a} \tau_{ja,c'a}\right) \quad \textbf{Eq 2-53}$$

$$G_{ca,m} = \exp\left(-\alpha_{ca,m} \tau_{ca,m}\right) \quad \textbf{Eq 2-54}$$

$$G_{im} = \exp\left(-\alpha_{im} \tau_{im}\right) \quad \textbf{Eq 2-55}$$

$$\tau_{ma,ca} = \tau_{am} - \tau_{ca,m} + \tau_{m,ca} \quad \textbf{Eq 2-56}$$

$$\tau_{mc,ac} = \tau_{cm} - \tau_{ca,m} + \tau_{m,ca} \quad \textbf{Eq 2-57}$$

The values of τ are used as temperature dependant fitting parameters using a linear polynomial. The sum of the long range and short range interaction are equal to the excess Gibbs energy in equation 2-58.

$$g^{E} = g^{E}_{PDH} + g^{E}_{BORN} + g^{E}_{NRTL} \qquad \textbf{Eq 2-58}$$

The advantage of the NRTL equation is the binary parameters of a multicomponent system and of its constituents binary systems are the same. This model has been used in the past to model the speciation and solubility of CO_2 in aqueous amine solutions (Hessen et al., 2010; Zhang and Chen, 2011; Ying Zhang et al., 2011).

2.3.5 Extended Universal Quasichemial Model / Extended UNIQUAC

The **Uni**versal **Qua**si**c**hemical model or UNIQUAC is one of the more complex local composition models created by (Abrams and Prausnitz, 1975) in 1975. The model includes theory from (Guggenheim E. A., 1952), where local composition is a result of the molecules are a combination of size differences between the molecules and energy the difference in intermolecular energies in the mixture. To accommodate electrolyte in solution the Debye Hückel term can be added. The idea has led to the concept that the excess Gibbs energies are a combination of three terms.

$$\frac{G^{E}}{RT} = \frac{G^{E}\left(combinatorial\right)}{RT} + \frac{G^{E}\left(residual\right)}{RT} + \frac{G^{E}\left(Extended\ Debye\text{-}Huckel\right)}{RT} \qquad \textbf{Eq 2-59}$$

The combinatorial term represents the size differences of the molecules, otherwise known as the entropic term, and is independent of temperature. The residual term represents the energy differences between the molecules, otherwise known as the enthalpic term. The extended Debye Huckel term

represent the electrostatic influence form ion interactions. The activity coefficients are represented by the following equations

$$\frac{G^E\left(combinatioral\right)}{RT}=\sum_i x_i \ln\left(\frac{\phi}{x_i}\right)-\frac{z}{2}\sum_i q_i x_{\ i} \ln\left(\frac{\phi_i}{\theta_i}\right) \qquad \textbf{Eq 2-60}$$

The express for the activity coefficients follow equation 2-61

$$\ln\gamma^c=\ln\left(\frac{\phi}{x_i}\right)+1-\frac{\phi}{x_i}-\frac{z}{2}q_i\left[\ln\left(\frac{\phi_i}{\theta_i}\right)+1-\frac{\phi_i}{\theta_i}\right] \qquad \textbf{Eq 2-61}$$

The parameter z is a coordination number that is usually set to 10. The values of θ_i is the area fraction of the species and ϕ_{i} is the volumes fraction of species are defined by the equations 2-62 and 2-63

$$\theta_i=\frac{x_i q_i}{\sum_j x_j q_j} \qquad \textbf{Eq 2-62}$$

Where q_i the surface area parameters.

$$\phi_i=\frac{x_i r_i}{\sum_j x_j r_j} \qquad \textbf{Eq 2-63}$$

and r_i *is* the volumes fraction of species defined by the size parameter. x_i is the molar fraction of the species. The residual parameters for the excess Gibbs energy and activity coefficients are related with the equation below.

$$\frac{G^E\left(residual\right)}{RT} = -\sum_i \left[x_i q_i \ln\left(\sum_j \theta_j \tau_{ji} \right) \right] \qquad \textbf{Eq 2-64}$$

$$\ln \gamma^R = q_i \left[1 - q_i \ln\left(\sum_j \theta_j \tau_{ji} \right) - \sum_j \frac{\theta_j \tau_{ij}}{\sum_k \theta_k \tau_{kj}} \right] \qquad \textbf{Eq 2-65}$$

$$\tau_{ij} = \exp\left(-\frac{u_{ij} - u_{jj}}{RT} \right) \qquad \textbf{Eq 2-66}$$

The values of τ_{ij} are equal to the average interaction energy u_{ij} for unlike species and u_{ii} for like species. The difference between u_{ij} and u_{ii} can be considered temperature dependant. The size and shape parameters, q and r, for organic compounds are calculated using the methods of Bondi (Arnold Aaron Bondi, 1968; Abrams and Prausnitz, 1975). For ionic species these species are determined from data regression. To describe the water and ions in solution the Debye-Hückel term recommended by (Fowler and Guggenheim, 1939) used,

$$\frac{G^E\left(Debye-Huckel\right)}{RT} = -x_w M_w 4 \frac{A}{b^3} \left[\ln\left(1 + bI^{0.5}\right) - bI^{0.5} + \frac{b^2 I}{2} \right] \qquad \textbf{Eq 2-67}$$

$$\ln \gamma_w^{DH} = M_w 4 \frac{2A}{b^3}\left[1 + bI^{0.5} - \frac{1}{1+bI^{0.5}} - 2\ln\left(1+bI^{0.5}\right)\right] \quad \textbf{Eq 2-68}$$

The value of x_w, M_w are the molar fraction and molar mass of water, A is the Debye Hückel constant. The b is a distance of closest approach set at 1.5 for this version and I is the ionic strength of the solution. Ions in solution follow equation 2-69.

$$\ln \gamma_i^{DH} = -z_i^2 \frac{AI^{0.5}}{1+bI^{0.5}} \quad \textbf{Eq 2-69}$$

The value for Z_i is the charge of the species. A lot of work on the development of this model was done by (Thomsen et al., 1996) based of the work from (Sander et al., 1986) for electrolyte solutions. The models have been used to calculate solubility and speciation models for CO_2 absorption by (Thomsen and Rasmussen, 1999; Faramarzi et al., 2009; Sadegh et al., 2015).

3 Liquid-Liquid Equilibrium of Piperidine

3.1 Introduction

The temperature of liquid-liquid phase separation has been determined for the aqueous solutions of piperidines for different CO_2 loading charges, using the cloud point method. The challenge in these measurements is the preparation of the sample containing an accurate quantity of dissolved gas. Two different apparatuses which use visual observation to identify the phase separation temperature were used depending on the temperatures range investigated: a Thar Instrument equilibrium cell, and a sapphire cell build in the "Centre Thermodynamique des Procédés" Mines ParisTech, Fontainebleau.

3.2 Experimental

3.2.1 Cloud Point Method

The liquid-liquid equilibrium temperature, LLE, data were obtained using the cloud point method. This method is based on the optical determination of the temperature at which point the solution is no longer homogeneous, and presents equilibrium between two liquid phases. This property is derived from the difference in the refractive index of a clear homogeneous solution versus an emulsion. In the case of emulsions, droplets of one liquid phase are dispersed in the volume of a second phase. This equilibrium leads to the appearance of opaque heterogeneous mixtures, while the homogeneous solutions have only one transparent phase.

The procedure for the cloud point identification is the same and independent of the system under measurement (visual isochoric method). Once the cell is entirely filled with the homogeneous solution (without any vapour phase), it is isolated from the pumps. At this point the solution appears to be clear. Then, the temperature in the cell is increased at a definite scanning rate (0.2 to 1 K/min) to find the

sharpest possible temperature interval in which the solution appears opaque: the second phase appears. At this point, increasing and decreasing the temperature slowly in this temperature interval leads to a fine determination of the cloud point temperature.

During this procedure, the cell is maintained at constant pressure. For that purpose the cell is connected to the buffer volume to avoid pressure increase due to thermal expansion. The change in turbidity is visually observed. The uncertainty on the temperature of the cloud point was estimated from reproducibility tests and is less than $\sigma T = 2$K, while uncertainty on such temperature determination for one experiment is $\sigma T = 0.5$ K.

3.2.2 Overview of the Methods

Aqueous solutions of amine loaded with controlled quantities of CO_2 are prepared in a custom-made flow mixing cell, described in detail in the section 4.3.3 of this manuscript. The experimental arrangements of the two apparatuses are depicted in Figure 3-1. The mixing point is built with the same structure as the one developed at ICCF for enthalpies of solution measurements (Arcis et al., 2011). The mixing point is constructed in a Y formation, where two 1/16" stainless steel tubes are soldered on the top branches of the Y, while a unique tube containing the final mixture move out from the bottom branch of the mixing unit.

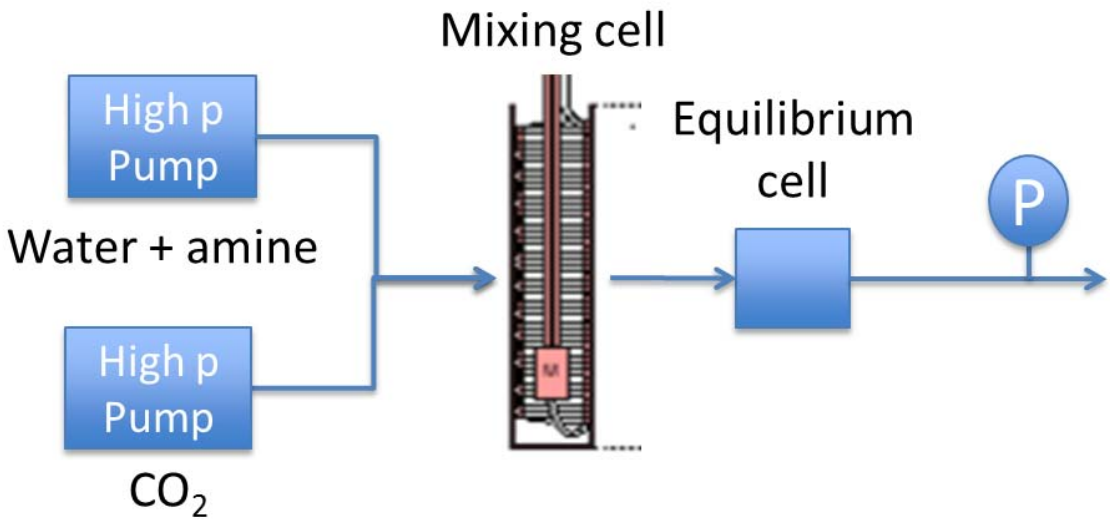

Figure 3-1: Overall experimental set-up of liquid-liquid equilibrium cells for solutions containing dissolved gas.

The two fluids, CO_2 and the aqueous amine solution, are injected into the mixing unit supplied by two ISCO model 100 DM high-pressure syringe pumps. As the syringe pumps deliver constant volumetric flow rates, they were regulated at a constant temperature of 298.15 K using a thermostatic bath in order to accurately calculate the composition of the aqueous solutions containing dissolved gas. The system pressure is maintained constant at ± 0.02 MPa using a buffer volume of 1 L equipped with a back pressure regulator and placed at the end of the flow line. The gas loading charge, α (mol CO_2 / mol amine), of the mixture leaving the mixing unit was calculated using the molar flow rates delivered by the two syringe pumps in equation 3-1.

$$\alpha = \frac{\dot{n}_{CO2}}{\dot{n}_{amine}} \qquad \textbf{Eq 3-1}$$

where $\dot{n}_{CO_2}$ and $\dot{n}_{amine}$ are the molar flow rates of CO_2 and aqueous amine solution respectively. To calculate the molar flow rates, the densities of the aqueous solution of amine and CO_2 are needed at the

experimental conditions of temperature and pressure. The densities of the solution as a function of the pressure were measured using an Anton Paar densimeter DMA HP. The densities of CO_2 were calculated using the equation of state from Span and Wagner (Span and Wagner, 1996). Details on the calculation of the loading charge and its uncertainty are found in (Arcis et al., 2011). The relative uncertainty on loading charge using this method is estimated to be less than 0.4%.

Two different apparatuses have been used to determine the cloud points of the mixtures, depending mainly on the range of temperature to be covered for these measurements. The next part will describe the specificity of each device.

3.2.3 Thar Equilibrium Cell

The first apparatus is a visual phase equilibrium cell SPM20 from Thar instruments. The overall representation of the equipment is represented in figure 3.2.

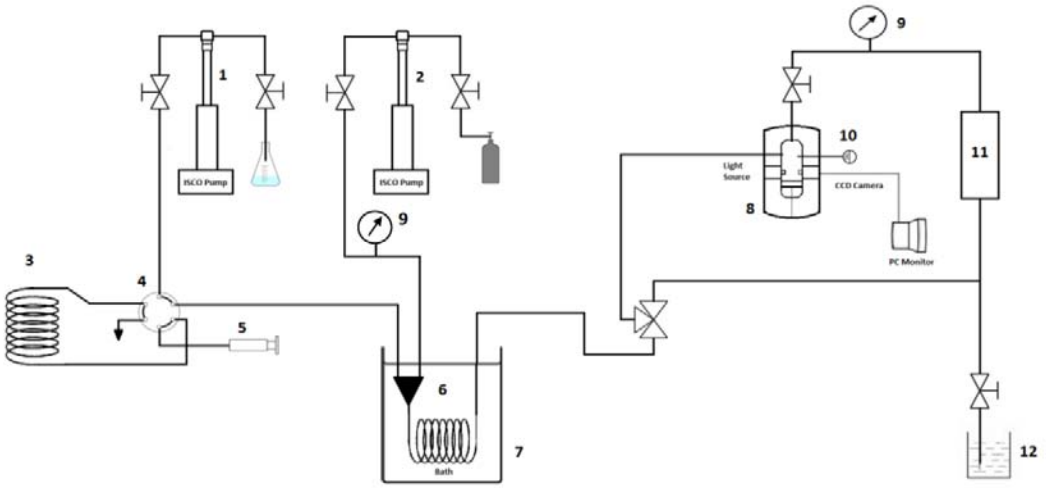

Figure 3-2 : General oberview of the SPM 20 Thar equilibrium apparatus. (1) Water pump; (2) CO_2 pump (3) Injection loop; (4) Six way valve; (5) Injection port for aqueous amine; (6) Mixing unit; (7) Isothermal bath; (8) Measurement cell; (9) Pressure gauges; (10) Thermocouple; (11) Buffer volume and back pressure regulator; (12) Waste bottle.

The equipment features a high pressure chamber (8) provided with a thick sapphire window, pressure and temperature sensors. Cloud points are observed with a light source and a CCD camera connected to a computer. The vessel body can be used to work from ambient temperature to 398 K and from atmospheric pressure to 70 MPa. The internal volume of the chamber can be adjusted from 10 mL to 20 mL. For the present experiment the volume of the chamber was set to 10 mL. The original chamber heating system uses four electrical heaters located at the bottom of the chamber with a separate controller. This was replaced by a heat tape which surrounds the vessel body and uniformly heats the internal chamber. A spherical magnet was placed inside the chamber driven from the exterior by a stir plate to mix the solution.

Each experiment using the equipment described in Figure 3-2 follows the same procedure: ISCO pumps were filled with water (1) and carbon dioxide (2). The amine solution of known composition was injected into the injection loop (3) isolated from the rest of the system. The water pump is set to the desired flow rate to push the amine solution through the injection loop in the direction of the mixing point (6). The injection loop is used to avoid damaging the internal cylinder and seals of the ISCO pump with amine solutions. The CO_2 filled pump flow rate is set and run to inject CO_2. 10 mL of CO_2 amine solution moved through the mixing cell to the trash cylinder (11) before the three way ball valve was switch to begin filling the equilibrium cell (8) from the bottom up. Once the cell was filled entirely (no vapour phase) the 3 way ball valve was shut to isolate the equilibrium cell from the pumps. The visual cell was placed in horizontal position and spherical magnet was started to maintain efficient mixing. The temperature in the cell was then increased using the heating tape until the cloud point was observed using the CCD camera and computer.

3.2.4 Sapphire cell

The second cell, supplied by CTP Mines ParisTech is fully made of sapphire, allowing the visualization of the entire sample, instead of a limited zone, as in the Thar sapphire window. The experimental device is schematically represented in Figure 3-3.

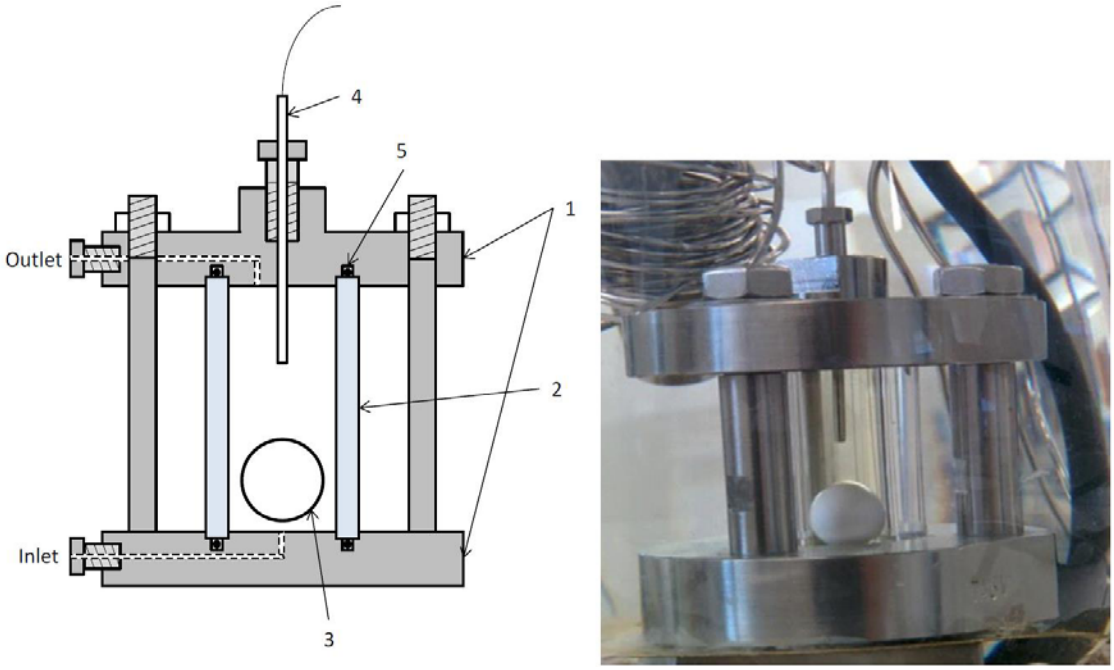

Figure 3-3 : Sapphire liquid-liquid equilibrium cell. (1) Titanium blocks; (2) Sapphire cell; (3) Spherical stirrer; (4) K-type Thermocouple; (5) O-ring.

The equilibrium cell is made of a sapphire tube (2) (25 mm O.D., 12.7 mm I.D., 35 mm height) tightly sealed by two titanium flanges (1) at the top and bottom. Its internal volume is approximately 4.4 mL. An inlet located at the bottom of the cell and an outlet at the top, allow loading operations. A spherical magnet (3) is located inside the sapphire vessel and is driven by a submersible magnetic stirrer placed right under the bottom flange. Temperature is monitored through a K-type thermocouple (4) entering the cell from the top flange.

The complete configuration of the equipment is reported in Figure 3-4. The cell (8) is immerged in a silicon oil cooling bath (9) to measure between the temperature range of 263 K, up to 393.15 K. The

maximum pressure allowed in the cell is 8 MPa. For this apparatus, the mixing unit (7) is immerged in the same bath as the measuring cell (8). Consequently the CO_2 amine solution is prepared at the exact same temperature as injection temperature of solution filling of the measuring cell.

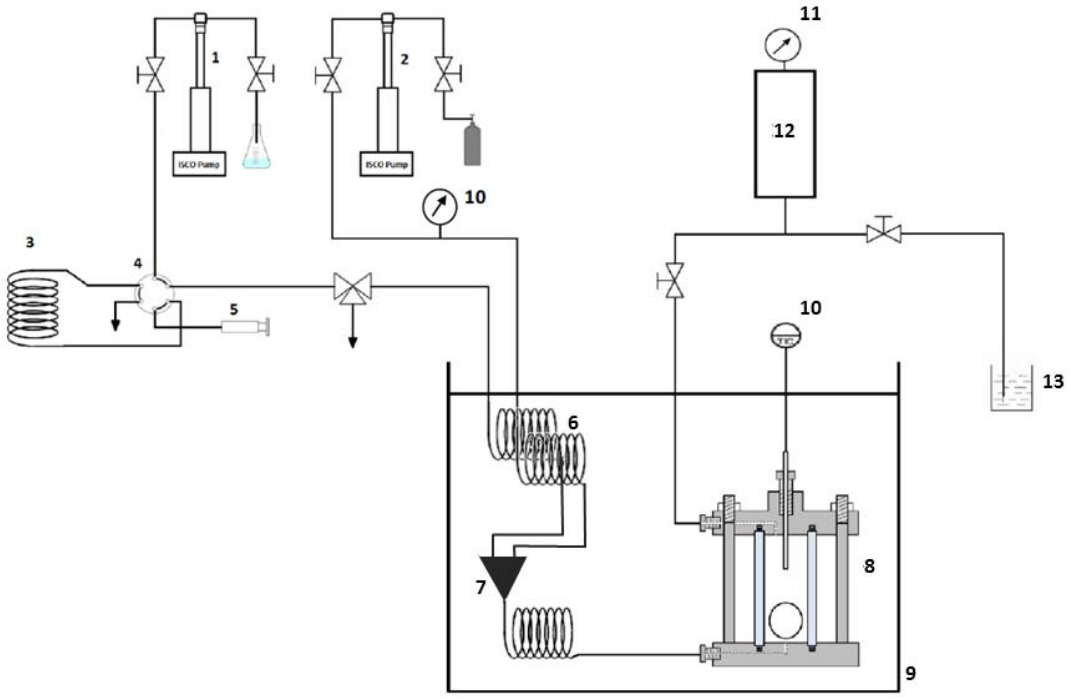

Figure 3-4 : General overview of the liquid-liquid equilibrium sapphire apparatus. (1) Water pump; (2) CO_2 pump; (3) Injection loop (4) Six-way valve; (5) Injection port for aqueous amine; (6) delay loop; (7) Mixing unit; (8) Sapphire equilibrium cell; (9) Jacketed glass reactor vessel; (10) Thermocouple; (11) Pressure gauges; (12) Buffer volume and back pressure regulator; (13) Waste bottle.

As shown in Figure 3-4, the complete procedure for the experiment is performed as follows. The ISCO pumps were filled with water (1) and carbon dioxide (2). The amine solution of known composition is injected into the injection loop (3) and isolated from the system. The water pump pushes water down the flow line in the direction of the loop to push the amine solution in the direction of mixing unit (7). Delay loops (6) are placed in the thermostated bath (9) to insure that the temperature of the solution and of the CO_2 are low enough to prepare homogenous mixtures before entering the sapphire cell (8). 20 mL of

mixed CO_2 and amine solution moved through the mixing cell before the valves were switch to isolate the pumps from the mixing point. The spherical stir ball was then activated to maintain the homogenous solution with increasing temperature. The temperature of the cell was slowly raised using a heating bath until the cloud point was reached.

3.2.5 Comparison of the Equilibrium Cells

The detailed characteristics of both apparatuses are given in Table 3-1.

Table 3-1 : Characteristics of the visual cells used for cloud point measurements

	Thar Equilibrium cell	**Sapphire Equilibrium cell**
T (K)	Room T – 393	270 – 393
Control of *T*	Heat tape	Thermostatic bath
p (MPa)	1 – 40	1 – 8
Control of *p*	Buffer volume	Buffer volume
Inner volume (mL)	10 - 20 adjustable	4.4
Visualization of the sample	sapphire window	Full sample

The Thar equilibrium cell has the ability to measure the LLE up to a pressure of 40 MPa and can measure solutions with critical solution temperature above room temperature. The sapphire equilibrium cell has a unique advantage to measure the critical solution temperature of ternary solutions at a low temperature of 270K. One advantage of the sapphire cell, is the ability to view the whole sample rather than through a small viewing window. The same devices are used to measure temperature of phase separation for solutions without dissolved gas. In that case, the solutions are directly injected in the visual cell, without using the mixing cell prior to the entrance of the visual cell.

3.2.6 Alternative Mixing Method

The challenge is in the preparation of the ternary mixture of aqueous alkyl piperidine with an accurate CO_2 composition. Most of the mixtures have been prepared using the mixing unit described in part 3.2.4 with the same design as the mixing points used with advantages in mixing enthalpy calorimeters (Arcis et al., 2011). In that configuration, the temperature of the mixing unit is adjusted to prevent phase separation during gas dissolution.

However, some systems have to be prepared directly at low temperature, specifically binary mixture with a lower critical solution temperature below room temperature. In that case, it is necessary to make sure that the reservoir containing the aqueous solution of amine is maintained at temperature below LCST. For that purpose, the flow mixing unit was replaced by a static system loaded with CO_2 and amine solution. The schematic view of this mixing unit is depicted in Figure 3-5. It consists in a 25 mL sample cylinder (8) with two openings at each end purchased from Swagelok. A small magnetic stir bar is placed inside the cylinder to mix the amine solution with CO_2. Swagelok 3-way ball valves (3) are attached to both ends of the sample cylinder. The volume of this system was calibrated by the difference in weight between the empty sample cylinder and the filled cylinder with degassed deionized water at room temperature.

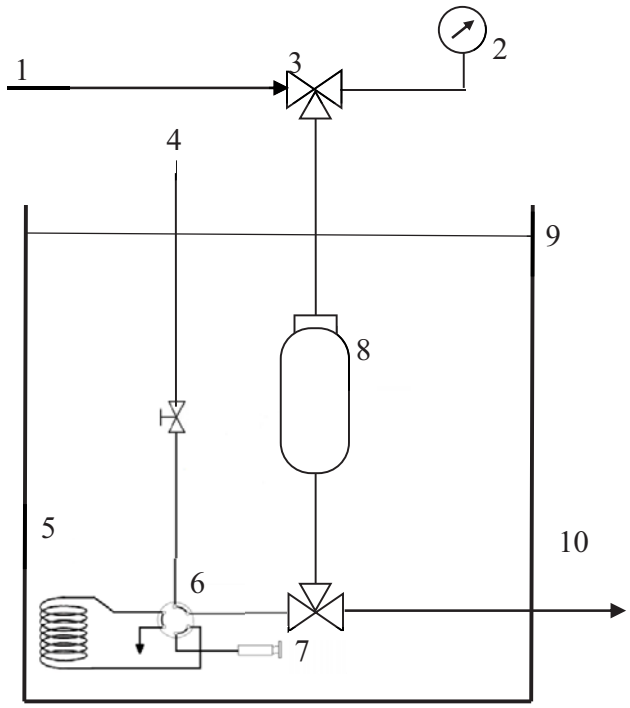

Figure 3-5 : General overview of the sample cell: (1) Direction of nitrogen flow from isco pump (2) Pressure gauge (3) 3-way ball valve (4) Source of water flow from ISCO pump (5) Sample loop (6) sixway valve (7) Injection port for solution. (8) Sample cylinder, with stir bar inside (9) Ice bath. (10) Direction of solution flow to the Thar cell.

The upper valve is connected to a D100 ISCO pump (1) filled with N_2 gas and a Keller barometer (2) to read the pressure to ± 0.002MPa. The lower valve is connected to a 40 mL injection loop (5) filled with amine solution. A D260 syringe pump (4) is filled with water to push the amine solution out of the loop and into the sample cylinder. The nder and the loop are immersed in a cooled bath filled with liquid water in equilibrium with ice, to maintain the temperature as close as possible to zero degree celsius to keep the amine solution homogenous both during mixing and injection.

The procedure to fill the cylinder is as follows: The sample cylinder is filled with a known pressure of CO_2 at a well-known temperature, allowing the determination of the number of mole of CO_2 in the cylinder. The cell is then submerged into an ice bath. Using an ISCO pump filled with water the amine is injected into the sample cylinder at a pressure higher than the CO_2. The cylinder was filled with amine until the full volume was reached. The solution was stirred overnight to produce a homogenous

solution. Once the system reaches equilibrium N_2 gas is used to inject the mixture into the Thar equilibrium cell (10). The estimated uncertainty is approximately ± 0.0005 in the solution composition.

3.3 Results and Discussion

3.3.1 Cloud Point Visualization

After mixing the solution and filling it with the cell the temperature is increased to reach the cloud point. Figure 3-6 show the images of the change in turbidity using the Thar Instrument. In image (a) the temperature is below the temperature of phase separation and the solution is homogenous and transparent. The sphere in the bottom right of the picture is a stir ball. Image (c) is the opaque heterogeneous solution. The temperature at this point is above the cloud point. Image (b) shows the solution approaching the demixing temperature and the solution is becoming turbid.

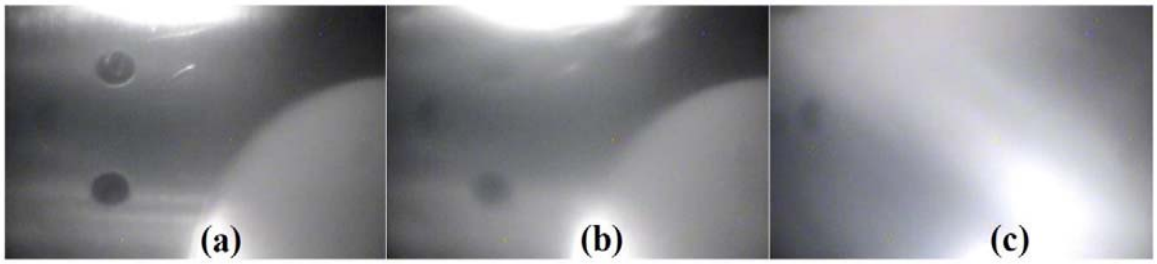

Figure 3-6 : CCD camera pictures of the internal chamber of the Thar Instrument measuring cell. (a) Transparent homogenous solution; (b) Cloud point; (c) Opaque heterogeneous mixture.

The sapphire cell results are shown in Figure 3-6. With this cell, the stirred solution appears transparent below cloud point (picture (a)), while it is opaque above cloud point (picture (b)).When stirring is stopped, the two phases in equilibrium separate (picture (c)). As the full volume is observable, it is also possible to quantify the proportion of each phase using this method.

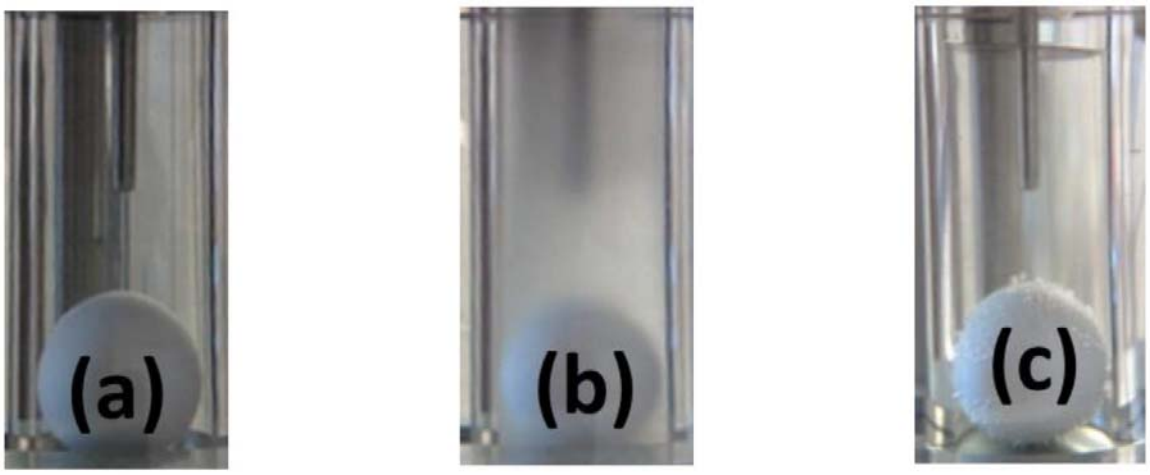

Figure 3-7 : Picture of phase transition in the Sapphire Equilibrium cell. (a) Transparent homogenous solution (b) Cloud Point (c) Decanted two phase mixture.

Experiments were performed to assess the reproducibility of these two instruments using identical ternary {water+amine+CO_2} with identical mass percent amine.

3.3.2 Liquid-Liquid Equilibrium of Alkyl piperidines

The temperatures of phase separation obtained for the different alkyl-piperidines in water and without CO_2 are listed in Table 3-3. Results were obtained using both visual methods described above. In the literature, the phase diagrams for most of the amine studied are referenced mainly by three groups:

- Flashner and coworkers from (Flaschner and MacEwen, 1908; Flaschner, Otto, 1908) worked mainly on methyl-piperidines. Flaschner's used the cloud point technique to measure the LLE of the alkyl piperidines. The low temperature experiments were conducted in sealed glass capillary tubes with a blown bulb at the end. Low temperature measurements contained a mixture of water and amine which was titrated and resealed after each titration. The higher temperature

measurements used single use thick walled Jena glass capillary tubes to measure up to temperature of 503 K.

- Stephenson and coworkers (Stephenson, 1993) studied most of the alkyl-piperidines. The experimental method used by Stephenson was the analytical method where the solutions were brought into equilibrium at a given temperature and samples were extracted by syringe. To each sample a higher boiling organic compounds was added as a standard and the ratio of peaks was measured by gas chromatography. The sample was analysed by gas chromatography using a thermal conductivity detector.
- Coulier and coworkers (Coulier et al., 2010) published data for N-MPD and 2-MPD. The data were collected using the Thar visual cell described earlier in this chapter and a calorimetric method. With this last method, the solution is inserted in a heat capacity cell at low temperature. When increasing the temperature, the calorimetric signal is linear and almost constant when the solution is homogeneous. When reaching the demixing temperature, an enthalpic peak appears followed by a strong change of the signal. This is due to the shift in equilibrium of two different phases which change the composition versus temperature.

Figure 3-8 shows the results obtained and available in literature with N-MPD and N-EPD. The results obtained in this work concern the N-ethylpiperidine (N-EPD). The lines are calculations of the phase envelop for the N-MPD and N-EPD (Stephenson data) using a scaling law model, which will be described in the section 3.3.3. Our results are mainly obtained for molar fraction from 0.01 up to 0.2. The results are in good agreement with data from Stephenson. As it can be observed in the Figure 3-8, the LCST with N-EPD is obtained at 281.5 K for a molar fraction of amine of 0.05. This value is located at the same molar fraction as N-methylpiperidine (N-MPD) but at a lower temperature, as the LCST for

N-MPD is around 318 K. The range of molar fraction where the demixion is observed is also larger for N-EPD than for N-MPD. On the range of temperature studied here, the demixion for N-MPD occurs for molar fraction lower than 0.65, according to Stephenson, while for the N-EPD demixion is observed for molar fraction up to 0.85, within the same temperature range.

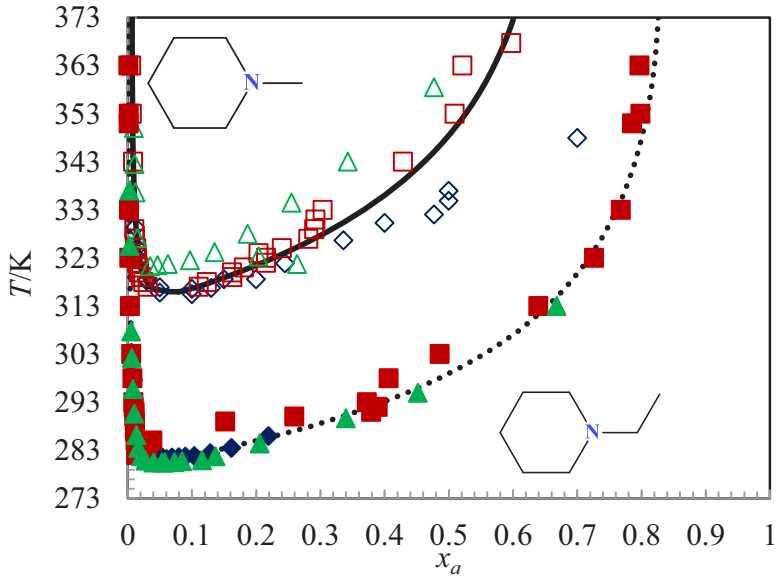

Figure 3-8: Comparison of the LLE for tertiary alkyl piperidines: N-MPD data (◇ (Coulier et al 2010), □ (Stephenson,1993) , △ (O.Flaschner, 1908), ___ (Scaling fit this work)) and N-EPD data (◆ (This work), ■ (Stephenson 1993), ▲ (O.Flaschner, 1908), …… (Scaling fit this work))

Figure 3-9 shows the results obtained for secondary amines with at least one substituent in position 2. Once again, the lines on this graph are a fit of the phase envelop using a scaling law. The results obtained for 2-EPD and 2,6-DPD are in very good agreement with Stephenson's data. The largest discrepancy is obtained with 2-MDP, where data from Stephenson are slightly overestimated, comparing to Stephenson and Coulier.

On Figure 3-9, it is observed that the molar fraction corresponding to the LCST is almost similar for the 3 amines with a value of 0.05. The main difference is with the LSCT temperature. The

temperature is of 343 K for the 2-MPD, 300 K for the 2,6-DPD and 280 K for the 2-EPD. These results lead to the conclusion that the addition of methyl groups on the methylpiperidine lowers the temperature of phase separation. Changing size of the substituent (from methyl to ethyl group), also decreases the LCST.

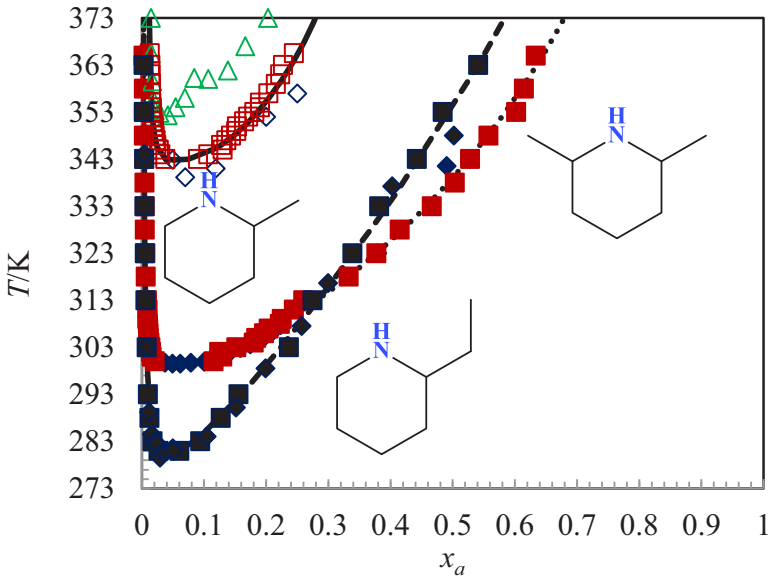

Figure 3-9: Comparison of the LLE for secondary hindered alkyl piperidines: LLE of 2-MPD, (◇ (Coulier et al. 2010), □ (Stephenson 1993) , △ Flaschner and MacEwan 1908), ___ (Scaling fits)) 2,6-DPD, (◆ (This work), ■ (Stephenson 1993), …… (Scaling fits)) and 2-EPD (◆ (This work), ■ (Stephenson 1993), _ _ (Scaling fits)) data.

The biggest difference with the tertiary amines studied in Figure 3-8 is the range of concentration where the demixion occurs. The secondary amines are narrower in comparison. Once again considering the maximum temperature of 373 K, the 2-MPD form two liquid phases only for a molar fraction lower than 0.3, compared to 0.65 for N-MPD. Similarly the 2-EPD demixes only for molar fraction lower than 0.6 (0.8 for N-EPD). The 2,6-DPD seems to be intermediate between the N-MPD and the N-EPD. This is probably due to the restriction of access to the nitrogen which is surrounded by methyl groups in the 2 and 6 positions. Thus it appears to behave as a tertiary amine.

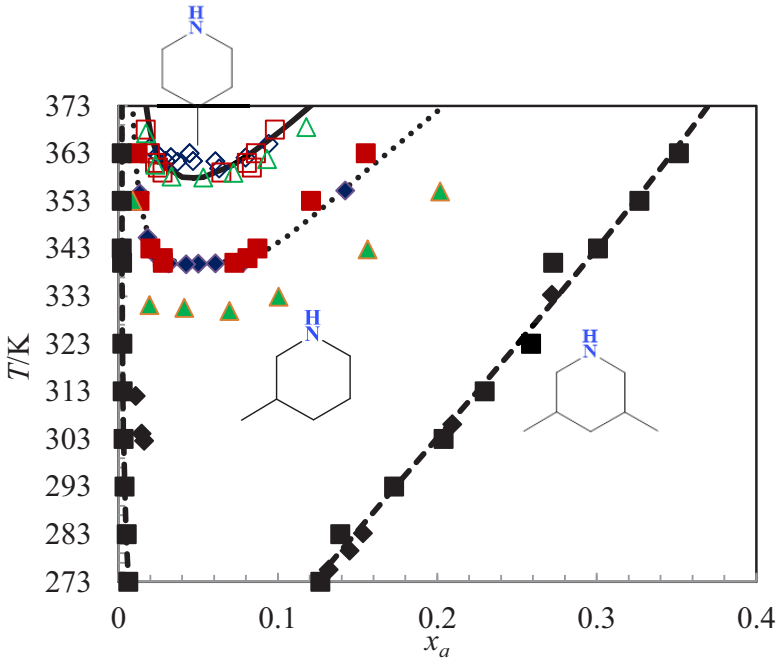

Figure 3-10: Comparison of the LLE for secondary alkyl piperidines: LLE of 4-MPD, (◇ (This work), □ (Stephenson, 1993) , △ (Flaschner, 1909), ___ (Scaling fit this work)). 3-MPD, (◆ (This work), ■ (Stephenson 1993), ▲ (Flaschner, 1909), …… (Scaling fit this work)) 3,5-DPD data (◆ (This work), ■ (Stephenson 1993), _ _ (Scaling fit this work)).

Finally, Figure 3-10 illustrates the results for the binary systems containing 3-MPD, 4-MPD and 3,5-DPD. The data set supplied by (Stephenson, 1993) shows the best agreement with our measurements with the 3-MPD and 4-MPD. The data reported by Flaschner, for 3-MPD is strongly under-evaluated comparing to Stephenson, and to our new data.

The most unexpected behaviour comes from the 3,5-DPD. Within the studied temperature range, this particular amine exhibits a domain, between the molar fraction of 0.01 and 0.12, where the mixture is never homogenous.

These amines have narrower LLE curves than the amines discussed in Figure 3-8 and Figure 3-9. It is expected that increasing the size of the alkyl-group from either the three or four position would have a similar effect on the LLE as observed from the increase in size of the alkyl group on 2-MPD. Future measurements should answer those questions.

3.3.3 Mathematical Regressions for Binary Liquid-Liquid Equilibrium Curves

The experimental results, with supporting literature, were regressed with a set of mathematical equations designed to reproduce the data to the best point necessary. Each equation set describes a water rich region, here denoted for the amount of amine x_1, and amine rich region denoted by (1-x_1). Depending on the phase envelop of each amine, different sets of equations have been used.

3.3.3.1 System with no Extremum

This set of equations is used to regressed data which does present neither a UCST nor measurable LCST.

$$\ln x_1 = \ln\left(x_{1,\min}\right) + C_1\left(T_{1,\min}/T - \ln\left(T_{1,\min}/T\right) - 1\right) \qquad \textbf{Eq 3-2}$$

$$\ln\left(1-x_1\right) = \ln\left(1-x_{1,\min}\right) + C_2\left(T_{2,\min}/T - \ln\left(T_{2,\min}/T\right) - 1\right) \qquad \textbf{Eq 3-3}$$

Where C_1, C_2, $T_{1,min}$ and $T_{2,min}$ are independent fitting parameters. Where $T_{i,min}$ are minimum temperatures for the fit. The parameters can be seen in Table 3-4: This set of equation has been used to fit the data obtained with 3,5-DPD.

3.3.3.2 Systems with only one Extremum

This set of equations is used when the phase diagram exhibits either a LCST or a UCST

$$\ln x_1 = \ln\left(x_{cs}\right) + a_1\left(T_{cs}/T - 1\right) + a_2\left|1 - T/T_{cs}\right|^{1/3} + a_3\left(1 - T/T_{cs}\right) \qquad \textbf{Eq 3-4}$$

$$\ln\left(1-x_1\right) = \ln\left(1-x_{cs}\right) + b_1\left(T_{cs}/T - 1\right) + b_2\left|1 - T/T_{cs}\right|^{1/3} + b_3\left(1 - T/T_{cs}\right) \qquad \textbf{Eq 3-5}$$

.

Where x_{cs} and T_{cs} are shared parameters between the two equations. The parameter a_i and b_i are regressed independently from the data sets. These equation were used to regressed 2-MPD, 3-MPD, 2,6-DPD, N-EPD, 2-EPD.

3.3.3.3 Closed Loop Systems

This set of equations is used for closed loop systems which have simultaneously UCST and LCST.

$$\ln x_1 = z_L \ln(x_L) + z_U \ln(x_U) + c_1 z_L z_U / T + c_2 |z_L z_U|^{1/3} + c_3 z_L z_U \quad \textbf{Eq 3-6}$$

$$\ln(1-x_1) = z_L \ln(1-x_L) + z_U \ln(1-x_U) + d_1 z_L z_U / T + d_2 |z_L z_U|^{1/3} + d_3 z_L z_U \quad \textbf{Eq 3-7}$$

$$z_L = (T_U - T)/(T_U - T_L) \quad \textbf{Eq 3-8}$$

$$z_U = 1 - z_L \quad \textbf{Eq 3-9}$$

Where T_U, T_L, x_U and x_L are parameters which are regressed together, with parameter c_i and d_i are regressed independently for each data. N-MPD parameters were regressed using the data provided by (Coulier et al., 2010) (Stephenson, 1993) and 4-MPD parameters were regressed using the data (Coulier et al., 2010) (Stephenson, 1993) (Flaschner, Otto, 1908; Flaschner, 1909).

3.3.4 Aqueous Solutions of Alkyl-Piperidine with Carbon Dioxide

After studying the binary mixtures, measurements have been realized with ternary systems, containing dissolved gas. For that purpose the mixing units described in part 3.2.3 and 3.2.4 have been used to prepare the mixture. The Table 3-1, below show the configurations of the apparatus/mixing unit used for each amine.

Table 3-2: Experimental method used to measure the phase equilibrium temperature.

Amine	Equilibrium cell	Mixing unit	Range of temperature of the LLE
N-MPD	Thar Instrument Sapphire cell	Flow mixing unit	From 273 K to 359K
2-MPD	Thar Instrument	Flow mixing unit	Greater than 343 K
3-MPD	Solution becomes completely miscible		
4-MPD	Solution becomes completely miscible		
2,6-DPD	Sapphire cell	Flow mixing unit Static mixing unit	280 K to 373 K
3,5-DPD	Experiments are not possible		
N-EPD	Thar cell	Flow mixing unit Static mixing unit	283 K to 363 K

Experiments have been conducted with both of the equilibrium cells with N-MPD to verify that there is no difference between the results due to the apparatus (section 3.2.3 and Figure 3-2). The influence of the mixing unit method was verified with 2,6-DPD, by comparing the results of the two methods for the same mixtures (section 3.2.4, Figure 3-3).

The results obtained for each amine will be presented in terms of:

- quantity of gas dissolved when the binary system {water + amine} is constant (loading charge)
- changing amine concentration when the loading charge is held constant

After presenting the results for each amine, they will be discussed to find the relationships between the chemical reactions occurring in the solution and the behaviour of the mixtures in the presence of CO_2.

3.3.4.1 Water + N-MPD + CO_2

Figure 3-11 illustrates the temperatures of phase separation obtained in ternary mixtures of N-MPD + water + CO_2 versus the loading charge of gas expressed as the number of mole of molecular CO_2 injected in the solution per initial mole of amine in the solution. The measurements have been

performed for three different concentrations of amines, specifically 10 w_a% (x_a=0.0198), 20 w_a% (x_a=0.0434) and 40 w_a% (x_a=0.1080) by mass percent of amine in water (w_a%).

All the solutions were prepared using the dynamic mixing unit. Most of the measurements have been conducted using the Sapphire cell equipment. The Thar equilibrium cell was used for four solutions with 20 w_a% (x_a=0.0434) by mass of amine to compare the results of the two apparatus.

The cell was filled at a constant pressure of 0.5 MPa and maintained for the duration for the experiment, to avoid both evaporation and degassing of the solution, while increasing the temperature. In order to determine the influence of pressure on the temperature of phase separation, experiments were performed at three different pressures as listed in Table 3-5. For the same composition of the ternary system {water+amine+CO_2}, specifically an aqueous solution of amine at 20% (x_a=0.0434) by mass, and a loading charge of CO_2 α=0.48, the temperature of phase separation was observed to be constant and equal to 308.4 K for pressure changing from 0.5 to 2 MPa. It is assumed for the rest of the experiments, that within this pressure range, there is no pressure effect on the temperature of phase separation.

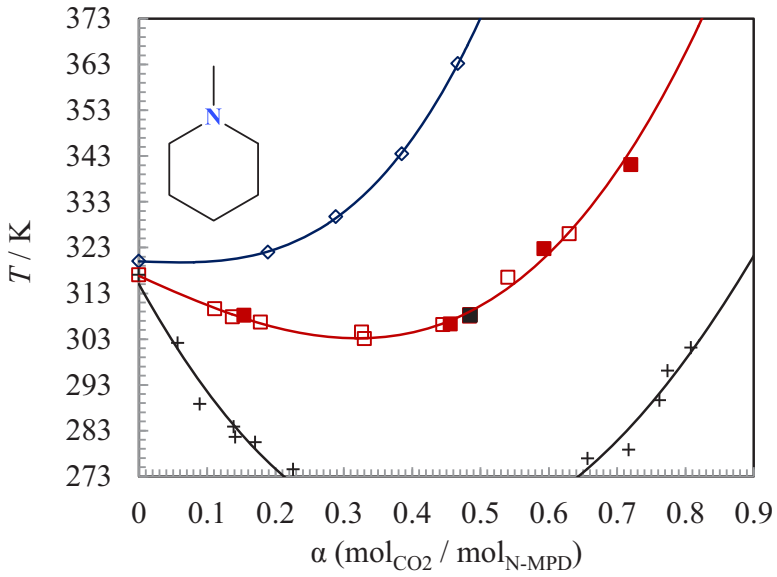

Figure 3-11: The LLE temperature with respect to the increasing loading charge of CO_2 in solutions of N-MPD using the sapphire cell. (◇ 10w_a% / x_a=0.0198) solutions, (□ 20w_a% / x_a=0.0434) solutions, ■ 20 w_a% solutions at 2 MPa,

(+ 40w_a% / x_a=0.1080), solutions ■ 20w_a% solutions measured using Thar cell. The solid lines are polynomial fits for a visual aid. The sizes of the markers represent the uncertainty in the temperature.

For each composition of aqueous amine solution, the temperatures of phase separation were observed to have a parabolic shape with a decrease at low CO_2 loading charge, α, and an increase at higher α. The initial decrease is steeper with the increasing quantity of amine in the aqueous solution, while the position of the minimum is shifted to higher loading charges. For the 10 w_a% (x_a=0.0198) by mass solution, the minimum is very small, and the temperature of phase separation starts to increase quickly. For aqueous solutions containing 40 w_a% (x_a=0.1080) by mass of amine, and loading charges between 0.22 and 0.64, the solution was observed to be diphasic on all the domain of temperature studied.

Figure 3-12 represents the data obtained versus molar fraction of N-MPD in the binary mixture {amine+water}, with no CO_2, and with a constant loading charge of 0.17. The listed data values for these experiments can be found in Table 3-5. The temperature of phase separation decreases dramatically when increasing the amine concentration. For amine molar fraction higher than 0.13, approximately 45 w_a%, the solutions were always demixed, on all the range of temperature studied.

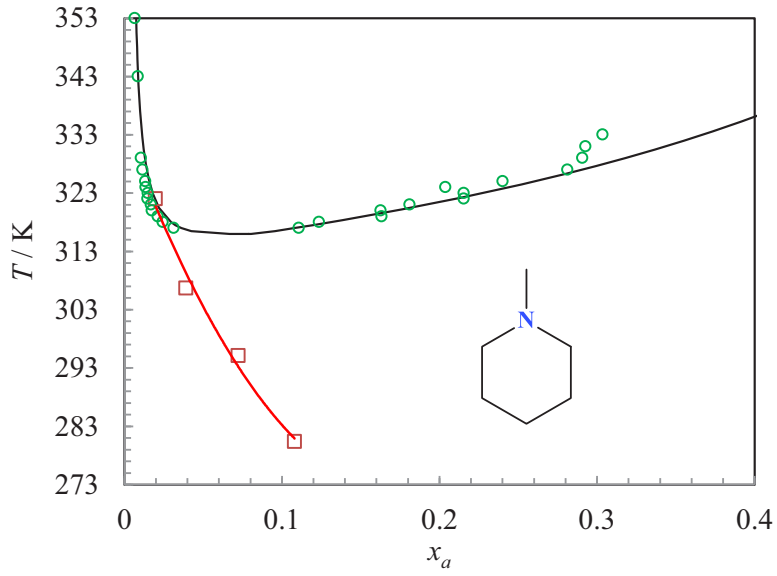

Figure 3-12 : LLE Temperature of N-MPD with increasing molar fraction of amine in solution at a constant loading charge of 0.17: □ CO_2 loaded N-MPD solution, — polynomial fit to loaded solution, ○ Unloaded N-MPD solution, ▬ Scaling fit to unloaded. The weight percent of loaded solution were increased 10 w_a% starting from 10 w_a% (x_a=0.0198) to 40 w_a% (x_a=0.1080)

3.3.4.2 Water + 2-MPD + CO_2

The experiments involving 2-MPD solutions and CO_2 were studied using the Thar equilibrium cell. The solution compositions with respect to the weight percent of 2-MPD are 20 w_a% (x_a=0.0434) and 40 w_a% (x_a=0.1080). They were performed at a pressure of 0.5 MPa. Results with respect to loading charge of CO_2 are presented in Figure 3-11. All the values are tabulated in Table 3-5.

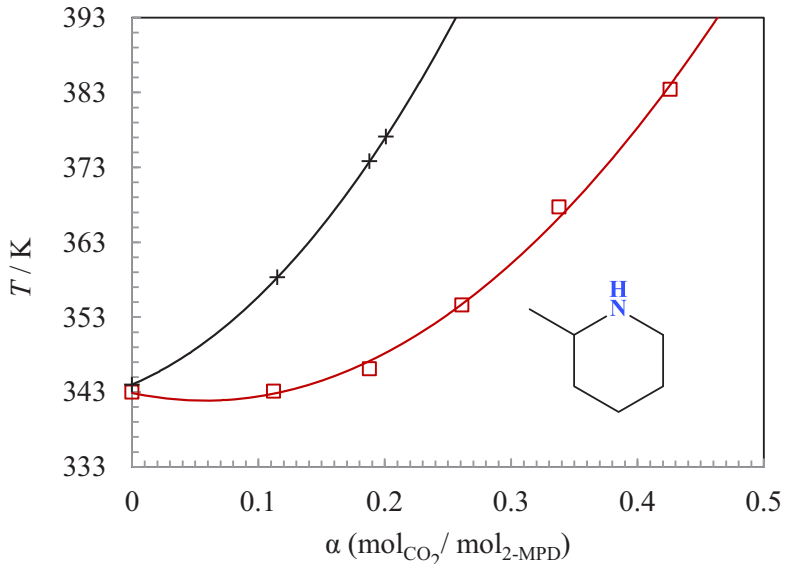

Figure 3-13: LLE temperature versus increasing loading charge of carbon dioxide, in aqueous 2-MPD solutions measured using the Thar cell. (+ 40 w_a%/x_a=0.1080),(□ 20 w_a%/ x_a=0.0434).

Increasing the amount of CO_2 in both solutions raises the critical solution temperature. The 40 w_a% (x_a=0.1080) solution of 2-MPD demonstrates the sharpest rise. In the presence of CO_2, and with loading charge higher than α=0.5 for the 20w_a% (x_a=0.0434) by weight solution, and α=0.25 for the 40w_a% (x_a=0.1080) by weight solution, the mixture remains fully soluble and homogeneous on the whole range of temperature investigated.

The effect of CO_2 versus the mass fraction of 2-MPD in the corresponding binary solution was examined at a constant loading charge of 0.2, mol of CO_2 per mol of 2-MPD, and compared to the unloaded solution. Results are presented in Figure 3-14

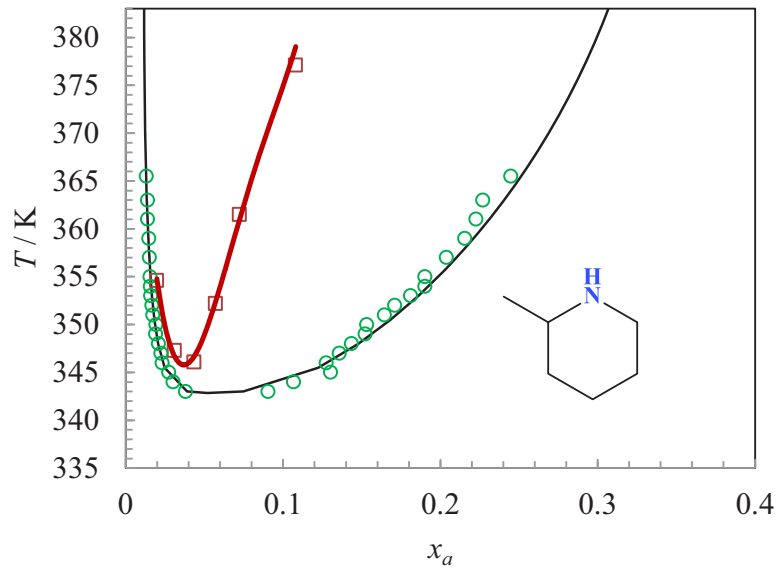

Figure 3-14: LLE temperature of a 2-MPD solution versus molar fraction with a constant loading charge of 0.2 of CO_2. (○ unloaded 2-MPD solutions), (▬Scaling fit to 2-MPD data), (□ 2-MPD solution loaded to 0.20), (▬ polynomial fit to the LLE data). The weight percent of loaded solution increases from 10w_a% (x_a=0.0198) to 30 w_a%(x_a=0.0722) increasing ever 5 w_a%. The last square is 40 w_a%(x_a=0.1080)

The phase separation temperature increases in presence of CO_2 for all the molar fraction of 2-MPD compared to unloaded solutions. Moreover, the range of concentration where the solution demixes is also reduced. For solutions containing more than 20% of amine in the mixture, the solution remains homogeneous, on the range of temperature studied.

3.3.4.3 Water + 2,6-MPD + CO_2

The effect of the restricting access to the nitrogen group was studied by studying a piperidine with two methyl groups in position 2 and 6. Due to low temperature requirements, the critical solution temperatures of 2,6-DPD were measured using the sapphire cell. For technical requirements, the 5w_a% (x_a=0.0174) solutions were measured at pressure lower than 0.5 MPa (0.1 MPa at its lowest), using the dynamic mixing unit. Few points have been obtained from solutions prepared in the static mixing unit (see section 3.2.6) to validate the procedure of mixing using this protocol.

Beyond 30 w_a% (x_a=0.0639) the addition of CO_2 caused white solids to precipitate in solution. A simple C^{13} NMR study has shown that these crystals are composed of carbonate and bicarbonate salts. This concentration was then the maximum concentration of amine taken into account for the LLE experiments.

A composition study with respect to changing quantity CO_2 and weight percent of 2,6-DPD was measured and are illustrated in and Figure 3-15 with the data listed in Table 3-7.

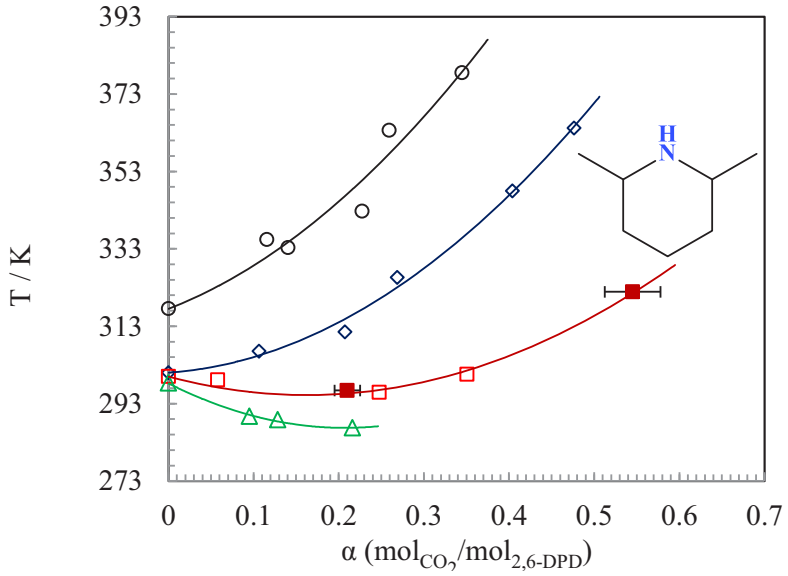

Figure 3-15: LLE temperature verusus CO_2 loading of 2,6-DPD in solution at a constant weight percent measured using the sapphire cell. ○ (5w_a% / x_a=0.0083), ◇ (10w_a% / x_a=0.0173), □ (20w_a% / x_a=0.0382), ■ (20w_a% / x_a=0.0382) solution mixed prepared using a static mixing unit, △ (30 w_a% / x_a=0.0959). The solid lines are polynomial fits to the data.

When comparing results obtained with the dynamic flow mixing unit and the static one (red curve on the graph, 20w_a% amine solution,) on the Figure 3-15, it can be seen that there is a very good agreement between the two methods.

For low amine concentration, the LLE temperature increases with CO_2 loading charge. When increasing the concentration of amine, the slope of the increase becomes smaller, and the shape of the

curve tends to a parabolic behaviour. This behaviour is very similar to the N-MPD studied before in section 3.3.4.1.

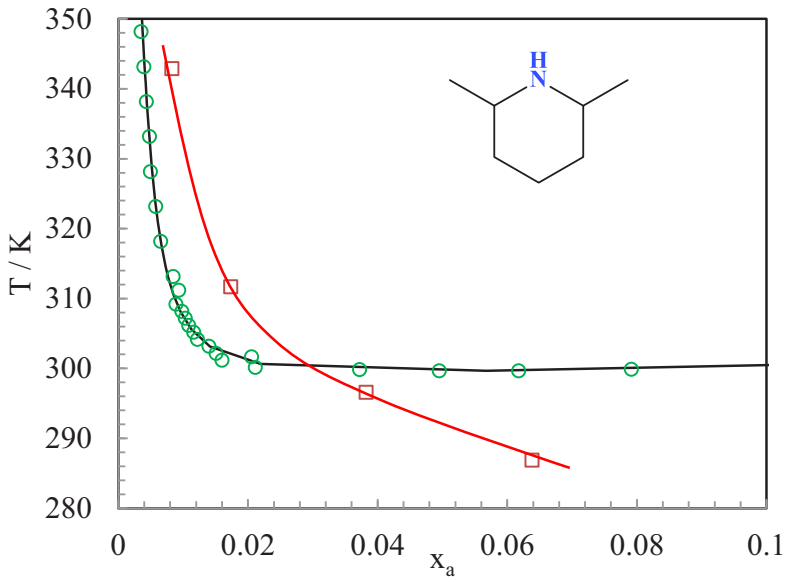

Figure 3-16: LLE temperature of 2,6-DPD versus molar fraction of amine at a constant loading charge 0.21: (□ CO_2 loaded aqueous 2,6-DPD solutions),(— data line to guide the eye), (○ unloaded aqueous 2,6-DPD solution),(— Scaling fit to unloaded data). The corresponding weight percent of solution from mole fraction are (5w$_a$% / x_a=0.0959), (10w$_a$% / x_a=0.0959), (20w$_a$% / x_a=0.0383), (30w$_a$% / x_a=0.0959)

When studying the effect of amine concentration versus mole fraction of amine, it is observable that at low amine mole fraction the CO_2 increases the LLE temperature while at higher mole fractions, its presence decreases the temperature, comparing to unloaded solutions. Once again, this trend is very similar to N-MPD results.

3.3.4.4 Water + N-EPD + CO_2

For these mixtures, most the CO_2 charged solutions, have been measured using the Thar Instruments equilibrium cell, and the static mixing unit. For the 5 w$_a$% (x_a=0.0959) solutions, some

experiments have also been performed using the flow mixing method, as shown in Figure 3-17 and Table 3-8.

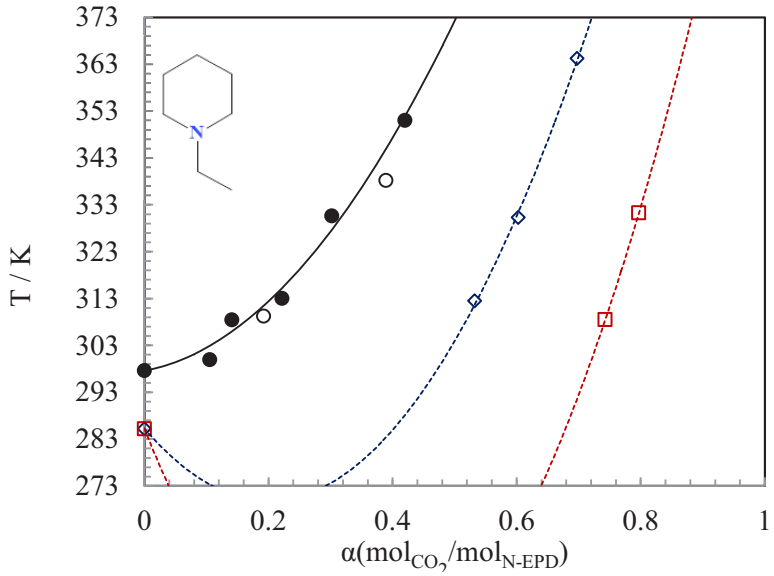

Figure 3-17: LLE temperature of N-EPD versus CO_2 loading charge. The solutions are prepared in a sample cylinder (○ 5 w_a%/, x_a=0.0083) (◇ 10 w_a%/ x_a=0.0173), (□ 20 w_a% x_a=0.0959) . The solution prepared by the flow mixing unit is labelled (● 5 w_a%/ x_a=0.0083), The lines are polynomial fits to the data. The size of the markers reflects the uncertainty in the data.

The binary N-EPD solutions have LLE values 35 K lower in temperature than N-MPD LLE. However, the trend is similar to N-MPD. For low amine concentrations (5 w_a%/x_a=0.0083) the behaviour is similar to the curve obtained for N-MPD with a 10w_a% (x_a=0.0198), concentration. For larger concentrations of N-EPD the temperatures of phase separation decrease a lot when added a small quantity of CO_2. Up to α=0.5 for 10 w_a% (x_a=0.0198) solutions of amine, and up to α=0.7 for 20 w_a% (x_a=0.0434), of amine, the solution demixes below room temperature. At higher loading charges for those two amine concentrations, the LLE temperature increases with a, giving the same tendency than N-MPD at 20 w_a% (x_a=0.0434) and 40 w_a% (x_a=0.1080)

To confirm the behaviour of the amine in presence of CO_2, experiments will be conducted in the laboratory, using the Sapphire cell equipment together with the static mixing unit.

3.3.4.5 Other Alkyl Piperidines

3-MPD and 4-MPD:

When adding CO_2 to 3-MPD and 4-MPD solutions, with in the molar fraction range of 0.009 to 0.108, the mixture remains fully soluble across the measurable temperature range. It was not possible to measure LLE temperature with our equipment. A 20 w_a% solution of 4-MPD was injected with CO_2 at a pressure of 0.1 MPa. The loading charge was below 0.05 with no phase equilibrium observed.

3,5-DPD

Solutions of 3,5-DPD precipitated white solids with the addition of CO_2 on a very large range of concentration. The white precipitate was measured using C^{13}, NMR the results of which show both carbonate and carbamate peaks. The spectra can be found at the end of this section in the appendix (Figure 3-18). This amine's phase equilibrium was then not studied with CO_2.

3.3.5 Discussion

3.3.5.1 Effect of the Position of the Methyl Group:

The effect of the position of the single methyl group on the LLE temperature can be conceived in terms of chemical equilibriums occurring in the solution. The reactions which are mainly considered in such mixtures are the formation of carbonates and bicarbonates. They exist for all the amine considered and the formation of carbamates that exist only for the secondary amines.

As N-MPD is a ternary amine, the N-MPD carbamates do not exist in solution and hydrogen bonding is much more limited. Adding CO_2 into the solution, profoundly changes the chemical

environment. The formation of carbonates and bicarbonates consume water and the increase of number of protonated N-MPD species. These ions cause a –salting out" effect which reduces the miscibility of the solution with low CO_2 loading concentrations. Increasing the CO_2 concentration consumes more neutral N-MPD thus leading to the rise in LLE temperature.

2-MPD, 3-MPD and 4-MPD are secondary amines. These amines are able to react with aqueous carbonate species to form carbamates in solution. They have previously been observed in solution using IR spectroscopy (Robinson et al., 2012) and Raman spectroscopy (Fandiño et al., 2016) for 3-MPD and 4-MPD. It can be assumed that carbamates play a significant role in the LLE. For 3-MPD and 4-MPD, where the quantity of carbamate is important, the solution is stabilized, and the phase separation was no longer observable within the range of temperature studied. The carbamate acts like a –stabilizer" or a –surfactant". 2-MPD is a secondary amine but the methyl group is in the 2-position, hindering slightly the Nitrogen group. As a result of this, 2-MPD form carbamates that are unstable, leading to a smaller effect on the stabilization of the mixture compared to 3- and 4- MPD.

3.3.5.2 Hindered Alkyl Piperidines:

2,6-DPD is an interesting case where the nitrogen group is located between the carbon atoms with bulky methyl groups attached, to the 2 and 6 positions. These substituents greatly hinder the accessibility to the nitrogen group. Nitrogen will be able to protonate but not react to form carbamates. The LLE temperatures of 2,6-DPD behaves similarly to N-MPD with the increasing loading charge and increasing weight percent of solutions. Inhibiting the carbamate reaction pathway of secondary amine produces a LLE pattern that mimics the tertiary amines.

3.3.5.3 Effect of the Alkyl Chain Length

N-EPD is a tertiary amine, and carbamates cannot be formed in solution. The CO_2 species are restricted to bicarbonates and carbonates. The effect is similar to N-MPD which has a sharper rise in temperature at high CO_2 composition. The effect of the chain length on tertiary amines is a pronounced drop-in of the LLE temperature.

3.4 Conclusions

The binary solutions of alkyl-piperidines correlate well with data from the literature. The structures of the substituted piperidines were compared with their LLE to identify the key traits of size, number and position of the functional groups. They are acknowledged as tertiary piperidine, secondary hindered piperidine and secondary piperidine.

Addition of CO_2 to the aqueous piperidine solutions has shown that there are significant trends when CO_2 is added to solution depending of the structure of the amine. Tertiary piperidines such as N-MPD and N-EPD, and strongly hindered amines such as 2,6-DPD show similar LLE behaviour in the presence of CO_2. Increasing the weight percent piperidine in solution causes the LLE to drop as CO_2 is added in low loading charges.

Secondary piperidines such as 3-MPD and 4-MPD are completely soluble in all proportions with the addition of CO_2, due to the presence of carbamate that stabilizes the solution. Secondary hindered amines like 2-MPD with unstable carbamates, show intermediate behaviour, increasing solubility across all concentration ranges with the addition of CO_2.

3.5 Appendix for Chapter 3

Table 3-3 : Mole fraction and measured liquid-liquid equilibrium temperatures of alkyl piperidines

x_a [a]	T [b] / K	x_a [a]	T [b] / K
3-MPD		4-MPD	
0.01347	354.8	0.01991	364.4
0.01842	345.5	0.02477	362.9
0.02356	341.8	0.02994	361.6
0.03170	340.1	0.03306	362.4
0.04262	339.9	0.03711	361.4
0.05018	340.0	0.04483	363.2
0.06100	340.1	0.04483	363.2
0.07900	340.5	0.04694	361.6
0.14243	355.4	0.06102	361.5
-	-	0.06334	360.0
-	-	0.07992	362.3
-	-	0.09429	365.2
2,6-DPD		3,5-DPD	
0.02059	301.7	0.01102	312.2
0.03726	299.8	0.01476	304.3
0.04956	299.7	0.01621	302.8
0.06181	299.7	0.13208	275.7
0.07918	299.9	0.14498	279.7
0.10074	300.1	0.15353	283.4
0.11879	300.8	0.20938	306.3
0.13915	301.8	0.27198	333.5
0.15864	303.0	-	-
0.17471	303.8	-	-
0.18520	304.7	-	-
0.19797	305.5	-	-
0.20687	306.3	-	-
0.21240	306.8	-	-
0.22354	307.9	-	-
0.37901	323.2	-	-
0.49058	341.7	-	-

N-EPD		2-EPD	
0.00832	297.8	0.00380	344.2
0.01741	285.2	0.00820	303.2
0.02039	283.6	0.01200	289.4
0.02545	282.5	0.01620	284.7
0.02703	282.6	0.02030	283.2
0.02833	282.3	0.02490	282.7
0.03275	282.2	0.02940	279.7
0.03311	282.2	0.03410	281.0
0.04258	281.8	0.03990	281.1
0.04586	281.7	0.05020	281.7
0.04969	281.6	0.05080	281.2
0.05006	281.6	0.10430	284.2
0.05386	281.6	0.15140	290.4
0.05403	281.5	0.19890	298.7
0.06073	281.3	0.25710	307.7
0.06925	281.6	0.29990	316.8
0.07984	281.7	0.40270	337.4
0.08994	281.8	0.50180	348.2
0.10413	281.9	0.68300	348.2
0.12887	282.5	-	-
0.16181	283.7	-	-
0.21938	286.1	-	-

a : uncertainty in the mol fraction σxa=0.00005

b : uncertainty in the temperature σT=0.5 K

Table 3-4: Scaling law parameter for aqueous alkyl piperidine solutions.

Parameters	N-MPD	2-MPD	3-MPD	4-MPD	2,6-DPD	3,5-DPD	N-EPD	2-EPD
LN $x_{1,min}$						-6.0749		
LN $x_{2,min}$						-0.0274		
C1						27.8198		
C2						-2.9763		
$T_{1,\min}$						355.501		
$T_{2,\min}$						206.1471		
Error 1						0.0102		
Error 2						0.0312		
LN x_{cs}		-2.8967	-3.0118		-3.0180		-2.6650	-2.8238
T_{cs}		342.9953	339.95		299.65		281.47	280.4152
A1		82.5784	7.5838		-1.3976		-2.2519	-0.7739
A2		-3.8276	-4.4052		-0.3417		-0.7043	0.0008
A3		5.8572	-13.1067		2.1548		2.1332	1.6211
B1		-4.8877	-4.6621		1.3658		6.4786	0.1467
B2		-0.3435	-0.2186		-5.5141		-6.0300	-4.9207
B3		5.8572	4.8114		-1.2272		5.8971	-1.1775
Error		0.0262	0.0892		0.0592		0.1683	0.054
LN X_U	-2.54211			-2.37086				
LN X_L	-1.21369			-3.05336				
T_U	316.1404			462.65				
T_L	548.1424			358.05				
C1	-3534.96			-2598.39				
C2	-4.7559			-1.6302				
C3	9.071			4.6842				
D1	-2913.82			616.6778				
D2	-0.0469			-0.061				
D3	3.796			-1.9961				
Error	0.1992			0.1604				

Table 3-5: LLE of aqueous N-MPD solutions with CO_2 measured with the sapphire equilibrium cell and the Thar Instruments equilibrium cell.

w_a%	α		$\sigma\alpha$	T	p
	mol $_{CO_2}$/mol $_{N\text{-}MPD}$			K	MPa
	0		-	320.2	-
	0.189		0.009	322.2	0.45
10.00%	0.467		0.003	363.4	0.48
	0.385		0.002	343.7	0.54
	0.288		0.002	329.9	0.52
	0		-	317.2	-
	0.111		0.011	309.8	0.52
	0.137		0.001	308.0	0.52
	0.178		0.009	306.9	0.51
	0.326		0.016	304.7	0.50
	0.33		0.017	303.3	0.51
	0.445		0.022	306.3	0.50
	0.484		0.002	308.5	0.52
20.00%	0.484		0.002	308.2	1.15
	0.485		0.001	308.4	2.12
	0.54		0.027	316.7	0.50
	0.63		0.031	326.2	0.52
	0.154	c	0.006	308.4	0.51
	0.72	c	0.014	341.3	0.51
	0.593	c	0.012	322.9	0.52
	0.456	c	0.014	306.5	0.53
30.00%	0.178		0.009	295.3	0.52
	0		-	317.2	-
	0.057		0.01	302.3	0.49
	0.089		0.01	289.0	0.51
	0.139		0.01	284.0	0.52
	0.141		0.01	281.8	0.51
	0.17		0.01	280.6	0.53
40.00%	0.226		0.01	274.7	0.51
	0.657		0.004	277.1	1.04
	0.717		0.01	279.0	1.09
	0.762		0.01	289.8	1.06
	0.774		0.01	296.3	1.14
	0.808		0.01	301.3	1.15

a : uncertainty in the temperature σT=0.5 K

b : uncertainty in the pressure σp=0.02 MPa

c : Thar equilibrium cell

Table 3-6: LLE of aqueous 2-MPD solutions with CO_2 measured with the Thar Instruments equilibrium cell

w_a%	α	$\sigma\alpha$	T^a	p^b
	mol $_{CO_2}$/mol $_{2\text{-MPD}}$		K	MPa
10.00%	0.194	0	354.8	0.5
15.00%	0.202	0.002	347.5	0.52
	0		343.2	
	0.112	0.001	343.3	0.53
	0.188	0.001	346.3	0.53
20.00%	0.261	0.001	354.8	0.53
	0.338	0.001	367.9	0.53
	0.426	0.001	383.6	0.51
25.00%	0.207	0.002	352.4	0.52
30.00%	0.209	0.003	361.7	0.52
	0		344.2	
	0.115	0	358.5	0.53
40.00%	0.188	0.003	374.0	0.5
	0.201	0.007	377.3	0.53

a : uncertainty in the temperature σT=0.5 K

b : uncertainty in the pressure σp=0.02 MPa

Table 3-7: LLE of aqueous 2,6-DPD solutions with CO_2 measured with the sapphire equilibrium cell

w_a%	α	$\sigma\alpha$	T	p
	mol CO_2/mol 2,6-DPD		K	MPa
5.00%	0.0000	-	317.7	-
	0.1403	0.0029	333.5	0.14
	0.1158	0.0024	335.6	0.12
	0.2274	0.0047	342.9	0.13
	0.2592	0.0054	363.8	0.25
	0.3449	0.0072	378.7	0.33
10.00%	0.0000	-	301.2	
	0.1066	0.0011	306.7	0.225
	0.2073	0.0022	311.7	0.229
	0.2690	0.0029	325.8	0.523
	0.4042	0.0044	348.1	0.525
	0.4763	0.0051	364.4	0.493
20.00%	0.0000	-	300.2	
	0.0580	0.0003	299.3	0.25
	0.2100 [c]	0.0150	296.6	0.99
	0.2477	0.0015	296.1	0.51
	0.3505	0.0021	300.8	0.516
	0.5451 [c]	0.0327	322.1	0.515
30.00%	0.0000	-	298.5	
	0.0953	0.0004	289.9	0.55
	0.1285	0.0006	289.0	0.53
	0.2162	0.0010	286.9	0.53

a : uncertainty in the temperature σT=0.5 K

b : uncertainty in the pressure σp=0.02 MPa

c: static mixing unit.

Table 3-8: LLE of aqueous N-EPD solutions with CO_2 measured with the static mixing unit and Thar cell.

w_a%	α		$\sigma\alpha$	T^a	p^b
	mol CO_2/mol N-EPD			K	MPa
	0			297.8	
	0.1055		0.0009	300.1	0.20
	0.1412		0.0012	308.6	0.13
5	0.2219		0.0019	313.2	0.20
	0.3024		0.0025	330.8	0.29
	0.4204		0.0035	351.2	0.21
	0.1924	C	0.0001	309.4	0.20
	0.3894	C	0.0002	338.4	0.50
	0.0000		-	285.4	
10	0.5327	C	0.0003	312.7	0.96
	0.6029	C	0.0004	330.5	0.72
	0.6975	C	0.0004	364.4	0.72
	0.0000		-	285.4	
20	0.7430	C	0.0004	308.7	0.50
	0.7972	c	0.0005	331.5	0.47

a : uncertainty in the temperature σT=0.5 K

b : uncertainty in the pressure σp=0.02 MPa

c : static mixing unit.

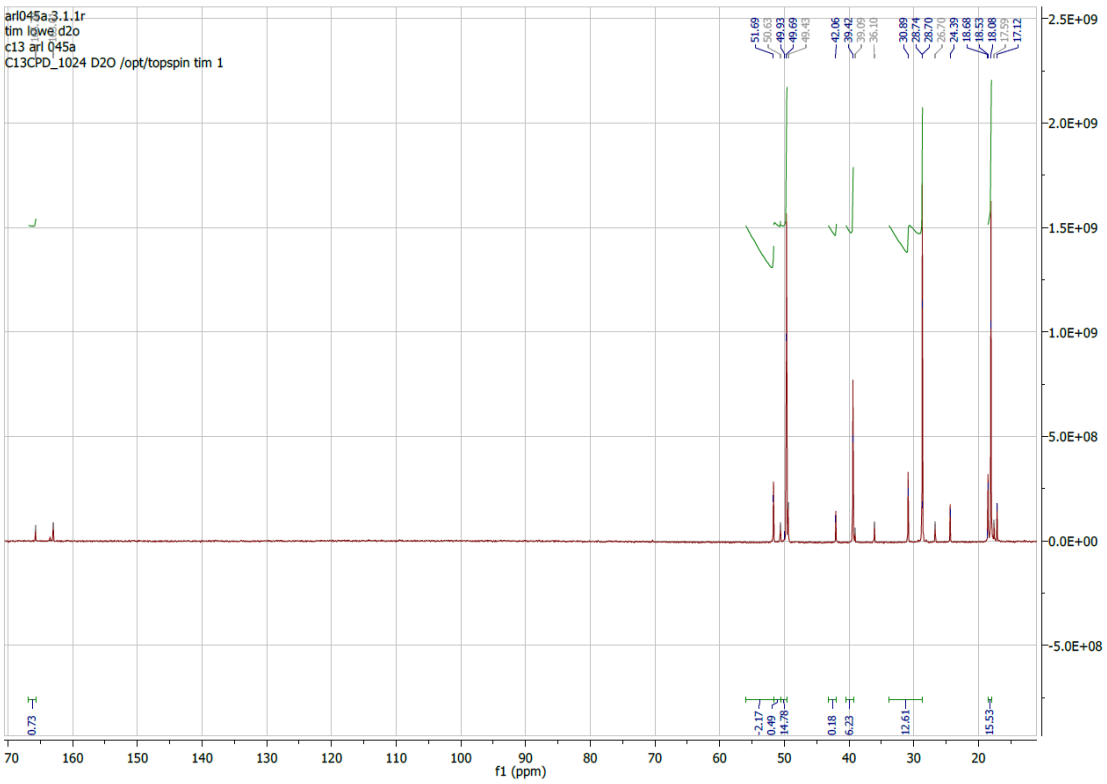

Figure 3-18: Carbon 13 NMR spectra of precipitated 3,5-dimethylpiperidine in D_2O solvent. The chemical shifts between 10 and 55 ppm are part of the ring structure. The down field shifts between 160 and 170 ppm are carbonate, bicarbonate and carbamate salts.

4 Thermodynamic Properties of Alkyl-Piperidines.

4.1 Introduction

There are few thermodynamic data related to the aqueous solutions of alkyl piperidine and their excess properties. In the recent past the lab has previously investigated the excess properties of N-MPD and 2-MPD (Coulier et al., 2010; Coulier et al., 2015). The work presented in this chapter expands the thermodynamic data of the alkyl piperidine in water mixtures. Each of the alkyl piperidine thermodynamic data collected is compared to molecular structure into find structure property relations.

4.2 Chemicals and Solution Preparation

The chemicals their purities and supplier information are listed in Table 4-1. Gas cylinders containing nitrogen gas and carbon dioxide gas was purchased from Air Products. Water was deionized and then degassed under vacuum at a temperature of 40˚C.

Aqueous amine solutions were prepared by mass; with solution volumes below 30 mL weighed on an analytical balance and volumes over 150 mL were weighed using a top loading balance. The standard deviations in the molar fractions of solutions are less than ± 0.00005. The solutions were blanked with N_2 gas to minimise exposure to atmospheric CO_2. The solutions were stirred overnight, with a magnetic stir bar, to ensure a homogenous solution prior to injection into instruments.

4.3 Experimental Instrumentation.

4.3.1 Densities of Amine Solutions

4.3.1.1 Atmospheric Pressure Measurements

The densities of solutions of amines and pure liquids were measured, at atmospheric pressure, using a Sodev-D02 and D03 picker type vibrating tube densitometers (Picker et al., 1973). The operation

of these densitometers has been rigorously described in the past to measure solution densities of aqueous solutions (Visser et al., 1977; Perron et al., 1993; Ballerat-Busserolles et al., 2000; Afzal et al., 2008; Coulier et al., 2010; Coulier et al., 2016). For these experiments the temperature of the densitometer cell was thermally regulated by a Julabo F12 model cytostatic circulation bath. The temperature is controlled to a precision of ± 0.03 K. The densitometer was operated as a static cell, using a syringe to inject the liquids into the U-tube. The period of vibration is picked up using a digital frequency meter and the data is transferred to a computer and is plotted as a function of time as shown in Figure 4-1.

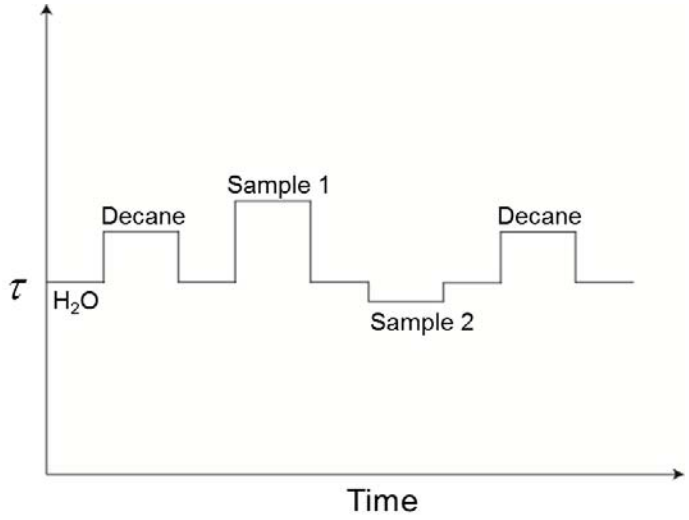

Figure 4-1: Example of calibration and measurement of the period of vibration.

The density of liquids relative to water are related to the period of vibration by Hooke's Law as applied to a harmonic oscillator,

$$\left(\rho_l - \rho_w\right) = k_\rho \left(\tau_l^2 - \tau_w^2\right) \qquad \textbf{Eq 4-1}$$

where ρ_l is the density of the liquid; ρ_w is the density of water; τ_l and τ_w are the periods of vibration for the liquids and water; and k_ρ is the calibration of the cell at the specific temperature. The calibration constant was calculated using deionized and degassed water (Wagner and Pruß, 2002), octane (Span and Wagner, 2003b), decane (Lemmon and Span, 2006) and dodecane (Span and Wagner, 2003a) with their reference densities take from the NIST data base. The calibration was performed for each temperature. The calibration of the cell and measurement of the solutions were performed in a sequence of water, solution/calibration liquid then water again for each temperature. The standard deviation of the calibration constants, for example, at 298.15 K is 7.0874×10^{-7} with a standard deviation of $\pm 4 \times 10^{-11}$. The standard deviation in the period of vibration for water 2942.727 is ± 0.002**.**

The experimental procedure for the measurements were as followed. The degassed deionized water was injected into the instrument using a syringe connected to an injection line. Once the period of vibration was observed to reach stable plateau it was recorded. The amine solution was then injected. Once again the period of vibration was measured once the signal reached a stable plateau. The densitometer tube was rinsed, 3 times, with acetic acid, followed by ethanol finishing with water. The period of vibration of water was compared to the previous water measurement to verify that the cell is clean. The 278.15 K measurement of N-EPD was done using ice cooled syringes with the injection line submerged in the ice as well. This was done to prevent demixing before injection into the densimeter tube. The procedure was repeated for each measurement and the same procedure was used to measure the period of vibration for the calibration solutions.

4.3.1.2 Pressure and Temperature Dependant Measurements

The fluid densities of aqueous amine solutions and pure liquids at the pressures of 0.5 and 1.0 MPa were determined using an Anton Paar External Measuring Cell DMA HPM densitometer. This

densitometer follows the same operation principle that the previously mentioned Sodev densitometer. The cell was enclosed within polystyrene insulation and then placed in a wooden container and kept inside a fume hood. A cytostatic circulation bath, a Julabo F12 model, regulated the temperature of the measuring cell using Julabo Thermal H2OS oil. Liquids are injected into the cell using an Azura P4.1S isocratic pump at a constant flow rate of 0.200 mL min^{-1} through stainless steel tubing. Pure liquids are injected into the measurement cell via 25 mL injection loop placed in between the pump and the densitometer cell to protect the pump from corrosion. The connection between the pump, injection loop and the densitometer cell was made using a 6 port valve. A PMP 4010 pressure transducer with DRUCK DPI 282 digital readout is connected to the end of the flow line after the densitometer cell. The pressure is measured to approximately ±0.005 MPa. The pressure in the cell is maintained constant using a 1L stainless steel sample cylinder filled with N_2 gas located at the end of the circulating line.

4.3.2 Differential Scanning Calorimeter

The heat-capacity-density products, $c_p\rho$, of amine solutions and pure amines were measured using a heat-flux differential-scanning-microcalorimeter from SETARAM (microSC). The operation principles for this method have been rigorously tested by (Ballerat-Busserolles et al., 2000) and many different measurements have been completed in the lab of Earl Woolley (Woolley, 2007). The experimental procedure using this calorimeter has been previously published by (Coulier et al., 2015). Here, a quick review of the experiment is presented.

The calorimeter is a Calvet type, of calorimeter, where the heating and cooling of the calorimeter block is performed by peltier elements. Detection of the heat flux, J_q, between the reference and sample cells is made using ~~"3~~D Calvet Sensors" which surround the calorimeter wells. To measure $c_p\rho$ of the sample, calorimetric cells with a 1 mL internal volume were placed in the wells and enclosed within an

insulated box. Once filled and isolated the experiment begins with a 20 min isothermal step at 278.15 K. The scan rate was set to 0.5 K·min^{-1}, to reach the final temperature of 333.15 K. The initial value of J_q when the cells filled with an identical compound is equal to the structural differences between the two calorimeter cells and their environments. The base line experiment has both cells filled with N_2 gas the heat flux, J_{N_2}, is represented by the following expression.

$$J_{N_2}k_c = \left([\{c_{p,N_2}\cdot\rho_{N_2}\}+\{c_{p,cell}\cdot\rho_{cell}\}]_{sample} - [\{c_{p,N_2}\cdot\rho_{N_2}\}+\{c_{p,cell}\cdot\rho_{cell}\}]_{reference}\right) \quad \textbf{Eq 4-2}$$

The exact values of $c_{p,cell}\rho_{cell}$ for sample and reference well are unknown and are not necessary for the final calculation. The difference between the $c_{p,N_2}\rho_{N_2}$ in each cell are equal to 0. The value of k_c is a calibration constant relating the thermal flux to the difference in the cell. In an experiment with a sample solution, the reference cell is filled with N_2 gas while the sample cell is filled using a 5 mL chromatography syringe to fill the cell from the bottom up. The excess fluid exits the cell via the top of the cell and is collected by a waste container. The relative difference between $c_p\rho$ of solution and nitrogen is related to the difference in heat flux, J_s, is related to equation 4-3.

$$J_s k_c = \left([\{c_{p,s}\cdot\rho_s\}+\{c_{p,cell}\cdot\rho_{cell}\}]_{sample} - [\{c_{p,N_2}\cdot\rho_{N_2}\}+\{c_{p,cell}\cdot\rho_{cell}\}]_{reference}\right) \quad \textbf{Eq 4-3}$$

By subtracting equations 4-2 with equation 4-3, an expression is created for the heat-capacity-density product of solution and nitrogen without any extra information relating to the differences in the cell's structure or environment.

$$\left(J_s - J_{N_2}\right)k_c = \left(\left[c_{p,s} \cdot \rho_s\right]_{sample} - \left[c_{p,N_2} \cdot \rho_{N_2}\right]_{sample}\right) \quad \textbf{Eq 4-4}$$

Dividing by the solution density, ρ_s which is measured using the Sodev densitometer yields an expression for the specific heat capacity of solution, c_{ps}.

$$c_{p,s} = \frac{(J_s - J_{N_2})k_c}{\rho_s} + \frac{c_{p,N_2} \cdot \rho_{N_2}}{\rho_s} \quad \textbf{Eq 4-5}$$

To calibrate the calorimeter, the equations of state for water and nitrogen are taken from the NIST data base. The accuracy of the calibration constant was tested using octane. The values are listed in Table 4-2.

4.3.3 Enthalpies of Mixing Experiments

The heats of mixing amine and water were measured using a custom designed flow-mixing cell, constructed to fit in a SETARAM BT2.15 heat conduction differential calorimeter. The experimental setup has a long history and has been described in detail in the work by Mathonat (Mathonat et al., 1994; Mathonat et al., 1997), Koshel (Koschel et al., 2006) and Arcis (Arcis et al., 2007; Arcis et al., 2011; Arcis et al., 2012b; Arcis et al., 2012a). This mixing cell was housed in the calorimetric block, where the heats of mixing were detected by Tian-Calvet thermopiles. The two fluids were injected into the mixing unit supplied by two ISCO model 100 DM high-pressure syringe pumps. The syringe pumps were regulated at a constant temperature of 303.15 K. The flow line was constructed with stainless steel of 1.6 mm outer diameter and 1.0 mm inner diameter. The design of the mixing cell is the same as described by Arcis et al. The stainless steel tubing was placed in contact with one another in a small chamber at

the bottom of the cell in Figure 4-2. Here the two input tubes and 2.8 m mixing chamber were silver soldered together. The quantitative mixing occurs in this 2.8 M long mixing chamber which consisted of a (1.6 mm o.d.) stainless steel tube placed in good thermal contact with the inner wall of the confinement cylinder a stainless steel tube of 18.7 mm i.d., and 80mm in height. The system pressure was maintained constant up to a pressure of 1.5 MPa using a 1L stainless steel sample cylinder filled with N_2 gas. The pressure of the flow line was measured using a PDCR 900-1021 pressure transducer, placed on the solution flow line. The pressure in the flow line is measured to be within ± 0.02 MPa. The temperature of the calorimeter was controlled using a SETARAM G11 electronic control device.

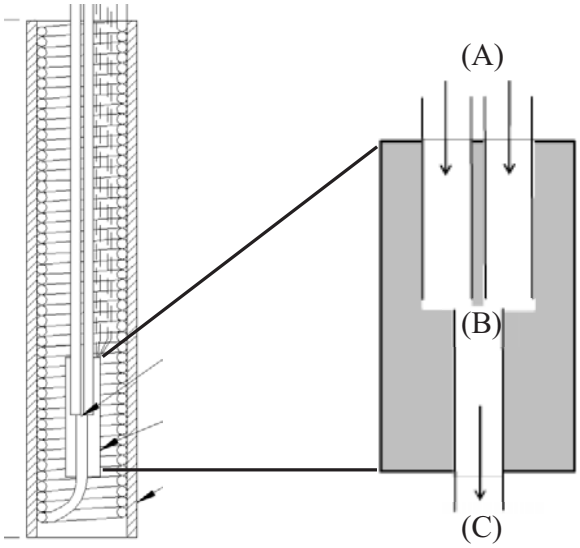

Figure 4-2: Diagram of the mixing chamber with zoom up to the mixing point. (A) stainless steel injection tubes (B) mixing point of the cell (C) mixing chamber made of stainless steel tubing.

4.3.4 Cell Calibration and Solution Measurement

4.3.4.1 Mixing Calorimeter Cell Calibration

The calibration of the BT2.15 calorimeter is representative of the heat flow from the mixing cell to out of the well, depending on thermal conductivity, contact between the mixing cell and the calorimeter well and thermal leaks. The preheaters are first adjusted to give a baseline which is independent of flow rate at the set temperature of the calorimeter. Water was used and the flow rate remained linear up to 0.6 mL min^{-1}. The chemical reference data used for calibration came from Ott *et al.* (Ott, et al., 1986), who rigorously measured the excess enthalpy, H^E, of ethanol, {ethanol-water} systems from 298.15 K to 473.15 K for a pressure from 0.4 to 15 MPa (Ott, et al., 1986; Ott, et al., 1986; Ott et al., 1987). The advantage of using ethanol water mixtures as a calibration fluid is that it is inexpensive to purchase in it anhydrous form, stable, non-toxic and easy to dispose of. The excess enthalpies, H^E, of mixing are insensitive to small amounts impurities and the accuracy is equal to or better than 1%.

The cell constant is calculated using the following relationship:

$$k_h = \left(S_M - S_{BL}\right) / H^E \dot{n}_t \qquad \textbf{Eq 4-6}$$

where k_h is the cell constant, S_{BL} and S_M are the signal base line for thermal flux (in mV) with pure water moving through the mixing cell and the signal from mixing between two fluids respectively. The total molar flow rate, $\dot{n}_t$, is calculated from the volumetric flow rate, $\dot{v}$, density of the fluid, ρ, and molecular weight, M, using the following equation:

$$\dot{n}_t = \frac{\rho_w \dot{v}_w}{M_w} + \frac{\rho_{eth} \dot{v}_{eth}}{M_{eth}} \qquad \textbf{Eq 4-7}$$

Ethanol was added into the flow system via the injection loop. The water and ethanol mixing signal, S_M, reaches a plateau at equilibrium in the calorimeter after an average time of 15 minutes. Densities of ethanol and water were taken from the NIST database. Multiple data points were measured between the mole fraction ranges of 0.2 to 0.6. The cell constants for each the measurement were averaged together and the relative standard errors are calculated to a value better than 3%.

4.3.4.2 Measuring Excess Enthalpies

To calculate the amount of amine in solution during the measurement, equation 4-7 can be redefined in terms of alkyl piperidine, *a*.

$$\dot{n}_t = \frac{\rho_w \dot{v}_w}{M_w} + \frac{\rho_a \dot{v}_a}{M_a} \qquad \textbf{Eq 4-8}$$

The densities of the pure substances are taken from the densitometer measurements made in section 4.2.1. The excess enthalpy H^E is then derived from equation 4-6.

$$H^E = \left(S_M - S_{BL}\right) / k_h \left(\dot{n}_a + \dot{n}_w\right) \qquad \textbf{Eq 4-9}$$

4.4 Results and Discussion

4.4.1 Densities and Excess Molar Volumes

As the density of the solutions have to be determine only for homogeneous solutions, the range of temperature and concentration covered depends on the liquid-liquid phase diagrams of the binary mixtures {water+amine}. According to the phase diagrams described in section 3.3.2, 3-MPD and 4-MPD densities were measured between 288.15 K and 328.15 K with a 10 K interval, on the whole range of concentration. They are listed in Table 4-3 and Table 4-4 respectively. 2,6-DPD was measured between 288.15 K and 318.15 K and are listed in Table 4-5. 3,5-DPD was measured between the temperature range of 288.15 K to 308.15 K and are listed in Table 4-6. N-EPD was measured from 278.15 K to 298.15 K as the temperature of phase separation is very low and is listed in Table 4-7. The density experiments were conducted at atmospheric pressure. The standard deviations for multiple measurements of the pure substances are at most ± 0.00008 g cm^{-3}. The uncertainty in the excess volumes is equal to ± 0.02 mol cm^{-3}.

4.4.1.1 Molar Volumes of Pure Alkyl Piperidine

The molar volumes of the pure substances, V^*, are plotted in Figure 4-3. The piperidine data was taken from the work of (Afzal et al., 2008). N-MPD and 2-MPD data were taken from the work of (Coulier et al., 2010). Figure 4-3 shows the temperature dependence of the molar volumes, V^*. The curves remain parallel to each other independent of the amine considered. Also, it has to be observed that the volumes obtained for the substituted amines are larger than for piperidine.

The molar volume of 2-MPD, 3-MPD and 4-MPD are mostly similar. The addition of the methyl group to the N position has the biggest effect on the molar volumes: V^* is 5cm^3mol^{-1} larger when the methyl group is branched on the nitrogen. In general, the methyl group affects the packing structure of

the liquid. The difference in pure molar volumes of N-MPD versus 2-MPD, 3-MPD and 4-MPD shows that hydrogen bonding has a larger effect in reducing the molar volume of the liquid.

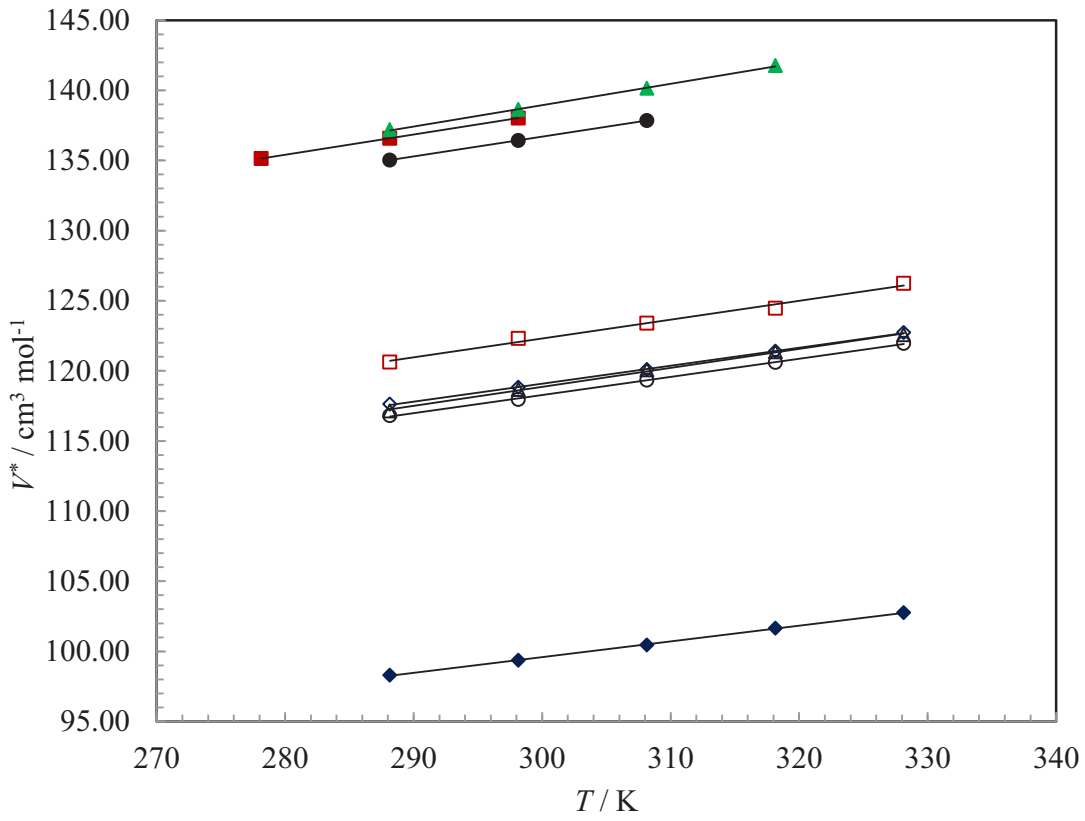

Figure 4-3: Comparison of the molar volumes of pure alkyl-piperidines: ◆ Piperidine (Afzal et al., 2008), ○ 3-MPD, △ 2-MPD (Coulier et al., 2010), ◇ 4-MPD, □ N-MPD (Coulier et al., 2010), ● 3,5-DPD, ■ N-EPD, ▲ 2,6-DPD. Solid lines are polynomial fits. The size of the markers reflects the uncertainty of the data.

The molar volumes of 2,6-DPD, 3,5-DPD and N-EPD are similar, and larger than the methyl ones. This is linked to the molar mass of the piperidine that is larger in the case of ethyl and dimethyl substituents compared to methyl ones. Nevertheless small differences can be seen between those amines. 3,5-DPD exhibits a volume slightly smaller than 2,6-DPD. For this amine, the access to nitrogen is not restricted by the methyl groups around the nitrogen and hydrogen bonding can be formed. The addition of methyl groups to the 2 and 6 positions restricts intermolecular hydrogen bonding.

When comparing N-EPD and N-MPD, the increase of the chain length increases the molar volume of the piperidine, proportionally to the molar mass of the molecule.

4.4.1.2 Excess Volumes of Aqueous Alkyl Piperidines

The excess volumes of the alkyl-piperidines are calculated using the following equation:

$$V^E = V - x_a V^* + x_w V^* = \frac{\left(x_w M_w + x_a M_a\right)}{\rho_s} - \frac{x_w M_w}{\rho_w^*} - \frac{x_a M_a}{\rho_a^*} \qquad \textbf{Eq 4-10}$$

Where x_w and M_w are the molar fraction and molecular mass of water, x_a and M_a are the molar fraction and molecular weight of amine. ρ_w^*, ρ_a^* and ρ_s are the densities for pure water, pure amine and solution respectively.

The excess properties at each temperature were fitted to the Redlich-Kister equation, given in equation 4-11:

$$Y^E = x_w x_a \sum_k A_k \left(x_w - x_a\right)^k \qquad \textbf{Eq 4-11}$$

Where Y^E is the excess molar property, in this case V^E, A_i are the regression parameters.

The Levenberg-Marquardt non-linear least squares algorithm within the commercial software package SigmaPlot 11® was used to fit the polynomials. The parameters are listed in Table 4-9.

Figure 4-4 to Figure 4-8 show the excess volumes and Redlich-Kister fits for the alkyl piperidines measured. One should note that for 2,6-DPD, 3,5-DPD and N-EPD, some domains of concentration have not been studied. In this domain and for the highest temperatures the solutions are

demixed, and the density cannot be measured. The straight line shown in the figures do not represent a fit but is only the connection between the last measurable points. The curves are represented by Redlich-Kister type polynomials.

For all the amine+water solutions studied the excess molar volume doesn't change significantly with temperature. However, as the temperature of the solution is increased the excess volume becomes less negative, with a maximum change of 0.2 cm^3mol^{-1} in 40 K variation. The local minima for the excess molar volumes do not move with increasing temperature, and is located around x_a=0.45.

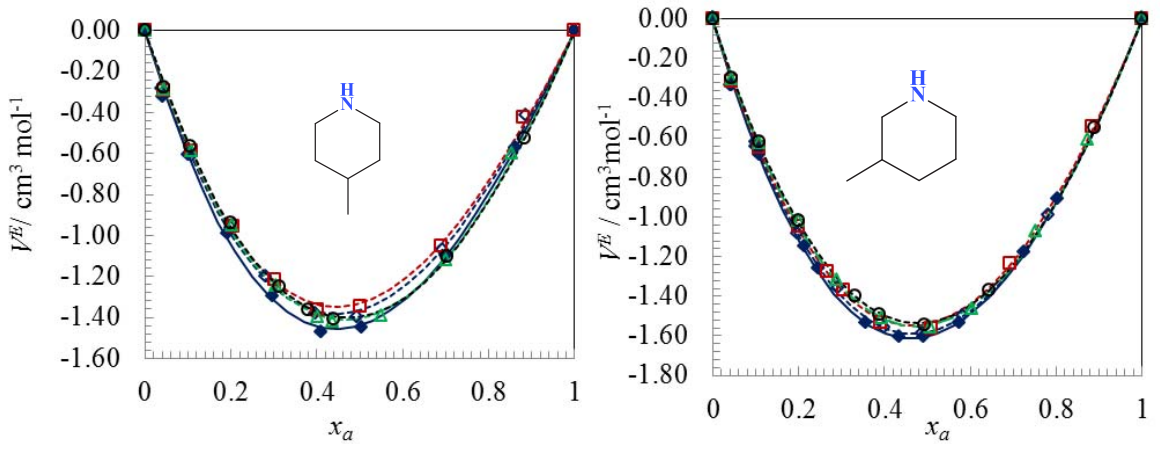

Figure 4-4 and Figure 4-5: Excess molar volumes of 4-MPD (left) and 3-MPD (right) measured at atmospheric pressure, with Redlich Kisters fits to the data. (◆,—— 288.15 K) (◇, - - - 298.15 K) (□,- - - 308.15 K) (△,- - - 318.15K) (○,- - - 328.15 K). The sizes of the markers reflect the uncertainty in the data.

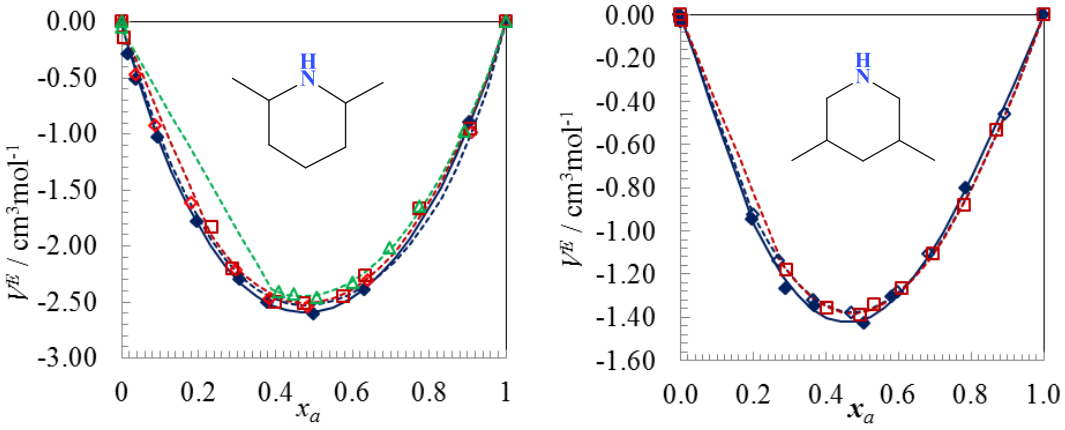

Figure 4-6 and Figure 4-7: Excess molar volumes of 2,6-DPD (left) and 3,5-DPD (right) measured at atmospheric pressure with Redlich Kisters fits and polynomial fits to the data. (◆,— 288.15 K) (◇, - - - 298.15 K) (□,- - - 308.15 K) (△,- - - 318.15K). The size of the markers reflects the uncertainty in the data.

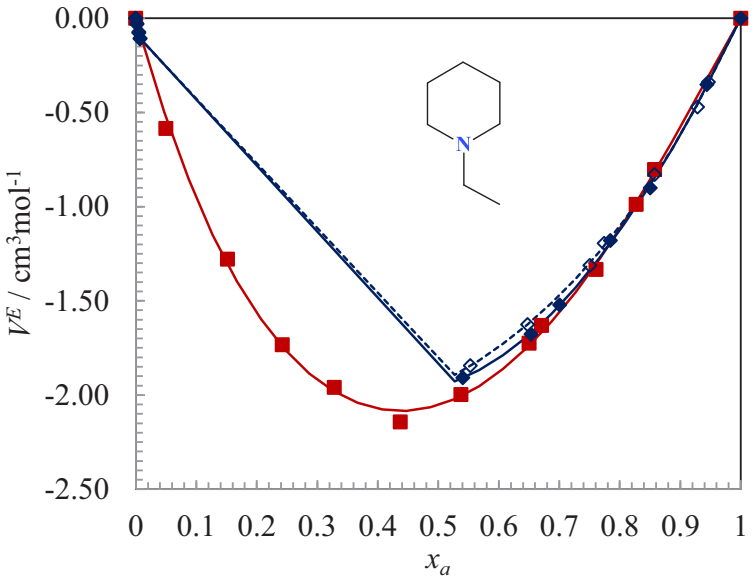

Figure 4-8: Excess molar volumes of N-EPD measured at atmospheric pressure, with polynomial fits to the data. (■, - - - 278.15 K) (◆,— 288.15 K) (◇, - - - 298.15 K). The size of the markers reflects the uncertainty in the data.

The partial molar property of each component, $\overline{V}_i$, is expressed by the following equation:

$$\overline{V}_i = \left(\frac{\partial V}{\partial n_i}\right)_{T,p,n_j} \qquad \textbf{Eq 4-12}$$

Where V is molar volume of the liquid and n_i is the number of mole of the component i. To calculate the partial molar volume of the amine $\overline{V}_a$ equations 4-12 in combination with equation 4-10, expressed as.

$$\overline{V}_a = V^E + V_a^* - x_w \left(\frac{\partial V^E}{\partial x_w} \right)_{T,p} \qquad \textbf{Eq 4-13}$$

By combining this equation with the Redlich-Kister equation, 4-13 with respect to the water component, the following relations are obtained:

$$\overline{V}_a = V_a^* + x_w^2 \sum A_k \left(1 - 2x_w\right)^{k-1} + 2x_w^2 \left(1 - x_w\right)^2 \sum A_k \left(k - 1\right)\left(1 - 2x_w\right)^{k-2} \qquad \textbf{Eq 4-14}$$

$$\overline{V}_w = V_w^* + \left(1 - x_w\right) \sum A_k \left(1 - 2x_w\right)^{k-1} - 2x_w \left(1 - x_w\right) \sum A_k \left(k - 1\right)\left(1 - 2x_w\right)^{k-2} \qquad \textbf{Eq 4-15}$$

These equations help in determining the partial molar volumes at infinite dilution $\overline{V}^{\infty}$ with respect to the amine and water using the following equations:

$$\overline{V}_a^{\infty} = V_a^* + \sum A_k \left(-1\right)^k \left(x_a \longrightarrow 0\right) \qquad \textbf{Eq 4-16}$$

$$\overline{V}_w^{\infty} = V_w^* + \sum A_k \left(x_w \longrightarrow 0\right) \qquad \textbf{Eq 4-17}$$

Subtracting the pure values from both sides of equation 4-15 and 4-16 results in the partial molar excess volumes, $\overline{V^E}^{\infty}$.

$$\overline{V^E}_a^{\infty} = \sum A_k \left(-1\right)^k \left(x_a \longrightarrow 0\right) \qquad \textbf{Eq 4-18}$$

$$\overline{V^E}_w^{\infty} = \sum A_k \left(x_w \longrightarrow 0\right) \qquad \textbf{Eq 4-19}$$

The infinite dilution properties for the alkyl piperidines have been calculated only for temperatures were the amine is fully miscible with water. The values are found in Table 4-9.

The temperature dependant infinite dilution properties 3,5-DPD and N-EPD were not measured. Their critical solution temperatures are too low and prevent the measurement of complete excess volume curve.

The infinite dilution values of 3-MPD are almost constant on all the range of temperature studied, while the value for 4-MPD and 2,6-DPD show a linear increase with increasing temperature. The increase in partial molar volume with increasing temperature can be interpreted as destruction of the solution structure (Patterson, 1994). Hepler theorised that the water structure is related to the second derivative of the infinite dilution partial molar volumes, $\partial\overline{\mathrm{V}}^{\infty 2}/\partial^2\mathrm{T}$. Linear equations can be fitted to the values 3-MPD and 4-MPD. Since the second derivative in both cases are zero the amines are neither structure making or breaking solutes in solution (Hepler, 1969).

The magnitude of the excess volumes and their minima were compared to the parent piperidine molecule at 298.15 K (Afzal et al., 2008) and are listed in Table 4-10. The exception to this comparison is the N-EPD which uses the temperature of 278.15 K.

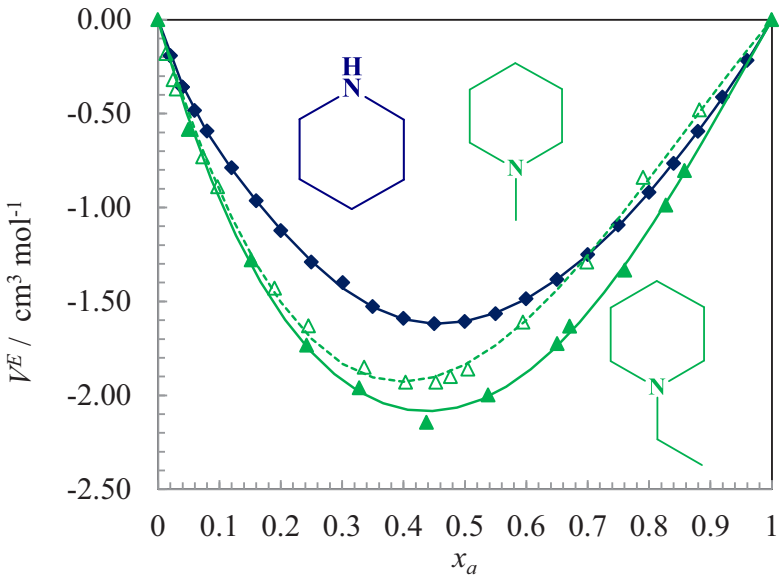

Figure 4-9: Excess molar volumes of tertiary alky piperidines and piperidine at 298.15 K. ◆ Piperidine (Afzal et al., 2008) N-MPD△ (Coulier et al., 2010) N-EPD▲ (278.15 K). The size of the markers reflect the uncertainty of the data

In Figure 4-9 it is observed that adding an alkyl group to the nitrogen of piperidine increase the magnitude of the excess volume. For the reference molecule of piperidine the curve minima of -1.61 is found at a molar fraction of 0.455. The addition the methyl group shifts the curve minima to a molar fraction value of 0.40 and a V^E magnitude of -1.93 cm^3 mol^{-1}. Increasing the chain length from methyl to ethyl increases the V^E to -2.08 cm^3 mol^{-1} and increases the curve minima to 0.44. The difference between the minima excess volumes of N-MPD and N-EPD is about 0.2 cm^3 mol^{-1}. The difference in the increased V^E suggests that the amine and water have stronger intermolecular interactions when increasing the chain length.

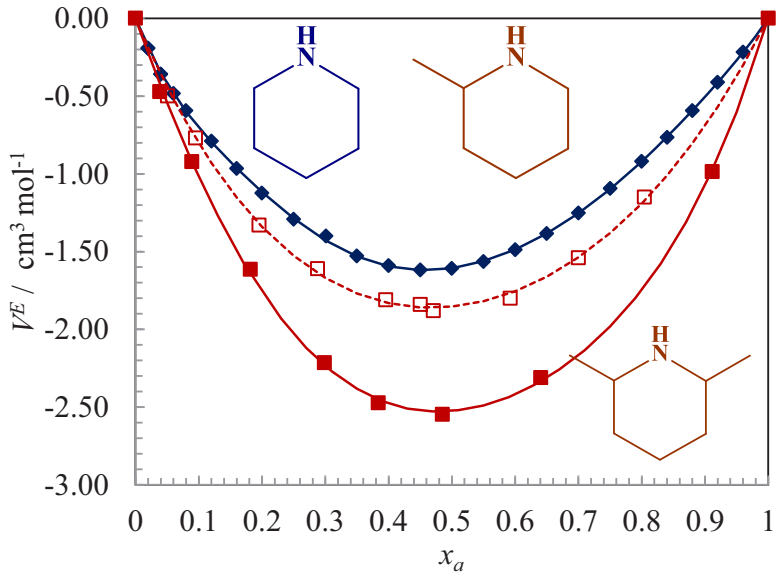

Figure 4-10: Excess molar volumes of secondary hindered alkyl piperidines and piperidine at 298.15 K. ◆ Piperidine (Afzal et al., 2008), □ 2-MPD (Coulier et al., 2010), ■,2,6-DPD. The size of the markers reflect the uncertainty of the data

In Figure 4-10 it is observed that adding an alkyl group to the 2 and 6 position of piperidine increase the magnitude of the excess volume. Adding the methyl group to the 2 position shifts the curve minima to a molar fraction value of 0.47 and a V^E magnitude of -1.86 cm^3 mol^{-1}. Adding another methyl group to the 6 position increases the V^E to -2.53 cm^3 mol^{-1} and increases the curve minima to 0.48. The increase in the V^E may be due to a combination of access restriction to the N group in the ring system, limiting access to one set of loan pair elections inductive effect from the methyl groups attached to the carbons in the 2 and 6 positions. This combined influence would explain the increase in the excess volumes with the addition of methyl groups.

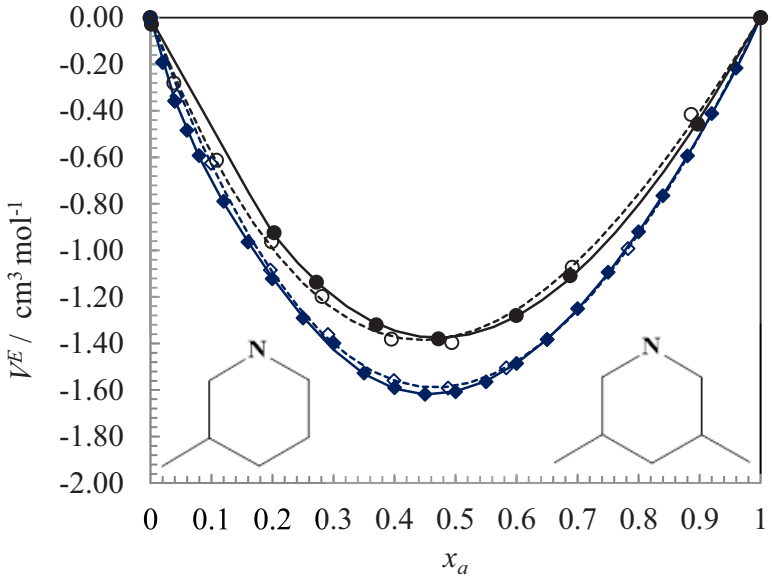

Figure 4-11: Excess molar volumes of secondary alkyl piperidines and piperidine at 298.15 K. ◆ Piperidine (Afzal et al., 2008), ◇ 4-MPD, ○ 3-MPD , ● 3,5-MPD . The size of the markers reflect the uncertainty of the data

In Figure 4-11 it is observed that adding an alkyl group to the 3 and 5 position of piperidine decrease the magnitude of the excess volume. Adding the methyl group to the 3 position does not shift the minima curve and a V^E magnitude is reduced to -1.38 cm^3 mol^{-1}. Adding another methyl group to the 5 position had no effect on the excess volume, when compared to 3-MPD, and the curve minima increases to 0.47. The 4-MPD excess volumes are very similar to piperidine with only slightly smaller V^E of about 0.02 cm^3 mol^{-1}. In this case the interactions maybe dominated by hydrophobic effects. These effects produce larger bulkier tails which reduce the interactions with water. When the molecule is symmetrical like 4-MPD and 3,5-DPD, the effects of the interactions appear to be reduced.

The tertiary and secondary hindered amines have much more negative excess volume than that of piperidine. 2,6-DPD is the most negative followed by N-EPD, N-MPD and 2-MPD. These observations can be seen in Figure 4-9 and Figure 4-10. The secondary amines have a slightly different trend and can be seen in Figure 4-11. 4-MPD is equivalent to that of the piperidine value while 3-MPD and 3,5-DPD share similar excess volumes and are less negative than piperidine.

The magnitude of the volume curves is representative of the strength of the interactions between water and alkyl piperidine. In this case tertiary piperidines and secondary hindered piperidines display the strongest water amine interaction. The secondary unhindered piperidines possess weaker interactions with the water molecules.

The trend in the minima follows a different trend than the magnitude of the excess volumes. The local minima of 4-MPD is equal to the local minima of piperidine. 3-MPD is a secondary piperidine with a local minimum at 0.45 next to piperidine. The rest of the secondary piperidines in general have local minima closer to the midpoint, 0.5, while the tertiary piperidines such as N-MPD, 0.40, and N-EPD, 0.44, local minima are closest to the x_a of 0. The other alkyl piperidines minima are found at, 2,6-DPD, 0.48, 2-MPD, 0.47, and 3,5-DPD, 0.47. For all the alkyl piperidines there is a preference for the minima to be located in the aqueous region between, (x_a = 0 and 0.5). This suggests that there is a preference for water amine interactions.

4.4.1.3 Pressure Effects on Excess Volumes.

The densities and calculated excess molar volumes of 3-MPD and 4-MPD from the Sodev and Anton Parr densitometers are listed in the Table 4-12, at the temperature of 303 K and at atmospheric pressure, 0.5 MPa and 1.0 MPa, respectively. The excess molar volumes were regressed to Redlich-Kister curves and can be seen in Figure 4-12 and Figure 4-13 with the parameters listed in Table 4-11. The excess molar volumes are not really influenced by the pressure on the range covered here. However, they were observed to decrease slightly with increasing pressure with no change to the position of the local minima.

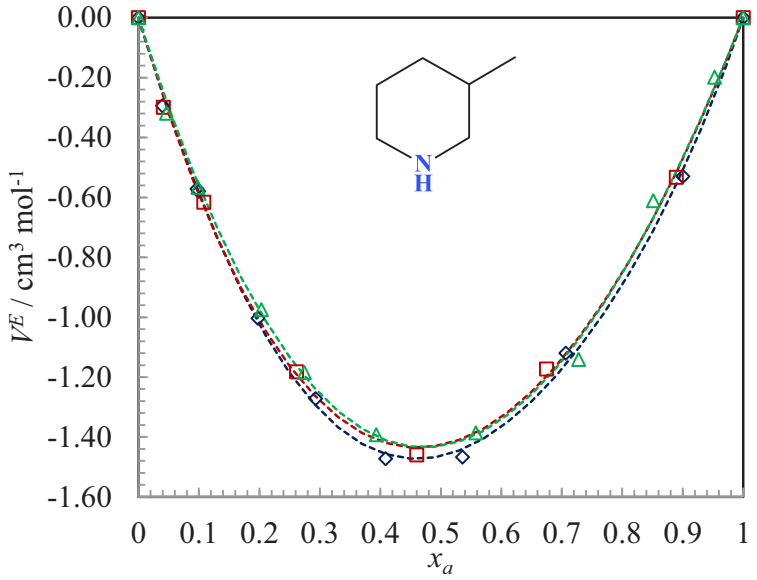

Figure 4-12: Excess molar volumes of 3-MPD at 303.15 K with increasing pressure and Redlich Kisther fits: ◇ (atmospheric pressure), □ (0.5 MPa), △ (1.0 MPa). The size of the markers reflect the uncertainty of the data

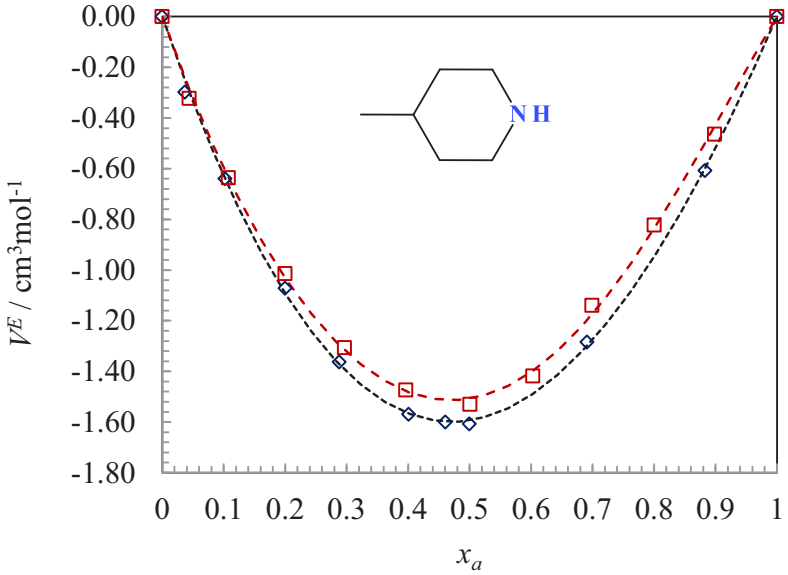

Figure 4-13: Excess molar volumes of 4-MPD at 303.15 K with increasing pressure and Redlich Kishter fits. ◇ (atmospheric pressure), □ (0.5 MPa). The size of the markers reflects the uncertainty of the data.

4.4.2 Excess Molar Enthalpies of Methyl Piperidines

The excess molar enthalpies, H^E for 3-MPD and 4-MPD were measured at 303.15 K, 313.15 K 323.15 K and 333.15K at a pressure of 1.0 MPa using the calorimeter and the mixing cell described in

section 4.2.4. The excess enthalpies are measured between the molar fraction of 0.01 and 0.6. The 3-MPD and 4-MPD excess enthalpies beyond this mole fraction cannot be measured for two reasons. The total flow rates needed to measure beyond this mole fraction causes a baseline shift which reduces the accuracy of the measurement. The second is the difference in the magnitude of the flow rates between each pump cannot maintain efficient mixing between both the alkyl piperidine and water. The maximum uncertainty in the composition is ± 0.0023. The uncertainties in the excess enthalpies are at most ± 21 J mol^{-1}. The data were fit with the Redlich-Kishter equation and are listed in Table 4-15.

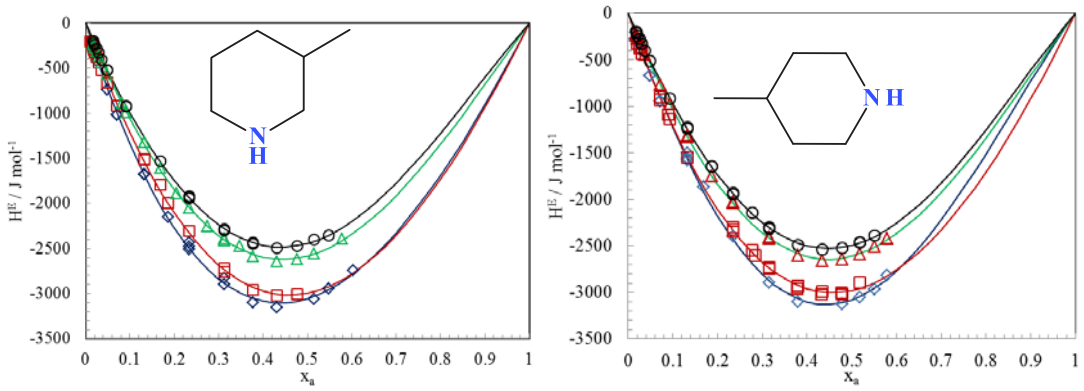

Figure 4-14 and Figure 4-15 : Excess Molar Enthalpies of 3-MPD (left) and 4-MPD (right) measured at 1.0 MPa (◇, — 303.15 K) (□,— 313.15 K) (△,— 323.15K) (○,— 333.15 K). The size of the markers reflects the uncertainty of the data.

The values are listed in Table 4-13 and Table 4-14 and can be seen in Figure 4-14 and Figure 4-145. For both amines H^E is exothermic and the value is less negative when increasing the temperature.

On Figure 4-16, The excess molar enthalpies of 4-MPD and 3-MPD at 303.15 K are compared with the N-MPD data at 303.15 K and the 2-MPD data measured at 308.15K by (Coulier et al., 2015) and piperidine data measured at 298.15 K from (Kul and Lieu, 2010). 3-MPD and 4-MPD have comparable excess molar enthalpies and the value is larger than the other piperidines, with excess molar enthalpy at the extremum around -3000 J mol^{-1}. Moving the methyl group close to the nitrogen reduces the exothermicity of the mixing, as it can be seen on 2-MPD+water curve. N-MPD has excess molar

enthalpies close to the values obtained with piperidine. The local minima of the excess enthalpies is located around x_a=0.45 for piperidine and for the methylpiperidines with methyl branched on carbon group. When the methyl group is located on the nitrogen, the minimum is shifted to lower molar fractions (x_a = 0.35).

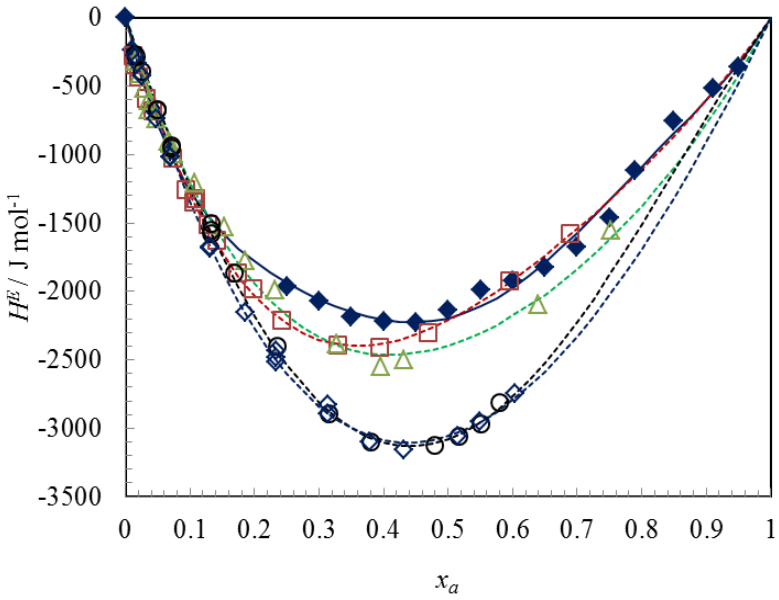

Figure 4-16: Excess molar enthalpies of alkyl piperidine and Redlich Kister fits, ◆ Piperidine (Kul and Lieu, 2010), □ N-MPD (Coulier et al., 2015), △ 2-MPD (Coulier et al., 2015), ○ 3-MPD, ◇ 4-MPD. The size of the markers reflects the uncertainty of the data.

Classically the reduction of the exothermicity with respect to the temperature is related to an increase of the first derivative properties of the excess Gibbs energy, and represent the destruction of the liquid structure (Patterson, 1994). This principle can also be applied to the change of methyl group position on the piperidine ring and provide some insight into the relationship between the molecular structure and thermodynamic properties. With the excess molar enthalpy representing the change between the pure state and the solution states, it can be argued that the 3-MPD and 4-MPD create more ordered or stable solution structure. Moving the methyl group towards the nitrogen group represents a

less ordered structure, which is observed with the less negative values obtained for N-MPD and 2-MPD at the same temperature.

4.4.2.1 Infinite dilution Excess Molar Enthalpies

The excess molar enthalpies give access to the reduced excess molar enthalpies, $H^E/(x_1x_2)$. These reduced values have been used to calculate the infinite dilution partial molar enthalpy $\overline{H}^{\infty}$ for 3-MPD and 4-MPD as shown in Figure 4-17 and Figure 4-18. The results are listed in Table 4-17.

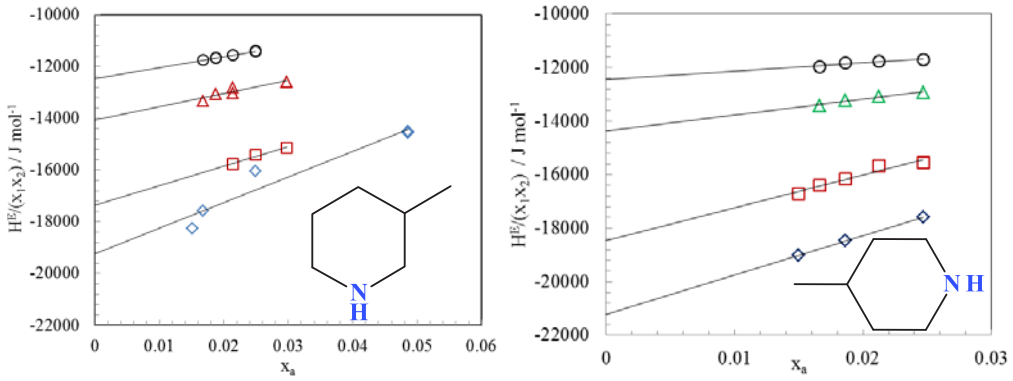

Figure 4-17 and Figure 4-18 : Reduced molar enthalpies of 3-MPD (left) and 4-MPD (right): (◇ 303.15 K), (□ 313.15 K), (△ 323.15K), (○ 333.15 K). The solid lines are linear regressions for infinite dilution. The size of the markers reflects the uncertainty of the data

The Figure 4-19 shows the evolution of $\overline{H}^{\infty}$ versus temperature for the 3-MPD and 4-MPD. The evolution is linear on the range of temperature studied and increases with temperature. From those results it appears that the slope of the regression versus temperature is larger for 4-MPD than for 3-MPD. From those results $\overline{H}^{\infty}$ was extrapolated at 298.15 K to be compared with literature. The values of the infinite dilution partial molar enthalpy at 298.15 K are -20.6 ± 9 kJ mol-1 for 3-MPD and -22.6 ±

7 kJ mol-1 for 4-MPD. $\overline{H}^{\infty}$ are in agreement within the experimental uncertainty with (Berthon et al., 1979) who obtained -23.37 ± 0.03 kJ mol-1 for 3-MPD and -23.67 ± 0.07 kJ mol-1 for 4-MPD. The values with respect to N-MPD at -27 ± 3.2 kJ mol-1 and 2-MPD at -28 ± 2 kJ mol-1 are more negative.

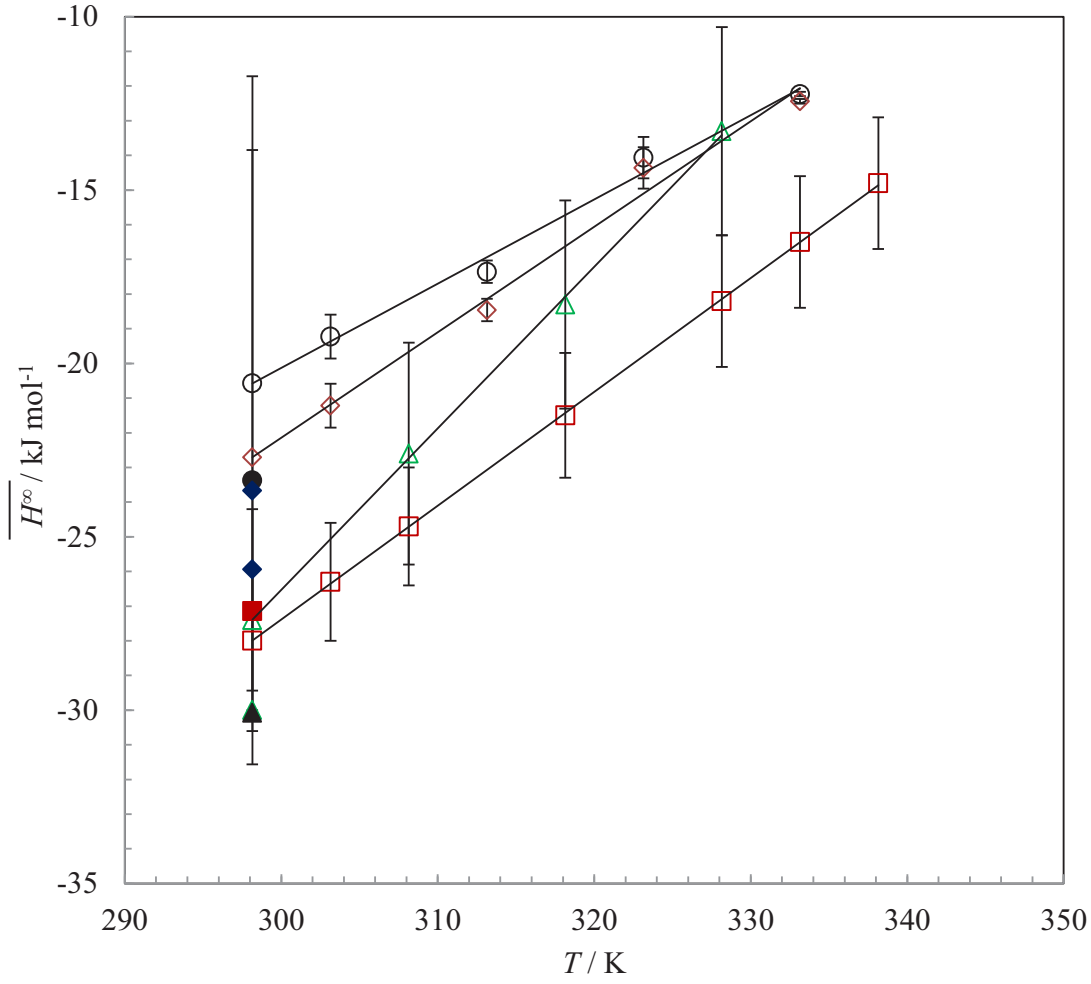

Figure 4-19: Temperature dependent infinite dilution enthalpies of alkyl piperidines. , ◆ Piperidine at 298.15 K (Dohnal et al., 1994), □ N-MPD (Coulier et al., 2015), ■ N-MPD (Dohnal and Rehak, 2011), △ 2-MPD (Coulier et al., 2015), ▲ 2-MPD at 298.15 K (Berthon et al., 1979), ○ 3-MPD, ● 3-MPD at 298.15 K (Berthon et al., 1979), ◇ 4-MPD, ◇ 4-MPD at 298.15 K (Berthon et al., 1979).

4.4.3 Specific Heat Capacities and Excess Molar Heat Capacities

3-MPD and 4-MPD specific heat capacities were measured between for the range from 288.15 K to 343.15 K using the method described in section 4.2.2 and are listed in Table 4-18 and Table 4-19 respectively. The specific heat capacity experiments were conducted at atmospheric pressure in a nitrogen environment. The standard deviations for multiple measurements of the pure substances are ± 0.006 J g^{-1} K^{-1}. The uncertainty was propagated with solution composition to a value of ± 0.008 J g^{-1} K^{-1}. The maximum uncertainties for the excess heat capacities are ± 0.7 J mol^{-1} K^{-1}. The values for N-MPD and 2-MPD were taken from the previously reported data from (Coulier et al., 2015).

4.4.3.1 Heat Capacities of pure Alkyl Piperidines

The molar heat capacities, C_p*, of the pure substances are plotted in Figure 4-20. The pure values of piperidine and 2-MPD data were taken from the work of (Messerly et al., 1988). The experimental data for N-MPD and 2-MPD were reported in work of (Coulier et al., 2015) and from (Conti, G et al., 1976). The pure values of 3-MPD and 4-MPD obtained here are similar and very close to the values obtained with 2-MPD. However, the slope versus temperature is similar to piperidine. The increase of C_p* is then probably mainly due to the increase of the molar mass of the compound. An interesting difference is observed between piperidines substituted on nitrogen: the methyl group on the N position lower the molar heat capacity of the methyl piperidines. Moreover, the slope versus temperature with N-MPD is very different from the slope obtained for piperidine and for the others methyl-piperidines. This may be due to N-MPD lacks the ability to hydrogen bonds with other N-MPD molecules.

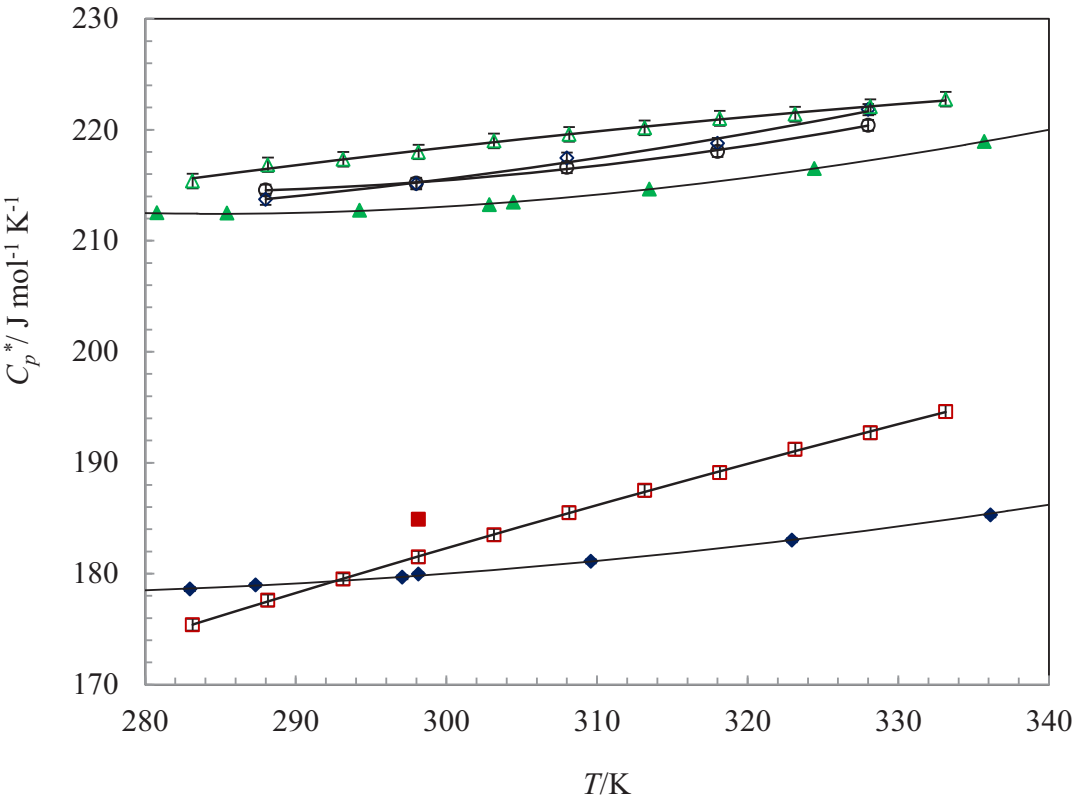

Figure 4-20: Molar heat capacities of pure alkyl-piperidine. ◆ Piperidine (Messerly et al., 1988), □ N-MPD (Coulier et al., 2015), ■ N-MPD (Conti, G et al., 1976), ▲ 2-MPD (Messerly et al., 1988), ○ 3-MPD, ◇ 4-MPD,(3-MPD and 4-MPD are overlapped) △ 2-MPD (Coulier et al., 2015), ,.

4.4.3.2 Excess Molar Heat Capacities of Alkyl Piperidine

The excess molar heat capacities were calculated using equation 4-20,

$$C_p^E = \left(x_w M_w + x_a M_a\right) c_{p,s} - x_w M_w c_{p,w} - x_a M_a c_{p,a}, \qquad \textbf{Eq 4-20}$$

where $c_{p,s}$ is the specific heat capacity of solution, $c_{p,w}$ is the specific heat capacity of water, $c_{p,a}$, is the specific heat capacity of measured 3-MPD and 4-MPD. The results are listed in Table 4-18 and Table 4-19. The excess properties were fitted to equation 5-10 and the fitting parameters are listed in. The data are plotted in Figure 4-21 and Figure 4-22. Low temperature data at 288.15 K and 298.15 K showed the largest amount of scatter in the data. The scatter is caused by chemical relaxation equilibrium in the

solution and was impossible to fit to Redlich Kister polynomial curves. The Redlich Kister equation used 5 parameters to fit the data at 308.15 K and was chosen to fit the lower temperature data.

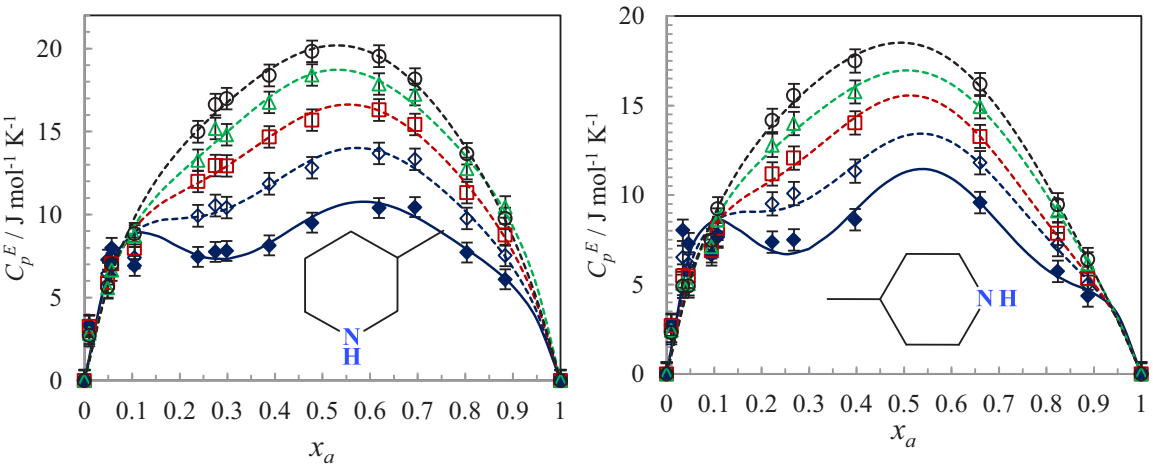

Figure 4-21 and Figure 4-22: Excess molar heat capacities of 3-MPD (left) and 4-MPD (right) at atmospheric pressure: (◆,— 288.15 K) (◇, - - - 298.15 K) (□,- - - 308.15 K) (△,- - - 318.15K) (○,- - - 328.15 K)

The excess heat capacity data, demonstrate two separate regions of molar fraction where the evolution of the excess properties differs. At molar fractions lower than 0.08, the excess molar heat capacities decrease with increasing temperature for both 3-MPD and 4-MPD as illustrated in Figure 4-23. For molar fraction higher than 0.08, the excess molar heat capacities increase with temperature.

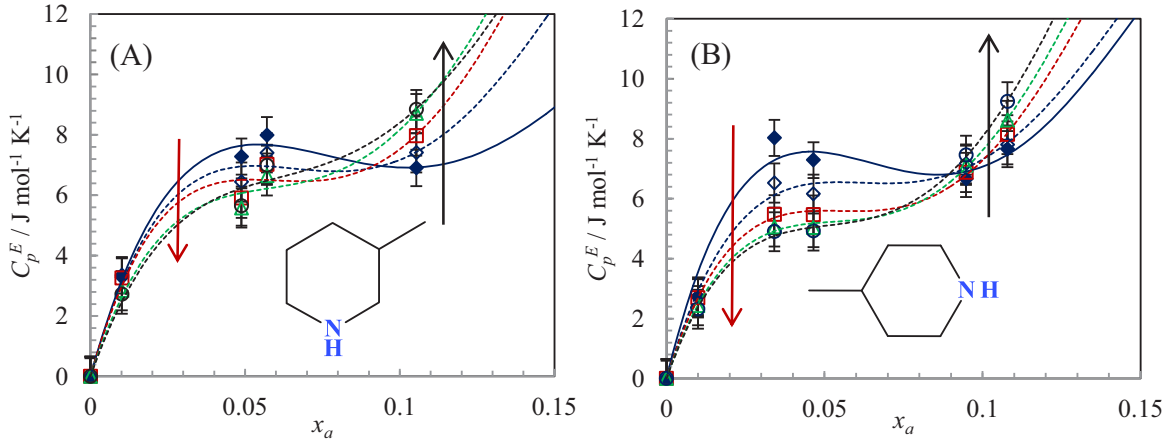

Figure 4-23: Zoom in of excess molar heat capacities in the crossover concentration. (A) 3-MPD (◆,— 288.15 K) (◇, - - - 298.15 K) (□,- - - 308.15 K) (△,- - - 318.15K) (○,- - - 328.15 K), (B) 4-MPD (◆,— 288.15 K) (◇, - - - 298.15 K) (□,- - - 308.15 K) (△,- - - 318.15K) (○,- - - 328.15 K). The lines in the figure are polynomial fits to the data. The arrows show the direction of increasing, black, and decreasing, red, heat capacity with temperature.

This behaviour has been observed with the heat capacity results of N-MPD which crosses at a mole fraction of 0.1 in the work of (Coulier et al., 2015) as seen in

Figure 4-24.

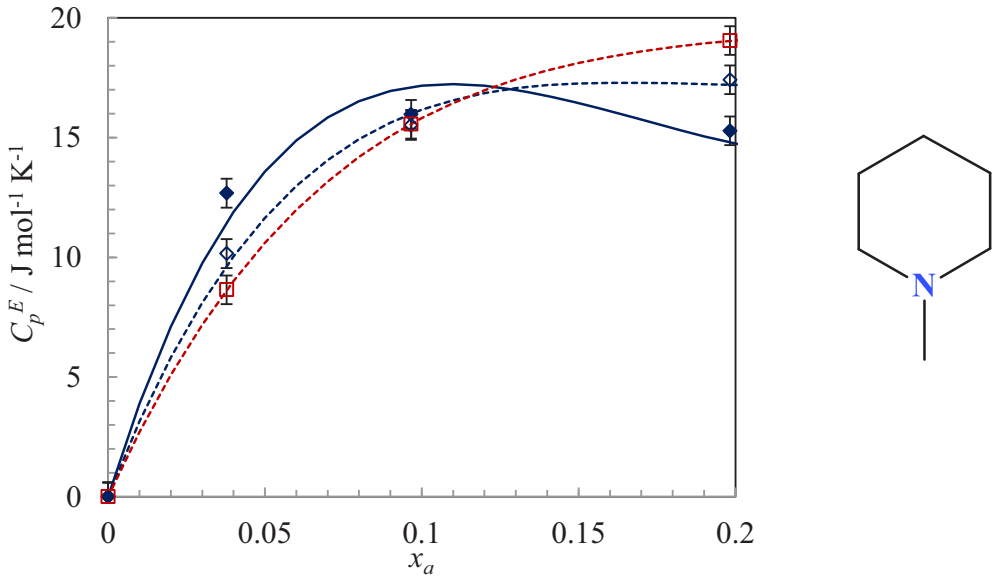

Figure 4-24: Excess molar heat capacities of N-MPD from (Coulier *et al.* 2015), (◆,— 288.15 K), (◇, - - - 298.15 K), (□,- - - 308.15 K).

The work from (Visser et al., 1977) has commented that heat capacity measurements are more sensitive to structural changes in solution. This give rise to the observed excess heat capacity curves but not in excess enthalpy or excess volume curves. The excess heat capacity curves in the more dilute region are related to hydrophobic interaction between water and the alkyl groups creating what is thought to be micro phases in solution. Similar heat capacity behaviour has been seen in 2,6-dimethylpyridine, and 2-isobutoxyethanol by (Perron et al., 1993), and (Doi et al., 2000). The work of (Doi et al., 2000) has found that curve fitting is impossible for excess heat capacity for 2-isobutoxyenthanol+water using the Redlich-Kishter and Myers-Scott equations. More recent investigations involving the heat capacities of organic species in water within the mole fraction range of

0 to 0.2 have been investigated by (Zemánková et al., 2015; Zemánková et al., 2016). They demonstrate that a variety of alcohols and amines with one polar head group and large bulky alkyl groups showed decreasing heat capacities with increasing temperature. If the number of hetero-atoms in the piperidine skeleton are increased these heat capacity effects are no longer prevalent (Zemánková et al., 2015). Small-angle neutron scattering studies have shown that N-methylpiperidine and piperidine form aggregates within the concentration range of the heat capacity inversion (Marczak et al., 2013; Marczak et al., 2015). As in the case of (Doi et al., 2000), the excess heat capacities are over-fitted and are unable to reproduce the excess heat capacities at low concentrations.

A comparison of the results at 308.15 K has been done for the 4-MPD studied. The results are plotted on figure 5.24 and the maxima and magnitude of the C_p^E are listed in Table 4-21.

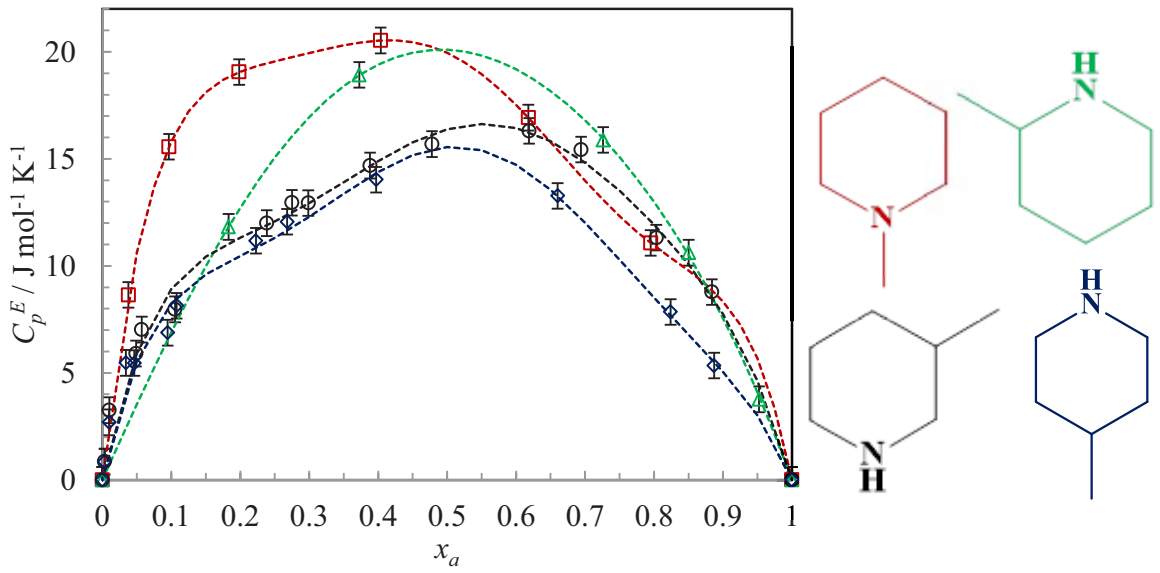

Figure 4-25: Comparison of excess molar heat capacities at 318.15 K. □ N-MPD (Coulier et al., 2015), △ 2-MPD (Coulier et al., 2015), ○ 3-MPD, ◇ 4-MPD

The largest values of the excess molar heat capacities are obtained with N-MPD, at 20.54 J mol^{-1} K^{-1}. As the methyl group moves further from the nitrogen group, the magnitude of the excess heat capacities decreases. It can be also noticed that the maximum of the curve is shifted from x_a=0.35 to x_a=

0.55 when moving the methyl group from the nitrogen to the carbon on the piperidine ring. This trend is similar to the results obtained for excess molar volumes and shown in 4.3.1.2.

4.5 Conclusions

The data have demonstrated that there is a relationship between the thermodynamic properties and molecular structures of the alkyl piperidines. The observations in the changes of the magnitude, position of the local maxima and minima and partial molar properties are related to the location of the alkyl group on the piperidine skeleton. The tertiary alkyl piperidines have in general a trend different from the other methyl piperidines. The excess heat capacities of the methylpiperidine show the same trends as the excess volumes. However the curves are more complicated in that the excess volumes and excess enthalpy experiments. The difference in the excess heat capacity curve structures are from chemical relaxation effects. The source of the chemical relaxation may be due to aggregation phenomena in the aqueous regions which are not yet well understood.

To conclude it is possible to maintain the classification in the previous chapters where the structures are divided into tertiary alkyl piperidines, secondary hindered alkyl piperidine and secondary alkyl piperidine.

4.6 Appendix for Chapter 4

Table 4-1: List of chemicals suppliers and purities

Chemicals & Abbreviation	Molecular weight g mol^{-1}	Supplier	C.A.S.	Supplier Purity by w%
N-Methylpiperidine (N-MPD)	99.1741	Sigma-Aldrich	626-67-5	99.90%
2-Methylpiperidine (2-MPD)	99.1741	Sigma-Aldrich	109-05-7	98.30%
3-Methylpiperidine (3-MPD)	99.1741	Sigma-Aldrich	626-56-2	99.70%
4-Methylpiperidine (4-MPD)	99.1741	Sigma-Aldrich	626-58-4	99.20%
2,6-Dimethylpiperidine (2,6-DPD)	113.2007	TCI	504-03-0	99.90%
3,5-Dimethylpiperidine (3,5-DPD)	113.2007	TCI	35794-11-7	99.50%
N-Ethylpiperidine (N-EPD)	113.2007	TCI	766-09-6	99.20%
Octane	114.2285	Sigma-Aldrich	111-65-9	99.30%
Decane	142.2817	Sigma-Aldrich	124-18-5	99.50%
Dodecane	170.3348	Sigma-Aldrich	112-40-3	99.50%
Absolute Ethanol	46.0684	VWR	64-17-5	99.50%
Nitrogen Gas	28.0134	Air Products	7727-37-9	99.995%
Carbon Dioxide Gas	44.0095	Air Products	124-38-9	99.995%

Table 4-2: Experimental and literature of molar isobaric heat capacities of n-octane.

T^a	$C_{p,exp}$	$\sigma(C_{p,exp})$	$C_{p,lit}{}^b$	%RD[d]
K		$J \cdot mol^{-1} \cdot K^{-1}$		
283.15	248.16	0.05	248.23	0.03
288.15	250.10	0.05	250.36	0.10
293.15	252.24	0.05	252.32	0.03
298.15	253.98	0.04	254.34	0.14
303.16	256.50	0.05	256.40	0.04
308.15	258.05	0.04	258.28	0.09
313.16	260.87	0.05	260.66	0.08
318.15	262.70	0.06	262.86	0.06
323.15	264.78	0.05	265.09	0.12
328.15	267.24	0.05	267.36	0.05
333.15	269.31	0.06	269.67	0.13

*a:*uncertainty in T ±0.01 K

b*:*(Lemon, E.W.; Huber,M.L.; McLinden, M.O., 2010)

d: $\%RD = |(C_{p,exp} - C_{p,lit}) / C_{p,lit}| \times 100$ uncertainty in T ± 0.03 K

Table 4-3: Densities and excess molar volumes of aqueous 3-MPD solutions and pure liquid at atmospheric pressure. [a,b,c,d]

x_a	ρ	V^E	x_a	ρ	V^E
	g cm^{-3}	mol cm^{-3}		g cm^{-3}	mol cm^{-3}
	288.15 K			298.15 K	
0.000000	0.99910	0.00	0.000000	0.99705	0.00
0.040754	0.98102	-0.32	0.038391	0.97730	-0.28
0.098778	0.95768	-0.61	0.108361	0.94802	-0.61
0.192360	0.93291	-0.99	0.198882	0.92387	-0.96
0.296096	0.91437	-1.30	0.281119	0.90837	-1.20
0.409657	0.89895	-1.47	0.395139	0.89188	-1.38
0.505046	0.88764	-1.45	0.494059	0.88021	-1.39
0.699313	0.86927	-1.09	0.691374	0.86139	-1.07
0.860487	0.85743	-0.57	0.886412	0.84710	-0.41
1.000000	0.84902	0.00	1.000000	0.84082	0.00
	308.15 K			318.15 K	
0.000000	0.99403	0.00	0.000000	0.99021	0.00
0.043331	0.96942	-0.29	0.043504	0.96353	-0.29
0.107788	0.94144	-0.59	0.108452	0.93401	-0.59
0.205981	0.91441	-0.96	0.201147	0.90749	-0.95
0.302319	0.89659	-1.22	0.304775	0.88764	-1.24
0.400886	0.88258	-1.36	0.402068	0.87368	-1.40
0.500753	0.87044	-1.35	0.435879	0.86940	-1.42
0.688685	0.85271	-1.05	0.550801	0.85670	-1.39
0.879377	0.83872	-0.43	0.699354	0.84307	-1.12
1.000000	0.83208	0.00	0.854223	0.83125	-0.60
-	-	-	1.000000	0.82233	0.00

x_a	ρ	V^E
	g cm^{-3}	mol cm^{-3}
	328.15 K	
0.000000	0.98569	0.00
0.043198	0.95745	-0.28
0.105419	0.92767	-0.56
0.199810	0.89958	-0.94
0.313845	0.87745	-1.25
0.381113	0.86751	-1.36
0.438152	0.86012	-1.41
0.704200	0.83359	-1.11
0.883256	0.82055	-0.52
1.000000	0.81327	0.00

*a:*uncertainty in xa ±0.00005

*b:*uncertainty in ρ ± 0.00005 g cm-3

*c:*uncertainty in VE ± 0.02 cm3 mol-1

d: uncertainty in T ± 0.03 K

Table 4-4: Densities and excess molar volumes of aqueous 4-MPD solutions and pure liquid at atmospheric pressure. [a,b,c,d]

x_a	ρ	V^E	x_a	ρ	V^E
	g cm^{-3}	mol cm^{-3}		g cm^{-3}	mol cm^{-3}
	288.15 K			298.15 K	
0.000000	0.99910	0.00	0.000000	0.99705	0.00
0.040000	0.98084	-0.34	0.043555	0.97424	-0.34
0.099980	0.95573	-0.65	0.099569	0.94985	-0.63
0.106751	0.95384	-0.69	0.196879	0.92322	-1.08
0.212133	0.92704	-1.15	0.291160	0.90450	-1.36
0.244717	0.92071	-1.26	0.398985	0.88868	-1.56
0.357171	0.90282	-1.54	0.487763	0.87778	-1.59
0.432937	0.89281	-1.61	0.583183	0.86753	-1.50
0.491358	0.88589	-1.61	0.782854	0.84990	-0.99
0.573248	0.87719	-1.54	1.000000	0.83462	0.00
0.724748	0.86313	-1.18	-	-	-
0.803913	0.85681	-0.91	-	-	-
1.000000	0.84322	0.00	-	-	-
	308.15 K			318.15 K	
0.000000	0.99403	0.00	0.000000	0.99021	0.00
0.042559	0.96939	-0.32	0.043383	0.96309	-0.31
0.108269	0.94000	-0.65	0.108075	0.93288	-0.63
0.199564	0.91410	-1.05	0.199519	0.90597	-1.03
0.266694	0.90049	-1.27	0.289717	0.88789	-1.32
0.392094	0.88101	-1.53	0.394787	0.87175	-1.52
0.694046	0.84811	-1.23	0.506570	0.85807	-1.56
0.304541	0.89386	-1.37	0.604094	0.84794	-1.47
0.509124	0.86655	-1.56	0.752465	0.83444	-1.07
0.883518	0.83331	-0.54	0.874083	0.82528	-0.61
1.000000	0.82585	0.00	1.000000	0.81696	0.00

x_a	ρ	V^E
	g cm^{-3}	mol cm^{-3}
	328.15 K	
0.000000	0.98569	0.00
0.043159	0.95697	-0.30
0.107336	0.92573	-0.62
0.200430	0.89752	-1.02
0.331369	0.87222	-1.40
0.387640	0.86383	-1.49
0.494121	0.85037	-1.54
0.643465	0.83502	-1.37
0.890781	0.81528	-0.55
1.000000	0.80809	0.00

*a:*uncertainty in xa ±0.00005

*b:*uncertainty in ρ ± 0.00005 g cm-3

*c:*uncertainty in VE ± 0.02 cm3 mol-1

d: uncertainty in T ± 0.03 K

Table 4-5: Densities and excess molar volumes of aqueous 2,6-DPD solutions and pure liquid at atmospheric pressure. ***a,b,c,d***

x_a	ρ	V^E	x_a	ρ	V^E
	g cm^{-3}	mol cm^{-3}		g cm^{-3}	mol cm^{-3}
	288.15 K			298.15 K	
0.00000	0.99910	0.000	0.00000	0.99705	0.000
0.01736	0.99257	-0.285	0.03828	0.97510	-0.472
0.03824	0.98113	-0.516	0.08893	0.95015	-0.921
0.09369	0.95623	-1.029	0.18149	0.92056	-1.615
0.19735	0.92556	-1.786	0.29857	0.89551	-2.214
0.30812	0.90272	-2.298	0.38395	0.88161	-2.472
0.37819	0.89151	-2.506	0.48491	0.86734	-2.547
0.50063	0.87472	-2.608	0.64069	0.84941	-2.310
0.63099	0.85969	-2.394	0.91155	0.82514	-0.987
0.90481	0.83348	-0.893	1.00000	0.81652	0.000
1.00000	0.82519	0.000			
	308.15 K			318.15 K	
0.00000	0.99403	0.000	0.00000	0.99021	0.000
0.00832	0.98984	-0.138	0.00240	0.98903	-0.044
0.23486	0.89814	-1.832	0.41061	0.85841	-2.410
0.40182	0.87023	-2.501	0.44906	0.85279	-2.431
0.47679	0.85918	-2.512	0.50841	0.84541	-2.460
0.57672	0.84738	-2.453	0.69745	0.82467	-2.022
0.77671	0.82664	-1.669	0.77680	0.81717	-1.644
0.63360	0.84066	-2.265	0.60022	0.83477	-2.334
0.29017	0.88915	-2.205	0.89351	0.80761	-0.978
0.90903	0.81618	-0.957	1.00000	0.79858	0.000
1.00000	0.80779	0.000			

*a:*uncertainty in xa ±0.00005

*b:*uncertainty in ρ ± 0.00005 g cm-3

*c:*uncertainty in VE ± 0.02 cm3 mol-1

d: uncertainty in T ± 0.03 K

Table 4-6: Densities and excess molar volumes of aqueous 3,5-DPD solutions and pure liquid at atmospheric pressure. ***a,b,c,d***

x_a	ρ	V^E	x_a	ρ	V^E
	g cm^{-3}	mol cm^{-3}		g cm^{-3}	mol cm^{-3}
	288.15 K			298.15 K	
0.000000	0.99910	0.00	0.000000	0.99705	0.00
0.002074	0.99818	-0.03	0.002074	0.99600	-0.03
0.201264	0.91486	-0.95	0.202664	0.90703	-0.92
0.290992	0.89977	-1.27	0.369897	0.87936	-1.32
0.372948	0.88721	-1.35	0.471919	0.86759	-1.38
0.509215	0.87276	-1.43	0.599463	0.85571	-1.28
0.584836	0.86535	-1.31	0.272050	0.89378	-1.14
0.787282	0.85017	-0.80	0.688154	0.84872	-1.11
1.000000	0.83838	0.00	0.896868	0.83538	-0.46
-	-	-	1.000000	0.82980	0.00

	308.15 K	
0.000000	0.99403	0.00
0.002074	0.99264	-0.02
0.292807	0.88244	-1.18
0.403224	0.86711	-1.36
0.495526	0.85699	-1.39
0.697569	0.83967	-1.11
0.782319	0.83389	-0.88
0.535206	0.85288	-1.34
0.872608	0.82807	-0.53
0.610374	0.84635	-1.27
1.000000	0.82122	0.00

*a:*uncertainty in xa ±0.00005

*b:*uncertainty in ρ ± 0.00005 g cm-3

*c:*uncertainty in VE ± 0.02 cm3 mol-1

d: uncertainty in T ± 0.03 K

Table 4-7: Densities and excess molar volumes of aqueous N-EPD solution and pure liquid at atmospheric pressure. ***a,b,c,d***

x_a	ρ	V^E	x_a	ρ	V^E
	g cm^{-3}	mol cm^{-3}		g cm^{-3}	mol cm^{-3}
	278.15 K			288.15 K	
0.00000	0.99997	0.00	0.00000	0.99910	0.00
0.04977	0.97820	-0.58	0.00187	0.99822	-0.03
0.15182	0.94061	-1.28	0.00490	0.99692	-0.07
0.24209	0.91990	-1.73	0.00691	0.99616	-0.11
0.32814	0.90393	-1.96	0.54058	0.86613	-1.91
0.43752	0.88901	-2.14	0.65358	0.85497	-1.68
0.53772	0.87604	-2.00	0.70094	0.85070	-1.52
0.65038	0.86444	-1.73	0.78441	0.84375	-1.18
0.67084	0.86228	-1.63	0.85037	0.83904	-0.90
0.76069	0.85493	-1.33	0.94409	0.83240	-0.35
0.82729	0.84945	-0.99	1.00000	0.82882	0.00
0.85782	0.84701	-0.80			
1.00000	0.83775	0.00			

	298.15 K	
0.00000	0.99705	0.00
0.00203	0.99605	-0.03
0.00500	0.99462	-0.08
0.00705	0.99373	-0.11
0.55284	0.85583	-1.84
0.64773	0.84633	-1.63
0.75042	0.83775	-1.31
0.77445	0.83570	-1.19
0.85782	0.82965	-0.83
0.92871	0.82496	-0.47
0.94678	0.82361	-0.34
1.00000	0.82020	0.00

*a:*uncertainty in xa ±0.00005

*b:*uncertainty in ρ ± 0.00005 g cm-3

*c:*uncertainty in VE ± 0.02 cm3 mol-1

d: uncertainty in T ± 0.03 K

Table 4-8: Temperature dependent Redlich-Kishter parameters for excess molare volumes of alkyl piperidines.

T / K	A_0			A_1			A_2			A_3			A_4			Error
							3-MPD									
288.15	-5.7588	±	0.05	-1.295	±	0.12	0	±	-	0	±	-	0	±	-	0.023
298.15	-5.4726	±	0.05	-1.2274	±	0.12	0	±	-	0	±	-	0	±	-	0.024
308.15	-5.3267	±	0.06	-1.2295	±	0.16	0	±	-	0	±	-	0	±	-	0.03
318.15	-5.6216	±	0.08	-0.7725	±	0.22	0	±	-	0	±	-	0	±	-	0.015
328.15	-5.5958	±	0.16	-0.6393	±	0.40	0	±	-	0	±	-	0	±	-	0.012
							4-MPD									
288.15	-6.4092	±	0.04	-0.9913	±	0.10	0	±	-	0	±	-	0	±	-	0.019
298.15	-6.3286	±	0.03	-0.8592	±	0.08	0	±	-	0	±	-	0	±	-	0.013
308.15	-6.17	±	0.05	-0.86	±	0.11	0	±	-	0	±	-	0	±	-	0.022
318.15	-6.192	±	0.07	-0.6301	±	0.19	0	±	-	0	±	-	0	±	-	0.039
328.15	-6.135	±	0.13	-0.5387	±	0.40	0	±	-	0	±	-	0	±	-	0.064
							3,5-DPD									
288.15	-5.5949	±	0.02	-1.0935	±	0.07	0.5863	±	-	0	±	-	0	±	-	0.025
298.15	-5.4847	±	0.02	-0.6376	±	0.06	0.2319	±	-	0	±	-	0	±	-	0.01
308.15	-5.5078	±	0.07	-0.609	±	0.20	0.2614	±	-	0	±	-	0	±	-	0.012
							2,6-DPD									
288.15	-10.3568	±	0.11	-0.8626	±	0.26	-1.4882	±	0.5	0	±	-	0	±	-	0.043
298.15	-10.0989	±	0.07	-0.6725	±	0.30	-2.3864	±	0.4	1.6796	±	0.7	0	±	-	0.029
308.15	-10.0287	±	0.14	-0.6169	±	0.33	-1.0929	±	0.8	0	±	-	0	±	-	0.06
318.15	-9.7746	±	0.05	-0.92	±	0.29	-1.3865	±	0.6	0	±	-	0	±	-	0.023
							N-EPD									
278.15	-8.2163	±	0.08	-1.9665	±	0.3	-0.4586	±	0.4	-1.0334	±	0.8	0	±	-	0.03
288.15	-7.8254	±	0.08	-1.7794	±	0.7	-1.6999	±	1.2	-2.5202	±	0.8	-1.629	±	1.5	0.01
298.15	-7.7491	±	0.06	-3.0465	±	0.29	-3.5076	±	0.5	-1.3449	±	0.5	0	±	-	0.009

Table 4-9: Temperature dependent excess partial infinite dilution molar volumes and infinite dilution partial molar properties of alkyl piperidine.

T	3-MPD		4-MPD	
K	$\overline{V^E}^{\infty}$	$\overline{V}^{\infty}$	$\overline{V^E}^{\infty}$	$\overline{V}^{\infty}$
	$cm^3\ mol^{-1}$		$cm^3\ mol^{-1}$	
278.15	-	-	-	-
288.15	-4.5	112.3	-7.4	110.2
298.15	-4.2	113.7	-7.2	111.6
308.15	-4.1	113.9	-7	113.1
318.15	-4.8	113.1	-6.8	114.6
328.15	-4.8	113.1	-6.7	116.1

	2,6-DPD		N-EPD	
	$\overline{V^E}^{\infty}$	$\overline{V}^{\infty}$	$\overline{V^E}^{\infty}$	$\overline{V}^{\infty}$
	$cm^3\ mol^{-1}$		$cm^3\ mol^{-1}$	
278.15	-	-	-11.7	123.4
288.15	-12	125.2	-	-
298.15	-11.5	127.2	-	-
308.15	-11.7	128.4	-	-
318.15	-12.1	129.7	-	-
328.15			-	-

Table 4-10: Magnitude and local minima of excess molar volumes at 298.15 K. The table is arranged by decreasing magnitude of the excess molar volumes.

Alkyl piperidine	2,6-DPD	N-EPD	N-MPD	2-MPD	Piperidine	4-MPD	3-MPD	3,5-DPD
local minimum (x_a)	0.48	0.44	0.40	0.47	0.455	0.46	0.45	0.47
V^E $cm^3\ mol^{-1}$ at Minimum	-2.53	-2.08	-1.93	-1.86	-1.61	-1.59	-1.38	-1.38

Table 4-11: Pressure dependant Redlich-Kister parameters for excess molar volumes at 303.15 K

p	T	A_0		A_1		A_2		A		Error
MPa	K									
						3-MPD				
atm	303	-5.8550	± 0.07	-0.9132	± 0.25	-0.3656	± 0.29	0.6130	± 0.6	0.03
0.5	303	-5.7100	± 0.07	-0.8369	± 0.15	-0.3158	± 0.30	-		0.024
1.0	303	-5.7209	± 0.07	-0.6466	± 0.16	-		-		0.033
						4-MPD				
atm	303	-6.3745	± 0.03	-0.7430	± 0.10	-		-		0.02
0.5	303	-6.0282	± 0.06	-0.9977	± 0.12	0.5041	± 0.26	-		0.03

Table 4-12: Densities and excess molar volumes of 3-MPD and 4-methylpiperidine at 303 K at atmospheric pressure, 0.5 MPa and 1.0 MPa.

4-MPD			3-MPD		
x_a	ρ	V^E	x_a	ρ	V^E
	g cm^{-3}	mol cm^{-3}		g cm^{-3}	mol cm^{-3}
		Atmospheric Pressure 303.15 K			
0.00000	0.99565	0.00	0.00000	0.99565	0.00
0.03695	0.97526	-0.30	0.04007	0.97385	-0.29
0.10197	0.94544	-0.64	0.09708	0.94824	-0.57
0.19984	0.91750	-1.07	0.09962	0.94719	-0.58
0.28782	0.90033	-1.36	0.19766	0.92013	-1.00
0.40081	0.88333	-1.57	0.29321	0.90156	-1.27
0.46084	0.87566	-1.60	0.40907	0.88523	-1.47
0.49986	0.87126	-1.61	0.53596	0.87066	-1.47
0.69102	0.85197	-1.29	0.70706	0.85444	-1.12
0.88304	0.83701	-0.61	0.90059	0.84090	-0.53
1.00000	0.82901	0.00	1.00000	0.83414	0.00
		0.5 MPa 303.15 K			
0.00000	0.99583	0.00	0.00000	0.99583	0.00
0.04416	0.97164	-0.32	0.04131	0.97352	-0.30
0.10792	0.94402	-0.64	0.10838	0.94468	-0.62
0.20007	0.91837	-1.01	0.26146	0.90778	-1.18
0.29641	0.90009	-1.31	0.46057	0.87952	-1.46
0.39625	0.88544	-1.47	0.67474	0.85797	-1.17
0.50059	0.87325	-1.53	0.88930	0.84245	-0.53
0.60308	0.86261	-1.42	1.00000	0.83528	0.00
0.69908	0.85326	-1.14			
0.80041	0.84525	-0.82			
0.89855	0.83859	-0.46			
1.00000	0.83226	0.00			

4-MPD			3-MPD		
x_a	ρ	V^E	x_a	ρ	V^E
	g cm^{-3}	mol cm^{-3}		g cm^{-3}	mol cm^{-3}
		1.0 MPa 303.15 K			
0.00000	0.99605	-	0.00000	0.99605	0.00
0.04402	0.97182	-	0.04649	0.97085	-0.32
0.10801	0.94420	-	0.09858	0.94832	-0.57
0.30228	0.89925	-	0.20334	0.91898	-0.97
			0.27460	0.90529	-1.18
			0.39360	0.88775	-1.39
			0.55809	0.86933	-1.39
			0.72800	0.85516	-1.14
			0.85152	0.84496	-0.61
			0.95281	0.83850	-0.20
			1.00000	0.83584	0.00

*a:*uncertainty in xa ±0.00005

*b:*uncertainty in ρ ± 0.00005 g cm-3

*c:*uncertainty in VE ± 0.02 cm3 mol-1

d: uncertainty in T ± 0.03 K

Table 4-13: Excess molar enthalpies of mixing water and 3-MPD at a pressure of 1.0 MPa

x_a	σx_a	H^E	σH^E	x_a	σx_a	H^E	σH^E
		J mol^{-1}				J mol^{-1}	
303.15 K / 1.12± .10 MPa				313.15 K / 1.04 ± 0.1 MPa			
0.0151	0.0001	-271	3	0.0214	0.0001	-331	1
0.0167	0.0001	-289	3	0.0249	0.0001	-374	2
0.0249	0.0001	-389	3	0.0297	0.0001	-437	3
0.0486	0.0002	-670	3	0.0711	0.0003	-933	4
0.0486	0.0002	-673	3	0.0711	0.0003	-896	3
0.0711	0.0003	-938	7	0.0905	0.0004	-1093	5
0.0711	0.0003	-950	3	0.0926	0.0004	-1139	5
0.1328	0.0005	-1581	6	0.1328	0.0005	-1551	6
0.1328	0.0005	-1501	12	0.2345	0.0009	-2347	9
0.1328	0.0005	-1553	5	0.2345	0.0009	-2299	11
0.1695	0.0007	-1865	7	0.2345	0.0009	-2321	8
0.2345	0.0009	-2399	8	0.2769	0.0011	-2546	8
0.3148	0.0012	-2897	11	0.2848	0.0011	-2604	12
0.3799	0.0014	-3102	21	0.3148	0.0012	-2726	19
0.4788	0.0018	-3129	11	0.3148	0.0012	-2743	12
0.5174	0.0019	-3056	11	0.3781	0.0014	-2958	10
0.5506	0.0020	-2966	11	0.3798	0.0014	-2925	12
0.5795	0.0022	-2814	10	0.3799	0.0014	-2928	11
-	-	-	-	0.3799	0.0014	-2933	13
-	-	-	-	0.4318	0.0016	-3021	11
-	-	-	-	0.4337	0.0016	-2991	11
-	-	-	-	0.4770	0.0018	-3005	10
-	-	-	-	0.4788	0.0018	-3020	10
-	-	-	-	0.5174	0.0019	-2896	11

x_a	σx_a	H^E	σH^E	x_a	σx_a	H^E	σH^E
		J mol^{-1}				J mol^{-1}	
323.15 K / 10.9 ±0.9 MPa				333.15 K / 0.96 ±.12 MPa			
0.0167	0.0001	-219	1	0.0167	0.0001	-193	1
0.0188	0.0001	-241	1	0.0188	0.0001	-215	2
0.0214	0.0001	-273	1	0.0188	0.0001	-215	1
0.0214	0.0001	-268	1	0.0214	0.0001	-242	1
0.0297	0.0001	-363	2	0.0249	0.0001	-277	1
0.0369	0.0002	-437	2	0.0249	0.0001	-277	1
0.0711	0.0003	-765	5	0.0297	0.0001	-328	2
0.0926	0.0004	-976	4	0.0297	0.0001	-326	2
0.1328	0.0005	-1313	5	0.0369	0.0002	-401	3
0.1328	0.0005	-1326	6	0.0486	0.0002	-513	3
0.1328	0.0005	-1317	11	0.0926	0.0004	-913	3
0.1868	0.0007	-1745	7	0.1328	0.0005	-1225	6
0.2345	0.0009	-2027	8	0.1328	0.0005	-1242	5
0.2345	0.0009	-2041	8	0.1868	0.0007	-1648	6
0.3148	0.0012	-2423	10	0.1868	0.0007	-1647	6
0.3148	0.0012	-2405	8	0.2345	0.0009	-1926	7
0.3798	0.0014	-2600	10	0.2345	0.0009	-1945	7
0.4336	0.0016	-2659	10	0.2769	0.0011	-2141	8
0.4788	0.0018	-2643	10	0.3148	0.0012	-2301	8
0.5173	0.0019	-2587	9	0.3148	0.0012	-2321	8
0.5506	0.0020	-2507	9	0.3148	0.0012	-2300	8
0.5795	0.0022	-2420	8	0.3799	0.0014	-2489	9
-	-	-	-	0.4337	0.0016	-2542	9
-	-	-	-	0.4789	0.0018	-2525	9
-	-	-	-	0.5173	0.0019	-2461	8
-	-	-	-	0.5174	0.0019	-2471	9
-	-	-	-	0.5506	0.0020	-2392	8

Table 4-14: Excess molar enthalpies of mixing water and 4-MPD at a pressure of 1.0 MPa

x_a	σx_a	H^E	σH^E	x_a	σx_a	H^E	σH^E
		J mol^{-1}				J mol^{-1}	
303.15 K/ 1.1 ±.12 MPa				313.15 K / 1.06 ±0.12 MPa			
0.01497	0.00006	-281	1	0.01156	0.00005	-202	1
0.01864	0.00008	-338	1	0.01251	0.00005	-215	1
0.02471	0.00011	-424	2	0.01363	0.00006	-229	1
0.04822	0.00021	-739	3	0.01497	0.00006	-246	1
0.07063	0.00030	-1018	5	0.01661	0.00007	-268	1
0.07063	0.00030	-1017	5	0.01865	0.00008	-296	1
0.13194	0.00054	-1677	6	0.02125	0.00009	-326	1
0.13195	0.00054	-1679	6	0.02471	0.00011	-375	2
0.13195	0.00054	-1681	6	0.02950	0.00013	-434	2
0.18567	0.00074	-2152	7	0.03661	0.00016	-523	3
0.23313	0.00092	-2481	9	0.04823	0.00021	-662	3
0.23313	0.00092	-2434	9	0.04823	0.00021	-662	3
0.23314	0.00092	-2513	8	0.07063	0.00030	-919	4
0.31319	0.00120	-2896	11	0.13194	0.00054	-1518	6
0.31321	0.00120	-2828	9	0.13195	0.00054	-1506	5
0.37812	0.00143	-3103	11	0.16853	0.00068	-1799	6
0.43183	0.00162	-3155	11	0.18568	0.00074	-1997	12
0.51552	0.00192	-3059	11	0.23313	0.00092	-2310	10
0.54875	0.00204	-2948	10	0.23315	0.00092	-2310	12
0.60319	0.00225	-2743	10	0.31319	0.00120	-2762	9
-	-	-	-	0.31320	0.00120	-2718	10
-	-	-	-	0.37812	0.00143	-2958	9
-	-	-	-	0.43183	0.00162	-3021	10
-	-	-	-	0.47700	0.00178	-3005	10

x_a	σx_a	H^E	σH^E	x_a	σx_a	H^E	σH^E
		J mol^{-1}				J mol^{-1}	
323.15 K / 1.15±0.14 MPa				343.15 K / 1.08 ± 0.08 MPa			
0.01661	0.00007	-219	1	0.01661	0.00007	-196	1
0.01864	0.00008	-242	1	0.01865	0.00008	-216	1
0.02125	0.00009	-272	1	0.02125	0.00009	-244	1
0.02471	0.00011	-311	2	0.02471	0.00011	-282	1
0.02950	0.00013	-364	2	0.02950	0.00013	-331	1
0.03661	0.00016	-439	2	0.03661	0.00016	-405	2
0.04822	0.00021	-566	3	0.04822	0.00021	-520	3
0.08208	0.00034	-891	4	0.04823	0.00021	-520	3
0.09201	0.00038	-985	4	0.09201	0.00038	-923	5
0.13195	0.00054	-1326	5	0.09202	0.00038	-920	3
0.13195	0.00054	-1319	5	0.16852	0.00068	-1530	6
0.16852	0.00068	-1608	5	0.23313	0.00092	-1925	10
0.20535	0.00082	-1893	7	0.23314	0.00092	-1917	7
0.23314	0.00092	-2050	7	0.23314	0.00092	-1940	11
0.27536	0.00107	-2252	7	0.31319	0.00120	-2282	9
0.31318	0.00120	-2389	8	0.31320	0.00120	-2300	8
0.31320	0.00120	-2412	8	0.37811	0.00143	-2449	9
0.34724	0.00132	-2474	11	0.37812	0.00143	-2434	8
0.37811	0.00143	-2591	10	0.43181	0.00162	-2498	9
0.43182	0.00162	-2645	10	0.47698	0.00178	-2469	9
0.47700	0.00178	-2616	9	0.51549	0.00192	-2402	14
0.51551	0.00192	-2561	9	0.54875	0.00204	-2357	9
0.57771	0.00215	-2397	8	0.57771	0.00215	-2270	8

Table 4-15: Redlich-Kister parameters for the excess molar enthalpies

T / K	A_0		A_1		A_2		Error
				3-MPD			
303.15	-12323.4781	±80	-3479.6793	±500	2204.8389	±800	47
313.15	-11901.978	±50	-2199.1776	±140	-		20
323.15	-10439.5811	±30	-2593.8728	±190	1464.4277	±300	14
333.15	-9986.2405	±25	-2523.5377	±160	1774.3313	±250	10
				4-MPD			
303.15	-12239.3793	±70	-3270.4	±170	-		39
313.15	-11990	±100	-1948.3	±230	-		33
323.15	-10334.25	±40	-2629.3902	±210	1014.79	±300	20
333.15	-9774.2111	±20	-2742.4565	±120	1372.5557	±200	12

Table 4-16: Magnitude and local minima of excess molar enthalpies. The table is arranged by decreasing magnitude of the excess molar volumes.

alkyl-piperidine	4-MPD	3-MPD	2-MPD	N-MPD	Piperidine
Local maximum (x_a)	0.43	0.47	0.42	0.37	0.45
H^E J mol^{-1} at Maximum	-3155	-3129	-2547	-2411	-2225

Table 4-17: Infinite dilution partial molar enthalpies of 3-MPD and 4-MPD.

T	$\overline{H}^{\infty}$	$\sigma\overline{H}^{\infty}$	$\overline{H}^{\infty}$	$\sigma\overline{H}^{\infty}$
K	kJ mol^{-1}		kJ mol^{-1}	
	3-MPD		4-MPD	
298.15[a]	-20.6	9	-22.7	12
303.15	-19.2	0.6	-21.218	0.019
313.15	-17.4	0.3	-18.4	0.3
323.15	-14.1	0.6	-15.1	0.14
333.15	-12.2	0.07	-12.4	0.18

a: estimated from a liner regression of higher temperature data.

*b:*estimated excluding temperature of 313.15 K

Table 4-18: Specific heat capacities and excess molar heat capacities of aqueous 3-MPD solution and pure liquid at atmospheric pressure. [a,b,c,d]

x_a	$c_{p,s}$	C_p^E	x_a	$c_{p,s}$	C_p^E
	J g^{-1} K^{-1}	mol^{-1} K^{-1}		J g^{-1} K^{-1}	mol^{-1} K^{-1}
	288.15 K			298.15 K	
0.00000	4.189	0.0	0.00000	4.181	0.0
0.01016	4.258	3.4	0.01016	4.248	3.3
0.04882	4.074	7.3	0.04882	4.031	6.4
0.05705	4.036	8.0	0.05705	4.006	7.4
0.10536	3.652	6.9	0.10536	3.669	7.4
0.23842	3.107	7.5	0.23842	3.175	9.9
0.27503	3.012	7.8	0.27503	3.084	10.5
0.29867	2.955	7.8	0.29867	3.019	10.4
0.38813	2.780	8.1	0.38813	2.858	11.9
0.47798	2.667	9.5	0.47798	2.730	12.8
0.61886	2.521	10.4	0.61886	2.574	13.7
0.69426	2.455	10.4	0.69426	2.499	13.3
0.80329	2.344	7.7	0.80329	2.374	9.8
0.88389	2.280	6.1	0.88389	2.302	7.5
1.00000	2.165	0.0	1.00000	2.171	0.0
	308.15 K			318.15 K	
0.00000	4.179	0.0	0.00000	4.180	0.0
0.01016	4.246	3.3	0.01016	4.225	2.8
0.04882	4.009	5.9	0.04882	3.998	5.6
0.05705	3.992	7.0	0.05705	3.979	6.6
0.10536	3.695	8.0	0.10536	3.729	8.7
0.23842	3.240	12.0	0.23842	3.282	13.3
0.27503	3.153	13.0	0.27503	3.218	15.2
0.29867	3.089	12.9	0.29867	3.143	14.8
0.38813	2.927	14.7	0.38813	2.979	16.8
0.47798	2.793	15.7	0.47798	2.852	18.4
0.61886	2.626	16.3	0.61886	2.661	17.9
0.69426	2.542	15.4	0.69426	2.578	17.2
0.80329	2.408	11.3	0.80329	2.438	12.8
0.88389	2.331	8.8	0.88389	2.363	10.5
1.00000	2.187	0.0	1.00000	2.200	0.0

x_a	$c_{p,s}$	C_p^E
	J g^{-1} K^{-1}	mol^{-1} K^{-1}
	328.15 K	
0.00000	4.183	0.0
0.01016	4.223	2.7
0.04882	4.008	5.6
0.05705	4.002	7.0
0.10536	3.745	8.8
0.23842	3.343	15.0
0.27503	3.269	16.6
0.29867	3.210	17.0
0.38813	3.030	18.4
0.47798	2.896	19.8
0.61886	2.706	19.5
0.69426	2.611	18.2
0.80329	2.470	13.7
0.88389	2.376	9.8
1.00000	2.222	0.0

*a:*uncertainty in xa ±0.00005

*b:*uncertainty in cp,s ± 0.006 J g -1K-1

*c:*uncertainty in CPE ± 0.7 J mol-1 K-1

d: uncertainty in T ± 0.01 K

Table 4-19: Specific heat capacities and excess molar heat capacities of aqueous 4-MPD solution and pure liquid at atmospheric pressure

x_a	$c_{p,s}$	C_p^E	x_a	$c_{p,s}$	C_p^E
	J g^{-1} K^{-1}	J mol^{-1} K^{-1}		J g^{-1} K^{-1}	J mol^{-1} K^{-1}
	288.15 K			298.15 K	
0.00000	4.189	0.0	0.00000	4.181	0.0
0.00996	4.226	2.7	0.00996	4.221	2.7
0.03413	4.243	8.0	0.03413	4.167	6.5
0.04650	4.093	7.3	0.04650	4.038	6.2
0.09477	3.704	6.7	0.09477	3.724	7.2
0.10787	3.662	7.7	0.10787	3.668	7.8
0.22269	3.149	7.4	0.22269	3.213	9.5
0.26797	3.018	7.5	0.26797	3.090	10.1
0.39705	2.766	8.6	0.39705	2.830	11.3
0.66026	2.463	9.6	0.66026	2.506	11.8
0.82397	2.299	5.7	0.82397	2.330	7.2
0.88720	2.249	4.4	0.88720	2.270	5.0
1.00000	2.155	0.0	1.00000	2.169	0.0
	308.15			318.15	
0.00000	4.179	0.0	0.00000	4.180	0.0
0.00996	4.218	2.7	0.00996	4.206	2.4
0.03413	4.119	5.5	0.03413	4.102	5.1
0.04650	4.009	5.5	0.04650	3.993	5.0
0.09477	3.720	6.9	0.09477	3.735	7.1
0.10787	3.689	8.1	0.10787	3.713	8.6
0.22269	3.273	11.2	0.22269	3.326	12.8
0.26797	3.155	12.1	0.26797	3.213	14.0
0.39705	2.901	14.0	0.39705	2.947	15.8
0.66026	2.548	13.3	0.66026	2.583	14.9
0.82397	2.359	7.8	0.82397	2.387	9.1
0.88720	2.297	5.3	0.88720	2.319	6.2
1.00000	2.193	0.0	1.00000	2.206	0.0

x_a	$c_{p,s}$	C_p^E
	J g^{-1} K^{-1}	$Jmol^{-1}$ K^{-1}
	328.15	
0.00000	4.183	0.0
0.00996	4.204	2.3
0.03413	4.102	4.9
0.04650	3.997	4.9
0.09477	3.761	7.5
0.10787	3.750	9.2
0.22269	3.385	14.2
0.26797	3.274	15.6
0.39705	3.006	17.5
0.66026	2.629	16.2
0.82397	2.421	9.5
0.88720	2.352	6.4
1.00000	2.237	0.0

*a:*uncertainty in xa ±0.00005

*b:*uncertainty in cp,s ± 0.006 J g -1K-1

*c:*uncertainty in CPE ± 0.7 J mol-1 K-1

d: uncertainty in T ± 0.01 K

Table 4-20: Redlich-Kister fitting parameters for excess molar heat capacities.

T / K	A_0		A_1		A_2		A_3		A_4		Error
					N-MPD						
288.15	64.0011	±4	30.6121	±15	-151.911	±50	23.3363	±50	458.0154	±30	1.0
298.15	73.9555	±1.7	31.1487	±6	-80.9046	±19	37.8726	±20	276.153	±40	0.4
308.15	79.793	±0.04	29.9809	±0.15	-20.2544	±0.4	34.2076	±0.5	164.5129	±0.9	0.009
					2-MPD						
288.15	53.7675	±0.14	3.0566	±0.4	8.8331	±0.5	-2.9271	±1.0	-		0.031
298.15	67.7397	±0.4	3.634	±1.0	5.6262	±1.4	-9.5306	±3	-		0.08
308.15	80.3791	±0.5	2.6989	±1.5	-0.1318	±2	-11.4361	±4	-		0.12
318.15	88.817	±1.1	9.8267	±3	-2.6959	±4	-31.9716	±8	-		0.24
328.15	98.5787	±1.3	8.4864	±4	-2.4318	±5	-35.0119	±10	-		0.29
					3-MPD						
288.15	40.6965	±2.5	-26.6632	±7	-20.2916	±24	74.8683	±18	127.9026	±39	0.9
298.15	54.3463	±2.2	-22.9477	±6	-13.1846	±22	57.2086	±17	98.8296	±35	0.8
308.15	65.5376	±2.1	-17.7415	±6	-9.4137	±20	40.3677	±16	80.9123	±32	0.7
318.15	74.5611	±1.8	-11.0934	±5.1	-11.9804	±18	15.2194	±14	85.503	±28	0.6
328.15	80.4837	±1.7	-9.7111	±5	3.446	±16	24.6143	±13	44.0855	±26	0.6
					4-MPD						
288.15	45.0196	±6	-20.7781	±13	-83.5627	±50	76.7368	±29	198.0662	±68	1.2
298.15	53.192	±4	-15.0293	±9	-47.7129	±30	62.4607	±21	125.0679	±51	0.8
308.15	62.1875	±4	-5.2232	±8	-42.0334	±29	42.8508	±18	94.425	±43	0.8
318.15	67.8366	±3	-2.1583	±7	-15.5718	±26	34.0323	±16	50.1353	±39	0.8
328.15	74.0278	±3	2.2654	±7	-9.8358	±25	30.5146	±16	31.8518	±40	0.6

Table 4-21: Magnitude and local minima of excess molar heat capacities at 318.15K. The table is arranged by decreasing magnitude of the excess volumes.

alkyl-piperidine	2-MPD	N-MPD	4-MPD	3-MPD
global maximum (x_a)	0.50	0.43	0.50	0.50
C_p^E J mol^{-1} K^{-1} at Maximum	20.09	20.54	15.56	16.63

5 Enthalpy of Carbon Dioxide Dissolution in Aqueous 3-methylpiperidine and 4-methylpiperidine; A Solubility Model

Here, are presented direct measurements data of the enthalpy of solution ($\Delta_{sol}H$) for CO_2 absorption by aqueous solutions of 3-methylpiperidine (3-MPD) and 4-methylpiperidine (4-MPD). Both binary systems {X-MPD – H_2O} have lower critical solution temperatures above 338 K (Stephenson, 1993). The $\Delta_{sol}H$ of 3-MPD and 4-MPD are measured at the temperatures of 318 K and 338 K and at pressures of 0.5, 1.0 and 1.5 MPa. Aqueous solution of 3-MPD and 4-MPD were prepared within the composition range from $15w_a\%$ to $40w_a\%$. CO_2 reacts with amine to form carbamate species with respect to temperature conditions of the solutions. The measurements were made with the SETARAM BT 2.15 calorimeter using a custom made mixing cells unique to this laboratory. The measured data have been used with a modified Pitzer model developed to represent the absorption of CO_2 in aqueous solutions of 2-methylpiperidine (2-MPD) to attempt to find a carbamate formation constant for 3-MPD and 4-MPD. The carbamate constants of 3-MPD and 4-MPD are derived from the measured solubility and enthalpy data.

5.1 Experimental

5.1.1 Technic and Procedure

The experimental design uses the same equipment and procedure mentioned in section 4.3.3 for measuring excess molar enthalpies. The mixing point and calculation of the loading charge composition is found in section 3.2.2. The relative uncertainty on the loading charge in this work is estimated to be about 1.5%. The complete experimental design and detail on uncertainties calculation are given in the work of from this lab, (Arcis et al., 2011; Arcis et al., 2012b; Arcis et al., 2012a).

5.1.2 Results

The enthalpy of solution of CO_2 dissolution in the aqueous amine solutions ($w_{3\text{-MPD}}$%=19 and 40 and $w_{4\text{-MPD}}$%=17 and 40) was measured at 318 K and 338 K and at pressures from 0.5 MPa to 1.5 MPa. Experiments were conducted for different loadings (α) up to the saturation of the absorbent solution, together with the experimental uncertainties they are listed in Table 5-4 to Table 5-10. At 338 K a single 3-MPD solution of 40.00 w_a% was measured. The dissolution of CO_2 into the 20.00 w_a% solution of 3-MPD could not be measured, due to instability in the calorimetric signal, before adding the CO_2. When studying the liquid-liquid phase diagram of this amine in water, it is observed that at this composition (20 w_a%) corresponds to a molar fraction of amine of 0.04, which is located near the LCST of the diagram. For this amine, the temperature of phase separation is very close to the temperature of the calorimeter. Then, the binary mixture arriving at the mixing point is oscillating between heterogeneous and homogeneous solutions, leading to instability of the signal. Even so the solution after adding CO_2 is homogenous, the measurements cannot be conducted.

The experimental enthalpies have been plotted versus the gas loading charge α (mole of CO_2/mole of amine) and are given in Figure 5-7 to Figure 5-13 together with the corresponding tables (Table 5-4 to Table 5-10) in appendix 5.4. Large exothermic effects were observed at both temperatures and for both systems. As an example, the enthalpies of solution versus the loading charge measured at T = 318 K and $w_{4\text{-MPD}}$% = 39.86, are illustrated in Figure 5-1 and Figure 5-2. When the enthalpy of solution $\Delta_{sol}H_{CO_2}$ is expressed in kJ·mol^{-1} of CO_2 (Figure 5-1), the graph exhibits plateaus for the lowest loadings, up to 0.5, and then the exothermic effect decreases as the loading increases. At the lowest loadings (Figure 5-1), the energetic effect per mole of gas appears to be constant, within experimental uncertainty, and independent of CO_2 loading. This behaviour was also observed and reported in the literature. (Arcis et al., 2011; Arcis et al., 2012a; Coulier et al., 2016).

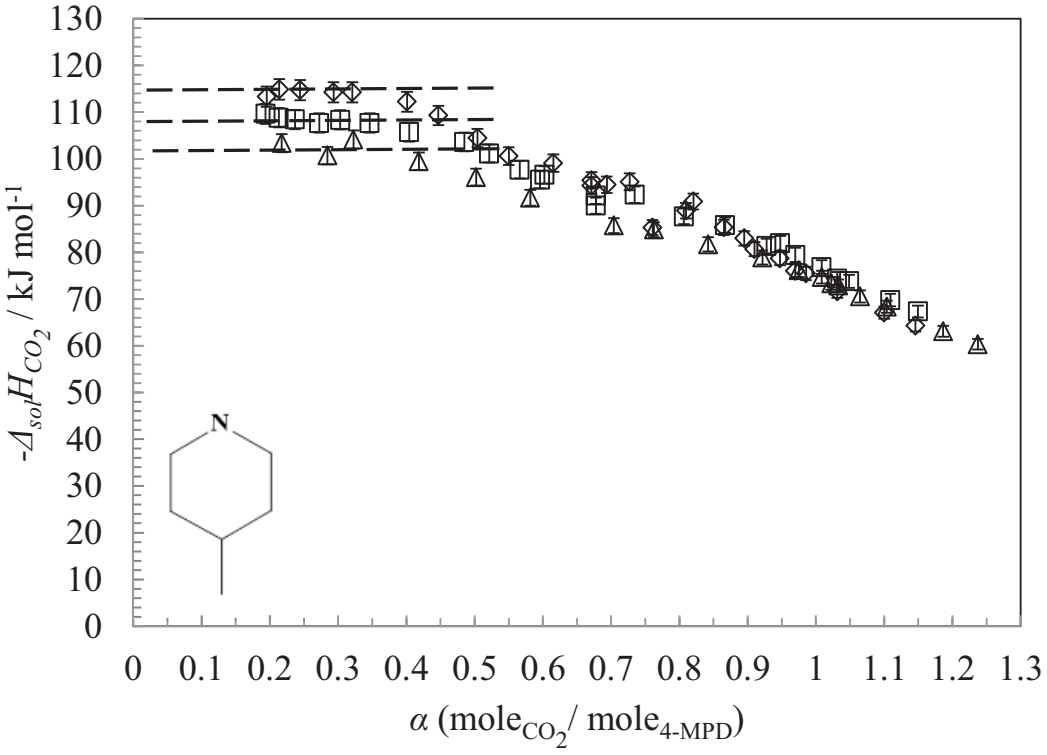

Figure 5-1: Solution enthalpies per mole of carbon dioxide for a 39.86 w_a% 4-MPD solution. The dashed lines represent the data selected for the average enthalpy of dissolution for CO_2 in solution. (◇(0.43 MPa), □ (0.95 MPa), △ (1.45 MPa))

The average enthalpy values $\Delta_{sol}H^{av}{}_{CO_2}$, for $\alpha < 0.5$, expressed in kJ·mol^{-1} of CO_2 and all experimental conditions investigated are reported in table 5.1 and table 5.2. A small decrease of $\Delta_{sol}H^{av}{}_{CO_2}$ is observed as the composition rises for the same condition of pressure and temperature. A small reduction of the exothermic effect is noticed when the temperature or the pressure increases. The migration of the methyl group has no apparent effect on the $\Delta_{sol}H^{av}{}_{CO_2}$.

In Figure 5-2, experimental enthalpies of solution expressed in kJ mol^{-1}of 4-MPD show three different domains. In the first domain ($0 < \alpha < 0.5$), $\Delta_{sol}H_a$ increases linearly with the loading charge. The value of the slope in this domain is equal to $\Delta_{sol}H^{av}{}_a$ obtained previously (Figure 5-1). Then, $\Delta_{sol}H_a$ keep rising but with a different slope to reach a plateau. The change in slope is usually due to a change

in the absorption mechanism. This change is described by the thermodynamic modeling in the next section. The last domain where the enthalpy of solution stays constant is characteristic of a saturated solution. The intersection between unsaturated (enthalpy increase) and saturated (plateau) domains yields the solubility limit (α_s). The experimental uncertainty is dependent on the precision on the identification of the first point of the plateau. This based on the reproducibility of the measurements and systematic errors affecting the solution enthalpy, or the tolerance of the pump flow rates. The relative cumulative uncertainty in the solubility data is within, 5 to 9 %. Experimental solubility limits in aqueous 3-MPD and 4-MPD solutions were graphically determined at 318 K and 338 K, values are listed in Table 5-1 and Table 5-2 together with their uncertainties.

Table 5-1: Enthalpies of solution for CO_2 dissolution and solubility of CO_2 in aqueous solutions of 3-MPD

p	σp	$-\Delta_s H^{av}_{CO2}$	$\sigma -\Delta_s H^{av}_{CO2}$	α_s	$\sigma \alpha_s$	p	σp	$-\Delta_s H^{av}_{CO2}$	$\sigma -\Delta_s H^{av}_{CO2}$	α_s	$\sigma \alpha_s$
MPa		kJ mol^{-1}		$mol_{CO_2}/mol_{3\text{-MPD}}$		MPa		kJ mol^{-1}		$mol_{CO_2}/mol_{3\text{-MPD}}$	
T=318 K											
		$w_{3\text{-MPD}}$ %=19.36							$w_{3\text{-MPD}}$ %=40.44		
0.43	0.02	113.5	0.7	0.940	0.07	0.56	0.02	89.4	2.8	0.850	0.06
0.96	0.02	112.3	3.0	1.018	0.07	1.07	0.02	93.8	1.9	0.948	0.07
1.47	0.02	102.4	2.0	1.029	0.07	1.47	0.02	95.3	1.6	0.960	0.07
T=338 K											
		$w_{3\text{-MPD}}$ %=20.00							$w_{3\text{-MPD}}$ %=40.00		
		-	-	-		0.46	0.02	106.1	2.1	0.813	0.06
		-	-	-		0.99	0.02	99.7	1.6	0.880	0.06
		-	-	-		1.51	0.02	96.8	0.9	0.920	0.06

Table 5-2: Enthalpies of solution for CO_2 dissolution and solubility of CO_2 in aqueous solutions of 4-MPD

p	σp	$-\Delta_s H^{av}_{CO2}$	$\sigma -\Delta_s H^{av}_{CO2}$	α_s	$\sigma \alpha_s$	p	σp	$-\Delta_s H^{av}_{CO2}$	$\sigma -\Delta_s H^{av}_{CO2}$	α_s	$\sigma \alpha_s$
MPa		kJ mol^{-1}		$mol_{CO_2}/mol_{4\text{-MPD}}$		MPa		kJ mol^{-1}		$mol_{CO_2}/mol_{4\text{-MPD}}$	
T=318 K											
		$w_{4\text{-MPD}}$ %=16.57							$w_{4\text{-MPD}}$ %=39.86		
0.43	0.02	118.6	2.3	0.928	0.06	0.43	0.02	113.9	1	0.824	0.06
0.96	0.02	108.2	1.1	0.977	0.07	0.95	0.02	108.0	1.2	0.915	0.06
1.48	0.02	103.7	2.9	0.991	0.07	1.45	0.02	102.7	1.8	0.949	0.07
T=338 K											
		$w_{4\text{-MPD}}$ %=20.00							$w_{4\text{-MPD}}$ %=40.00		
0.47	0.02	101.1	1.3	0.876	0.06	0.47	0.02	99.8	2.4	0.804	0.06
0.98	0.02	96.3	2.7	0.958	0.07	0.96	0.04	96.6	2.1	0.920	0.06
1.50	0.02	95.4	1.9	0.960	0.07	1.47	0.02	89.6	1.7	0.935	0.07

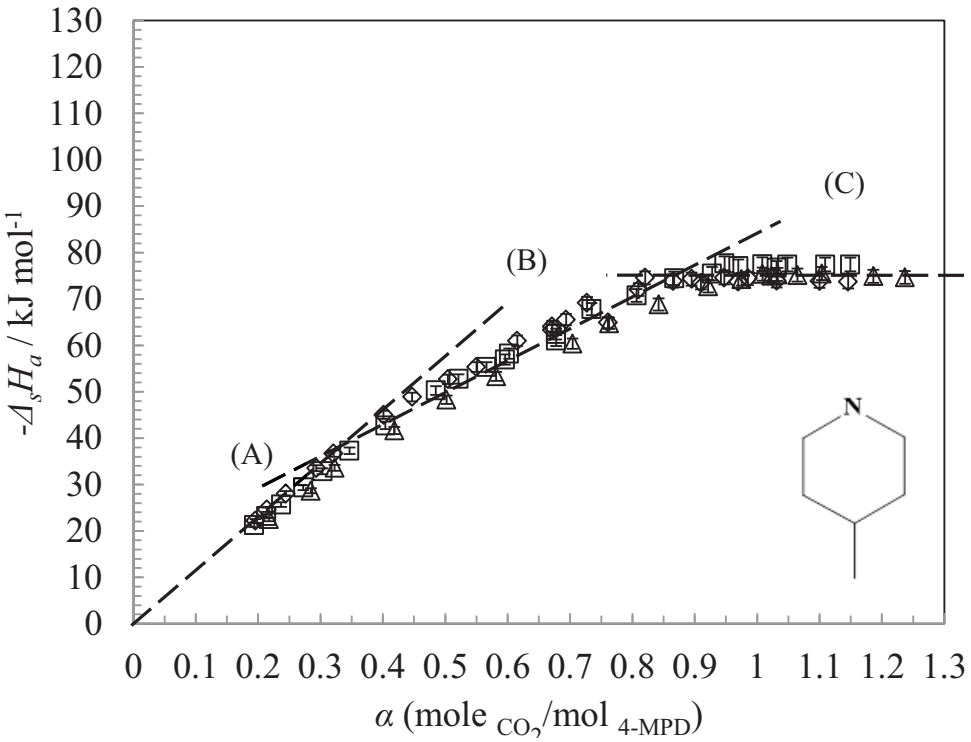

Figure 5-2: Solution enthalpies per mol of amine for a 39.86 w_a% 4-MPD solution. The dashed lines represent the three separate regions for the solution enthalpies. (A) The initial slope. (B) the second slope representing the change in absorption mechanism (C) Plateau representing the saturation of the solution. The intercepts of slops B and C reveal the solubility limits for each solution. (◇(0.43 MPa), □ (0.95 MPa), △ (1.45 MPa))

5.2 Thermodynamic Framework

The model presented here is similar with the model used by (Coulier *et al.* 2015) to represent the absorption of CO_2 in aqueous solutions of 2-methylpiperidine. It is based on two types of equilibria, namely chemical reactions and vapour-liquid-phase equilibria for molecular species. Ionic species are treated as non-volatile compounds. The solution is treated as a single solvent system. All other species in the liquid phase are considered to be molecular or ionic solute.

5.2.1 Modelling Speciation and Absorption

Illustrated in the Figure 5-3 are the species present at the equilibrium in the system.

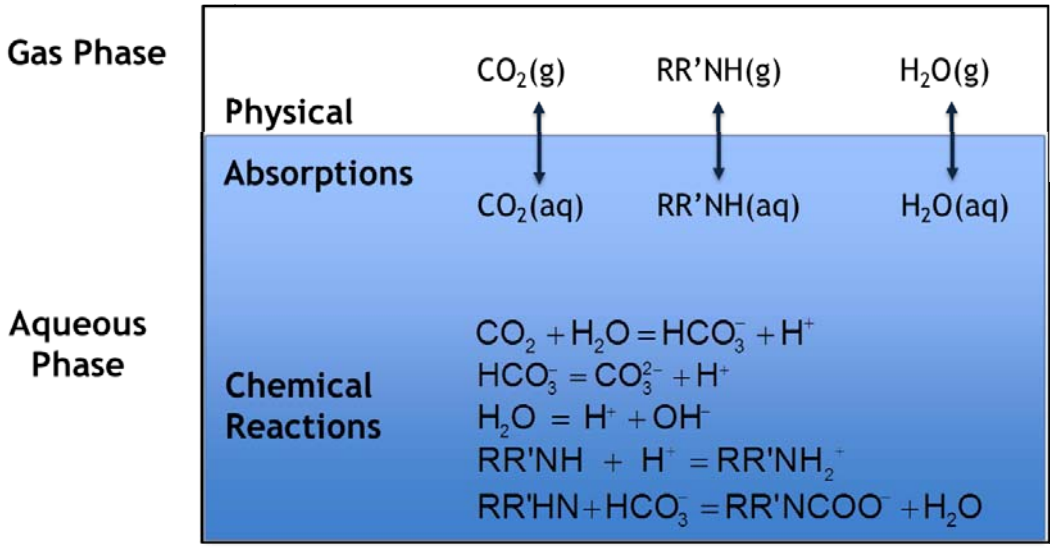

Figure 5-3: Illustration of the different equilibrium conditions and reactions in the system to be modelled.

Chemical equilibria involved in the dissolution of CO_2 in an aqueous solution of amine are:

$$H_2O \rightleftharpoons H^+ + OH^- \qquad \textbf{Eq 5-1}$$

$$CO_2 + H_2O \rightleftharpoons HCO_3^- + H^+ \qquad \textbf{Eq 5-2}$$

$$HCO_3^- \rightleftharpoons CO_3^{2-} + H^+ \qquad \textbf{Eq 5-3}$$

$$RR'NH_2^+ \rightleftharpoons RR'NH + H^+ \qquad \textbf{Eq 5-4}$$

$$RR'NCOO^- + H_2O \rightleftharpoons RR'NH + HCO_3^- \qquad \textbf{Eq 5-5}$$

Chemical equilibria are governed by their equilibrium constant, K:

$$K = \prod_i a_i^{\upsilon_i} \qquad \textbf{Eq 5-6}$$

where a_i is the activity of species i and υ_i is the stoichiometric coefficient for the component i in the considered reaction. Equilibrium constants are based on molality scale. The dissociation constant of water, equation 5-1, was taken from Marshall and Franck (Marshall and Franck, 1981). The temperature dependence of equilibria 5-1 to 5-5 is represented by the following function:

$$\ln K = A/(T/\mathrm{K}) + B + C \cdot \ln(T/\mathrm{K}) \qquad \textbf{Eq 5-7}$$

First and second dissociation constants of CO_2 (reaction equations 5-2 and 5-3) were obtained from H. Renon (Renon, 1980). The dissociation constants of 3-MPD and 4-MPD (reaction equation 5-4) used in this work was derived from calorimetric measurements obtained in the laboratory (Brethes and Chassagnette, 2014) and not yet published. The experimental determination of equilibrium constant for carbamate formation is challenging and no values have been reported yet for 3-MPD and 4-MPD. Hence, the carbamate formation constant was treated as an adjustable parameter of the model. Values of coefficients A, B and C for reaction equations 5-2 to 5-5 are summarized in Table 5-3.

Table 5-3: Parameters for equilibrium constants

Equation number	A	B	C
	K^{-1}		
5-2	-12092.1	235.482	-36.7816
5-3	-12431.7	220.67	-35.5819
5-4(3-MPD)	-6820.8	-2.2497	-
5-4(4-MPD)	-6755.9	-2.6023	-
5-5(3-MPD)	4375.3	-9.6849	-
5-5(4-MPD)	3700.6	-7.6337	-

Considering the chemical reactions (5-1 to 5-5), the conservation equations for the overall amounts $\overline{n}_i$ of methylpiperidine, carbon dioxide and water were applied:

$$n_{HCO_3^-} + n_{CO_3^{2-}} + n_{CO_2} + n_{RR'NCOO^-} = \overline{n}_{CO_2} \quad \textbf{Eq 5-8}$$

$$n_{RR'NH_2^+} + n_{RR'NCOO^-} + n_{RR'NH} = \overline{n}_{RR'NH} \quad \textbf{Eq 5-9}$$

$$n_{HCO_3^-} + n_{CO_3^{2-}} + n_{HO^-} + n_{H_2O} = \overline{n}_{H_2O} \quad \textbf{Eq 5-10}$$

Together with the condition of electroneutrality:

$$n_{HCO_3^-} + 2n_{CO_3^{2-}} + n_{HO^-} + n_{RR'NCOO^-} = n_{RR'NH_2^+} + n_{H^+} \quad \textbf{Eq 5-11}$$

The vapour-liquid equilibria encountered are defined by equations 5-12 to 5-14

$$RR'NH^{(l)} \rightleftharpoons RR'NH^{(v)} \qquad \textbf{Eq 5-12}$$

$$H_2O^{(l)} \rightleftharpoons H_2O^{(v)} \qquad \textbf{Eq 5-13}$$

$$CO_2^{(l)} \rightleftharpoons CO_2^{(v)} \qquad \textbf{Eq 5-14}$$

The conservation equation of the vapour phase is expressed as follows:

$$y_{CO_2} + y_{H_2O} + y_{RR'NH} = 1 \qquad \textbf{Eq 5-15}$$

To represent the liquid-vapour equilibrium of water the extended Raoult's law is used equation 5-16. For CO_2 and MPD phase equilibria the extended Henry's law is employed equation 5-17. These equations can be applied to calculate the total pressure and the composition of the gas phase:

$$y_{H_2O}\phi_{H_2O}p = a_{H_2O}\phi^{sat}_{H_2O}p^{sat}_{H_2O}\exp\left(\frac{v_{H_2O}\left(p - p^{sat}_{H_2O}\right)}{RT}\right) \qquad \textbf{Eq 5-16}$$

$$y_a\phi_a p = \gamma_a m_a k_{H,a}\left(T, p^{sat}_{H_2O}\right)\exp\left(\frac{\bar{v}^{\infty}_a\left(p - p^{sat}_{H_2O}\right)}{RT}\right), \text{ where } a\text{=3-MPD, 4-MPD or } CO_2 \qquad \textbf{Eq 5-17}$$

In order to solve equations 5-16 and 5-17, the knowledge of Henry's constant k_{H,CO_2}, on the molality scale, for carbon dioxide in pure water, the vapour pressure $p^{sat}_{H_2O}$ and the molar volume v_{H_2O} of pure water, and the partial molar volumes $\bar{v}^{\infty}_{CO_2}$ of the dissolved carbon dioxide at infinite dilution in water, are required. All the correlations used to calculate these thermodynamic properties are given by Arcis *et al.*(Arcis et al., 2009). The temperature dependence of the partial molar volumes $\bar{v}^{\infty}_{RR'NH}$ of 3-MPD and

4-MPD at infinite dilution in water were measured by McGregor (Christine McGregor, 2017) in the University of Guelph but have not been published yet (equations 5-18 and 5-19):

$$\bar{v}^{\infty}_{\text{3-MPD}}/\text{cm}^3\cdot\text{mol}^{-1} = 1.8149\cdot10^{-4}(T/K)^2 + 7.1507\cdot10^{-3}(T/\text{K}) + 92.449 \qquad \textbf{Eq 5-18}$$

$$\bar{v}^{\infty}_{\text{4-MPD}}/\text{cm}^3\cdot\text{mol}^{-1} = 2.2706\cdot10^{-4}(T/K)^2 - 2.2913\cdot10^{-2}(T/\text{K}) + 97.400 \qquad \textbf{Eq 5-19}$$

The Henry's constants for $k_{\text{H,3-MPD}}$ and $k_{\text{H,4-MPD}}$ in pure water are not available in the literature and are estimated for this model. The method given by (Edwards et al., 1978) could not be used since no values for the VLE equilibria for both of the binary systems {X-MPD – H_2O} have been measured. Hence the temperature dependence of the Henry's law constant was derived from the combination of the activity coefficient at infinite dilution of piperidine measured by Bernauer and Dohnal (Bernauer and Dohnal, 2009) with the vapour pressure of the pure compounds measured in our laboratory:

$$k_{H,a} = \gamma_a^{\infty}\cdot p_a^{\text{sat}} \qquad \text{where } a\text{=3-MPD or 4-MPD} \qquad \textbf{Eq 5-20}$$

Soave's modification of the Redlich-Kwong equation of state is used to represent the equilibrium behaviour of the vapour phase. Fugacity coefficients for all species in the vapour phase ϕ_i (equations 5-16 and 5-17), are calculated using the Soave-Redlich-Kwong equation of state (SRK).

$$p = \frac{RT}{V-b} - \frac{a\alpha(T,\omega)}{V(V+b)} \qquad \textbf{Eq 5-21}$$

where the values of *a* and *b* are

$$a = 0.42748 \frac{R^2 T_c^2}{p_c} \alpha(T)$$ **Eq 5-22**

$$b = 0.08664 \frac{RT_c}{p_c}$$ **Eq 5-23**

where $\alpha(T)$ is equal to

$$\alpha(T) = \left[1 + \left(0.48508 + 1.55171\,\omega - 0.15613\,\omega^2\right)\left(1 - \sqrt{T_r}\right)\right]^2$$ **Eq 5-24**

Where ω is the acentric factor, T_c and p_c are the critical temperature and pressure of the pure species and T_r is the reduced temperature. The values of these critical properties for 3-MPD and 4-MPD are found in (Yaws, 2014). The original mixing rules used by Redlich and Kwong (Redlich and Kwong, 1949) are used in this work to calculate equation of state parameters for gas mixtures:

$$a_m = \sum_i \sum_j y_i y_j \left(a_i \alpha_i a_j \alpha_j\right)^{0.5}$$ **Eq 5-25**

$$b_m = \sum_i y_i b_i$$ **Eq 5-26**

By proper rearrangement, the SRK equation of state can also be written as a cubic equation in volume:

$$V^3 - \frac{RT}{p} V^2 + \frac{1}{p}\left(a\alpha - bRT - pb^2\right)V - \frac{a\alpha b}{p} = 0$$ **Eq 5-27**

As discussed in section 2.1.1, the fugacity coefficient of any component in a gas mixture can be calculated through application of the following equation:

$$\mathrm{R}T\ln\varphi_i = \int_0^P \left(\overline{V}_i - V_i\right) dp \qquad \textbf{Eq 2-7}$$

The partial molar volume, $\overline{V}_i$, of any molecular component is calculated from the previous equation and the mixing rules equations. From equation 2-7, equation 5-25, equation 5-26 and equation 5-27 the fugacity coefficient based on the SRK equation of state is:

$$\ln\varphi_i = \frac{b_i}{b_{\mathrm{m}}}(z-1) - \ln\left[z\left(1-\frac{b_m}{V}\right)\right] + \frac{(a\alpha)_m}{b_m RT}\left[\frac{b_i}{b_m} - \frac{2}{(a\alpha)_m}\sum_j y_j (a\alpha)_{ij}\right]\ln\left(1+\frac{b_m}{V}\right) \qquad \textbf{Eq 5-28}$$

where:

$$z = pV/RT \qquad \textbf{Eq 5-29}$$

$$(a\alpha)_{ij} = \left[(a_i\alpha_i)(a_j\alpha_j)\right]^{1/2} \qquad \textbf{Eq 5-30}$$

$$(a\alpha)_m = \sum_i \sum_j y_i y_j (a\alpha)_{ij} \qquad \textbf{Eq 5-31}$$

In order to calculate φ_i it is first necessary to calculate V of the mixture. For that purpose, equation 5-27 is solved using Newton-Raphson procedure. Then, equation 5-29 is used to calculate the fugacity coefficient of all components in the vapour phase.

Activity coefficients γ_i, of both neutral and ionic species were calculated, using Pitzer model modified by Edwards et al., 1978.

$$\ln \gamma_i = -A_\phi z_i^2 \left[\frac{\sqrt{I}}{1+b\sqrt{I}} + \frac{2}{b} \ln\left(1+b\sqrt{I}\right) \right] + 2 \sum_{j \neq H_2O} m_j \left\{ \beta_{i,j}^0 + \frac{\beta_{i,j}^1}{2I} \left[1 - \left(1+2\sqrt{I}\right) \exp\left(-2\sqrt{I}\right) \right] \right\} - \frac{z_i^2}{4I^2} \sum_{j \neq H_2O} \sum_{k \neq H_2O} m_j m_k \beta_{j,k}^1 \left[1 - \left(1+2\sqrt{I}\right) \exp\left(-2\sqrt{I}\right) \right] \quad \textbf{Eq 5-32}$$

where, m_i, z_i, are molality, and charge of species i; m_j, m_k, are molality of species j and k; I is the ionic strength in mol·kg^{-1}; A_ϕ, in units of (kg/mol)$^{-1/2}$, is the Debye-Hückel limiting slope for osmotic coefficient at the experimental temperature and pressure; $\beta_{i,j}^0$ and $\beta_{i,j}^1$ are binary Pitzer interaction parameters in unit of kg of water per mole; and Pitzer parameter b = 1.2 kg$^{1/2}$·mol$^{-1/2}$. Interaction parameters between ions of like charge are all assigned to zero. The influence of the temperature on those parameters was expressed as follows:

$$\beta_{i,j}^0 = \beta_{i,j}^0(\mathrm{a}) + \frac{\beta_{i,j}^0(\mathrm{b})}{T(K)} \quad \textbf{Eq 5-33}$$

The activity of water is determined from the Gibbs-Duhem equation:

$$\ln a_{H_2O} = M_{\mathrm{H_2O}} \left\{ \frac{2A_\varphi I^{3/2}}{1+b\sqrt{I}} - \sum_{i\neq \mathrm{H_2O}} \sum_{j\neq \mathrm{H_2O}} m_i m_j \left[\beta^0_{i,j} + \beta^1_{i,j} \exp\left(-2\sqrt{I}\right) \right] - \sum_{i\neq \mathrm{H_2O}} m_i \right\} \qquad \textbf{Eq 5-34}$$

5.2.2 Modelling Enthalpies

The enthalpy of solution is the combination of all reaction enthalpies, ΔH_N associated to the previously discussed physical and chemical equilibria.

$$\Delta H_N = \Delta H^\circ_N + \sum_i \upsilon_{i,N} \overline{H}^E_i \qquad \textbf{Eq 5-35}$$

Where the ΔH°_N, is the standard enthalpy of reaction, v_i is the stoichiometric coefficients, and $\overline{H}^E_i$ is the excess partial molar enthalpies from species *i*. The reaction enthalpies are calculated using the van't Hoff equation where

$$\left(\frac{\partial ln K_N}{\partial T} \right)_p = \frac{\Delta H^\circ_N}{RT^2} \qquad \textbf{Eq 5-36}$$

Excess enthalpies for species *i* and water are calculated using the temperature differentiation of the activity coefficient and activity of water respectively.

$$H^E_i = -RT^2 \left(\frac{\partial \ln \gamma_i}{\partial T} \right)_{\mathrm{p}} \qquad \textbf{Eq 5-37}$$

$$H^E_w = -RT^2 \left(\frac{\partial \ln a_w}{\partial T} \right)_p \qquad \textbf{Eq 5-38}$$

The heat of the absorption Q_N is calculated using the sum of the $\Delta H°_{N,}$ and H^E_i with respect to the extent of reaction.

$$Q_N = \xi_N \sum \left(\Delta H^{\circ}_N + v_i H^E_N \right) \qquad \textbf{Eq 5-39}$$

The enthalpy of physical dissolution is calculated using the Gibbs-Helmoltz equation,

$$\left(\frac{\partial \Delta_r G/T}{\partial T} \right)_p = - \frac{\Delta H_G}{T^2} \qquad \textbf{Eq 5-40}$$

The Gibbs free energy of reaction $\Delta_r G$ for the solubility of carbon dioxide in water is defined by

$$\Delta_r G = RT \left[\begin{array}{l} \ln k_{H,CO_2}\left(T, p_w^{sat}\right) + \ln\left(\gamma_{CO_2} m_{CO_2} \exp\left\{ \frac{\bar{V}^{\infty}_{CO_2}\left(p - p_w^{sat}\right)}{RT} \right\} \right) \\ -\ln\left(\varphi_{CO_2} y_{CO_2} p \right) \end{array} \right] \qquad \textbf{Eq 5-41}$$

The first derivative of equation 5-41 results by equation 5-42 results in the following relationship

$$\Delta H_G = -RT^2 \left[\frac{\partial \ln k_{H,CO_2}\left(T, p_w^{sat}\right)}{\partial T} + \frac{\partial \ln \gamma_{CO_2}}{\partial T} + \frac{\bar{V}^{\infty}_{CO_2}\left(p - p_w^{sat}\right)/RT}{\partial T} - \frac{\partial \ln \varphi_{CO_2}}{\partial T} \right] \qquad \textbf{Eq 5-42}$$

The enthalpy of solution $\Delta_{sol}H$ in sum of enthalpies of reactions for physical dissolution ΔH_G and heats of absorption Q_N.

$$\Delta_s H = \Delta H_G + \sum_N Q_N \Big/ n^{dis}_{CO_2} \qquad \textbf{Eq 5-43}$$

5.2.3 Modelling Strategy

The Pitzer parameters determined by Coulier *et al.* to represent the absorption of CO_2 in aqueous solutions of 2-MPD were used for {CO_2 – 3-MPD – H_2O} and for {CO_2 – 4-MPD – H_2O} systems. The solubility and enthalpy data determined in this study were used to adjust equilibrium constant of carbamate formation. The carbamate formation equation takes the same form as equation 5-8 with parameters A and B fitted to generate the carbamate values as seen in Table 5-3. The equilibrium of the system was resolved using the Newton-Raphson algorithm. The regression was conducted using Minuit Software (James, 1994) written for Fortran 77. The simplex fitting algorithm in Minuit was used to optimize the carbamate formation constant for 3-MPD and 4-MPD using the normalized objective function below.

$$F_1 = \sum_i^{n_1} \left(\frac{\Delta_{sol} H_i^{exp} - \Delta_{sol} H_i^{calc}}{\delta \Delta_{sol} H_i^{exp}} \right)^2 + \sum_i^{n_2} \left(\frac{p_i^{exp} - p_i^{calc}}{\delta p_i} \right)^2 \qquad \textbf{Eq 5-44}$$

where $\delta\Delta_{sol}H_i^{exp}$ and $\delta p_{,i}$ are the experimental uncertainties; n_i are the number of experimental data points. The resulting parameters for equation 5-8 are listed in Table 5-3.

5.2.4 Model Results

The ability of the thermodynamic model to describe the solubility of CO_2 in aqueous solutions of amine (3-MPD and 4-MPD) was assessed by comparing calculated total equilibrium pressure at different loadings with the experimental value determined from the measured enthalpies of solution in this study. As shown in Figure 5-1, a good agreement is observed for both systems.

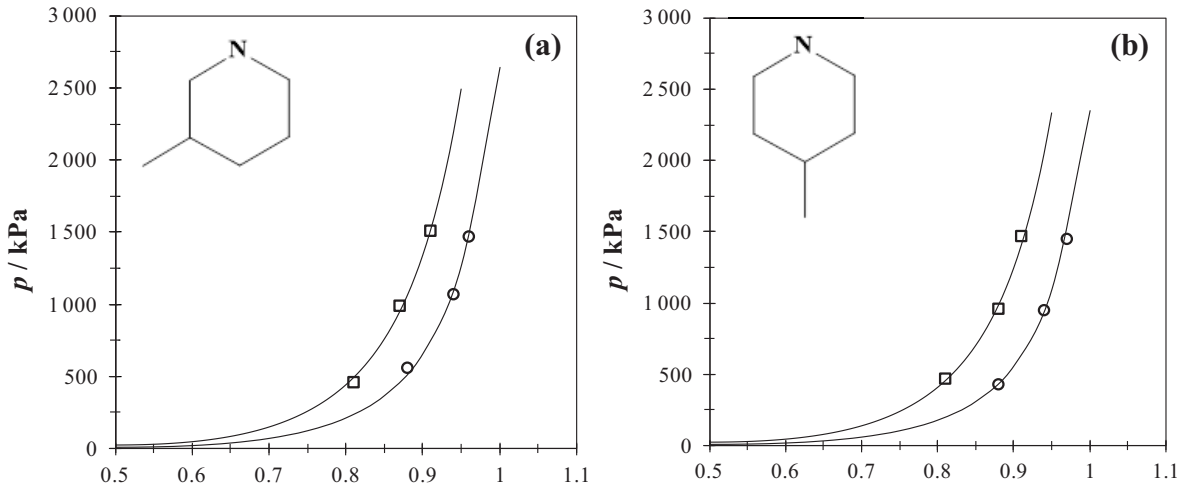

Figure 5-4: Experimental Solubility (*s*) of CO_2 in aqueous, (a), 3-MPD and, (b), 4-MPD solutions (w_a%=40) vs total pressure. (○), 318 K and (□), 338 K. Solid lines are the calculated solubility at 318 and 338 K.

The thermodynamic model used in this study is aimed at providing a reliable representation of the heat of absorption of CO_2 in an aqueous solution of 3-MPD or 4-MPD. Correlations of the experimental enthalpies of solution for different loadings at 318 K and 338 K and w_a%= 40 are shown in Figure 5-5 for both systems. The agreement is excellent for the 3-MPD solutions at all temperatures within ±5% deviation. For the 4-MPD solutions, good agreement is observed at 338 K. At 318 K, the model underestimates the energetic effect, especially at low loadings where the deviation is about 10%.

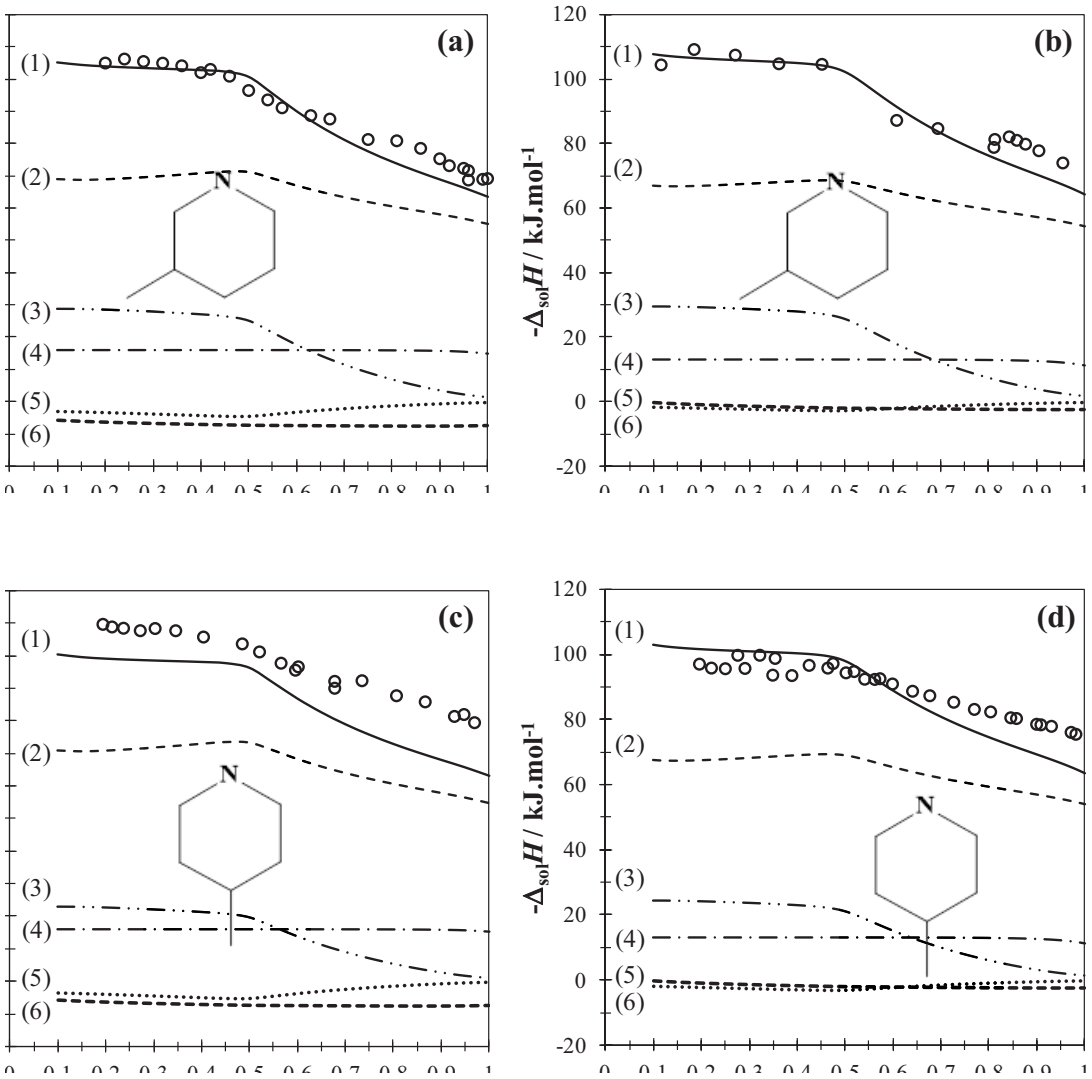

Figure 5-5: Enthalpies of solution ($\Delta_{sol}H$ / kJ·mol$^{-1}_{CO_2}$) versus CO_2 loading for aqueous solutions of 3-MPD and 4-MPD: ○, experimental data. From the thermodynamic model: (1), total enthalpy of solution; enthalpic contribution from equilibria: (2), amine protonation (eq 6-4); (3), carbamate formation (eq 6-5); (4), CO_2 vapour – liquid equilibrium; (5), second ionization of CO_2 (eq 6-2); (6), first ionization of CO_2 (eq 6-3). (a): T = 318 K and $w_{3\text{-MPD}}$%= 40; (b): T = 338 K and $w_{3\text{-MPD}}$ %= 40; (c): T = 318 K and $w_{4\text{-MPD}}$ %=40; (d): T = 338 K and $w_{4\text{-MPD}}$ %=40.

These enthalpy data are derived from the speciation of the chemical system at equilibrium. Activity coefficients calculated with the adjusted interaction parameters are used to determine the

equilibrium concentrations of these species. Activity coefficients and equilibrium concentrations at various loadings are given in Figure 5-6 at 318 K and w_a%= 20.

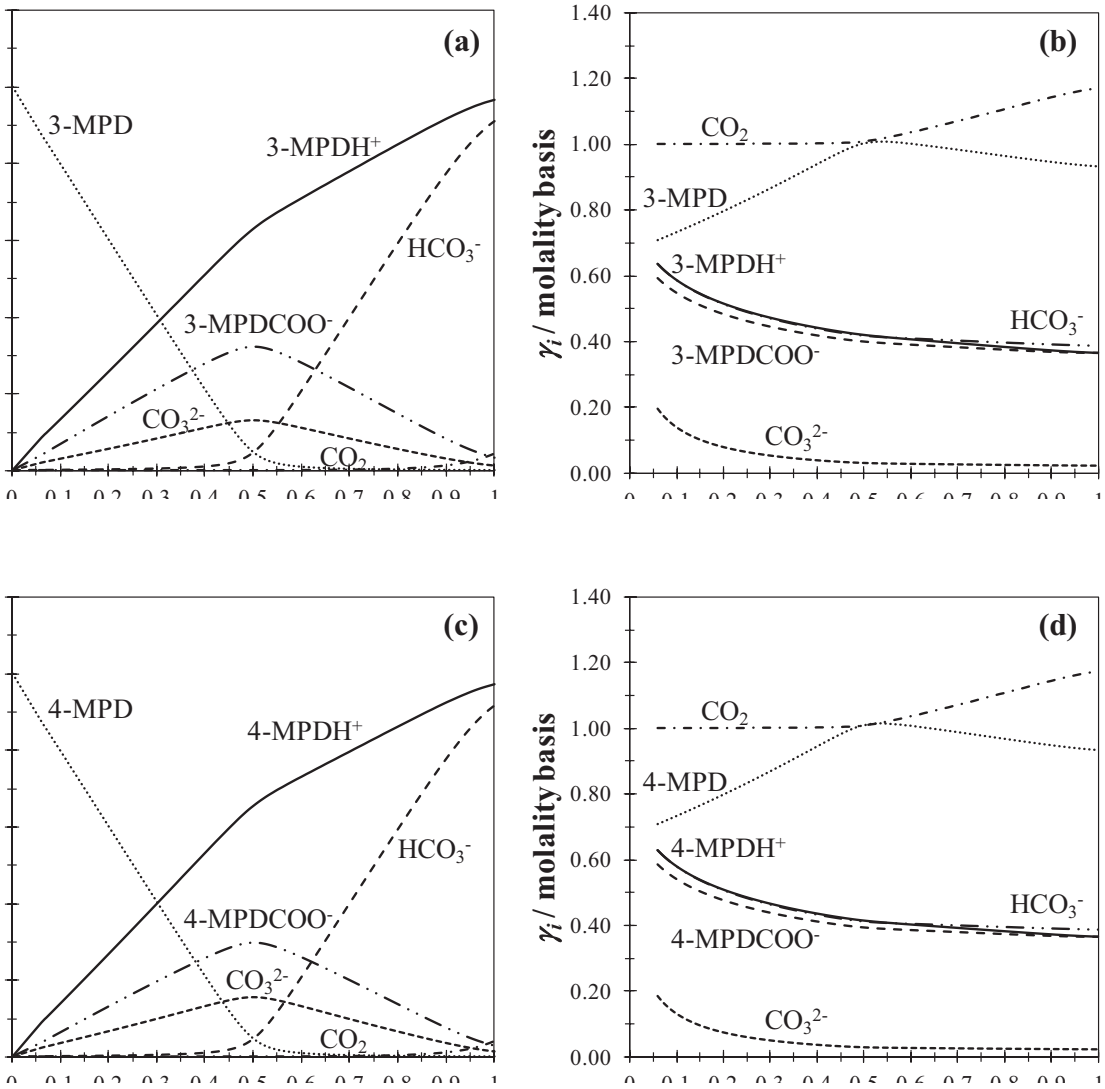

Figure 5-6: Activity coefficients (γ_i) and liquid phase composition (m_i, molal concentration) of aqueous solutions of 3-MPD and 4-MPD versus gas loading charge as calculated from the model. (a) and (b): T = 318 K and $w_{3\text{-MPD}}$%= 20; (c) and (d): T=318 K and $w_{4\text{-MPD}}$%= 20.

A typical experimental trend for unhindered primary and secondary amines is that the enthalpy of solution remains constant at low loadings up to α = 0.5. Then, $\Delta_{sol}H$ decreases because of carbamate

hydrolysis. The thermodynamic model reproduces these experimental trends for both 3-MPD and 4-MPD solutions. The chemical reactions involved in the overall dissolution process, yield different enthalpies of reaction. Details of the different energetic contributions taking place during the dissolution process are given in Figure 5-5. At both temperatures, the contribution of the reaction of protonation of 3-MPD or 4-MPD (equation 5-4) plays a major role in the final value of the enthalpy of solution. The thermodynamic model shows that CO_2 dissolution in 3-MPD or 4-MPD solutions yields mostly to bicarbonates (HCO_3^-) formation. Nevertheless, due to the high pK_a values of 3-MPD and 4-MPD aqueous solutions, bicarbonates are converted in carbonates for gas loading charges less than 0.5. The concentration profiles of species in liquid phase as a function of the loading charge show that after a loading of 0.5, carbamate and carbonate compositions decrease to the benefit of bicarbonate formation. It explains the slope change observed for the experimental enthalpy expressed in kJ per moles of amine in Figure 5-5.

As described by Arcis et al. in their work (Arcis et al., 2011; Arcis et al., 2012b; Arcis et al., 2012a), equilibrium constants play a major role in the modeling of VLE and enthalpy data. In this study, while the equilibrium constants of the first and second dissociation of CO_2 (equations 5-2 and equations 5-3) are known accurately, small inconsistencies for equilibrium constants of amine protonation (equations 6-4) and carbamate formation (equations 5-5) can affect the model. The model may also be influenced by the choice of the parameters of the activity coefficient model. To improve this thermodynamic representation, the acquisition of VLE and speciation data is required. Speciation will be obtained from Pr Tremaine work: in DACOOTA project, his role is to obtain speciation in solution using NMR and RAMAN spectroscopy. VLE data are actually measured in the laboratory using calorimetric methods. This will improve the model calculations.

5.3 Conclusions

This section describes a thermodynamic model which calculated the carbamate formation constant of 3-MPD and 4-MPD. Using the carbamate constant the model was able to reproduce both the solubility of carbon dioxide in 3-MPD and 4-MPD solutions as well as the enthalpy of solution for dissolving CO_2. The experimental results also show that there is no significant difference in the solubility or enthalpies of solution for dissolving CO_2 in aqueous solutions of methyl piperidine.

5.4 Appendix for Chapter 5

Table 5-4: Experimental enthalpies of solution of CO_2 in aqueous 3-MPD (w_a%=19.36) at 318 K

α	$\sigma\alpha$	$-\Delta_{sol}H_{amine}$	σH	$-\Delta_{sol}H_{CO_2}$	σH
mole $_{CO_2}$/ mole $_{amine}$		kJ mol^{-1}		kJ mol^{-1}	
		0.43±0.02 MPa			
0.230	0.095	25.9	0.5	112.7	2.3
0.276	0.066	31.3	0.6	113.5	2.3
0.359	0.039	41.1	0.8	114.5	2.3
0.404	0.031	46.0	0.9	113.7	2.3
0.448	0.025	50.7	1.0	113.0	2.2
0.525	0.018	55.6	1.1	105.9	2.1
0.538	0.017	57.3	1.1	106.5	2.1
0.613	0.014	61.4	1.2	100.1	2.0
0.628	0.013	62.9	1.2	100.2	2.0
0.700	0.011	66.1	1.3	94.4	1.8
0.753	0.010	68.9	1.3	91.5	1.8
0.788	0.009	72.7	1.4	92.3	1.8
0.846	0.008	75.5	1.5	89.2	1.7
0.884	0.008	76.7	1.5	86.8	1.7
0.897	0.008	78.7	1.5	87.7	1.7
0.940	0.007	77.3	1.5	82.1	1.6
0.945	0.007	78.4	1.5	82.9	1.6
0.997	0.007	76.2	1.5	76.4	1.5
1.035	0.007	75.5	1.5	73.0	1.4
1.129	0.007	75.5	1.5	66.9	1.3
		0.96±0.02 MPa			
0.204	0.121	22.9	0.4	112.3	2.2
0.255	0.077	28.5	0.6	111.9	2.2
0.306	0.054	34.6	0.7	113.2	2.2
0.346	0.042	40.7	0.8	117.4	2.3
0.403	0.031	43.9	0.8	109.0	2.1
0.427	0.028	46.9	0.9	109.9	2.1
0.498	0.020	53.3	1.0	107.1	2.1
0.509	0.019	52.9	1.0	103.9	2.0
0.527	0.018	54.5	1.0	103.4	2.0
0.596	0.014	59.5	1.1	100.0	1.9
0.597	0.014	59.8	1.2	100.1	2.0

0.597	0.014	60.2	1.2	100.7	2.0
0.677	0.011	64.2	1.2	94.8	1.8
0.753	0.010	67.6	1.3	89.8	1.7
0.840	0.008	71.4	1.4	85.0	1.6
0.878	0.008	73.0	1.4	83.1	1.6
0.945	0.007	76.1	1.5	80.5	1.6
0.998	0.007	78.7	1.5	78.9	1.5
1.018	0.007	78.7	1.5	77.3	1.5
1.043	0.007	78.7	1.5	75.5	1.5
1.088	0.007	78.7	1.5	72.4	1.4
1.134	0.007	78.6	1.5	69.3	1.3
1.208	0.007	77.8	1.5	64.4	1.2
		1.47±0.02 MPa			
0.202	0.123	19.9	0.4	98.5	1.9
0.221	0.103	22.5	0.4	101.8	2.0
0.289	0.060	29.7	0.6	102.9	2.0
0.334	0.045	34.9	0.7	104.7	2.0
0.407	0.030	41.9	0.8	103.0	2.0
0.434	0.027	44.4	0.9	102.3	2.0
0.500	0.020	52.3	1.0	104.6	2.0
0.563	0.016	56.9	1.1	101.0	1.9
0.629	0.013	60.5	1.2	96.2	1.8
0.695	0.011	63.7	1.2	91.6	1.8
0.762	0.009	66.8	1.3	87.7	1.7
0.828	0.008	69.1	1.3	83.5	1.6
0.901	0.008	72.1	1.4	80.0	1.5
0.927	0.007	74.2	1.4	80.0	1.5
0.932	0.007	74.3	1.4	79.7	1.5
0.964	0.007	76.5	1.5	79.4	1.5
0.997	0.007	76.4	1.5	76.6	1.5
1.029	0.007	77.2	1.5	75.1	1.4
1.068	0.007	77.2	1.5	72.3	1.4
1.093	0.007	77.8	1.5	71.1	1.4
1.125	0.007	78.1	1.5	69.4	1.3
1.168	0.007	77.9	1.5	66.7	1.3

Table 5-5: Experimental enthalpies of solution of CO_2 in aqueous 3-MPD (w_a%=40.44) at 318 K

α	$\sigma\alpha$	$-\Delta_{sol}H_{amine}$	σH	$-\Delta_{sol}H_{CO_2}$	σH
mole $_{CO_2}$/ mole $_{amine}$		kJ mol^{-1}		kJ mol^{-1}	
		0.56±0.02 MPa			
0.253	0.078	28.1	1.0	111.2	3.8
0.295	0.058	32.8	1.1	111.2	3.8
0.354	0.040	38.8	1.4	109.7	4.0
0.377	0.035	41.0	1.4	108.7	3.7
0.400	0.031	43.8	1.6	109.5	3.9
0.421	0.028	45.7	1.5	108.6	3.7
0.453	0.024	46.3	1.6	102.3	3.5
0.458	0.024	46.7	1.6	102.0	3.5
0.475	0.022	47.7	1.6	100.5	3.4
0.484	0.021	49.6	1.7	102.4	3.4
0.516	0.019	52.1	1.8	100.8	3.4
0.549	0.017	54.3	1.8	99.0	3.3
0.581	0.015	56.0	1.9	96.3	3.3
0.620	0.013	57.2	1.9	92.4	3.1
0.646	0.012	59.4	2.0	92.1	3.1
0.678	0.011	60.1	2.0	88.6	3.0
0.736	0.010	64.4	2.3	87.5	3.1
0.775	0.009	64.5	2.4	83.3	3.0
0.813	0.008	65.2	2.2	80.1	2.7
0.813	0.008	67.2	2.3	82.7	2.8
0.852	0.007	69.5	2.4	81.6	2.7
0.872	0.007	70.4	2.4	80.8	2.7
0.881	0.007	71.5	2.4	81.1	2.7
0.891	0.007	69.3	2.4	77.8	2.6
0.930	0.006	70.0	2.4	75.2	2.5
0.968	0.006	70.4	2.4	72.7	2.5
1.007	0.006	69.9	2.4	69.4	2.3
1.060	0.006	70.1	2.4	66.1	2.2
1.085	0.005	70.7	2.4	65.2	2.2
1.098	0.005	70.4	2.4	64.1	2.2
1.136	0.005	70.4	2.4	61.9	2.1
		1.07±0.02 MPa			
0.202	0.123	21.2	0.7	105.0	3.5
0.242	0.086	25.7	0.9	106.2	3.6

0.282	0.063	29.7	1.0	105.4	3.5
0.322	0.048	33.8	1.1	104.9	3.5
0.344	0.042	36.8	1.3	107.0	3.6
0.363	0.038	37.8	1.3	104.1	3.5
0.403	0.031	41.1	1.4	102.0	3.4
0.417	0.029	42.9	1.5	103.0	3.5
0.458	0.024	46.2	1.6	100.9	3.4
0.500	0.020	48.2	1.7	96.4	3.3
0.542	0.017	50.7	1.7	93.5	3.2
0.573	0.015	52.2	1.8	91.1	3.1
0.625	0.013	55.4	1.9	88.7	3.0
0.667	0.011	58.4	2.0	87.6	3.0
0.750	0.009	61.0	2.1	81.2	2.8
0.813	0.008	65.7	2.2	80.9	2.7
0.858	0.007	67.3	2.3	78.5	2.6
0.902	0.007	67.9	2.3	75.3	2.5
0.917	0.007	67.1	2.3	73.1	2.5
0.946	0.006	68.4	2.3	72.3	2.4
0.956	0.006	68.5	2.3	71.6	2.4
0.959	0.006	65.8	2.2	68.7	2.3
0.990	0.006	68.2	2.3	68.9	2.3
0.996	0.006	68.9	2.3	69.1	2.3
1.039	0.006	65.9	2.2	63.4	2.1
1.042	0.006	65.9	2.2	63.3	2.1
1.065	0.006	65.0	2.2	61.0	2.1
1.111	0.005	64.9	2.2	58.4	2.0
1.146	0.005	64.9	2.2	56.6	1.9
1.146	0.005	65.7	2.2	57.4	1.9
1.209	0.005	68.1	2.3	56.3	1.9

1.47±0.02 MPa

0.210	0.113	19.8	0.7	94.0	3.2
0.231	0.094	22.4	0.8	97.0	3.3
0.240	0.087	22.6	0.8	93.8	3.2
0.280	0.064	26.5	0.9	94.5	3.2
0.337	0.044	31.6	1.1	93.8	3.2
0.344	0.042	33.5	1.1	97.5	3.3
0.410	0.030	39.5	1.3	96.5	3.3
0.475	0.022	44.7	1.5	94.1	3.2
0.485	0.021	45.3	1.5	93.5	3.1
0.538	0.017	48.6	1.6	90.3	3.0
0.572	0.015	50.1	1.7	87.6	3.0

0.619	0.013	52.0	1.8	84.0	2.8
0.673	0.011	56.5	1.9	83.9	2.8
0.683	0.011	54.8	1.9	80.2	2.7
0.722	0.010	57.6	2.0	79.8	2.7
0.740	0.009	59.2	2.0	79.9	2.7
0.808	0.008	61.9	2.1	76.6	2.6
0.841	0.008	64.5	2.2	76.7	2.6
0.869	0.007	66.9	2.3	77.0	2.6
0.935	0.006	68.7	2.3	73.5	2.5
0.963	0.006	70.1	2.4	72.8	2.4
1.002	0.006	70.7	2.4	70.6	2.4
1.006	0.006	68.3	2.3	67.8	2.3
1.069	0.006	71.0	2.4	66.5	2.2
1.098	0.005	66.7	2.3	60.8	2.0
1.102	0.005	66.3	2.2	60.1	2.0
1.136	0.005	69.2	2.3	60.9	2.0
1.161	0.005	68.3	2.3	58.8	2.0
1.178	0.005	67.5	2.3	57.3	1.9

Table 5-6: Experimental enthalpies of solution of CO_2 in aqueous 3-MPD (w_a%=40.00) at 338 K

α	$\sigma\alpha$	$-\Delta_{sol}H_{amine}$	σH	$-\Delta_{sol}H_{CO_2}$	σH
mole $_{CO_2}$/ mole $_{amine}$		kJ mol^{-1}		kJ mol^{-1}	
		0.46±0.02 MPa			
0.116	0.373	12.1	0.3	104.4	2.7
0.185	0.146	20.2	0.5	109.2	2.8
0.271	0.068	29.2	0.8	107.4	2.8
0.362	0.038	37.9	0.9	104.7	2.6
0.452	0.024	47.3	1.2	104.6	2.6
0.608	0.014	53.0	1.3	87.2	2.2
0.694	0.011	58.8	1.5	84.7	2.1
0.811	0.008	63.9	1.6	78.8	2.0
0.813	0.008	66.1	2.1	81.3	2.5
0.843	0.008	69.2	1.8	82.1	2.1
0.859	0.007	69.6	1.7	81.0	2.0
0.877	0.007	70.0	1.7	79.8	2.0
0.905	0.007	70.3	1.8	77.8	1.9
0.955	0.006	70.6	1.8	74.0	1.9
1.079	0.005	70.8	1.8	65.6	1.6
1.167	0.005	71.1	1.8	60.9	1.6
		0.99±0.02 MPa			
0.147	0.230	14.6	0.4	98.9	2.5
0.157	0.203	15.6	0.4	99.1	2.5
0.194	0.132	20.0	0.5	102.8	2.7
0.222	0.101	22.5	0.6	101.1	2.7
0.270	0.069	27.1	0.7	100.3	2.5
0.311	0.052	31.2	0.8	100.2	2.6
0.357	0.039	35.4	0.9	99.1	2.5
0.389	0.033	38.0	0.9	97.8	2.4
0.456	0.024	44.8	1.1	98.1	2.4
0.578	0.015	53.6	1.3	92.7	2.3
0.682	0.011	60.0	1.5	88.0	2.2
0.745	0.009	63.4	1.7	85.1	2.2
0.843	0.008	69.9	1.7	82.9	2.0

0.916	0.007	72.4	1.9	79.1	2.1
0.948	0.006	73.0	1.9	77.0	2.0
0.958	0.006	73.0	1.9	76.2	2.0
0.958	0.006	72.9	1.9	76.0	2.0
0.990	0.006	73.2	1.9	73.9	1.9
1.032	0.006	73.2	1.8	70.9	1.7
1.075	0.006	73.2	1.8	68.2	1.7
1.117	0.005	73.1	1.8	65.4	1.6
1.159	0.005	73.2	1.8	63.1	1.5

1.51±0.02 MPa

0.203	0.122	19.8	0.5	97.5	2.4
0.254	0.078	24.7	0.6	97.5	2.4
0.268	0.069	25.5	0.7	95.1	2.4
0.285	0.061	27.8	0.8	97.5	2.6
0.307	0.053	29.4	0.7	95.8	2.4
0.317	0.050	30.7	0.8	96.9	2.5
0.347	0.041	33.7	0.8	97.1	2.4
0.389	0.033	37.0	0.9	95.1	2.3
0.426	0.028	40.2	1.0	94.5	2.4
0.447	0.025	42.5	1.1	95.3	2.4
0.460	0.024	43.4	1.1	94.3	2.3
0.507	0.020	46.4	1.3	91.5	2.6
0.511	0.019	49.4	1.2	96.7	2.4
0.596	0.014	54.5	1.4	91.4	2.3
0.642	0.012	56.7	1.4	88.3	2.2
0.666	0.011	59.2	1.5	88.9	2.2
0.681	0.011	58.7	1.5	86.1	2.1
0.731	0.010	63.4	1.6	86.8	2.1
0.766	0.009	62.2	1.6	81.1	2.0
0.800	0.008	66.3	1.6	82.8	2.0
0.870	0.007	69.5	1.7	80.0	2.0
0.926	0.007	72.2	1.8	77.9	1.9
0.972	0.006	72.9	1.9	75.0	1.9
1.002	0.006	73.5	1.8	73.3	1.8
1.022	0.006	74.2	1.8	72.6	1.8
1.022	0.006	73.5	1.9	72.0	1.9

1.036	0.006	73.3	1.8	70.7	1.7
1.063	0.006	73.4	1.8	69.1	1.7
1.090	0.005	73.4	1.8	67.4	1.7
1.199	0.005	73.8	1.8	61.5	1.5
1.251	0.005	74.0	1.8	59.1	1.4

Table 5-7: Experimental enthalpies of solution of CO_2 in aqueous 4-MPD (w_a%=16.57) at 318 K

α	$\sigma\alpha$	$-\Delta_{sol}H_{amine}$	σH	$-\Delta_{sol}H_{CO_2}$	σH
mole $_{CO_2}$/ mole $_{amine}$		kJ mol^{-1}		kJ mol^{-1}	
		0.43±0.02 MPa			
0.196	0.130	23.6	0.5	120.6	2.5
0.214	0.109	24.5	0.5	114.7	2.6
0.222	0.101	27.1	0.5	121.9	2.5
0.257	0.076	29.9	0.6	116.6	2.5
0.293	0.058	35.4	0.7	121.1	2.5
0.321	0.049	37.6	0.8	117.0	2.4
0.329	0.046	39.6	0.8	120.4	2.5
0.359	0.039	42.6	0.9	118.6	2.4
0.381	0.034	45.2	0.9	118.6	2.4
0.404	0.031	47.9	1.0	118.7	2.4
0.448	0.025	52.2	1.0	116.3	2.3
0.493	0.021	55.9	1.1	113.3	2.2
0.538	0.017	58.7	1.2	109.1	2.1
0.570	0.016	60.4	1.2	106.1	2.1
0.592	0.015	61.7	1.2	104.2	2.0
0.614	0.014	62.8	1.2	102.4	2.0
0.627	0.013	63.2	1.2	100.8	2.0
0.648	0.012	64.8	1.3	100.0	2.0
0.679	0.011	66.4	1.3	97.8	1.9
0.701	0.011	67.3	1.3	96.0	1.9
0.706	0.011	66.3	1.3	93.9	1.8
0.731	0.010	68.4	1.3	93.5	1.8
0.773	0.009	70.6	1.4	91.3	1.8
0.794	0.009	71.1	1.4	89.5	1.7
0.836	0.008	72.9	1.4	87.2	1.7
0.836	0.008	73.5	1.4	88.0	1.7
0.856	0.008	74.5	1.4	87.0	1.7
0.918	0.008	76.5	1.5	83.4	1.6
0.920	0.007	77.6	1.5	84.3	1.6
0.940	0.007	77.9	1.5	82.9	1.6
0.979	0.007	77.8	1.5	79.5	1.5
1.008	0.007	77.6	1.5	77.0	1.5
1.020	0.007	77.8	1.5	76.3	1.5
1.045	0.007	76.9	1.5	73.6	1.4
1.074	0.007	77.9	1.5	72.6	1.4
1.092	0.007	78.2	1.5	71.6	1.4

1.096	0.007	78.0	1.5	71.2	1.4
1.113	0.007	78.3	1.5	70.4	1.4
1.121	0.007	78.0	1.5	69.5	1.4
1.124	0.007	78.1	1.5	69.5	1.3
1.142	0.007	78.2	1.5	68.5	1.3
1.161	0.007	77.9	1.5	67.1	1.3
1.162	0.007	78.4	1.5	67.5	1.3
1.223	0.007	77.4	1.5	63.2	1.2
1.227	0.007	77.9	1.5	63.5	1.2
1.249	0.007	77.8	1.5	62.3	1.2
1.271	0.007	77.3	1.5	60.8	1.2

0.96±0.02 MPa

0.204	0.120	22.2	0.4	108.9	2.2
0.245	0.083	26.7	0.5	109.2	2.2
0.318	0.049	34.3	0.7	107.8	2.1
0.398	0.032	43.2	0.8	108.7	2.1
0.455	0.024	48.4	0.9	106.4	2.1
0.525	0.018	54.0	1.0	102.8	2.0
0.630	0.013	61.2	1.2	97.2	1.9
0.727	0.010	65.7	1.3	90.4	1.8
0.799	0.009	69.3	1.3	86.7	1.7
0.848	0.008	70.8	1.4	83.5	1.6
0.886	0.008	73.4	1.4	82.8	1.6
0.945	0.007	76.2	1.5	80.6	1.6
1.001	0.007	77.8	1.5	77.7	1.5
1.076	0.007	77.7	1.5	72.2	1.4
1.102	0.007	78.6	1.5	71.3	1.4
1.126	0.007	78.2	1.5	69.5	1.3
1.150	0.007	78.2	1.5	68.0	1.3

1.48±0.02 MPa

0.195	0.131	19.3	0.4	99.1	1.9
0.319	0.049	33.4	0.6	104.6	2.0
0.384	0.034	40.0	0.8	103.9	2.0
0.429	0.027	44.4	0.9	103.5	2.0
0.471	0.023	51.0	1.0	108.2	2.1
0.550	0.017	56.5	1.1	102.7	2.0
0.624	0.013	60.9	1.2	97.6	1.9
0.702	0.011	64.7	1.2	92.1	1.8
0.774	0.009	68.2	1.3	88.1	1.7

0.852	0.008	71.5	1.4	84.0	1.6
0.929	0.007	74.8	1.4	80.5	1.5
1.007	0.007	77.1	1.5	76.6	1.5
1.084	0.007	78.2	1.5	72.1	1.4
1.145	0.007	77.2	1.5	67.4	1.3
1.250	0.007	77.5	1.5	62.0	1.2

Table 5-8: Experimental enthalpies of solution of CO_2 in aqueous 4-MPD (w_a%=39.86) at 318 K

α	$\sigma\alpha$	$-\Delta_{sol}H_{amine}$	σH	$-\Delta_{sol}H_{CO_2}$	σH
mole $_{CO_2}$/ mole $_{amine}$		kJ mol^{-1}		kJ mol^{-1}	
		0.43±0.02 MPa			
0.196	0.131	22.2	0.4	113.3	2.2
0.214	0.109	24.6	0.5	114.9	2.2
0.244	0.084	28.0	0.5	114.7	2.2
0.293	0.058	33.5	0.6	114.2	2.2
0.321	0.049	36.7	0.7	114.3	2.2
0.401	0.031	45.0	0.9	112.2	2.1
0.447	0.025	48.8	0.9	109.3	2.1
0.504	0.020	52.7	1.0	104.5	2.0
0.550	0.017	55.3	1.0	100.6	1.9
0.615	0.014	61.0	1.1	99.1	1.9
0.671	0.012	63.3	1.2	94.3	1.8
0.671	0.012	64.0	1.2	95.4	1.8
0.694	0.011	65.5	1.2	94.5	1.8
0.727	0.010	69.2	1.3	95.1	1.8
0.761	0.009	64.9	1.2	85.3	1.6
0.810	0.009	72.0	1.4	88.9	1.7
0.820	0.008	74.6	1.4	90.9	1.7
0.865	0.008	73.8	1.4	85.4	1.6
0.895	0.008	74.3	1.4	83.0	1.6
0.910	0.008	73.4	1.4	80.7	1.5
0.947	0.007	74.6	1.4	78.7	1.5
0.970	0.007	73.7	1.4	76.0	1.4
0.985	0.007	74.4	1.4	75.5	1.4
1.031	0.007	73.9	1.4	71.6	1.4
1.100	0.007	73.8	1.4	67.1	1.3
1.146	0.007	73.7	1.4	64.3	1.2
		0.95±0.02 MPa			
0.194	0.133	21.2	0.4	109.6	2.1
0.213	0.110	23.2	0.4	108.8	2.1
0.237	0.089	25.7	0.5	108.4	2.1
0.272	0.067	29.3	0.6	107.7	2.1
0.303	0.054	32.8	0.6	108.4	2.1
0.346	0.042	37.3	0.7	107.7	2.1
0.404	0.031	42.7	0.8	105.7	2.0

0.485	0.021	50.3	1.0	103.6	2.0
0.521	0.019	52.7	1.0	101.2	1.9
0.566	0.016	55.3	1.1	97.7	1.9
0.596	0.014	56.9	1.1	95.5	1.8
0.602	0.014	58.2	1.1	96.6	1.8
0.678	0.011	62.4	1.2	92.1	1.8
0.678	0.011	61.0	1.2	90.0	1.7
0.735	0.010	67.8	1.3	92.3	1.8
0.807	0.009	70.7	1.4	87.7	1.7
0.867	0.008	74.4	1.4	85.8	1.6
0.928	0.007	75.5	1.4	81.3	1.6
0.948	0.007	77.7	1.5	81.9	1.6
0.970	0.007	77.0	1.5	79.4	1.5
1.008	0.007	77.5	1.5	76.8	1.5
1.031	0.007	76.7	1.5	74.4	1.4
1.049	0.007	77.4	1.5	73.8	1.4
1.109	0.007	77.4	1.5	69.8	1.3
1.149	0.007	77.4	1.5	67.3	1.3
		1.45±0.02 MPa			
0.218	0.106	22.5	0.4	103.4	1.9
0.285	0.062	28.7	0.5	100.7	1.9
0.323	0.048	33.6	0.6	104.1	2.0
0.418	0.029	41.6	0.8	99.5	1.9
0.502	0.020	48.3	0.9	96.1	1.8
0.582	0.015	53.3	1.0	91.7	1.7
0.704	0.011	60.4	1.1	85.7	1.6
0.763	0.009	64.7	1.2	84.9	1.6
0.842	0.008	68.8	1.3	81.7	1.5
0.922	0.007	72.7	1.4	78.9	1.5
0.975	0.007	74.2	1.4	76.1	1.4
1.009	0.007	75.3	1.4	74.7	1.4
1.023	0.007	75.0	1.4	73.3	1.4
1.033	0.007	75.3	1.4	72.9	1.4
1.065	0.007	75.1	1.4	70.6	1.3
1.104	0.007	75.5	1.4	68.4	1.3
1.186	0.007	74.9	1.4	63.1	1.2
1.237	0.007	74.6	1.4	60.3	1.1

Table 5-9: Experimental enthalpies of solution of CO_2 in aqueous 4-MPD (w_a%=20.00) at 338 K

α	$\sigma\alpha$	$-\Delta_{sol}H_{amine}$	σH	$-\Delta_{sol}H_{CO_2}$	σH
mole $_{CO_2}$/ mole $_{amine}$		kJ mol^{-1}		kJ mol^{-1}	
		0.47±0.02 MPa			
0.140	0.254	14.6	0.4	103.9	2.6
0.171	0.170	17.6	0.4	102.9	2.6
0.193	0.134	19.7	0.5	102.2	2.5
0.240	0.087	24.4	0.6	101.6	2.5
0.262	0.073	26.4	0.7	101.0	2.6
0.276	0.066	28.1	0.7	101.7	2.5
0.301	0.055	30.6	0.8	101.7	2.5
0.305	0.054	30.3	1.1	99.4	3.4
0.342	0.043	34.6	0.9	101.2	2.6
0.377	0.035	38.4	1.0	101.8	2.5
0.385	0.034	38.6	1.0	100.4	2.5
0.402	0.031	39.9	1.2	99.2	3.1
0.411	0.030	41.5	1.1	100.8	2.5
0.428	0.027	42.5	1.1	99.4	2.4
0.446	0.025	45.2	1.1	101.3	2.5
0.452	0.025	45.1	1.2	99.8	2.6
0.483	0.022	48.4	1.3	100.4	2.6
0.492	0.021	48.4	1.2	98.3	2.5
0.523	0.018	51.6	1.3	98.7	2.5
0.535	0.018	52.0	1.4	97.2	2.6
0.563	0.016	54.3	1.4	96.5	2.4
0.656	0.012	63.2	1.2	96.3	1.8
0.716	0.010	67.4	1.3	94.2	1.8
0.748	0.010	68.0	1.4	91.0	1.8
0.780	0.009	69.8	1.3	89.4	1.7
0.780	0.009	70.1	1.3	89.8	1.7
0.814	0.009	71.6	1.4	88.0	1.7
0.835	0.008	73.4	1.4	87.9	1.6
0.847	0.008	73.6	1.4	86.9	1.7
0.854	0.008	73.4	1.4	85.9	1.6
0.878	0.008	75.0	1.4	85.4	1.6
0.878	0.008	74.4	1.5	84.7	1.7
0.902	0.008	75.7	1.4	83.9	1.6
0.911	0.008	75.5	1.4	82.8	1.6
0.927	0.007	76.7	1.4	82.7	1.5
0.974	0.007	75.2	1.4	77.2	1.4

0.988	0.007	76.3	1.4	77.3	1.4
1.018	0.007	75.0	1.4	73.7	1.4
1.062	0.007	74.9	1.4	70.5	1.3

0.98±0.02 MPa

0.209	0.114	20.0	0.5	95.6	2.4
0.262	0.073	25.9	0.6	99.0	2.4
0.307	0.053	30.1	0.8	98.1	2.5
0.345	0.042	34.2	0.9	99.1	2.5
0.401	0.031	39.1	1.0	97.7	2.4
0.414	0.029	40.6	1.0	98.0	2.4
0.473	0.022	46.3	1.2	97.8	2.4
0.556	0.016	53.6	1.5	96.4	2.7
0.608	0.014	56.6	1.4	93.1	2.3
0.609	0.014	58.6	1.1	96.2	1.8
0.660	0.012	61.1	1.1	92.6	1.7
0.710	0.011	65.1	1.2	91.6	1.7
0.771	0.009	67.3	1.3	87.3	1.6
0.801	0.008	68.4	1.9	85.4	2.3
0.833	0.008	70.4	1.3	84.5	1.6
0.889	0.008	73.3	1.4	82.4	1.5
0.898	0.007	72.1	1.8	80.3	2.0
0.926	0.007	75.5	1.4	81.5	1.5
0.949	0.007	75.7	1.4	79.8	1.5
0.949	0.007	76.4	1.4	80.5	1.5
0.972	0.007	77.1	1.4	79.3	1.5
0.991	0.006	78.1	2.0	78.9	2.0
0.995	0.007	77.2	1.4	77.5	1.5
1.042	0.007	77.4	1.4	74.3	1.4
1.053	0.007	76.3	1.4	72.5	1.4
1.076	0.007	77.8	1.5	72.3	1.4
1.111	0.007	77.8	1.5	70.0	1.3
1.170	0.007	78.3	1.5	66.9	1.3
1.216	0.007	77.4	1.5	63.7	1.2
1.316	0.007	77.3	1.4	58.7	1.1
1.504	0.008	77.6	1.5	51.6	1.0

1.50±0.02 MPa

0.347	0.042	33.2	0.9	95.8	2.4
0.379	0.035	36.2	0.9	95.6	2.4
0.431	0.027	40.8	1.1	94.8	2.4

0.467	0.023	45.7	1.2	97.9	2.6
0.544	0.017	52.5	1.0	96.5	1.9
0.545	0.017	51.2	1.0	93.9	1.7
0.545	0.017	51.3	1.0	94.0	1.8
0.545	0.017	52.7	1.3	96.6	2.4
0.596	0.014	55.5	1.1	93.0	1.8
0.609	0.014	56.4	1.4	92.6	2.3
0.642	0.012	57.8	1.4	90.1	2.2
0.650	0.012	56.9	1.1	87.6	1.6
0.665	0.011	58.4	1.5	87.9	2.2
0.696	0.011	60.9	1.2	87.5	1.7
0.708	0.010	61.2	1.5	86.5	2.1
0.750	0.010	63.8	1.2	85.1	1.6
0.770	0.009	64.7	1.6	84.0	2.1
0.812	0.009	66.6	1.2	82.1	1.5
0.818	0.009	66.6	1.2	81.5	1.5
0.820	0.008	67.6	1.7	82.4	2.0
0.820	0.008	66.8	1.7	81.5	2.0
0.865	0.008	69.7	1.3	80.6	1.5
0.894	0.008	70.5	1.3	78.8	1.5
0.898	0.007	70.7	1.8	78.7	1.9
0.935	0.007	72.4	1.4	77.5	1.4
0.958	0.007	73.2	1.4	76.4	1.4
0.982	0.007	74.6	1.5	76.0	1.5
0.996	0.007	73.3	1.4	73.6	1.4
1.021	0.007	75.4	1.5	73.9	1.5
1.036	0.007	74.1	1.4	71.6	1.3
1.069	0.007	76.4	1.7	71.5	1.6
1.069	0.006	75.7	2.7	70.8	2.6
1.106	0.007	76.3	1.5	69.0	1.4
1.138	0.005	77.3	2.4	67.9	2.1
1.161	0.005	78.3	2.5	67.4	2.1
1.174	0.007	76.8	1.6	65.5	1.4

Table 5-10: Experimental enthalpies of solution of CO_2 in aqueous 4-MPD (wa%=40.00) at 338 K

α	$\sigma\alpha$	$-\Delta_{sol}H_{amine}$	σH	$-\Delta_{sol}H_{CO_2}$	σH
mole $_{CO_2}$/ mole $_{amine}$		kJ mol^{-1}		kJ mol^{-1}	
		0.47±0.02 MPa			
0.151	0.218	15.3	0.4	101.1	2.5
0.166	0.180	17.0	0.4	102.4	2.6
0.174	0.165	17.7	0.4	101.4	2.5
0.185	0.146	18.9	0.5	102.3	2.5
0.191	0.137	19.0	0.5	99.8	2.5
0.194	0.133	19.4	0.5	100.1	2.5
0.238	0.088	23.7	0.6	99.3	2.4
0.262	0.073	26.3	0.7	100.2	2.5
0.294	0.058	29.1	0.7	99.1	2.5
0.320	0.049	31.0	0.8	97.1	2.5
0.349	0.041	34.1	0.9	97.8	2.5
0.364	0.038	36.0	0.9	98.8	2.4
0.393	0.032	39.7	1.0	101.0	2.6
0.434	0.027	42.5	1.1	98.0	2.4
0.444	0.025	42.8	1.1	96.4	2.4
0.452	0.025	44.4	1.1	98.3	2.4
0.455	0.024	44.1	1.1	96.9	2.4
0.496	0.020	46.2	1.2	93.2	2.4
0.506	0.020	48.5	1.2	96.0	2.4
0.524	0.018	49.6	1.3	94.7	2.5
0.542	0.017	50.8	1.4	93.8	2.5
0.594	0.014	54.1	1.3	91.0	2.2
0.627	0.013	55.5	1.4	88.5	2.2
0.646	0.012	55.9	1.4	86.5	2.1
0.648	0.012	56.8	1.4	87.7	2.2
0.679	0.011	57.5	1.4	84.6	2.1
0.722	0.010	59.4	1.5	82.3	2.0
0.724	0.010	61.1	1.5	84.5	2.1
0.755	0.009	62.5	1.7	82.8	2.2
0.759	0.009	63.8	2.0	84.1	2.6
0.835	0.008	67.2	1.7	80.5	2.0
0.873	0.008	70.7	1.1	81.0	1.3
0.878	0.008	70.4	1.1	80.2	1.3
0.878	0.008	71.0	1.1	80.8	1.3
0.879	0.007	69.8	1.7	79.4	2.0
0.919	0.007	70.8	1.8	77.0	1.9

0.920	0.007	70.6	1.1	76.7	1.2
0.923	0.007	70.8	1.1	76.7	1.2
0.974	0.007	70.8	1.1	72.7	1.2
1.026	0.007	70.7	1.1	69.0	1.1
1.026	0.007	70.5	1.2	68.7	1.1
1.067	0.007	70.2	1.1	65.8	1.1

0.96±0.04 MPa

0.196	0.130	19.0	0.5	97.0	2.4
0.221	0.103	21.1	0.5	95.8	2.3
0.250	0.080	23.9	0.6	95.6	2.3
0.276	0.066	27.5	0.7	99.7	2.5
0.291	0.059	27.9	0.7	95.7	2.3
0.322	0.048	32.1	0.8	99.7	2.5
0.349	0.041	32.7	0.8	93.6	2.3
0.354	0.040	35.0	0.9	98.8	2.4
0.389	0.033	36.4	1.0	93.5	2.5
0.425	0.028	41.1	1.0	96.6	2.4
0.464	0.023	44.4	1.1	95.8	2.4
0.475	0.022	46.2	1.2	97.2	2.5
0.502	0.020	47.4	1.2	94.3	2.3
0.519	0.019	49.1	1.2	94.7	2.3
0.541	0.017	50.0	1.3	92.4	2.3
0.562	0.016	51.9	1.3	92.3	2.3
0.573	0.015	53.0	1.4	92.5	2.4
0.599	0.014	54.4	1.4	90.9	2.2
0.641	0.012	56.9	1.4	88.7	2.2
0.677	0.011	59.1	1.5	87.3	2.1
0.727	0.010	62.0	1.5	85.3	2.1
0.770	0.009	64.0	1.6	83.1	2.0
0.804	0.008	66.2	1.6	82.3	2.0
0.846	0.007	68.1	1.8	80.5	2.1
0.858	0.007	68.9	1.8	80.3	2.1
0.900	0.007	70.6	1.9	78.5	2.0
0.909	0.007	71.3	2.6	78.4	2.8
0.931	0.006	72.5	1.8	77.9	1.9
0.972	0.006	73.9	1.9	76.0	1.9
0.982	0.006	74.1	1.8	75.5	1.8
1.026	0.006	74.6	1.8	72.7	1.8
1.058	0.006	74.7	1.9	70.6	1.8
1.071	0.006	73.9	1.8	69.0	1.7
1.115	0.005	74.2	1.8	66.5	1.6

1.160	0.005	74.1	1.8	63.9	1.6
		1.47±0.02 MPa			
0.218	0.105	19.3	0.5	88.7	2.3
0.261	0.073	23.4	0.6	89.7	2.3
0.331	0.046	30.2	0.8	91.4	2.3
0.460	0.024	40.8	1.0	88.7	2.2
0.522	0.018	45.3	1.1	86.8	2.2
0.583	0.015	49.5	1.2	84.9	2.1
0.643	0.012	54.4	1.4	84.6	2.1
0.647	0.012	56.2	1.4	86.9	2.1
0.712	0.010	59.5	1.5	83.6	2.1
0.742	0.010	63.2	1.0	85.2	1.4
0.757	0.010	64.8	1.0	85.6	1.4
0.825	0.008	68.0	1.1	82.5	1.3
0.887	0.008	71.9	1.2	81.1	1.3
0.928	0.007	73.4	1.2	79.1	1.3
0.969	0.007	74.8	1.2	77.2	1.2
1.031	0.007	75.1	1.2	72.8	1.2
1.101	0.007	74.8	1.2	68.0	1.1
1.172	0.007	74.6	1.2	63.7	1.0

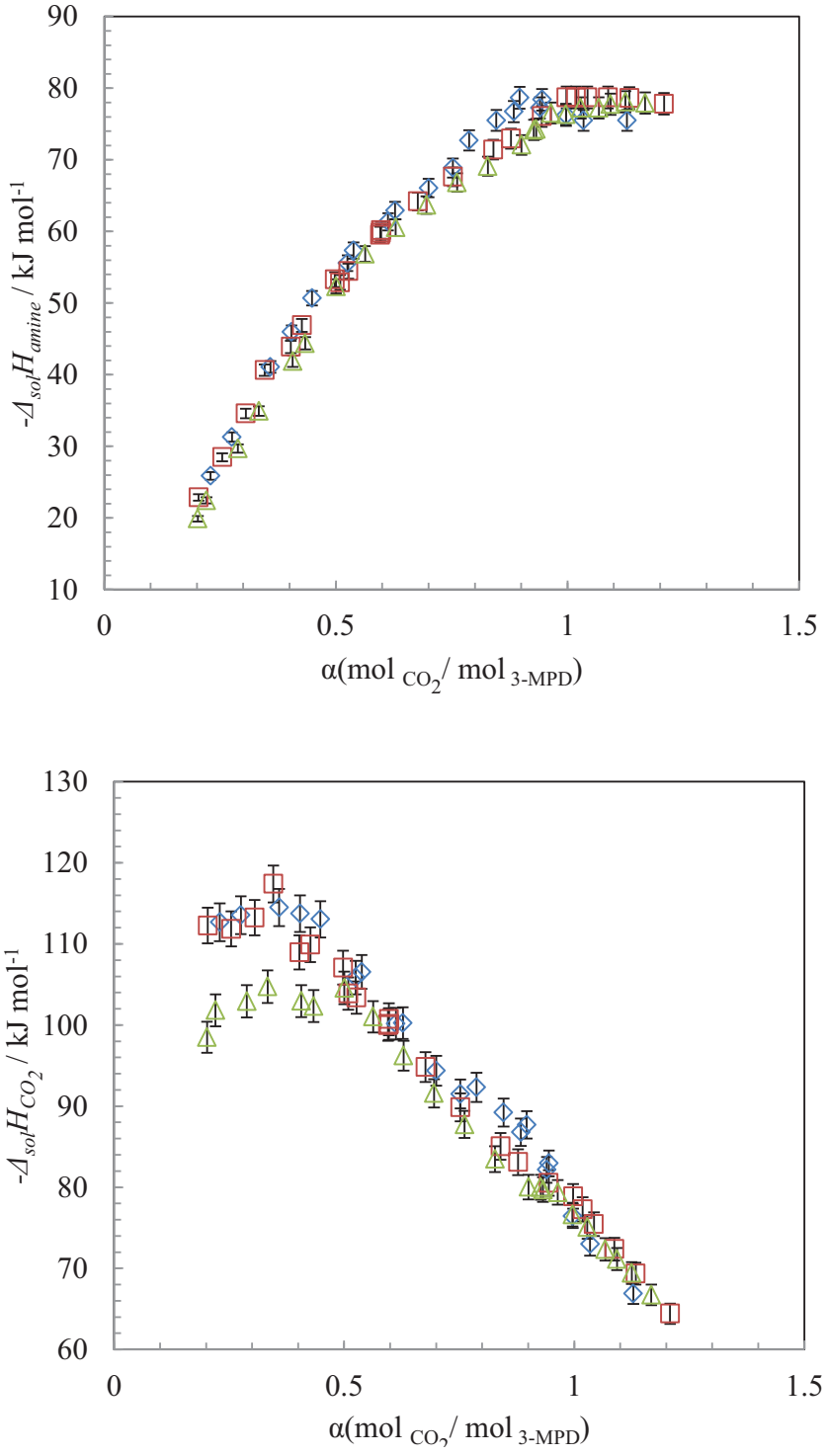

Figure 5-7: Enthalpies of solution per mole of amine (above) and per mole of CO_2 (below). 3-MPD corresponding to table 6-1 (◇ 0.5 MPa), (□ 1.0MPa) (△1.5MPa)

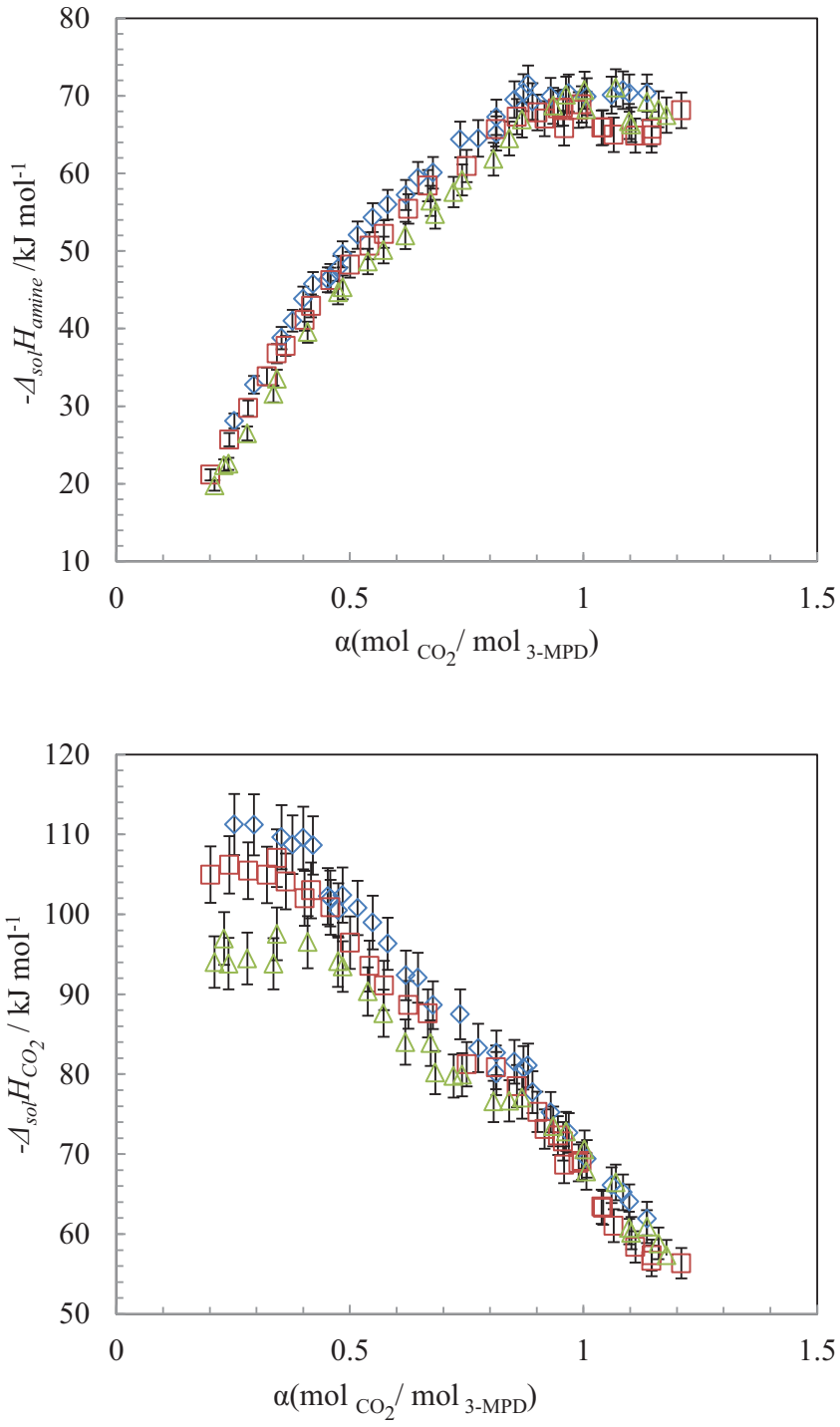

Figure 5-8: Enthalpies of solution to per mole of amine (above) and per mol of CO_2 (below). 3-MPD corresponding to table 6-2(◇ 0.5 MPa), (□ 1.0MPa) (△1.5MPa)

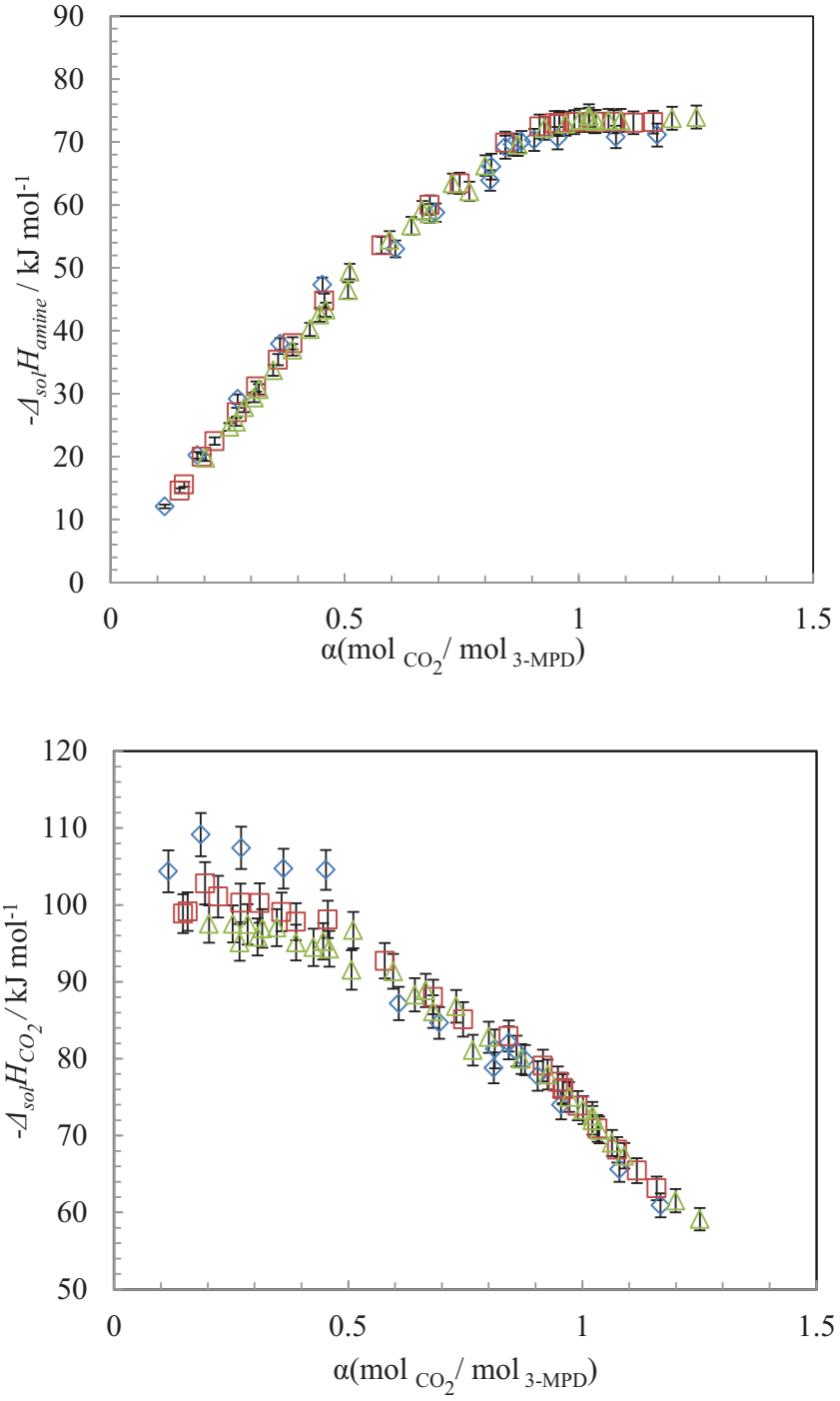

Figure 5-9: Enthalpies of solution to per mole of amine (above) and per mol of CO_2 (below). 3-MPD corresponding to table 6-3 (◇ 0.5 MPa), (□ 1.0MPa) (△1.5MPa)

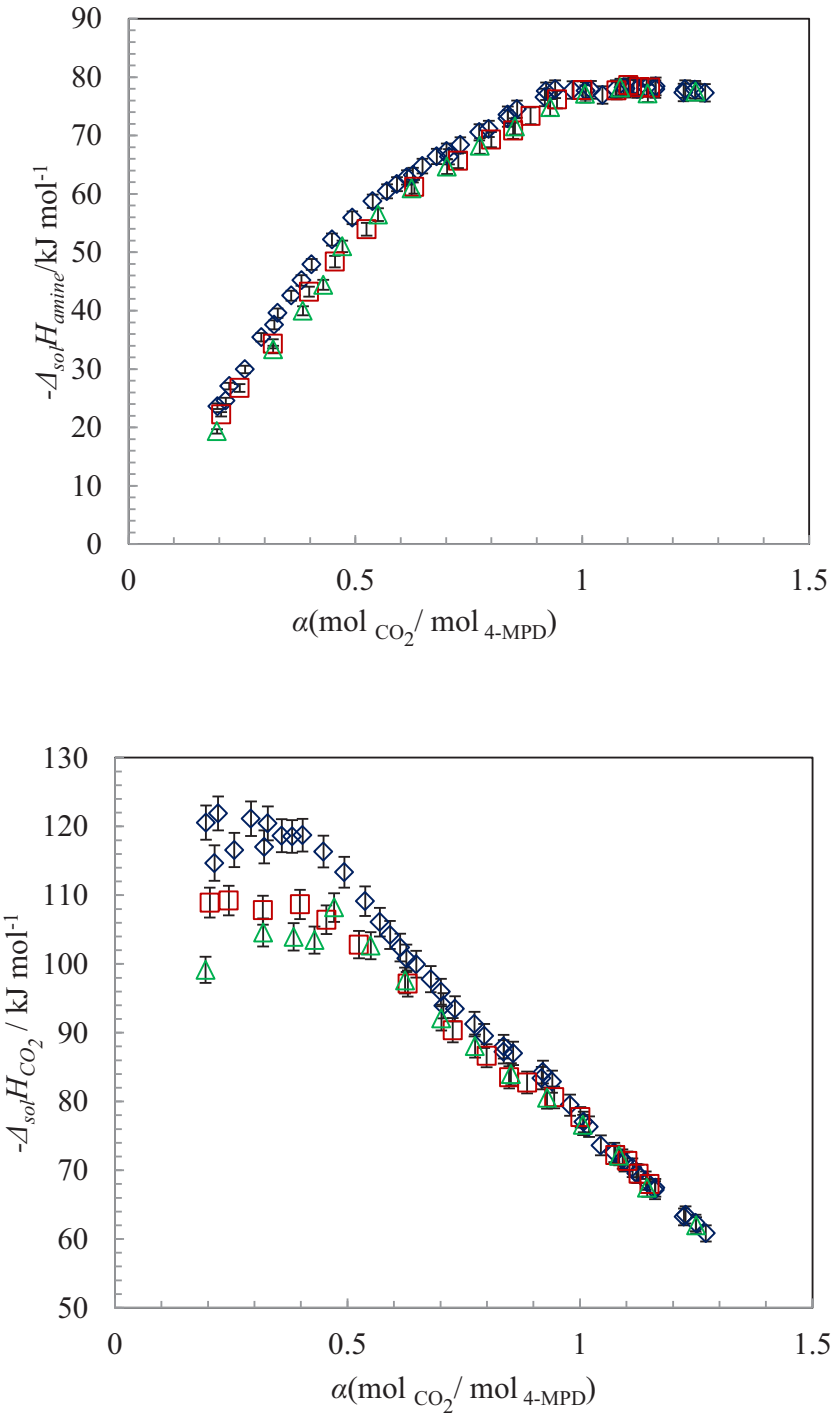

Figure 5-10: Enthalpies of solution to per mole of amine (above) and per mol of CO_2 (below). 4-MPD corresponding to table 6-4 (◇ 0.5 MPa), (□ 1.0MPa) (△1.5MPa)

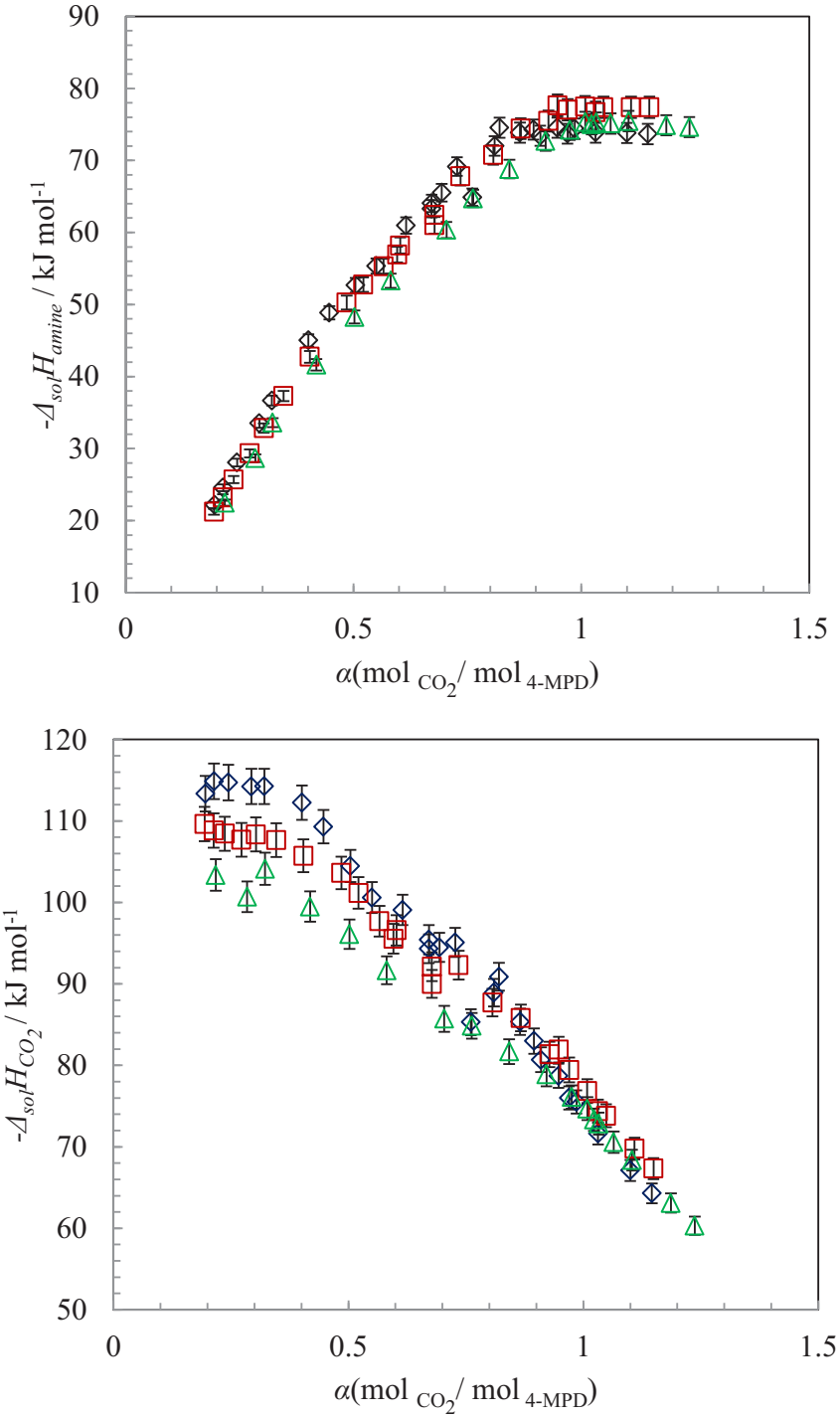

Figure 5-11: Enthalpies of solution to per mole of amine (above) and per mole of CO_2 (below). 4-MPD corresponding to table 6-5 (◇ 0.5 MPa), (□ 1.0MPa) (△1.5MPa)

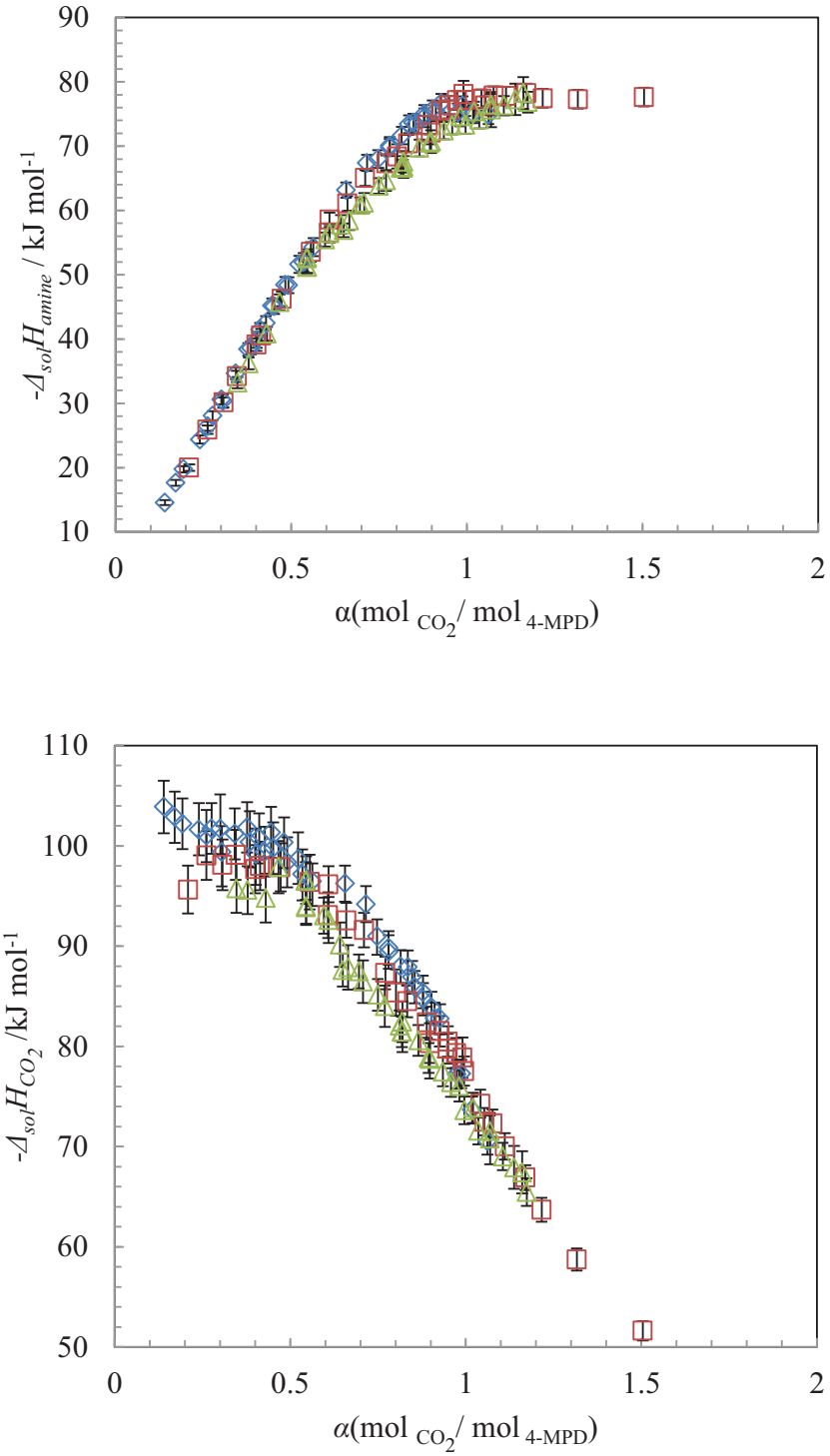

Figure 5-12: Enthalpies of solution per mole of amine (above) and per mole of CO_2 (below). 4-MPD corresponding to table 6-6 (◇ 0.5 MPa), (□ 1.0MPa) (△1.5MPa)

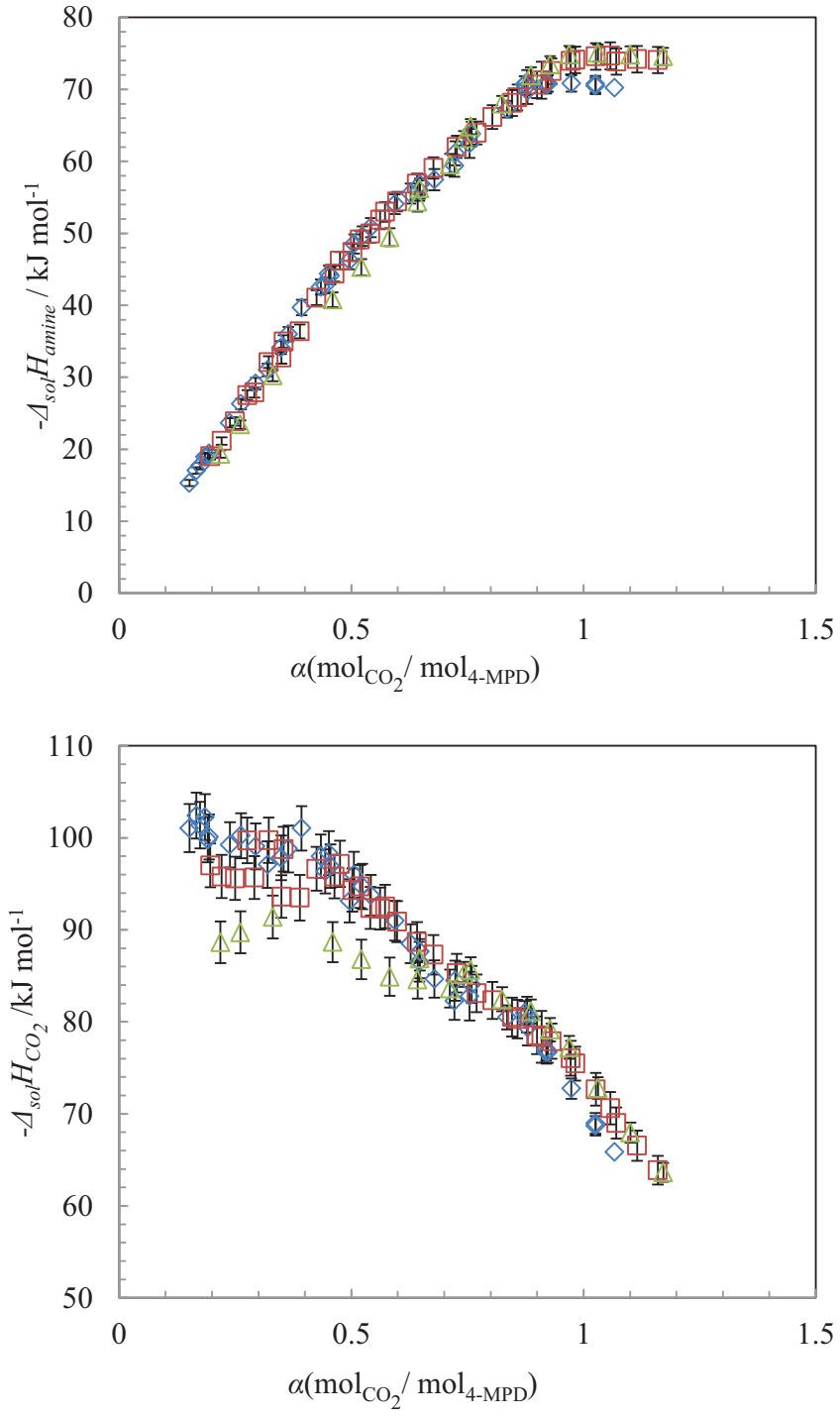

Figure 5-13: Enthalpies of solution per mole of amine (above) and per mole of CO_2 (below). 4-MPD corresponding to table 6-7. (◇ 0.5 MPa), (□ 1.0MPa) (△1.5MPa)

6 Conclusions

To summarize, two novel dynamic flow methods and a static mixing method were developed to measure the LLE for ternary solutions of aqueous alkyl piperidines with carbon dioxide from 273 K to 373 K. The instruments and the collected data have been demonstrated to be highly accurate and reproducible. The results have allowed for the division of the alkyl piperidines into different categories based on their physical structure and chemical equilibrium. Tertiary alkyl piperidines, such as N-MPD and N-EPD, do not produce any carbamates with carbon dioxide and thus show a unique LLE behaviour in the presence of CO_2. The increasing weight percent of alkyl piperidine in solution causes the LLE to decrease in temperature with addition of small amount of CO_2. Secondary hindered amine like 2-MPD show increasing solubility across all concentration ranges with the addition of CO_2. By adding another methyl group to the 6 position, the LLE behaviour will be similar to that of the tertiary piperidines which was observed with 2,6-DPD. Finally, secondary piperidines such as 3-MPD and 4-MPD are become completely soluble in all proportions with the addition of CO_2. This suggests that by allowing carbamates to form in solution this eliminates the phase equilibrium due to the carbamates ability to stabilise the solution.

These are the first temperature dependant thermodynamic data to be collected for many of the alkyl piperidine species in the pure state or the solution states. The extrapolation of the data to 298.15 K has shown to be in good agreement with literature data. The excess enthalpies and excess heat capacities were shown to be consistent with each other and reveal that there is a complex relationship between water and alkyl piperidines. The observations are clear that the changes of the magnitude, position of the local maxima and minima and partial molar properties are related to the location of the alkyl group on the piperidine skeleton. The tertiary alkyl

piperidines have, in general, the largest excess volumes, infinite dilution partial molar enthalpies and excess heat capacities and the weakest excess enthalpies. Increasing the chain length has a weak effect on the excess properties when compared to increase the number of methyl group on the piperidine ring. The secondary hindered alkyl piperidines have second largest excess volumes, infinite dilution partial molar enthalpies and excess heat capacities, with the second weakest excess enthalpies. The addition of an extra methyl group, as seen with 2,6-DPD, has a large effect on the excess volume, infinite dilution partial molar enthalpy and quite a significant effect on the LLE. This maybe be due to a combination of restricting access to the N group and through weak electron inductive effects the secondary alkyl piperidines which include the 3-MPD, 4-MPD and 3,5-DPD, have the least intense excess molar volumes, infinite dilution partial molar enthalpies and excess heat capacities, while having the most intense excess enthalpies. Adding a methyl groups to the 3-MPD and 3,5-MPD reduces the magnitude of the excess volume.

The thermodynamic and phase equilibrium data have shown that there is a large variation of the thermodynamic properties with the structure of the amine. The secondary alkyl piperidines would not be suitable for the demixing absorption solvent because a small amount of CO_2 prevent the miscibility gap. To design new molecules which would be useful for carbon capture, sterically hindered amine groups and tertiary amine are the most suitable candidates. They have LLE which are low temperature, with large heat capacities and low solution enthalpies. Depending on the concentration of alkyl piperidine in solution, the phase equilibrium temperature can be tuned to optimize carbon dioxide absorption.

Using the Pitzer ion interaction model was useful to predict the temperature dependent carbamate equilibrium constants for 3-MPD and 4-MPD. The constants were calculated from the

combination of solubility data and solution enthalpy data. These carbamate constants complete the model which is necessary to understand the equilibrium of species in solution during the absorption. The model also provides the necessary information to predict the regeneration enthalpies. The regeneration enthalpies can be used to calculate the amount of heat need to complete the regeneration cycle.

7 Lingering Questions and Future Work

The thermodynamic data for binary solution needs to be completed to finish characterising each alkyl piperidine. Each of the four methylpiperidines displayed closed loop LLE envelops which were measured at the turn of the century but do not agree with the modern data. As well as many alkyl piperidines have not had their entire envelopes measured. Completing the measurements of these systems would provide more insight into the differences between this class of molecule and water. Using computer modelling it may be possible to understand the relationship between liquid-liquid phase equilibria and thermodynamic properties.

For tertiary solutions of other aqueous alkyl piperidine solutions with CO_2, they do not have the same symmetric alkylated structure, for example 2,5-dimethylpiperidine, or are double methylated on the same carbon, for example 3,3-dimethylpiperidine. The structures of these alkyl piperidines are different enough that they may produce different phase equilibria behaviour when exposed to CO_2. It may also show which positions of the alkyl group are the most beneficial to modify. It would be a good idea to measure the LLE with other ionisable gases to see if they have different effects on the LLE for each of the solutions. While industrial processes do primarily produce CO_2 other contaminating gases like H_2S are present and may have an effect on the phase equilibria.

With the amount of data that exists it may be possible to find a way to combine both the LLE phase data and the thermodynamic data to create a speciation model. However the model would have to be able to work without the knowledge of the change in the dielectric constant of solution, as well as the lack of carbamate constants for other alkyl piperidines. It would also need to solve for the changes in vapour-liquid-liquid phase equilibrium. Example models would include the electrolyte-NRTL and extended UNIQUAC model.

8 Research Acknowledgments

This work was funded as part of an international research program called DACOOTA, (**D**emixing **A**mines for **CO**$_2$ capture: **T**hermodynamic and Spectroscopic **A**pproach), which was funded by the French National Research Agency (ANR) and the Natural Science and Engineering Research Council of Canada (NSERC). The project was a collaboration between the –CO_2 Capture Group" whom are specialised in measuring experimental solubilities of CO_2, liquid-liquid phase equilibrium, enthalpies of mixing heat capacities and densities of fluids. The Canadian partner is the –Hydrothermal Chemistry Group" in the University of Guelph and they are specialised in studying thermodynamic properties and transport properties of aqueous solution au high temperatures and pressures. In this project their contribution is to use RAMAN spectroscopy to determine the speciation of alkyl piperidine solutions following the absorption of CO_2 in both homogenous solution and both phases of demixed solution.

9 References

Abrams D. S. and Prausnitz J. M. (1975) Statistical thermodynamics of liquid mixtures: A new expression for the excess Gibbs energy of partly or completely miscible systems. *AIChE J.* **21**, 116–128. Available at: http://onlinelibrary.wiley.com/doi/10.1002/aic.690210115/abstract [Accessed July 29, 2016].

Afzal W., Valtz A., Coquelet C. and Richon D. (2008) Volumetric properties of (piperidine + water) binary system: Measurements and modeling. *J. Chem. Thermodyn.* **40**, 47–53. Available at: http://www.sciencedirect.com/science/article/pii/S0021961407001085 [Accessed June 23, 2016].

Arcis H., Ballerat-Busserolles K., Rodier L. and Coxam J.-Y. (2011) Enthalpy of Solution of Carbon Dioxide in Aqueous Solutions of Monoethanolamine at Temperatures of 322.5 K and 372.9 K and Pressures up to 5 MPa. *J. Chem. Eng. Data* **56**, 3351–3362. Available at: http://dx.doi.org/10.1021/je2002946.

Arcis H., Ballerat-Busserolles K., Rodier L. and Coxam J.-Y. (2012a) Enthalpy of Solution of Carbon Dioxide in Aqueous Solutions of Triethanolamine at Temperatures of 322.5 K and 372.9 K and Pressures up to 5 MPa. *J. Chem. Eng. Data* **57**, 3587–3597. Available at: http://dx.doi.org/10.1021/je300813c.

Arcis H., Ballerat-Busserolles K., Rodier L. and Coxam J.-Y. (2012b) Measurement and Modeling of Enthalpy of Solution of Carbon Dioxide in Aqueous Solutions of Diethanolamine at Temperatures of (322.5 and 372.9) K and Pressures up to 3 MPa. *J. Chem. Eng. Data* **57**, 840–855. Available at: http://dx.doi.org/10.1021/je201012e.

Arcis H., Rodier L., Ballerat-Busserolles K. and Coxam J.-Y. (2009) Modeling of (vapor + liquid) equilibrium and enthalpy of solution of carbon dioxide (CO2) in aqueous methyldiethanolamine (MDEA) solutions. *J. Chem. Thermodyn.* **41**, 783–789. Available at: http://www.sciencedirect.com/science/article/pii/S0021961409000111 [Accessed August 24, 2016].

Arcis H., Rodier L. and Coxam J. Y. (2007) Enthalpy of solution of CO2 in aqueous solutions of 2-amino-2-methyl-1-propanol. *J. Chem. Thermodyn.* **39**, 878–887. Available at: ://WOS:000247431400006.

Arnold Aaron Bondi (1968) *Physical Properties of Molecular Crystals, Liquids and Glasses*., Wiley, New York.

Arshad M. W., von Solms N., Thomsen K. and Svendsen H. F. (2013) Heat of Absorption of CO 2 in Aqueous Solutions of DEEA, MAPA and their Mixture. *Energy Procedia* **37**, 1532–1542.

Arshad M. W., Svendsen H. F., Fosbøl P. L., von Solms N. and Thomsen K. (2014) Equilibrium Total Pressure and CO2 Solubility in Binary and Ternary Aqueous Solutions of 2-(Diethylamino)ethanol (DEEA) and 3-(Methylamino)propylamine (MAPA). *J. Chem. Eng. Data* **59**, 764–774. Available at: http://dx.doi.org/10.1021/je400886w [Accessed July 4, 2016].

Atkins P. and de Paula J. (2010) *Atkins' Physical Chemistry*., OUP Oxford.

Ballerat-Busserolles K., Origlia M. L. and Woolley E. M. (2000) Calibration of a fixed-cell temperature-scanning calorimeter to measure precise solution heat capacities from 275 to

398 K at 0.35 MPa. *Thermochim. Acta* **347**, 3–7. Available at: http://www.sciencedirect.com/science/article/pii/S0040603199004281.

Ballerat-Busserolles K., Simond M. R., Coulier Y. and Coxam J.-Y. (2014) Protonation of alkanolamines and cyclic amines in water at temperatures from 293.15 to 373.15 K. *Pure Appl. Chem.* **86**, 233–243. Available at: http://www.degruyter.com/abstract/j/pac.2014.86.issue-2/pac-2014-5017/pac-2014-5017.xml [Accessed September 13, 2016].

Bates R. G. and Bower V. E. (1956) Dissociation Constant of Piperidinium Ion From 0 to 50 C and Related Thermodynamic Quantities. *J. Res. Natl. Bur. Stand.* **57**.

Bea S. A., Carrera J., Ayora C. and Batlle F. (2010) Modeling of concentrated aqueous solutions: Efficient implementation of Pitzer equations in geochemical and reactive transport models. *Comput. Geosci.* **36**, 526–538. Available at: http://www.sciencedirect.com/science/article/pii/S0098300409003264 [Accessed September 15, 2016].

Benamor A. and Aroua M. K. (2005) Modeling of CO2 solubility and carbamate concentration in DEA, MDEA and their mixtures using the Deshmukh–Mather model. *Fluid Phase Equilibria* **231**, 150–162. Available at: http://www.sciencedirect.com/science/article/pii/S037838120500018X [Accessed September 15, 2016].

Bernauer M. and Dohnal V. (2009) Temperature dependences of limiting activity coefficients and Henry's law constants for N-methylpyrrolidone, pyridine, and piperidine in water. *Fluid Phase Equilibria* **282**, 100–107. Available at: http://www.sciencedirect.com/science/article/pii/S0378381209001745 [Accessed October 10, 2016].

Berthon G., Angot B., Beden B. and Enea O. (1979) Quantitative comparison of substituent effects on solvation and proton-ionization standard enthalpies of methylpiperidines. *J. Chem. Thermodyn.* **11**, 539–546. Available at: http://www.sciencedirect.com/science/article/pii/0021961479900922 [Accessed October 1, 2016].

Blais M. J., Enea O. and Berthon G. (1974) Grandeurs thermodynamiques de protonation de la pipèridine et de ses dèrivès alkylsubstituès. *Thermochim. Acta* **8**, 433–438. Available at: http://www.sciencedirect.com/science/article/pii/0040603174851117 [Accessed October 4, 2016].

Boot-Handford M. E., Abanades J. C., Anthony E. J., Blunt M. J., Brandani S., Dowell N. M., Fernández J. R., Ferrari M.-C., Gross R., Hallett J. P., Haszeldine R. S., Heptonstall P., Lyngfelt A., Makuch Z., Mangano E., Porter R. T. J., Pourkashanian M., Rochelle G. T., Shah N., Yao J. G. and Fennell P. S. (2013) Carbon capture and storage update. *Energy Environ. Sci.* **7**, 130–189. Available at: http://pubs.rsc.org/en/content/articlelanding/2014/ee/c3ee42350f [Accessed September 18, 2016].

Bouillon P.-A., Jacquin M. and Raynal L. (2012) Method for deacidifying a gas by an absorbing solution with demixing control.

Brethes and Chassagnette (2014) Détermination du pKa d'amines démixantes par la méthode de l'électrode à hydrogène.

Carroll J. J. and Mather A. E. (1996) A Model for the Distribution of Acid Gases Between an Aqueous Alkanolamine Solution and Lpg. *Chem. Eng. Commun.* **144**, 95–101. Available at: http://dx.doi.org/10.1080/00986449608936448 [Accessed September 15, 2016].

Christine McGregor (2017) Master of Chemistry Thesis. Univeristy of Guelph.

Chue K. T., Kim J. N., Yoo Y. J., Cho S. H. and Yang R. T. (1995) Comparison of Activated Carbon and Zeolite 13X for CO2 Recovery from Flue Gas by Pressure Swing Adsorption. *Ind. Eng. Chem. Res.* **34**, 591–598. Available at: http://dx.doi.org/10.1021/ie00041a020.

Ciftja A. F., Hartono A. and Svendsen H. F. (2013) Experimental study on phase change solvents in CO 2 capture by NMR spectroscopy. *Chem. Eng. Sci.* **102**, 378–386.

Conti, G, Gianni, P, Matteoli, R and Mengheri, M (1976) Capacita termiche molari di alcuni composti organici mono- e bifunzionali nel liquido puro e in soluzione acquosa a 25C. *Chim Ind Milan* **58**, 225.

Coulier Y., Ballerat-Busserolles K., Mesones J., Lowe A. and Coxam J.-Y. (2015) Excess Molar Enthalpies and Heat Capacities of {2-Methylpiperidine–Water} and {N-Methylpiperidine–Water} Systems of Low to Moderate Amine Compositions. *J. Chem. Eng. Data* **60**, 1563–1571. Available at: http://dx.doi.org/10.1021/je5008444 [Accessed June 23, 2016].

Coulier Y., Ballerat-Busserolles K., Rodier L. and Coxam J.-Y. (2010) Temperatures of liquid–liquid separation and excess molar volumes of {N-methylpiperidine–water} and {2-methylpiperidine–water} systems. *Fluid Phase Equilibria* **296**, 206–212. Available at: http://www.sciencedirect.com/science/article/pii/S0378381210002475 [Accessed June 23, 2016].

Coulier Y., Lowe A., Tremaine P. R., Coxam J.-Y. and Ballerat-Busserolles K. (2016) Absorption of CO2 in aqueous solutions of 2-methylpiperidine: Heats of solution and modeling. *Int. J. Greenh. Gas Control* **47**, 322–329. Available at: http://www.sciencedirect.com/science/article/pii/S1750583616300597 [Accessed July 1, 2016].

Deshmukh R. D. and Mather A. E. (1981) A mathematical model for equilibrium solubility of hydrogen sulfide and carbon dioxide in aqueous alkanolamine solutions. *Chem. Eng. Sci.* **36**, 355–362. Available at: http://www.sciencedirect.com/science/article/pii/0009250981850154 [Accessed September 14, 2016].

Dohnal V. and Rehak K. (2011) Determination of Infinite Dilution Partial Molar Excess Enthalpies and Volumes for Some Ionic Liquid Precursors in Water and Methanol Using Tandem Flow Mixing Calorimetry and Vibrating-Tube Densimetry. *J. Chem. Eng. Data* **56**, 3047–3052.

Dohnal V., Roux A. H. and Hynek V. (1994) Limiting partial molar excess enthalpies by flow calorimetry: Some organic solvents in water. *J. Solut. Chem.* **23**, 889–900. Available at: http://link.springer.com/article/10.1007/BF00972752 [Accessed September 12, 2016].

Doi H., Tamura K. and Murakami S. (2000) Thermodynamic properties of aqueous solution of 2-isobutoxyethanol atT= (293.15, 298.15, and 303.15) K, below and above LCST. *J. Chem. Thermodyn.* **32**, 729–741. Available at: http://www.sciencedirect.com/science/article/pii/S0021961499906456 [Accessed June 26, 2016].

Edwards T. J., Maurer G., Newman J. and Prausnitz J. M. (1978) Vapor-liquid equilibria in multicomponent aqueous solutions of volatile weak electrolytes. *AIChE J.* **24**, 966–976. Available at: http://onlinelibrary.wiley.com/doi/10.1002/aic.690240605/abstract [Accessed August 24, 2016].

Eliel E. L., Kandasamy D., Yen C. and Hargrave K. D. (1980) Conformational analysis. 39. Carbon-13 NMR spectra of saturated heterocycles. 9. Piperidine and N-methylpiperidine. *J. Am. Chem. Soc.* **102**, 3698–3707. Available at: http://dx.doi.org/10.1021/ja00531a006.

Ellina Levina, Simon Bennett and Sean McCoy (2013) *Technology Roadmap: Carbon Capture and Storage*. 2013th ed., International Energy Agency, Paris.

Fan L.-S., Zeng L., Wang W. and Luo S. (2012) Chemical looping processes for CO2 capture and carbonaceous fuel conversion – prospect and opportunity. *Energy Environ. Sci.* **5**, 7254–7280. Available at: http://pubs.rsc.org/en/content/articlelanding/2012/ee/c2ee03198a [Accessed September 23, 2016].

Fandiño O., Yacyshyn M., Cox J. S. and Tremaine P. R. (2016) Speciation in Liquid-Liquid Phase-Separating Solutions of Aqueous Amines for Carbon Capture Applications by Raman Spectroscopy. In *Acid Gas Extraction for Disposal and Related Topics* (eds. Y. Wu, J. J. Carroll, and W. Zhu). John Wiley & Sons, Inc. pp. 81–94. Available at: http://onlinelibrary.wiley.com/doi/10.1002/9781118938652.ch7/summary [Accessed August 24, 2016].

Faramarzi L., Kontogeorgis G. M., Thomsen K. and Stenby E. H. (2009) Extended UNIQUAC model for thermodynamic modeling of CO2 absorption in aqueous alkanolamine solutions. *Fluid Phase Equilibria* **282**, 121–132. Available at: http://www.sciencedirect.com/science/article/pii/S037838120900171X.

Flaschner O. (1909) LXXXI.—The miscibility of the pyridine bases with water and the influence of a critical-solution point on the shape of the melting-point curve. *J. Chem. Soc. Trans.* **95**, 668–685.

Flaschner O. and MacEwen B. (1908) XCVI.-The mutual solubility of 2-methylpiperidine and water. *J. Chem. Soc. Trans.* **93**, 1000–1003.

Flaschner, Otto (1908) *Z Phys Chem* **62**, 493.

Fowler R. H. and Guggenheim E. A. (1939) *Statistical Thermodynamics: A Version of Statistical Mechanics for Students of Physics and Chemistry, by R. H. Fowler,... and E. A. Guggenheim,...*, University Press (printed by W. Lewis).

Freytag M. and Jones P. G. (1999) Hydrogen bonding in two piperidinium derivatives. *Acta Crystallogr. C* **55**, 1874–1877. Available at: http://scripts.iucr.org/cgi-bin/paper?S0108270199009567 [Accessed September 16, 2016].

Goeppert A., Czaun M., Prakash G. K. S. and Olah G. A. (2012) Air as the renewable carbon source of the future: an overview of CO2 capture from the atmosphere. *Energy Environ. Sci.* **5**, 7833–7853. Available at: http://pubs.rsc.org/en/content/articlelanding/2012/ee/c2ee21586a [Accessed September 23, 2016].

Gomez A., Briot P., Raynal L., Broutin P., Gimenez M., Soazic M., Cessat P. and Saysset S. (2014) ACACIA Project – Development of a Post-Combustion CO2 Capture Process.

Case of the DMXTM Process. *Oil Gas Sci Technol – Rev IFP Energ. Nouv.* **69**, 1121–1129. Available at: http://dx.doi.org/10.2516/ogst/2014035.

Góral M., Shaw D. G., Mączyński A., Wiśniewska-Gocłowska B. and Oracz P. (2012a) IUPAC-NIST Solubility Data Series. 96. Amines with Water Part 1. C4–C6 Aliphatic Amines. *J. Phys. Chem. Ref. Data* **41**, 43106. Available at: http://scitation.aip.org/content/aip/journal/jpcrd/41/4/10.1063/1.4755288 [Accessed June 27, 2016].

Góral M., Shaw D. G., Mączyński A., Wiśniewska-Gocłowska B. and Oracz P. (2012b) IUPAC-NIST Solubility Data Series. 96. Amines with Water Part 2. C7–C24 Aliphatic Amines. *J. Phys. Chem. Ref. Data* **41**, 43107. Available at: http://scitation.aip.org/content/aip/journal/jpcrd/41/4/10.1063/1.4755953 [Accessed June 27, 2016].

Guggenheim E. A. (1952) *Mixtures*., Oxford University Press, Oxford.

Gulluoglu M. T., Erdogdu Y. and Yurdakul S. (2007) Molecular structure and vibrational spectra of piperidine and 4-methylpiperidine by density functional theory and ab initio Hartree-Fock calculations. *J. Mol. Struct.* **834**, 540–547.

Hanming L., Junhua H. and Phillip P. (2012) Tailoring Ionic Liquids for Post-Combustion CO2 Capture. In *Recent Advances in Post-Combustion CO2 Capture Chemistry* ACS Symposium Series. American Chemical Society. pp. 153–175. Available at: http://dx.doi.org/10.1021/bk-2012-1097.ch008 [Accessed March 3, 2014].

Hepler L. G. (1969) Thermal expansion and structure in water and aqueous solutions. *Can. J. Chem.* **47**, 4613–4617. Available at: http://www.nrcresearchpress.com/doi/abs/10.1139/v69-762 [Accessed September 7, 2016].

Hessen E. T., Haug-Warberg T. and Svendsen H. F. (2010) The refined e-NRTL model applied to CO2–H2O–alkanolamine systems. *Chem. Eng. Sci.* **65**, 3638–3648. Available at: http://www.sciencedirect.com/science/article/pii/S0009250910001582 [Accessed June 28, 2016].

James F. (1994) CERN Program Library Long Writeup D506. *MINUIT Funct. Minimization Error Anal. Ref. Man. Version* **94**.

Jiang H., Zhang S. and Jin R. (2008) NMR and FT-IR analysis of new molecular complex 1-piperidine-carboxylate-piperidinium-H2O. *Wuhan Univ. J. Nat. Sci.* **13**, 93–97. Available at: http://link.springer.com/article/10.1007/s11859-008-0118-0 [Accessed September 16, 2016].

Jiang H., Zhang S., Jin R. and Ma Y. (2007) New crystal structure of molecular complex 1-piperidine carboxylate-piperidinium-H2O studied by X-ray single crystal diffraction. *Wuhan Univ. J. Nat. Sci.* **12**, 1099–1104. Available at: http://link.springer.com/article/10.1007/s11859-007-0111-z [Accessed September 16, 2016].

Jou F. Y., Mather A. E. and Otto F. D. (1982) Solubility of hydrogen sulfide and carbon dioxide in aqueous methyldiethanolamine solutions. *Ind. Eng. Chem. Process Des. Dev.* **21**, 539–544. Available at: http://dx.doi.org/10.1021/i200019a001.

Kent, R. L. and Eisenberg, B. (1976) Better Data For Amine Treating. *Hydrocarb. Process.* **55**, 87.

Koschel D., Coxam J. Y., Rodier L. and Majer V. (2006) Enthalpy and solubility data of CO2 in water and NaCl(aq) at conditions of interest for geological sequestration. *Fluid Phase Equilibria* **247**, 107–120. Available at: ://WOS:000240563000015.

Kul I. and Lieu T. (2010) Thermodynamic properties of aqueous solutions of pyridine and piperidine. *Fluid Phase Equilibria* **290**, 95–102. Available at: http://www.sciencedirect.com/science/article/pii/S0378381209004191 [Accessed September 5, 2016].

Lee J. I., Otto F. D. and Mather A. E. (1976) The measurement and prediction of the solubility of mixtures of carbon dioxide and hydrogen sulphide in a 2.5 N monoethanolamine solution. *Can. J. Chem. Eng.* **54**, 214–219. Available at: http://onlinelibrary.wiley.com/doi/10.1002/cjce.5450540316/abstract [Accessed September 15, 2016].

Lemmon E. W. and Span R. (2006) Short Fundamental Equations of State for 20 Industrial Fluids. *J. Chem. Eng. Data* **51**, 785–850. Available at: http://dx.doi.org/10.1021/je050186n [Accessed June 23, 2016].

Lemon, E.W.; Huber,M.L.; McLinden, M.O. (2010) *NIST Standard Reference Database 23: REference Fluid Thermodynamic and Transport Properties-REFPROP*., National Institute of Standards and Technology, Gaitherburge, MD, USA.

Liebenthal U., Pinto D. D. D., Monteiro J. G. M.-S., Svendsen H. F. and Kather A. (2013) Overall Process Analysis and Optimisation for CO2 Capture from Coal Fired Power Plants based on Phase Change Solvents Forming Two Liquid Phases. *GHGT-11 Proc. 11th Int. Conf. Greenh. Gas Control Technol. 18-22 Novemb. 2012 Kyoto Jpn.* **37**, 1844–1854. Available at: http://www.sciencedirect.com/science/article/pii/S187661021300307X.

Luo X., Chen N., Liu S., Rongwong W., Idem R. O., Tontiwachwuthikul P. and Liang Z. (2016) Experiments and modeling of vapor-liquid equilibrium data in DEEA-CO2-H2O system. *Int. J. Greenh. Gas Control* **53**, 160–168. Available at: http://www.sciencedirect.com/science/article/pii/S175058361630425X [Accessed September 15, 2016].

Lüthi D., Le Floch M., Bereiter B., Blunier T., Barnola J.-M., Siegenthaler U., Raynaud D., Jouzel J., Fischer H., Kawamura K. and Stocker T. F. (2008) High-resolution carbon dioxide concentration record 650,000–800,000 years before present. *Nature* **453**, 379–382. Available at: http://www.nature.com/nature/journal/v453/n7193/abs/nature06949.html [Accessed September 23, 2016].

Maddox R. N., Mains G. J. and Rahman M. A. (1987) Reactions of carbon dioxide and hydrogen sulfide with some alkanolamines. *Ind. Eng. Chem. Res.* **26**, 27–31. Available at: http://dx.doi.org/10.1021/ie00061a006.

Marczak W., Hołaj-Krzak J. T., Lodowski P., Almásy L. and Fadda G. C. (2015) Hydrogen-bonded aggregates in the mixtures of piperidine with water: Thermodynamic, SANS and theoretical studies. *Chem. Phys. Lett.* **619**, 77–83. Available at: http://www.sciencedirect.com/science/article/pii/S0009261414009890 [Accessed August 1, 2016].

Marczak W., Łężniak M., Zorębski M., Lodowski P., Przybyła A., Truszkowska D. and Almásy L. (2013) Water-induced aggregation and hydrophobic hydration in aqueous solutions of

N-methylpiperidine. *RSC Adv.* **3**, 22053–22064. Available at: http://pubs.rsc.org/en/content/articlelanding/2013/ra/c3ra43168a [Accessed June 26, 2016].

Mathonat C., Hynek V., Majer V. and Grolier J.-P. E. (1994) Measurements of excess enthalpies at high temperature and pressure using a new type of mixing unit. *J. Solut. Chem.* **23**, 1161–1182. Available at: http://link.springer.com/article/10.1007/BF00974028 [Accessed September 19, 2016].

Mathonat C., Majer V., Mather A. E. and Grolier J.-P. E. (1997) Enthalpies of absorption and solubility of CO2 in aqueous solutions of methyldiethanolamine. *Fluid Phase Equilibria* **140**, 171–182. Available at: http://www.sciencedirect.com/science/article/pii/S0378381297001829 [Accessed September 30, 2016].

Messerly J. F., Todd S. S., Finke H. L., Good W. D. and Gammon B. E. (1988) Condensed-phase heat-capacity studies and derived thermodynamic properties for six cyclic nitrogen compounds. *J. Chem. Thermodyn.* **20**, 209–224. Available at: http://www.sciencedirect.com/science/article/pii/0021961488901565 [Accessed September 1, 2016].

Millward A. R. and Yaghi O. M. (2005) Metal−Organic Frameworks with Exceptionally High Capacity for Storage of Carbon Dioxide at Room Temperature. *J. Am. Chem. Soc.* **127**, 17998–17999. Available at: http://dx.doi.org/10.1021/ja0570032.

Monteiro J. G.-S., Majeed H., Knuutila H. and Svendsen H. F. (2015) Kinetics of CO 2 absorption in aqueous blends of N, N-diethylethanolamine (DEEA) and N-methyl-1, 3-propane-diamine (MAPA). *Chem. Eng. Sci.* **129**, 145–155.

Monteiro J. G.-S., Pinto D. D., Zaidy S. A., Hartono A. and Svendsen H. F. (2013) VLE data and modelling of aqueous N, N-diethylethanolamine (DEEA) solutions. *Int. J. Greenh. Gas Control* **19**, 432–440.

Mumford K. A., Wu Y., Smith K. H. and Stevens G. W. (2015) Review of solvent based carbon-dioxide capture technologies. *Front. Chem. Sci. Eng.* **9**, 125–141. Available at: http://link.springer.com/article/10.1007/s11705-015-1514-6 [Accessed September 12, 2016].

Olajire A. A. (2010) CO 2 capture and separation technologies for end-of-pipe applications–a review. *Energy* **35**, 2610–2628.

Ott J. B., Cornett G. V., Stouffer C. E., Woodfield B. F., Guanquan C. and Christensen J. J. (1986) Excess enthalpies of (ethanol+ water) at 323.15, 333.15, 348.15, and 373.15 K and from 0.4 to 15 MPa. *J. Chem. Thermodyn.* **18**, 867–875.

Ott J. B., Stouffer C. E., Cornett G. V., Woodfield B. F., Guanquan C. and Christensen J. J. (1987) Excess enthalpies for (ethanol+ water) at 398.15, 423.15, 448.15, and 473.15 K and at pressures of 5 and 15 MPa. Recommendations for choosing (ethanol+ water) as an H m E reference mixture. *J. Chem. Thermodyn.* **19**, 337–348.

Ott J. B., Stouffer C. E., Cornett G. V., Woodfield B. F., Wirthlin R. C., Christensen J. J. and Deiters U. K. (1986) Excess enthalpies for (ethanol+ water) at 298.15 K and pressures of 0.4, 5, 10, and 15 MPa. *J. Chem. Thermodyn.* **18**, 1–12.

Pachauri R. K., Allen M. R., Barros V. R., Broome J., Cramer W., Christ R., Church J. A., Clarke L., Dahe Q. and Dasgupta P. (2014) *Climate change 2014: synthesis Report.*

Contribution of working groups I, II and III to the fifth assessment report of the intergovernmental panel on climate change., IPCC.

Patterson D. (1994) Structure and the thermodynamics of non-electrolyte mixtures. *J. Solut. Chem.* **23**, 105–120. Available at: http://link.springer.com/article/10.1007/BF00973540 [Accessed September 4, 2016].

Perron G., Quirion F., Lambert D., Ledoux J., Ghaicha L., Bennes R., Privat M. and Desnoyers J. E. (1993) Thermodynamic properties of aqueous organic mixtures near the critical demixing: Cases of 2,6-dimethylpyridine and of 2-isobutoxyethanol. *J. Solut. Chem.* **22**, 107–124. Available at: http://link.springer.com/article/10.1007/BF00650678 [Accessed June 26, 2016].

Picker P., Tremblay E. and Jolicoeur C. (1973) A high-precision digital readout flow densimeter for liquids. *J. Solut. Chem.* **3**, 377–384. Available at: http://link.springer.com/article/10.1007/BF00646478 [Accessed July 18, 2016].

Pinto D. D., Knuutila H., Fytianos G., Haugen G., Mejdell T. and Svendsen H. F. (2014) CO 2 post combustion capture with a phase change solvent. Pilot plant campaign. *Int. J. Greenh. Gas Control* **31**, 153–164.

Pinto D. D., Zaidy S. A., Hartono A. and Svendsen H. F. (2014) Evaluation of a phase change solvent for CO 2 capture: absorption and desorption tests. *Int. J. Greenh. Gas Control* **28**, 318–327.

Pitzer K. S. (1980) Electrolytes. From dilute solutions to fused salts. *J. Am. Chem. Soc.* **102**, 2902–2906. Available at: http://dx.doi.org/10.1021/ja00529a006.

Pitzer K. S. (1973) Thermodynamics of electrolytes. I. Theoretical basis and general equations. *J. Phys. Chem.* **77**, 268–277. Available at: http://dx.doi.org/10.1021/j100621a026.

Pitzer K. S. and Kim J. J. (1974) Thermodynamics of electrolytes. IV. Activity and osmotic coefficients for mixed electrolytes. *J. Am. Chem. Soc.* **96**, 5701–5707. Available at: http://dx.doi.org/10.1021/ja00825a004.

Raynal L., Alix P., Bouillon P.-A., Gomez A., de Nailly M. le F., Jacquin M., Kittel J., di Lella A., Mougin P. and Trapy J. (2011) The DMX^{TM} process: an original solution for lowering the cost of post-combustion carbon capture. *Energy Procedia* **4**, 779–786.

Raynal L., Bouillon P.-A., Gomez A. and Broutin P. (2011) From MEA to demixing solvents and future steps, a roadmap for lowering the cost of post-combustion carbon capture. *Chem. Eng. J.* **171**, 742–752. Available at: http://www.sciencedirect.com/science/article/pii/S1385894711000350 [Accessed July 1, 2016].

Redlich O. and Kwong J. N. S. (1949) On the Thermodynamics of Solutions. V. An Equation of State. Fugacities of Gaseous Solutions. *Chem. Rev.* **44**, 233–244. Available at: http://dx.doi.org/10.1021/cr60137a013 [Accessed October 24, 2016].

Renon H. and Prausnitz J. M. (1968) Local compositions in thermodynamic excess functions for liquid mixtures. *AIChE J.* **14**, 135–144. Available at: http://onlinelibrary.wiley.com/doi/10.1002/aic.690140124/abstract [Accessed September 15, 2016].

Robinson K., McCluskey A. and Attalla M. I. (2012) The Effect Molecular Structural Variations Has on the CO2 Absorption Characteristics of Heterocyclic Amines. In *Recent Advances in Post-Combustion CO2 Capture Chemistry* ACS Symposium Series. American

Chemical Society. pp. 1–27. Available at: http://dx.doi.org/10.1021/bk-2012-1097.ch001 [Accessed March 3, 2014].

Rumpf B. and Maurer G. (1993) An Experimental and Theoretical Investigation on the Solubility of Carbon Dioxide in Aqueous Solutions of Strong Electrolytes. *Berichte Bunsenges. Für Phys. Chem.* **97**, 85–97. Available at: http://onlinelibrary.wiley.com/doi/10.1002/bbpc.19930970116/abstract [Accessed August 28, 2016].

Sadegh N., Stenby E. H. and Thomsen K. (2015) Thermodynamic modeling of CO2 absorption in aqueous N-Methyldiethanolamine using Extended UNIQUAC model. *Fuel* **144**, 295–306. Available at: http://www.sciencedirect.com/science/article/pii/S0016236114012113.

Sander B., Rasmussen P. and Fredenslund A. (1986) Calculation of solid-liquid equilibria in aqueous solutions of nitrate salts using an extended UNIQUAC equation. *Chem. Eng. Sci.* **41**, 1197–1202.

Span R. and Wagner W. (1996) A New Equation of State for Carbon Dioxide Covering the Fluid Region from the Triple-Point Temperature to 1100 K at Pressures up to 800 MPa. *J. Phys. Chem. Ref. Data* **25**, 1509–1596. Available at: http://scitation.aip.org/content/aip/journal/jpcrd/25/6/10.1063/1.555991 [Accessed June 23, 2016].

Span R. and Wagner W. (2003a) Equations of State for Technical Applications. I. Simultaneously Optimized Functional Forms for Nonpolar and Polar Fluids. *Int. J. Thermophys.* **24**, 1–39. Available at: http://link.springer.com/article/10.1023/A%3A1022390430888 [Accessed June 23, 2016].

Span R. and Wagner W. (2003b) Equations of State for Technical Applications. II. Results for Nonpolar Fluids. *Int. J. Thermophys.* **24**, 41–109. Available at: http://link.springer.com/article/10.1023/A%3A1022310214958 [Accessed June 23, 2016].

Stephenson R. M. (1993) Mutual solubility of water and pyridine derivatives. *J. Chem. Eng. Data* **38**, 428–431. Available at: http://dx.doi.org/10.1021/je00011a026.

Stewart C. and Hessami M.-A. (2005) A study of methods of carbon dioxide capture and sequestration—the sustainability of a photosynthetic bioreactor approach. *Energy Convers. Manag.* **46**, 403–420. Available at: http://www.sciencedirect.com/science/article/pii/S0196890404000883.

Tan, Y. H. (2010) *Study of CO2 absorption into Thermomorphic Lipophilic Amine Solvents*., Technical University of Dortmond, Dortmund, Germany.

Thomsen K. and Rasmussen P. (1999) Modeling of vapor–liquid–solid equilibrium in gas–aqueous electrolyte systems. *Chem. Eng. Sci.* **54**, 1787–1802. Available at: http://www.sciencedirect.com/science/article/pii/S0009250999000196 [Accessed October 21, 2016].

Thomsen K., Rasmussen P. and Gani R. (1996) Correlation and prediction of thermal properties and phase behaviour for a class of aqueous electrolyte systems. *Chem. Eng. Sci.* **51**, 3675–3683. Available at: http://www.sciencedirect.com/science/article/pii/0009250995004181 [Accessed October 13, 2016].

Visser C. de, Perron G. and Desnoyers J. E. (1977) The heat capacities, volumes, and expansibilities of tert-butyl alcohol – water mixtures from 6 to 65 °C. *Can. J. Chem.* **55**, 856–862. Available at: http://www.nrcresearchpress.com/doi/abs/10.1139/v77-119 [Accessed September 4, 2016].

Wagner W. and Pruß A. (2002) The IAPWS Formulation 1995 for the Thermodynamic Properties of Ordinary Water Substance for General and Scientific Use. *J. Phys. Chem. Ref. Data* **31**, 387–535. Available at: http://scitation.aip.org/content/aip/journal/jpcrd/31/2/10.1063/1.1461829 [Accessed June 23, 2016].

Wang M., Lawal A., Stephenson P., Sidders J. and Ramshaw C. (2011) Post-combustion CO 2 capture with chemical absorption: a state-of-the-art review. *Chem. Eng. Res. Des.* **89**, 1609–1624.

Wigley T. M. L. (1983) The pre-industrial carbon dioxide level. *Clim. Change* **5**, 315–320. Available at: http://dx.doi.org/10.1007/BF00140798.

Woolley E. M. (2007) A new tool for an old job: Using fixed cell scanning calorimetry to investigate dilute aqueous solutions. *J. Chem. Thermodyn.* **39**, 1300–1317. Available at: http://www.sciencedirect.com/science/article/pii/S0021961407000213 [Accessed September 24, 2016].

Xu Z., Wang S., Liu J. and Chen C. (2012) Solvents with low critical solution temperature for CO2 capture. *Energy Procedia* **23**, 64–71.

Xu Z., Wang S., Qi G., Trollebø A. A., Svendsen H. F. and Chen C. (2014) Vapor liquid equilibria and heat of absorption of CO 2 in aqueous 2-(diethylamino)-ethanol solutions. *Int. J. Greenh. Gas Control* **29**, 92–103.

Yaws C. L. (2014) *Thermophysical properties of chemicals and hydrocarbons*., William Andrew.

Ye Q., Wang X. and Lu Y. (2015) Screening and evaluation of novel biphasic solvents for energy-efficient post-combustion CO 2 capture. *Int. J. Greenh. Gas Control* **39**, 205–214.

Zemánková K., Troncoso J., Cerdeiriña C. A. and Romaní L. (2015) Generality of hydrophobic phenomena for aqueous solutions of amphiphiles. *Chem. Phys. Lett.* **640**, 184–187. Available at: http://www.sciencedirect.com/science/article/pii/S000926141500785X [Accessed September 4, 2016].

Zemánková K., Troncoso J., Cerdeiriña C. A., Romaní L. and Anisimov M. A. (2016) Hydrophobicity and thermodynamic response for aqueous solutions of amphiphiles. *Chem. Phys.* **472**, 36–43. Available at: http://www.sciencedirect.com/science/article/pii/S0301010415301749 [Accessed September 4, 2016].

Zhang J., Agar D. W., Zhang X. and Geuzebroek F. (2011) CO2 absorption in biphasic solvents with enhanced low temperature solvent regeneration. *10th Int. Conf. Greenh. Gas Control Technol.* **4**, 67–74. Available at: http://www.sciencedirect.com/science/article/pii/S1876610211000257.

Zhang J., Misch R., Tan Y. and Agar D. W. (2011) Novel Thermomorphic Biphasic Amine Solvents for CO2 Absorption and Low-Temperature Extractive Regeneration. *Chem. Eng. Technol.* **34**, 1481–1489. Available at:

http://onlinelibrary.wiley.com/doi/10.1002/ceat.201100099/abstract [Accessed July 1, 2016].

Zhang J., Nwani O., Tan Y. and Agar D. W. (2011) Carbon dioxide absorption into biphasic amine solvent with solvent loss reduction. *Spec. Issue Distill. Absorpt.* **89**, 1190–1196. Available at: http://www.sciencedirect.com/science/article/pii/S0263876211000633.

Zhang J., Qiao Y. and Agar D. W. (2012a) Improvement of lipophilic-amine-based thermomorphic biphasic solvent for energy-efficient carbon capture ed. N. H. Rokke MB Mazzetti,MJ. *Energy Procedia* **23**, 92–101.

Zhang J., Qiao Y. and Agar D. W. (2012b) Intensification of low temperature thermomorphic biphasic amine solvent regeneration for CO 2 capture. *Chem. Eng. Res. Des.* **90**, 743–749.

Zhang J., Qiao Y., Wang W., Misch R., Hussain K. and Agar D. W. (2013) Development of an energy-efficient CO 2 capture process using thermomorphic biphasic solvents. *Energy Procedia* **37**, 1254–1261.

Zhang Y. and Chen C.-C. (2011) Thermodynamic Modeling for CO2 Absorption in Aqueous MDEA Solution with Electrolyte NRTL Model. *Ind. Eng. Chem. Res.* **50**, 163–175. Available at: http://dx.doi.org/10.1021/ie1006855.

Zhang Y., Que H. and Chen C.-C. (2011) Thermodynamic modeling for CO2 absorption in aqueous MEA solution with electrolyte NRTL model. *Fluid Phase Equilibria* **311**, 67–75. Available at: http://www.sciencedirect.com/science/article/pii/S0378381211004043 [Accessed September 15, 2016].